PhD: Chiara Damiana Romano

Faculty of Life Sciences, Technology and Medicine

DISSERTATION

Presented on 24th October 2024 in Luxembourg

to obtain the degree of

DOCTEUR DE L'UNIVERSITÉ DU LUXEMBOURG EN BIOLOGIE

by

Chiara Damina Romano

Born on 23 September 1991 in Galatina (Italy)

STUDY OF α-SYNUCLEIN AGGREGATION IN A HUMANIZED YEAST MODEL

UNIVERSITÉ DU LUXEMBOURG

PhD-FSTM-2024-073
The Faculty of Science, Technology and Medicine

DISSERTATION

Defence held on 24/10/2024 in Esch-sur-Alzette

to obtain the degree of

DOCTEUR DE L'UNIVERSITÉ DU LUXEMBOURG

EN BIOLOGIE

by

Chiara Damiana ROMANO
Born on 23 September 1991 in Galatina, (LE) (Italy)

STUDY OF α-SYNUCLEIN AGGREGATION IN A HUMANIZED YEAST MODEL

Dissertation defence committee

Dr Carole Linster, dissertation supervisor
Professor, Université du Luxembourg

Dr Øyvind Halskau
Professor, University of Bergen

Dr Evan Williams, Chairman
Professor, Université du Luxembourg

Dr Peter Barbuti
Associate Research Scientist at Columbia University

Dr Enrico Glaab, Vice Chairman
Professor, Université du Luxembourg

Affidavit

I hereby confirm that the PhD thesis entitled "STUDY OF α-SYNUCLEIN AGGREGATION IN A HUMANIZED YEAST MODEL" has been written independently and without any other sources than cited.

Luxembourg, 24/09/2024 Chiara D. Romano

Name

Acknowledgments

I would like to express my gratitude to my supervisor, Professor Carole Linster, for accepting me as a PhD student and offering me the opportunity to work in the prestigious and stimulating environment of the LCSB. Through her guidance, I was able to develop and apply advanced molecular biology techniques while navigating the challenges of research.

I extend my deepest gratitude to the members of my CET committee for their review and support throughout these years. In particular, I wish to thank Professor Johannes Meiser for his constructive feedback and invaluable suggestions, which significantly enhanced the quality of my work. Taking part in the 'Metabolism and Biochemistry' course was a crucial formative part of my studies. I also want to express my sincere thanks to Professor Evan Williams for joining the CET committee during the final two years of my PhD and for his steadfast support and encouragement throughout this journey. Additionally, I would like to thank Professor Fay Betsou for allowing me to work on the Convince study during the first six months of my PhD, for supporting me during challenging times, and for providing valuable advice throughout my doctoral journey.

I am immensely grateful to my former post-doc Dr. Ursula Heins Marroquin, who always believed in my capabilities and academic potential. Thank you for encouraging me even in my most challenging moments and for supporting me during times of doubt. Your deep commitment to academic excellence, meticulous attention to detail and insightful critiques have significantly shaped my work and the level of this dissertation. Thank you Ursula for teaching me essential molecular biology techniques and how important and amazing is to work with yeasts. Thank you for being the ideal model of a scientist and a woman, which I have always aspired to become.

I would like to thank my colleagues and members of the BCM group for providing distractions when needed and encouragement when it seemed impossible to continue. Parisa you are the most precious colleague, friend and âbji I could have ever dreamed of. The time spent together was like a sunny day in Luxembourg and I would like to thank you also for staying with me in the lab until late during the RNA extraction, for helping me with the qPCR, for always indicating the right choice in my scientific and not decisions. You were there when I was completely alone, making

me laugh, loved and (more or less) proficient in cooking lubie tahdig. My dear Ana-maria, I will never forget our long chats and late lunches. Thank you for your support and for teaching me how to work with mammalian cells, perform RNA extraction, Western blotting, and BCA assays. Your encouragement pushed me to improve every day, and it has been a pleasure working beside you. Najme thank you for the nice moments and for improving my persian culture. I would like to thank Gezime, Agnes, Santi, Beatriz and Jean-Francois for the enjoyable times together and their support.

A special thanks to Martin for his assistance with the lipidomics analysis and for reviewing this lengthy dissertation. I also want to thank Floriane and Lisa from the Metabolomics Platform for their help in processing my samples and providing valuable data. Additionally, my gratitude goes to Paul Antony from the Bioimaging Platform for teaching me how to properly conduct microscopy analysis on yeast samples and for guiding me in analyzing the imaging data.
I would like to thank the members of ECM, MFN, NIM and TN groups. Thank you Bego, Federica, Maria and Vera for the nice coffees and the psychological support. Thank you Michele for your kindness and for often understanding my frustration. Thank you Ilaria for making the lab environment a better place and for always taking my side despite my stubborn moods.

A big thanks to my partner Paul whose patience and understanding, especially during the worst time of my PhD, have been my anchor. Thank you for always being by my side and supporting me in any decisions. I am also deeply grateful to Eric and Sandrine for always believing in me, even when I struggled to believe in myself. I would like to thank my friends Lorenzo, Giuliana, Reza, Amin, Rey, Alex and Sura for making this journey not only possible but also enjoyable. I would like to thank Leonardo for all the precious moments we shared.

Finally I would like to thank the Luxembourg National Research Fund for their financial support throughout my doctoral research.

"This PhD thesis was written in the pursuit of knowledge for all mankind."

Index

List of Figures

List of Tables

Summary

Parkinson's Disorder (PD) is one of the major age-related neurodegenerative disorders that mainly affects the motor system, leading to the loss of dopaminergic neurons. Although PD is a progressive neurodegenerative disorder that primarily affects individuals over the age of 60; mutations of genes associated with hereditary forms of early-onset PD have been identified. This project focuses on the *SNCA* gene that encodes α-synuclein (α-syn), the main component of Lewy bodies which are found in the substantia nigra pars compacta of PD patients. Missense mutations in *SNCA* (also known as PARK1) were the first to be identified in familial cases of PD. Furthermore, duplications and triplications of *SNCA* have a gene dosage effect on the severity of the disorder. Currently, there is no cure for PD, but treatments that reduce the symptoms and improve the patient's quality of life are available. Levodopa is the first-line drug in the treatment of the disorder and the more recent therapy of deep brain stimulation (DBS) effectively improves the patient's movement. This doctoral project aimed to investigate the mechanisms underlying α-syn toxicity by studying the protein in yeast, a simple and comprehensive model organism. The resulting findings define molecular pathways that in the future may be targeted for the treatment of synucleinopathies.

This work started with the observation that cobalt, nickel and deferoxamine can rescue the toxicity induced by α-syn aggregation in yeast cells. These compounds were identified as promising candidates in a phenotypic high-throughput screening of an FDA-approved drug library on yeast engineered to overexpress human α-syn fused to GFP. After confirming that the three highlighted compounds do not directly decrease the expression level of the human protein, we concluded that the observed protective effect must involve a more complex molecular mechanism. To uncover this mechanism, we performed different analyses. Fluorescence microscopy revealed that treatment with Cobalt, Nickel, and Deferoxamine significantly reduced the number of α-syn aggregates in yeast cells. The formation and clearance of the inclusions were quantitatively monitored by time-lapse imagining in cells grown in a microfluidic system. The three treatments reduced the number and size of aggregates affecting the α-syn aggregation kinetics. Cobalt, in particular, eliminated all aggregates within the first 6 hours and prevented the formation of new ones.

We also observe a rescue effect increasing the oxygenation level of the media. To assess the importance of oxygen, we cultivated the cells in different formats with decreased oxygenation until we reached complete anoxia. We were able to observe the toxic phenotype only when the cells were grown under hypoxia conditions.

To identify the key mechanisms involved, we performed transcriptomic profiling coupled with pathway enrichment analysis on the strains untreated and treated with Cobalt and Deferoxamine. Our analyses showed significant changes in fatty acid, ergosterol, iron, energetic metabolism and more unexpectedly, in the thiamine biosynthesis pathway. The importance of the thiamine biosynthetic process was further investigated by generating α-syn strains overexpressing the enzymes THI4, THI5, THI11, THI12 and THI13. A moderate growth rescue effect was observed for some of these overexpression strains correlated with an increased level of thiamine pyrophosphate.

Following a multi-omics approach, we conducted metabolomic and lipidomic profiling to assess the impact of α-syn expression on cell metabolism and membrane composition. We found that α-syn expression expression alters the metabolite levels within the oxidative branch of the TCA cycle and one-carbon metabolism, while also inducing notable changes in the cell phospholipids profile. In particular, we noticed that pyruvate accumulates 70% more in the yeast strain overexpressing α-syn compared to the control, with consequences on the cell metabolism and synthesis of fatty acids (FAs). The excess of FAs is accumulated in di- and tri-glycerides whose levels increased significantly. Furthermore, we noticed upregulation of intermediates involved in phosphatidylinositol biosynthesis in the strain that overexpresses α-syn. Interestingly, Cobalt and deferoxamine treatments inverted the observed trends, reducing the levels of FAs and phosphoinositide.

Our study highlights that hypoxia triggers α-syn aggregation and toxicity, suggesting that oxygen availability plays an important role in neurodegenerative processes. Furthermore, pathological α-syn expression compromises central metabolic processes, potentially altering membrane lipid composition and further promoting protein aggregation in a self-perpetuating cycle. Small molecules

able to modulate the hypoxia response, most likely at the level of lipid and iron metabolism, can protect against α-syn toxicity. The results offer important insights into the mechanisms of α-syn toxicity and potential therapeutic interventions for neurodegenerative diseases involving protein aggregation.

Chapter 1

Introduction

This chapter provides an overview of neurodegeneration, emphasizing the critical role of the protein α-synuclein in Parkinson's Disease and Synucleinopathies. It revisits and summarizes key classical literature, incorporating significant recent advancements in the field. The investigation of α-Synuclein began 30 years ago, and substantial progress has been made in elucidating its role in the context of neurodegenerative disorders and physiological conditions.

1.1 Neurodegenerative diseases and Synucleinopathies

For a long time, *Neurodegeneration* has been defined as chronic, pathological conditions associated with the aging process. Aging is a phase of the life cycle characterized by a progressive decline in physiological capacities and the accumulation of somatic mutations named "genosenium", which increase the risk of developing Alzheimer's disease (AD), Parkinson's disease (PD), Huntington's disease (HD), and frontotemporal lobar dementia[1, 2]. The challenge of neurodegenerative diseases lies in their irreversible nature, as they affect neuronal cells that cannot regenerate because of their terminally differentiated post-mitotic state[3, 4]. These diseases' progression follows a dynamo scheme in which the loss of neurons in the central and peripheral nervous system leads to a gradual decline of all the essential functional activities: memory, cognition, behavior, sensory and mobility[5]. The aggregation of misfolding proteins is a hallmark of many neurodegenerative disorders: AD, PD, Primary tauopathies, Frontotemporal dementia, Amyotrophic lateral sclerosis,

Dementia with Lewy bodies (DLB), Multiple system atrophy, HD, Polyglutamine disorders and Prion-like diseases (Fig 1.1, **a** and **b**). When amyloid-forming proteins fail to adopt their native, functional three-dimensional structure, they assume the most thermodynamically favorable conformation, enriching in β-sheets that tend to be stabilized in insoluble aggregates[6]. The cell evolved a sophisticated quality control system, known as unfolded protein response (UPR), which is based on a battery of chaperones that assist proteins during their folding inside the endoplasmic reticulum (ER). Proteins that do not assume a correct conformation are eliminated through the ER-associated protein degradation (ERAD) (reviewed [7]). The same system is responsible for protein turnover assuring their degradation at the end of their lifecycle. Besides the UPR and ERAD systems, the cell can eliminate protein aggregates also by activation of the autophagosome-lysosome degradative process (ALP), which recycles cell components and eliminates damaged organelles or unfolded proteins[8]. Considering the importance of the ALP system in removing toxic protein aggregates, lysosome dysfunctions are often linked with neurodegenerative diseases[9, 10]. The pathological accumulation of misfolded proteins due to alteration of these cellular mechanisms has been reported in several neurodegenerative disorders[11, 12]. In this PhD thesis, we will mostly focus on the neurodegeneration induced by the pathological accumulation of the α-synuclein (α-syn) protein, which is a characteristic feature of PD and synucleinopathies (Figure 1.1 **b**)

The word "Synucleinopathies" refers to a group of neurodegenerative diseases that share a common feature: the presence of inclusions mainly composed of insoluble α-syn aggregates. These inclusions mostly affect neurons and glial cells and lead to a broad and complex spectrum of symptoms. Among the members of the synuclein family (Fig.1.1, **c**), α-syn is the most studied due to its role in neuropathology, while β-synuclein (β-syn) and γ-synuclein (γ-syn) for a long time were not associated to disorders[13]. The three proteins share a high homology in sequence[14, 15]: β-syn shows 62% sequence identity with the α isoform[16], while γ-syn only 56%[17]. Synuclein proteins are mostly expressed in the synaptic vesicles and nuclear envelope of presynaptic neurons [18], where they participate in neuron homeostasis and development[19].
β-Syn is a 134 amino acid protein that compared to the α isoform is less prone to aggregate under

physiological conditions[20]. This reduced aggregation tendency is due to the missing amyloidogenic hydrophobic core in its sequence[21, 22] (Fig.1.1, **c**). Similarly to the other synuclein members, β-syn is an intrinsically disordered protein without a secondary and tertiary conformation[22], but with a more extended structure[22, 23]. β-Syn is considered the molecular chaperone of α-syn able to prevent its toxic aggregation[24, 25, 26]. Different mechanisms have been suggested regarding how it stabilizes the α-homolog preventing its fibrillar aggregation. Protein docking simulations demonstrated that β-syn can bind α-syn in stable heterodimers compromising the aggregates propagation[27]. Because electrostatic interactions are too weak to justify a molecular chaperon activity, other hypotheses are more in favor of an indirect mechanism. Considering the high degree of homology between the two proteins, they can easily compete for the same binding sites at the surfaces of lipid vesicles. In this scenario, β-syn decreases α-syn concentration near the membrane preventing lipid-induced aggregation[28]. β-Syn chaperone activity is particularly significant during the initial stages of α-syn aggregation, when it interferes with the recruitment of toxic α-syn oligomers on the surface of the preformed fibrils, blocking the secondary nucleation and the fibril elongation[20, 28, 29]. The alteration of the α-syn aggregation process by β-syn results in smaller aggregates[29] and shorter and more branched fibrils[30]. β-Syn chaperone activity is not significant when neurodegeneration is driven by α-syn E46K, H50Q, and A53T mutations which have more complex aggregation kinetics[29]. P123H and V70M are two point mutations of β-syn that lead to a pathological condition characterized by axonal swellings and alteration of the lysosomal degradation activity with β-syn inclusions accumulation[31].

γ-Syn is the third member of the synuclein family and is involved in different types of human tumors[32]. Compared to the α isoform, γ-syn has a shorter C-terminus, with a total length of 127 amino acids[15] (Fig.1.1, **c**). Structural analysis reveals that γ-syn can assume a partial secondary structure with β-sheet and globular motifs. Because of the presence of the amyloidogenic hydrophobic core, the protein can undergo fibrillation with a kinetics similar to the one described for α-syn, although this process is 20-fold slower in γ-syn. Similarly to the β isoform, γ-syn has as well the ability to decrease the α-syn aggregation[22]. Computational analyses suggest that γ-syn can work as molecular chaperon[33] stabilizing α-syn in a α,γ heterodimer complex[34].

At the pathological level, γ-syn aggregations were observed in neuronal body and axons of PD and DLB patients, leading researchers to propose a new subcategory of synucleinopathies called γ-*Synucleinopathy*. Expression of high levels of γ-syn in animal models leads to severe and fatal neurological disease associated with protein aggregation[35].

Synoretin (SN), the most recently discovered member of the synuclein family, was isolated from ocular tissues in a screen for novel phototransduction regulators[36]. While the specific functions of SN and its potential involvement in neurodegenerative diseases are not yet well-defined, preliminary evidence suggests that it plays a role in modulating signal transduction[36].

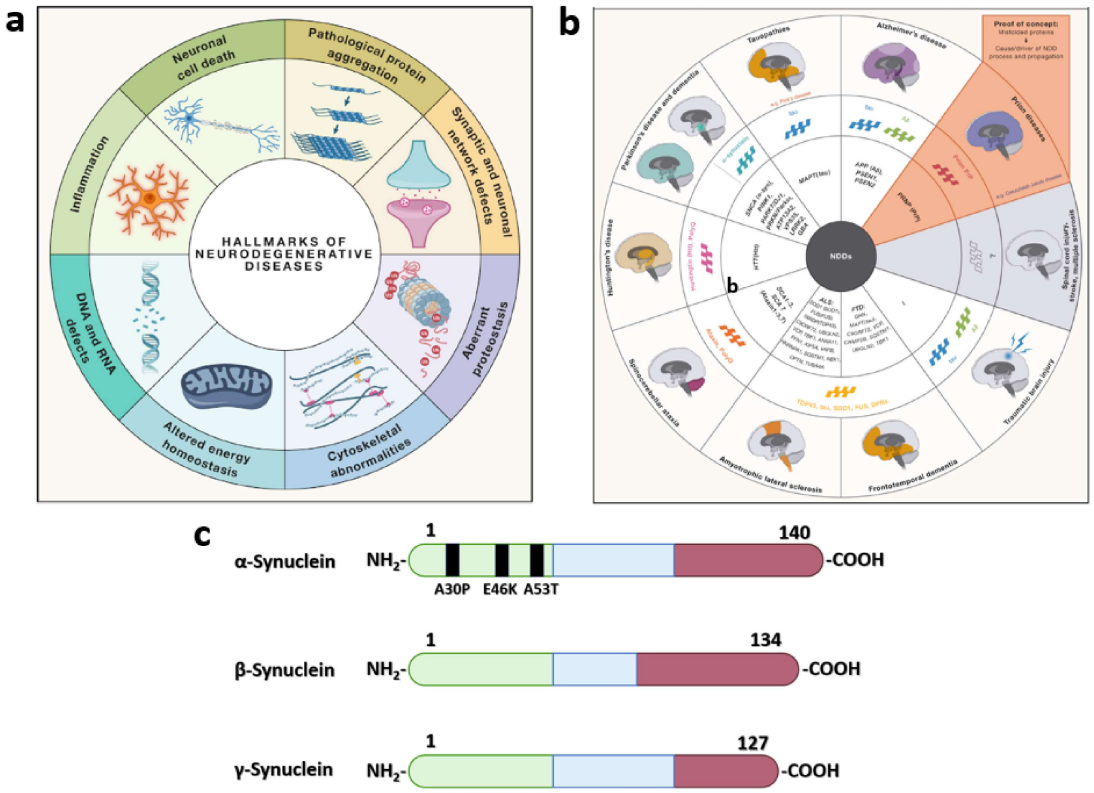

Figure 1.1: a and b Schemes of Hallmarks of Neurodegenerative Diseases with the respective proteins reported in *Wilson III et al.*[5] **c** Illustrative scheme of the Synuclein Family: α, β and γ with the relative amino acid count and the respective N-terminus in green, the central hydrophobic core in light blue and the C-terminus in red. In the N-terminus of the α-synuclein are reported three of the main point mutations associated with hereditary forms of PD: A30P, E46K and A53T.

1.2 Parkinson's Disease (PD)

A comprehensive analysis of the Global Burden of Disease conducted in 2018 reported 6 million cases worldwide of Parkinson's disease (PD) which has been identified as the second most common neurodegenerative disorder[37]. A more recent estimation indicates a significant increase with 9.4 million global cases reported in 2020[38], expected to rise up to 12 million by 2040. PD affects 1-2% of individuals over the age of 65[39], however, as indicated by the Parkinson's Foundation (`https://www.parkinson.org/`), 4% of people are diagnosed with PD before the age of 50. The

first clear medical description of PD was reported in 1817 by James Parkinson in his "Essay on the Shaking Palsy"[40]. PD was initially defined as "movement disorder" due to the characteristical uncontrolled tremor observed in the patients (Figure 1.2 **a**). Nowadays we learn that PD has a more complex and serious phenotype resulting from a combination of:

- Movement symptoms (tremor, bradykinesia, hypokinesia, akinesia, rigidity, postural instability and gait disturbances)
- Prodromal symptoms (rapid eye movement, sleep behavior disorder, hyposmia and constipation)
- Psychological or cognitive symptoms (depression, anxiety, apathy, hallucinations, psychosis, dementia and cognitive decline)

The PD symptoms are associated with a significant loss of dopaminergic neurons in the *substantia nigra* (SN), which leads to dopamine deficiency[41]. SN is one of the subcortical nuclei that constitute the basal ganglia, a brain region crucial for regulating movement, cognition, and emotions. These functions are coordinated through the basal ganglia-thalamo-cortical loop simplified in Figure 1.2 (**c**). Our ability to initiate movements relies on the direct pathway: from the *cortex*, where movement intentions originate, excitatory signals are sent to the *striatum*[42, 43] (Figure 1.2 **c**). The *striatum* then activates GABAergic neurons, which inhibit the suppression activity of the *globus pallidus* and SN on the *thalamus*. Disinhibited *thalamus* can send excitatory signals back to the cortex, facilitating the movement execution[42, 43, 44] (Figure 1.2 **c**). In contrast, the indirect pathway reduces the movement by activating the inhibition activity of *globus pallidus* and SN on the *thalamus*, which is no longer able to send excitatory signals to the cortex[42, 43, 44] (Figure 1.2 **c**). Dopaminergic neurons of SN regulate both the direct and indirect pathways, ensuring smooth and coordinated movements. Dopamine facilitates movement by enhancing excitatory inputs from the cortex and suppressing activity in the *globus pallidus*, as well as inhibiting the indirect pathway. In PD, dopamine loss disrupts the balance between these pathways, leading to excessive indirect pathway activation and impaired movement[44].

The second pathological hallmark of PD is the presence of proteinaceous inclusions in the monoaminergic and cholinergic neurons of the brainstem, diencephalon, basal forebrain[45], cerebral cortex and ganglia[46, 47]. These inclusions were first identified in 1912 by Friedrich Lewy and subsequently named Lewy bodies (LBs) in his honor[48]. In hematoxylin/eosin stained neurons, LBs appear as round complexes, but their morphology varies based on their location in the brain[49]. In particular, they show a thread-like profile (Lewy neurites) in the cortex and a serpiginous appearance in the sympathetic ganglia[50, 51]. Since the initial identification of α-syn as the primary component of LBs in the brains of PD and DLB patients[52], several studies tried to elucidate the role of this protein in the formation of LBs and LNs (Lewy neurites). The development of protocols for the LBs isolation from brain tissues[53, 54] opened an intense investigation aimed at deciphering the protein composition and ultrastructural organization of LB (reviewed[55]). Electron microscopy performed on LBs revealed a distinctive pattern characterized by a dense central core surrounded by radially arranged neurofilaments (Figure 1.2 **b**). The isolation of α-syn fibrils from LBs[56, 57], along with experimental evidence that α-syn is able to assemble in fibrils *in vitro*[58, 59] highlighted the essential role of α-syn in LBs formation. Years later, the LB model with a dense inner core and fibrillar periphery was revisited by Shahmoradian and colleagues[60]. By combining different high-resolution spectroscopy techniques, the authors analyzed LBs isolated from PD patients, finding that most of them lacked fibrillar features[60]. Their analysis concluded that LBs are mainly composed of membrane fragments, vesicular structures similar to lysosomes and autophagosomes and accumulated mitochondria at the periphery[60] (Figure 1.2 **b**). Considering all studies on LBs composition, it is not well understood how they contribute to the PD physiology[61], despite their presence in many neurodegenerative disorders[50, 62, 63] and being identified as one of the primary causes of dementia with Lewy bodies[64] and idiopathic Parkinson's disease[65].

For a long time and still nowadays there is a missing correlation between the presence or the number of LBs and the neuronal loss at the base of the neurodegeneration process[61, 66]. Because aggregated α-syn is the main component of LBs, their cytotoxicity is generally associated with the oligomeric and fibrillar forms of this protein[67]. However, the ultrastructural characterization

of LBs revealed that besides α-syn, proteins involved in the trafficking pathways such as microtubules, tubulin, and ubiquitin are as well present as components[68]. Vesicular aggregation in LBs deprives the cell of essential components, particularly microtubule and mitochondrial, leading to structural and energetic deficits, and ultimately, cell death [69]. This evidence supports the contribution of LBs in driving PD pathology.

There is no effective cure for PD, but the FDA has approved several drugs and treatments as therapies to improve the quality of life of PD patients. Levodopa or L-3,4-dihydroxyphenylalanine (L-DOPA) is the gold standard for PD treatment[70] and its development is intertwined with the discovery in 1957 of dopamine as a neurotransmitter that could control movement[71]. In the same period, Oleh Hornykiewicz reported dopamine deficiency in PD patients[41]. Because dopamine does not cross the blood-brain membrane and induces vasodilation as a side effect, initially D,L-dihydroxyphenylalanine (DOPA), the metabolic precursor of dopamine, was administrated to PD patients[72]. Due to the missing beneficial effect and the D-DOPA toxicity, only the L-enantiomer was used for the treatment[73]. PD patients responded to L-DOPA showing short-term symptom improvements and yet important side effects[73]. The weak efficiency of L-DOPA and its side effects were attributed to the decarboxylase enzyme's activity, which converts L-DOPA into dopamine. The significant advance came with the co-administration of L-DOPA with an L-aromatic amino acid decarboxylase inhibitor, carbidopa[74, 75]. L-DOPA/Carbidopa was approved in 1975 by the FDA as a treatment for PD symptoms. Despite the important improvements, the pharmacological replacement of dopamine has several complications in the long term such as fluctuation of PD symptoms and treatment resistance[76, 77]. The PD cases unresponsive to the pharmaceutical treatment are selected for deep brain stimulation. This invasive therapy is based on an implantable pulse generator, similar to the heart pacemaker, surgically implanted in the brain of the patients. An electrode applies high-frequency impulses to stimulate specific brain areas, such as the *ventrolateral thalamus*, *internal pallidum*, and *subthalamic nucleus*. In 2002, the FDA approved deep brain stimulation for the treatment of motor symptoms in advanced PD cases (more information on the therapy of deep brain stimulation is reported on the website of the National Institute of Neurological Disorders and Stroke `https://www.ninds.nih.gov`).

Novel approaches for the PD treatment currently tested in clinical trials use monoclonal antibodies against aggregates of α-syn. In this regard, Presinezumab is the first experimental therapeutic monoclonal antibody in the phase II trial designed to recognize and bind aggregated α-syn [78, 79].

An important step forward in PD research was the discovery of genetic mutations linked with hereditary forms of the disease which account for less than 10% of the total PD cases. The genes listed in Table 1.1 encode proteins involved in cellular mechanisms whose alteration drives PD neuropathology. How these genes are able to cause PD or increase the risk of developing this important neurodegenerative disease is still unclear. However, a large consensus arises from the evidence that genetic studies and experimental findings point to one key protein: α-synuclein.

Locus	Gene	Clinical features
Autosomal dominant inheritance		
PARK1, PARK4	SNCA	Missense mutations (PARK1) cause classic PD phenotype. Duplication or triplication of this gene (PARK4) causes early-onset PD with prominent dementia.
PARK8	LRRK2	Classical PD phenotype
PARK17	VPS35	Classical PD phenotype
Early-onset PD (autosomal recessive inheritance)		
PARK2	Parkin	Lower limb dystonia
PARK6	PINK1	PD psychiatric features
PARK7	DJ-1	Early-onset PD
PARK19B	DNAJC6	Early-onset PD
Complex genetic forms (autosomal recessive inheritance)		
PARK9	ATP13A2	Early-onset parkinsonism with a complex phenotype
PARK14	PLA2G6	Complex clinical phenotype without parkinsonism
PARK15	FBXO7	Early-onset parkinsonism with pyramidal signs and a variable complex phenotype
PARK19A	DNAJC6	Juvenile-onset parkinsonism with mental retardation and seizures
PARK20	SYNJ1	seizures, cognitive decline, abnormal eye movements and dystonia
PARK23	VPS13C	Young-adult-onset parkinsonism associated with progressive cognitive impairment that leads to dementia and dysautonomia

Table 1.1: This table, inspired by a similar one reported by Poewe et al. in their publication[69] summarizes genes and respective encoded proteins associated with hereditary forms of PD. Some of these proteins are involved in crucial molecular pathways that, when perturbed, lead to neuropathology with symptoms in the spectra of Parkinsonism and sporadic Parkinson's disease.

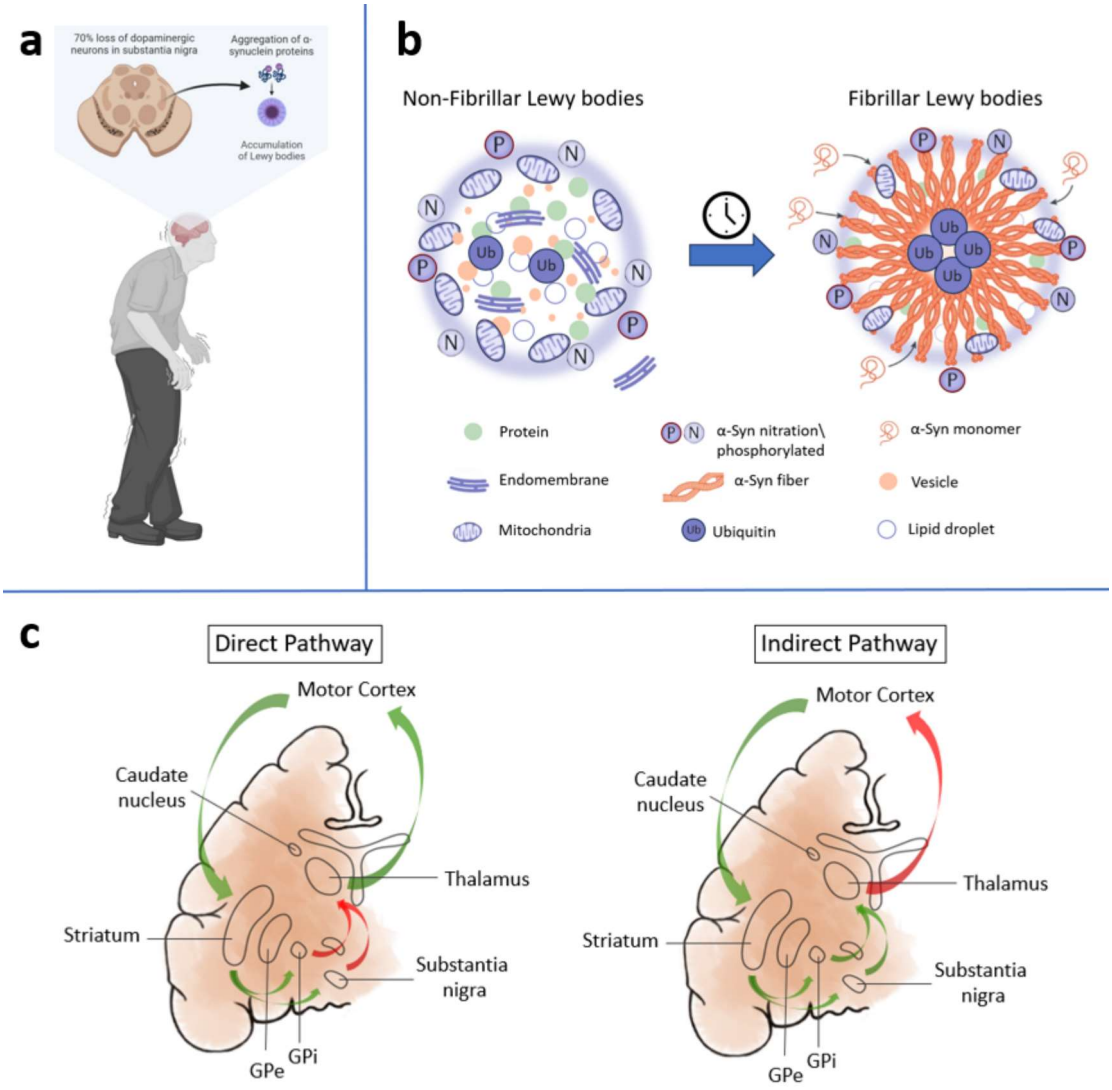

Figure 1.2: **a** Figurative representation of a PD patient with the typical motor symptoms: tremor, short shuffling steps because of postural instability, back rigidity, stooped posture and flexed elbows and wrists. In his brain, the two pathological features associated with the disease: loss of dopaminergic neurons in the SN and LBs. **b** Models of LBs composition based on the ultrastructures proposed in the literature. The fibrillar Lewy body shows the canonical structure, with a dense core surrounded by α-syn fibrils. The Non-fibrillar Lewy body is based on what was reported by Shahmoradian et al.[60] and it contains mainly the monomeric form of α-syn. Both models emphasize the presence of different proteins, membranous material, and organelles. These descriptions can be integrated into a more comprehensive framework, suggesting that α-syn fibers emerge only in the later stages of Lewy body maturation. **c** Representation of the basal ganglia-thalamo-cortical loop. In the Direct Pathway, the striatum inactivates globus pallidus and substantial nigra (red arrow) and the thalamus can send information (green arrow) back to the motor cortex. In the indirect Pathway, the globus pallidus and substantial nigra inhibit the thalamus which is no more able to communicate with the motor cortex. An illustration generated in Krita (5.2.3.100) is based on an online image of the direct and indirect pathways.

1.3 α-Synuclein

α-Synuclein is a small protein of 140 amino acids and a molecular weight of 14kDa. It is encoded by the SNCA gene located on the long arm of chromosome 4 (4q21) and mapped for the first time in 1995 by the geneticist Spillantini and her colleagues[80]. A few years later, in 1997, Polymeropoulos and colleagues identified the G209A point mutation in the SNCA gene of an Italian family affected by an autosomal dominant form of Parkinson's disease[81, 82]. This mutation results in the amino acids replacement A53T in the protein sequence[83]. The genetic link between α-syn and Parkinson's disease was subsequently consolidated with the advent of the genome-wide association studies that identified the SNCA locus as one of the main genes associated with the risk of Parkinson's development[84, 85, 86, 87, 88]. Despite the efforts to undercover the role of α-syn in the pathophysiology of neurodegenerative diseases, the complete physiological role of alpha-synuclein is still not fully understood, and ongoing research continue to uncover more details about its functions and mechanisms. α-Syn was first identified in the presynaptic terminations during a screening for proteins involved in the neurotransmission process[18]. As a definition, presynaptic proteins coordinate vesicle docking, priming and fusion to ensure the release of neurotransmitters[89]. The functional investigation of α-syn is further complicated by its native unfolded nature[90]. Because of its low hydrophobicity and high net charge[91], α-syn does not assume a well-defined structure in solution, at physiological pH, behaving as an intrinsically disordered protein[92, 93, 94].

1.3.1 Structure

The combination of advanced nuclear magnetic resonance techniques and circular dichroism allowed the resolution of the protein's secondary structure. The amino acids sequence can be subdivided into three main regions: the N-terminus, a central hydrophobic region and the negatively acidic C-terminus (Figure 1.3 **a**). The N-terminus (residues 1-60) is characterized by seven 11-amino acid imperfect repeats which assume a α-helix conformation similar to the A2 amphipathic-helix found in the lipid-binding domains of apolipoproteins[95, 96]. The N-terminus domain is the *binding domain* of the protein and mostly interacts with lipid membranes of vesicles

and micelles[97]. Depending on the curvature of the targeting membrane this part of the protein can fold in a broken α-helix with a discontinuity at the 43 and 44 residues level[98] (interaction with micelles) (Figure 1.3 **b**) or a continuous single α-helix (interaction with low-curvature membranes)[99]. The N-terminus ends in the non-amyloid-β component (NAC) domain (residues 61-95) (Figure 1.3 **a**) identified as the responsible sequence for the toxic aggregation of amyloid protein in Alzheimer's disease (AD)[100]. Several experiments showed that also the N-terminus plays a role in α-syn toxicity. Duplication of this part of the sequence increases the protein toxicity while deleting a few residues or the entire region significantly reduces or abolishes the protein's toxicity[101]. The C-terminus (residue 96-140) is the *solubilizing domain*[102, 103] and compared to the N-terminus, it preserves a random coil structure despite changes in external factors such as pH, temperature and solvent (Figure 1.3 **a, b**). It is negatively charged due to the presence of multiple aspartate and glutamate residues[102]. Truncations of the C-terminus tail exacerbate α-synuclein toxicity, accelerating the accumulation of protein fibrils in the cell[104] (α-Syn fibril structure in Figure 1.3 **c**). Furthermore, the combination of site-direct spin labeling with paramagnetic relaxation enhancement measurements performed on the native form of the protein, suggests that the flexibility of the C-terminus protects against aggregation, promoting packed conformations in which the C-terminus shields the NAC core and at the same time binds the N-terminus by electrostatic interactions[23]. The C-terminus is the part of the proteins involved in the interactions with other cellular effectors[105, 106], calcium[107], metals[108] and iron[109, 110]. These interactions inevitably affect the protein conformation and activity.

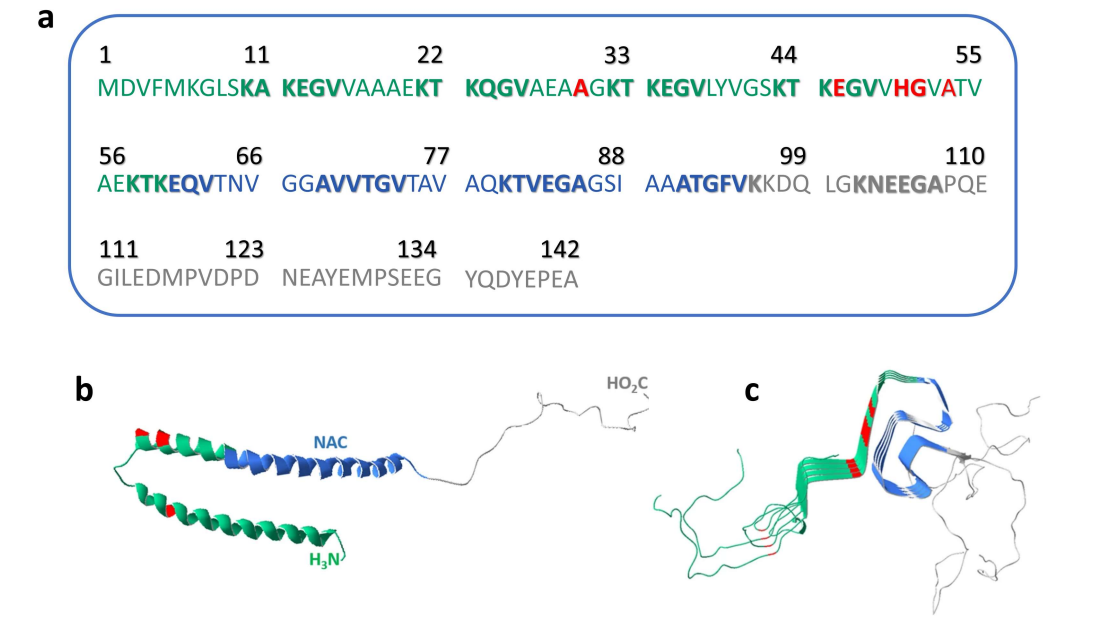

Figure 1.3: **a** Primary sequence of α-syn taken from the publication of Twohig and colleagues [111]. N-terminal residues 1-60 are in green, the non-amyloid component (NAC) residues 61-95 are in blue, C-terminus residues 96-140 are in grey. Disease-associated point mutations A30P, E46K, H50Q, G51D and A53T are in red. The seven 11-amino acids imperfect repeats are indicated below the sequence with the conserved KTKEGV hexameric motifs in bold. **b** Molecular model of NMR of micelle bound human α-syn, PDB 1XQ8[112] (same color scheme of **a**). **c** Molecular model of the structure of a α-syn fibrils, PDB 6H6B [113] (same color scheme of **a**).

1.3.2 Physiological functions

Based on the evidence that α-syn is a presynaptic protein able to interact with lipidic membranes and components of the neurotransmission machinery, researchers suggested that physiologically it works as a cytosolic regulator of neurotransmission. Synaptic neurotransmission is an organized and coordinated process that leads to the exocytosis of synaptic vesicles (SVs) upon an action potential. It is articulated in several steps reviewed in [114, 115]:

1. SVs recruitment in the synapses

2. SVs vesicles dock at the active zone, where the vesicle content can be released in the

extracellular domain.

3. syntaxin-1, SNAP-25, and VAMP2/synaptobrevin-2 assembly in the ternary SNARE complex.

4. The SVs and the presynaptic membrane are connected by the SNARE complex. Membrane fusion is possible only when Ca^{2+} binds the synaptotagmin protein exposed on the surface of the vesicles.

5. SVs release their contents into the extracellular space, while accessory proteins facilitate the disassembly of the SNARE complex and the reactivation of SNAREs for the next exocytosis event.

α-Syn modulates different steps of this cycle in two different ways:

- **Chaperoning SNARE-complex** (Figure 1.4). The SNARE complex formation in the synapsis requires initiation by accessory proteins. In this context, higher-order multimers of α-syn bind at the C-termini the VAMP2/synaptobrevin-2 exposed on the surface of the SVs already docked on the presynaptic membrane[105, 116]. α-syn is engaged in the SNARE complex, potentially increasing the driving force of the fusion process in favor of a broader opened fusion pore and more neurotransmitters releasing[117]. When α-syn forms less-ordered oligomers, it fails to engage in these processes, resulting in synaptic attenuation and decreased vesicle fusion events [118]. This further supports the toxic effect of α-syn oligomers on synaptic homeostasis.

- **Organization of SVs pools** (Figure 1.4). During neurotransmission, a group of SVs remains distal to the active zone serving as a reserve pool[119]. These vesicles are anchored in the presynaptic button ready to be recruited in the releasable pool by synapsins[120]. It has been proposed that this protein crosslinked the vesicles in a net-like structure[120]. Higher-order multimers of α-syn clustered on the surface of the SVs can contact the VAMP2/synaptobrevin-2 exposed on the adjacent vesicles forming an interconnection structure similar to the one reported for synapsins that help to maintain a physiological SVs cluster near the active zone[116, 117, 118, 121].

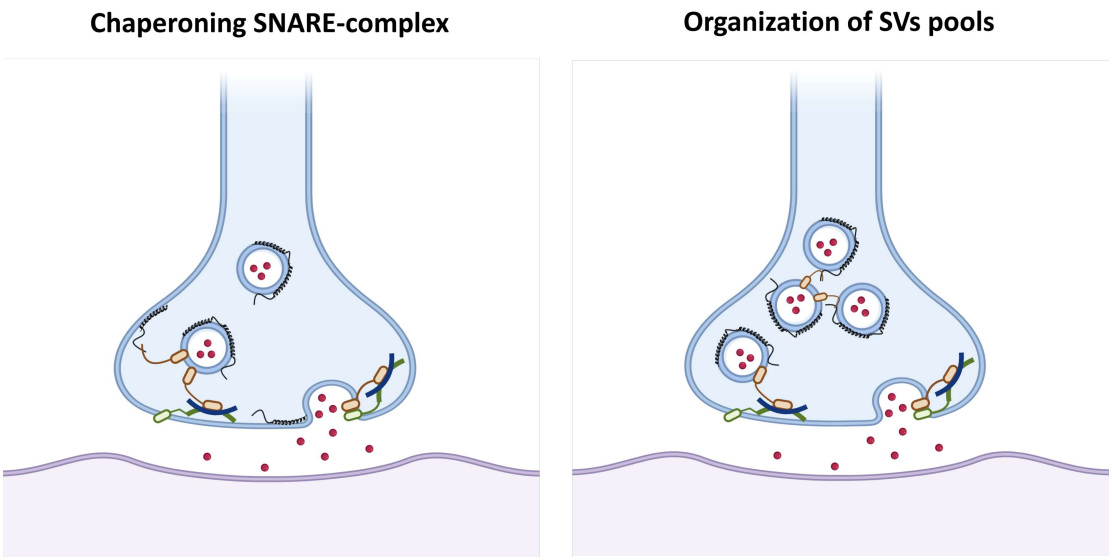

Figure 1.4: The primary physiological function reported for α-syn is the regulation and coordination of neurotransmission. This figure illustrates two main mechanisms proposed for α-syn (black): the chaperone role in the SNARE complex and the organization of synaptic vesicle pools. In the first mechanism, α-syn actively participates in the formation of the fusion pore for neurotransmitter release. In the second, the protein interconnects synaptic vesicles into a net-like structure, keeping them in proximity to the synaptic membrane. In the figure, α-syn is represented together with other important synaptic proteins involved in the neurotransmission: VAMP (orange), Synthaxin-1A (green) and SNAP-25 (blue).

Another physiological role addressed to α-syn is the modulation of the dopamine transporter activity. Dopamine (DA) is an important hormone whose signaling affects movement, cognition, executive functions, reward, motivation, and neuroendocrine control[122]. DA, like other neurotransmitters, is stored in vesicles at the presynaptic terminals. When an action potential arrives, it triggers the release of dopamine into the synaptic cleft, where it is captured by the dopamine receptors on the surface of the postsynaptic cells. DA reuptake in the dopaminergic neurons is performed by the dopamine transporter (DAT)[123]. This Na^+/Cl^- neurotransmitter transporter translocates the DA present in the synaptic cleft back to the cytoplasm, a process that requires the symport of two Na^+ and one Cl^- ions[124]. The DAT is the primary mechanism for the modulation of DA signaling as it clears DA from the synapses. DAT is particularly expressed in the SN, where the majority of dopaminergic neurons are located[125, 126]. The expression of DAT is half reduced in the brain of PD patients, due to the loss of dopaminergic neurons[126]. Nevertheless,

the reduced expression of the transporter could be a cellular adaptation response to increase the level of DA, in the attempt to compensate the dopaminergic neuronal death[127]. α-Syn has been proposed to regulate the homeostasis of monoamines in synapses by direct interaction with DAT. Lee and colleagues demonstrated that the NAC domain of α-Syn directly binds the C-terminus of DAT, resulting in a stable complex, also confirmed by further co-immunoprecipitation experiments[128, 129]. This interaction increases the transporter localization on the cell membrane[128], but it is unclear if α-syn enhances or decreases the transporter DA uptake activity[128, 130]. Further experiments have demonstrated that α-syn promotes the inactive conformational state of DAT, leading to impaired Na^+ and Cl^- translocation. This activity alteration explains the membrane depolarization observed in cells overexpressing both DAT and α-syn[129, 131] and support the hypothesis that the interaction between DAT and α-syn decreases dopamine uptake. Considering the homology between DAT and the serotonin transporter (SERT), the α-syn regulatory activity on this important neurotransmitter transporter has been investigated. Similarly to what was observed for DAT, α-syn interacts with SERT forming heteromultimeric complexes that involve the α-syn NAC domain and the C-terminus of the transporter[132]. It is unclear how this interaction affects the activity of the transporter as opposite results are reported in the literature when α-syn is differently expressed in raphe neurons[133, 134].

1.3.3 Aggregation kinetics

Aggregation is at the center of α-syn mediated toxicity in synucleinopathies and continues to be the focus of intensive research. Fully elucidating this process could provide insights into potential therapeutic strategies to inhibit or reverse the formation of α-syn toxic aggregates. Parallel studies on the amyloid-β fibrillation, a process implicated in Alzheimer's disease, contribute to the understanding of α-syn aggregation, which is defined as a nucleation-dependent polymerization reaction with sigmoidal growth kinetics[135]. The process is articulated in different steps summarized in Figure 1.5 **a**.

- At the beginning there is a slow growth phase (lag phase), in which α-syn monomers assemble into toxic oligomers. This species drives cellular toxicity by permeabilizing and disrupting cellular and mitochondrial membranes [136, 137, 138], dysregulating Ca^{2+} home-

ostasis[139], and inducing oxidative stress[140]. α-Syn aggregation results in a heterogeneous population of oligomers that leads to fibril polymorphism[141]. These oligomers can be classified according to their size into small (2-5 monomers), medium (5-15 monomers) and large (15-150 monomers)[142], or based on their shape[141]. In the latter case, there are two main types of α-syn oligomers: **spherical oligomers** less toxic and with a reduced tendency to interact with membranes; and **annular oligomers**, the highly toxic form of oligomers, able to insert in the lipid bilayers as a pore-like protein, destabilizing membrane permeability[141]. Annular oligomers also increase the Ca^{2+} influx in the cell, acting on calcium channels, activating indirectly caspase-3 and consequentially cell death[143]. α-Syn oligomers are named "critical nuclei" because their formation is the rate-limiting step of the aggregation process[144]. Due to the high interfacial energy associated with the surface area of small nuclei, their formation is energetically unfavorable. However, as they grow and reach a critical size, the intramolecular interactions make the assembly process thermodynamically possible[145, 146] and more prone to further growth. Li and colleagues reported that α-syn dimers have a self-aggregation rate 10.5-fold higher than monomers, a rate that increases 17-fold for tetramers, and 13.5-fold for octamers[147].

- The lag phase is followed by elongation with the formation of β-sheet-rich short fibrils. Because oligomers and not monomers are incorporated in the fibril elongation, it has been suggested a reconfiguration in a more ordered state upon addition[147]. The morphology transformation of α-syn intermediates during the aggregation process tracked by atomic force microscopy (AFM), revealed that oligomers are in a helix state at the beginning of the elongation[148]. Once incorporated in the fibril, there is a helix to β-sheet transition in the structure of the oligomers[149]. Further advanced spectroscopy analysis, specifically fourier transform infrared spectroscopy and nuclear magnetic resonance, clarified that not all oligomers can be incorporated into fibrils, therefore α-syn oligomers can be classified in two physical species[138], as shown in Figure 1.5 **b**. The "on-pathway type A" has a more disordered structure, it is more available in the cell and so more prone to be combined in fibrils[138, 150] (Figure 1.5 **b, type A**). the "off-pathway type B", due to its partial structural organization in α-helix and β-sheet, is mostly associated to the membrane and

not involved in the elongation process[138, 150] (Figure 1.5 **b, type B**).
During the elongation phase and the rise of mature amyloid fibers, some parallel processes occur which overall enhance the α-syn aggregation rate (reviewed at [151]). These processes are summarized as follows:

Membrane-induced α-Syn self-assembly When the N-terminus of α-syn monomers is folded in amphipathic α-helix, the protein tends to partition between the lipidic membrane and the aqueous cytosol[151]. If the protein concentration in the membrane proximity becomes critical, localized changes in pH and salt levels can trigger protein self-assembly as an alternative nucleation mechanism[152, 153].

Liquid-liquid Phase Separation The internal cytoplasmatic space is organized to facilitate essential cellular processes such as signaling, the secretory pathway, vesicular transport, and metabolic pathways. Interestingly, one of the cellular strategies for temporary storage biomolecules is to confine them in phase-separated liquid membraneless compartments (reviewed at [154]). Examples of these biomolecular condensates include P granules [155], nucleolus[156], Cajal bodies[157], Promyelocytic leukemia (PML) bodies[158], and stress granules[159]. These reservoirs are phase-separated from the surroundings but can easily exchange materials with the environment. At critical concentration and low pH, α-syn can similarly form liquid membraneless droplets[160]. The droplets increase their size rapidly through intense fusion events and undergo liquid-to-solid-like transition due to α-syn fibrillation [160].

Secondary nucleation Amyloid fibrils propagate in the elongation phase by fragmentation and secondary nucleation, as reported in Figure 1.5 **c**. The two processes depend on different factors and compete for the α-syn fibrils elongation/multiplication. Aggregation studies performed in quiescent conditions at mildly acidic pH (10 mM MES buffer pH 5.5, no shaking), which are more similar to the endosome microenvironment, demonstrated that

secondary nucleation dominates over fibrillation[161, 162]. Secondary nucleation is an autocatalytic process in which α-syn monomers are absorbed on the surface of amyloid fibrils by transient electrostatic interactions between the negative N-terminus of the monomer and the positive C-terminus of the fibril[163]. The surface of the preformed fibers works as templates for the deposited monomers that will start to assemble in oligomers. The latter will trigger a positive feedback mechanism increasing the pools of both toxic α-syn oligomers and α-syn fibrils in the cell[164] (Figure 1.5 **c**). Furthermore, the secondary aggregation requires less energy compared with the *de novo* seeding, leading to a short lag phase and a faster process[161].

Fibril fragmentation Similarly to secondary nucleation also fibril fragmentation is an autocatalytic process[164], mostly observed in experimental conditions that involved mechanical shaking as a stimulus to induce α-syn aggregation[165]. α-Syn fibrils can break into fragments of different sizes, whose ends recruit new monomers[161] or oligomers[147], acting as multiple elongations sites that increase the number of fibrils in the cell[165] (Figure 1.5, **c**).

- When monomers reach the solubility limit, the α-syn fibrils are in equilibrium with the α-syn monomeric form and the formation of new fibrils stop[161, 166]. Independently from how α-synuclein fibrils originate, once this equilibrium plateau is reached, preformed α-synuclein fibrils release oligomers, which act as seeds due to the higher proportion of fibrillar ends[167]. This process is important for the prion-like cell-to-cell propagation of α-synuclein toxicity.

  Although the factors triggering α-synuclein aggregation are unknown, once initiated, the aggregation process is irreversible and cannot be stopped[161].

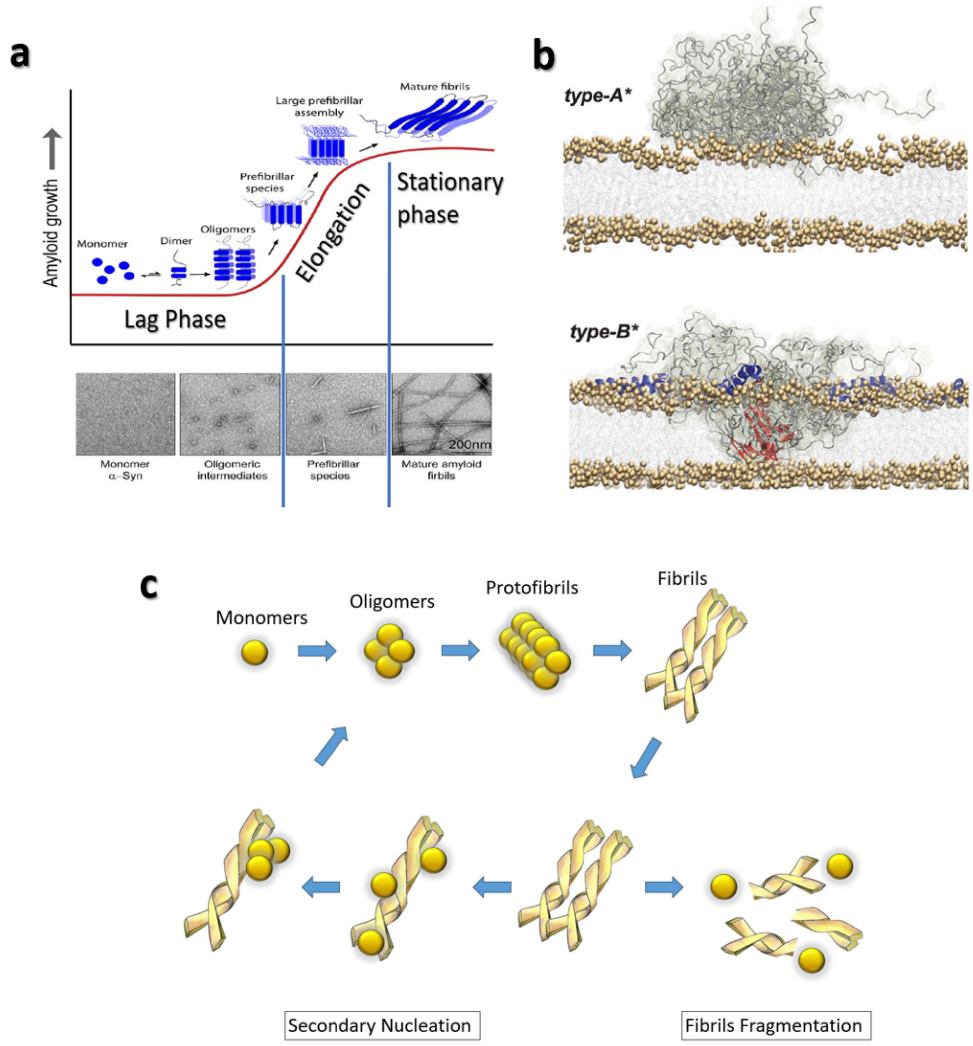

Figure 1.5: **a** Scheme of α-Syn amyloid aggregation adapted from the publication of Gadhe et al.[145]. The sigmoidal growth curve for α-Syn aggregation with lag, exponential and stationary phase and different conformational stages. On the bottom part, the transition of α-syn from monomers to fibrils. **b** Type-A α-syn oligomers are mainly disordered and bind exclusively to the membrane surface. Type-B α-syn oligomers feature both structured (red) and disordered (gray) regions and bind the surfaces of the lipid bilayers via the folding of N-terminal regions into amphipathic α-helices (blue) upon membrane binding[138]. **c** α-syn fibrils generated through the primary nucleation process can undergo secondary nucleation under quiescent and mild acidic conditions or they can elongate by fibrils fragmentation upon specific stimulus (such as mechanic sonication). Once a critical concentration of mature fibrils has formed, the surfaces of existing fibrils catalyze the nucleation of new aggregates from the monomeric state (secondary nucleation). Secondary nucleation reaction overtakes primary nucleation as the major source of new oligomers (positive feedback).

1.3.4 Prion-like propagation

Prions are unique infectious agents that lack genetic material[168, 169]. Essentially, a prion is a protein that induces neurodegeneration through the formation of cytotoxic amyloid aggregates[169]. These proteins impose their misfolded conformations to the host proteins initiating a pathological chain reaction[170]. Since the first observation that healthy neuronal cells grafted in PD patients also developed LBs[171, 172], extensive research has confirmed that α-syn can propagate in healthy cells through a prion-like mechanism[173]. In particular, α-syn aggregates can spread by neuron-to-neuron transmission via vesicular trafficking[174]. Based on this evidence, Braak and colleagues proposed a significant model in which α-syn aggregates, initially present in the lower brainstem, colonize distant brain areas, ultimately reaching the limbic and neocortical regions[175]. This model is currently used in diagnosis, to define the 6 stages of PD progression[175]. The ability of α-syn toxic aggregates to induce Parkinson's-like Lewy pathology in a prion-like infection has become an important tool in neurodegenerative disease research. For example, α-syn fibrils are injected into mouse brains to replicate PD-like phenotypes[176, 177].

1.3.5 α-Synuclein and Hypoxia

As aerobic organisms, our biological processes rely on oxygen consumption. During mitochondrial oxidative phosphorylation, oxygen (O_2) functions as the final electron acceptor, enabling the production of ATP. Considering the critical importance of this element, mammalian cells have evolved a tuned mechanism to adapt to oxygen levels. The response to hypoxia is regulated by the Hypoxia-Inducible Factor (HIF-1), a key transcription factor that activates the molecular adaptation program to ensure the maintenance of energy metabolism under low oxygen conditions. In Normoxic conditions (atmospheric oxygen level), the α-subunit of HIF-1 is hydroxylated by the proline hydroxylase-2 enzyme e and exposed to the Van Hippel-Lindau proteins (VHL). The VHL polyubiquitinates the hydroxylated α-subunit, converting it into a target for proteasome degradation. Under hypoxic conditions, the α-subunit cannot be hydroxylated and instead, it dimerizes with the β-subunit, generating the HIF-1 heterodimer. This transcription factor recognizes and binds to hypoxia-responsive elements (HREs) in the promoters of target genes, such

as erythropoietin, tyrosine hydroxylase, vascular endothelial growth factor, glycolytic enzymes and glucose transporters[178]. Neurons are high-energy-demand cells that consume 20% of the body's oxygen supply, and hypoxia can compromise their homeostasis, promoting neurodegeneration. There is, in fact, a link between aging and alteration of the hypoxia response (reviewed at [179, 180]). Breathing capacity is reduced with aging due to alteration in chemoreceptor function and decreased strength in the respiratory muscles that drive pulmonary compliance[181]. Furthermore, sleep apnea symptoms and downregulation of HIF-1[182] are common in aged individuals. Together, these factors can induce hypoxic stress that is toxic to the brain [182]. In the context of PD pathogenesis, there is an underlying connection between hypoxia and α-syn aggregation that passes by mitochondrial dysfunction. During chronic hypoxia, the isoform 2 of the HIF-1 factor (HIF-2) inhibits the α-syn phosphatase PP2A [183], which is responsible for dephosphorylating α-syn at the Ser129 residue. The missing activity of PP2A results in the accumulation of the hyperphosphorylated form of α-syn, which, among the various post-translational modifications of the protein, is more prone to aggregate [184]. At the same time, hypoxia decreases the mitochondrial membrane potential triggering the production of reactive oxygen species (ROS)[179, 185]. The combination of low oxygen and ROS deregulates cytochrome C (reviewed at [186]), an important component of the electron transport chain that, under optimal conditions, interacts with the phospholipid cardiolipin in the mitochondrial inner membrane to boost its activity[187]. During oxidative stress, cardiolipin migrates in the mitochondrial outer membrane, where it can interact with several effectors, including the hyperphosphorylated α-syn[188]. Ghio and colleagues demonstrated, through electrophysiology experiments, that α-syn oligomers can permeabilize mitochondrial membranes. In particular, they observed a more pronounced disruption when cardiolipin phospholipid was more abundant in the membrane[189].

Furthermore, the impact of oxygenation on α-syn is strongly supported by the observation that oxidation of the four Met residues (Met1, Met5, Met116 and Met126) reduces the fibrillation propensity of the protein[190].

Hypoxia Response in Yeast

Compared to mammalian cells, yeasts are facultative anaerobes organisms adapted to survive in low oxygen availability. Even in anaerobiosis, yeasts can metabolize sugar switching from respiratory to fermentative metabolism and producing CO_2 and ethanol, instead of CO_2 and water.

Aerobic Respiration Equation

$$C_6H_{12}O_6 + 6\,O_2 \longrightarrow 6\,CO_2 + 6\,H_2O + ATP \tag{1.1}$$

Anaerobic Fermentation Equation

$$C_6H_{12}O_6 \longrightarrow 2\,C_2H_5OH + 2\,CO_2 + ATP \tag{1.2}$$

The yeast hypoxia response differs from mammalian cells, as there is not a homologous of human HIF. The cellular oxygen sensors are represented by the heme biosynthetic enzymes. This process requires the coordinated activity of eight enzymes and the availability of two essential elements O_2 and Fe^{2+}[191]. In normoxia, heme activates the heme activator protein (HAP1). It remains unclear whether the activation of HAP1 in the presence of oxygen occurs through the direct binding of heme to the recognition motif on the protein[192], via heme precursors, oxygen level, or redox state by an intermediate enzyme[193]. Upon activation, the HAP1-heme complex binds to the promoter region of genes involved in cellular respiration and oxidative damage repair[194] (Enzymes listed in Table 1.2). In particular, the complex activates the aerobic repressor Rox1, which inhibits the expression of enzymes required for anaerobic growth (Hap1-heme signaling pathway in yeast reviewed in [195]). Rox1 binds the consensus sequence upstream of the heme-repressed genes and recruits the Ssn6 and Tup1 proteins[196]. The resulting repression complex recruits the histone deacetylase Hda1 that alters the chromatin structure of the TATA regions in the promoter[197]. Rox1 repressive activity requires the synergistic cooperation of a second transcription factor, Mot3. Despite the two transcription factors work differently, as Mot3 recruits just Ssn6 and not Tup1, both of them are required to achieve a complete inhibition of the hypoxic

response in the cell[198]. Under anaerobic conditions, Rox1 is not expressed, allowing heme-repressed genes to be transcribed. The cell optimizes the consumption of limited oxygen through two main strategies:

- To maintain a high reaction rate as oxygen concentration decreases, aerobic genes are replaced with anaerobic counterparts with higher oxygen consumption turnover numbers. A representative example is subunit V of the cytochrome oxidase enzyme. The Vb isoform, expressed in hypoxia, has a rearrangement in the binuclear reaction center (heme a_3 and Cu_B) that increases the enzyme turnover compared to the aerobic isoform Va[199, 200].

- To decrease oxygen-demanding processes like sterols biosynthesis, the cell prioritizes the expression of importer systems, such as the sterol importer Sut1[201].

Besides the canonical hypoxic genes, there are two groups of heme-repressed genes also involved in the hypoxia adaptation: the "DAN/TIR genes" and the "PAU family"[194, 201, 202, 203]. These genes are highly versatile and become active under specific stress conditions, such as hypoxia or cold shock, which necessitate cell wall remodeling. During hypoxia, desaturase enzymes are depleted decreasing the cellular pool of unsaturated fatty acids with consequences on the membrane and cell-wall fluidity. To compensate this situation, the cell replaces CWP1 and CWP2, the two most abundant mannoproteins responsible for cell wall stability under normal growth conditions[204, 205], with the mannoproteins: DAN1, DAN2, DAN3, DAN4, TIR1, TIR2, TIR3, TIR4, and TIP1[206]. Under aerobic conditions, these genes are inhibited by the repressor factors Mox1 and Mox2 which bind the consensus anaerobic response elements (AR1) in the promoter region. Interestingly, these genes can also be repressed by the canonical Rox1 and Mot3 assisted by the Tup1\Ssn6 repression complex[207]. In anaerobic conditions, the DAN/TIR genes are transcribed by the heme-repressed factors Mox4/Upc2 which recognize and bind as well the AR1 regions. The activation is asynchronous, DAN1, DAN4 and all the TIR genes are activated within 1 hour, while DAN2 and DAN3 are activated with 3.5 hours of delay, suggesting that cell wall remodeling follows a gradual model[208]. The later expression of DAN genes can be explained by the fact that TIR are essential for anaerobic growth compared to the DAN subgroup, indicating that the cell prioritizes their expression[206]. In hypoxia, Upc2 is also involved in the expression

of ERG genes, responsible for the biosynthesis of ergosterol[209, 210] and in the ergosterol uptake probably in synergy with SUT1, AUS1 and DAN1[211].

The Pau family includes 24 members and corresponds to one of the largest protein families in yeast. These proteins were identified during a yeast library screening and chromosome blotting against bombyxin A[212], an insect-like peptide involved in cellular aging and growing[213, 214]. All the PAU members share a high sequence homology and some common features, such as the presence of TATA box in the promoter region, the sub-telomeric localization and the low serine content which is the reason why they are also named as *seripauperins*[212]. The large number and the redundancy of these proteins make it challenging to define their biological function. Nevertheless, the partial homology with TIR proteins[212] suggests that PAU could be involved in hypoxia[215] and temperature stress response[216]. It has been proposed that the expression of these proteins in anaerobic conditions may contribute to cell growth and ergosterol uptake in low oxygen concentrations[207, 211]. Furthermore, gene expression studies on wine-making strains (*S. cerevisiae* strain A44) show upregulation of PAU genes during alcoholic fermentation, mostly due to the anaerobiosis stress[217, 218], suggesting that PAU family, as other anaerobic genes, could be regulated via heme repression[194, 195, 201].

Gene	Enzyme	Function
Induced by Heme		
CYC1	Iso-1-cytochrome c	Electron transport
CYT1	Cytochrome c_1	Electron transport
CYB2	Cytochrome b2 [L$^-$(+)-lactate cytochrome c oxireductase]	Electron transport
COR1	Subunit I of QH2:cytochrome c oxireductase	Electron transport
COR2	Subunit II of QH2:cytochrome c oxireductase	Electron transport
COX4	Subunit IV of cytochrome c oxidase	Electron transport
COX5A	Subunit Va of cytochrome c oxidase	Electron transport
COX6	Subunit VI of cytochrome c oxidase	Electron transport
CTT1	Catalase T	Oxydative damage
CTA1	Catalase A	Oxydative damage
SOD2	Manganese superoxide dismutase	Oxydative damage
HMG1	3-Hydroxy-3-methylglutaryl CoA reductase	Sterol synthesis
TIF51A	eIF5A	Translation initiation
ROX1	Heme-dependent repressor	Transcription repressor
Repressed by Heme		
COX5b	Subunit Vb of cytochrome c oxidase	Electron transport
ERG11	Cytochrome P450 (lanosterol 14α-demethylase)	Sterol synthesis
CPR1	NADPH-cytochrome P450 reductase	Sterol synthesis
HMG2	3-Hydroxy-3-methylglutaryl CoA reductase	Sterol synthesis
OLE1	Δ9 fatty acid desaturase	Fatty acid synthesis
HEM13	Coproporphyrinogen III oxidase	Heme synthesis
ANB1	eIF5A	Translation initiation

Table 1.2: This list of genes is inspired by the one reported in the publication of Zitomer and colleagues [194]. Heme promotes the expression of genes mostly involved in oxidative phosphorylation and oxidative damage repair, while repressing hypoxic genes, whose expression is not required under anaerobic conditions.

1.4 The Role of Iron Dysregulation in Parkinson's Disease

Although the etiology of PD and the factors that initiate the pathological aggregation of α-synuclein remain unclear, there is strong consensus that environmental conditions contribute to the development of PD and synucleinopathies[219]. There is, in fact, a positive correlation between neurodegeneration and industrialization that induces researchers to propose the hypothesis of "Parkinson's pandemic"[37]. Chronic exposure to synthetic compounds, such as herbicides, pesticides and metals, negatively affects neuron homeostasis. Epidemiological and population-based studies demonstrate that exposure to manganese, aluminum, lead, copper and iron induces PD[220, 221]. Furthermore, X-ray analysis and coupled plasma spectroscopy on post-mortem brain tissue of PD patients, revealed iron accumulation in Lewy bodies[222] and the basal ganglia[223]. In the substantia nigra of PD patients the ratio Fe^{2+}/Fe^{3+} shifts in favor of higher levels of Fe^{3+}, compared to healthy controls[224, 225]. In mammalian cells, ferritin is the main Fe^{3+} storage protein. Ferritin is a complex of 24 subunits arranged in a spherical shell that can incorporate 4500 iron atoms[226, 227]. In the brain, neuromelanine can also serve as iron storage, chelating Fe^{3+} and protecting neurons from the cytotoxic effect of insoluble iron[228, 229].
PD patients exhibit reduced levels of ferritin [223, 230] and iron content in neuromelanin[231], leading to an increased pool of free Fe^{3+} in the cytosol[222, 232], where it can undergo Fenton-like reactions (Eq. **R1** and **R2**) and generates harmful radical species[233].

1.4.1 α-Synuclein and Iron

There is an extensive literature on the effect of iron on α-syn aggregation with evidence both *in vivo* and *in vitro*, reviewed in [234]. It is well-established, *in vitro*, that micromolar concentrations of Fe^{3+} induce fibrillation of α-syn[235, 236] and that the fibrillation propensity increases in a dose-dependent manner[237]. This iron-induced aggregation is even more effective in mutant forms of α-syn, such as A53T and A30P[238]. Peng and colleagues were the first to measure the ES-MS spectra of α-syn-Fe^{2+} complex, finding a binding stoichiometry of 1:1[239]. Divalent ions, like iron, bind to the C-terminus of α-syn and specifically at the 121-123 residues which show more propensity to coordinate with metals[109]. The authors also estimated that α-syn-Fe^{2+}

complex has a low binding constant of 5.8 x 10^3 M^{-1}, which is reasonable given the tendency of Fe^{2+} to be oxidized to Fe^{3+}[239]. The binding constant measured for the α-syn-Fe^{3+} complex is even lower, of 1.2 x 10^{-13} M^{-1}[239]. Based on these results, the authors concluded that α-syn forms unstable complexes with iron, difficult to detect under physiological conditions[239]. Later, Davies and colleagues detected the α-syn-Fe^{3+} complex by isothermal titration calorimetry. They proposed a binding model where Fe^{3+} binds α-syn in two sites at the C-terminus with a constant of 0.70 M^{-1}[240]. The same authors proposed that α-syn works as ferrireductase, reducing Fe^{3+} in Fe^{2+}[240].

Iron binds to α-syn in both oxidation states affecting the protein's conformation depending on oxygen availability. TEM microscopy analysis has revealed that under aerobic conditions, Fe^{2+} and not Fe^{3+} promotes an antiparallel β-sheet oligomerization of α-syn, while under anaerobic conditions, both oxidation states lead to parallel β sheet[241]. Furthermore, the identification of an ire-like stem-loop at the 5'-UTR of the α-syn transcript, suggests that iron can modulate α-syn toxicity not necessarily by direct interaction, but at the transcriptional level through iron-responsive element-binding proteins (IRP1 and IRP2)[242, 243].

In vivo, Straumann and colleagues recently mapped α-syn aggregates and iron deposition in both the striatum and cortex of transgenic mice carrying the A53T mutation using a noninvasive imagining technique[244]. Their study provides direct evidence of iron-induced enhancement of α-syn toxicity in animal PD models. This evidence was demonstrated as well in Drosophila melanogaster[245] and SH-SY5Y cells[246].

All the above arguments inferred a fatal interaction between iron and α-syn, where iron contributes to α-syn aggregation either through direct binding or indirectly via oxidative stress and transcriptional regulation. On the other side, α-syn with its ferrireductase activity effects iron homeostasis.

The Molecular Mechanisms of Iron Toxicity

Iron is an essential element in living systems responsible for oxygen transportation, cell respiration, and DNA synthesis[247]. It coexists in two different oxidation states:

- **Ferrous iron Fe^{2+}** is the soluble and absorbable form of iron. It is less available at physi-

ological conditions because it is easily oxidized to Fe^{3+} by atmospheric O_2. Fe^{2+} is a soft Lewis acid that reacts with soft bases such as sulfur and nitrogen[248].

- **Ferric iron Fe^{3+}** is the insoluble and most abundant form of iron. It is the preferred oxidation state for iron storage in living systems. Fe^{3+} is a strong Lewis acid that prefers strong bases and it is generally found in combination with oxygen[248].

Living systems have evolved to stabilize iron within porphyrin complexes, exploiting the redox potential of the couple Fe^{2+}/Fe^{3+} in biochemical reactions. To give some examples, hemoglobin uses iron to fix and transport oxygen; peroxidases require iron to detoxify H_2O_2 in H_2O; iron is essential in the reduction of ribonucleotides and dinitrogen[249]; and iron-sulfur clusters facilitate electron transfer between the components of the electron transport chain[250].

In aqueous solutions, Fe^{2+} reduces hydrogen peroxide to form hydroxyl radicals and hydroxide, while being oxidized in Fe^{3+} (Eq. **R1**). This reaction also occurs when Fe^{2+} is bound to a ligand (Eq. **R2**) or in the presence of other transition metals[251]. Similarly, Fe^{3+} reacts with hydrogen peroxide generating hydroperoxyl radical (Eq. **R3**), which then reduces a new Fe^{3+} ion in Fe^{2+} (Eq. **R4**).

Fe^{2+} Fenton reactions

$$Fe^{2+} + H_2O_2 \longrightarrow Fe^{3+} + {}^{\bullet}OH + OH^- \quad \text{(R1)}$$

$$Fe^{2+}\text{–}L + H_2O_2 \longrightarrow Fe^{3+}\text{–}L + {}^{\bullet}OH + OH^- \quad \text{(R2)}$$

Fe^{3+} Fenton reactions

$$Fe^{3+} + H_2O_2 \longrightarrow Fe^{2+} + {}^{\bullet}OOH + H^+ \quad \text{(R3)}$$

$$Fe^{3+} + {}^{\bullet}OOH \longrightarrow Fe^{2+} + O_2 + H^+ \quad \text{(R4)}$$

Iron and other transition metals can react as well with lipid peroxides (ROOH) in Fenton-like reactions generating lipid alkoxy radicals (Eq. **R5 and R6**)[251].

Lipids Fenton reactions

$$Fe^{2+} + ROOH \longrightarrow Fe^{3+} + {}^{\bullet}OR + OH^{-} \tag{R5}$$

$$Fe^{2+}\text{–}L + ROOH \longrightarrow Fe^{3+}\text{–}L + {}^{\bullet}OR + OH^{-} \tag{R6}$$

$$\tag{R7}$$

Iron-dependent phospholipid peroxidation, along with the inactivation of the glutathione peroxidase enzyme GPX4, induces a specific form of cell death known as *ferroptosis*[252], reviewed in [253, 254]. Unlike apoptosis, ferroptosis is mostly a sabotage process in which the essential cellular functions are disrupted[254]. In the cell, GPX4 plays a protective role against ferroptosis, detoxifying phospholipid and cholesterol hydroperoxides to their corresponding alcohols, using glutathione (GSH) as a cofactor[255]. When GPX4 is inactivated, the cell tries to overcome the membrane disruption, induced by ferroptosis, increasing the cytosolic concentration of Ca^{2+}. In NIH-3T3 cells treated with the ferroptosis inducer Erastin-1, an increase in Ca^{2+} anticipates the cell transition to a rounded shape with a single swelling bleb[256]. Subsequently, small pores open in the membrane and water starts to influx inside due to the intracellular osmotic pressure[257]. In this critical state, Ca^{2+} plays an important role because it activates the membrane repair system ESCRT-III[258]. Under intense ferroptosis-inducing conditions, GPX4 and ESCRT-III can delay, but not prevent cell death, due to the excessive and irreversible membrane damages[257]. Furthermore, Fe^{2+} can directly induce ferroptosis through the activation of 15-LOX, a member of the LOXs dioxygenases family[253, 254, 259] responsible for polyunsaturated fatty acids (PUFAs) peroxidation. In particular, 15-LOX requires Fe^{2+} as a cofactor to convert arachidonoyl- and adrenoyl- phosphatidylethanolamine in free radicals that initiate a disruptive lipid radical chain reaction in the membrane[260].

Brain iron metabolism

Iron circulating in the bloodstream crosses the blood-brain barrier and reaches the brain's microvascular system, where it is captured by the plasma glycoprotein transferrin (Figure 1.6). This

proteins binds two Fe^{3+} ions, assuming the holo-conformation. Iron-laden transferrin is recognized by transferrin receptors (TfR1) on the apical surface of the brain's microvascular epithelial cells (Figure 1.6). The resulting Tf-TfR1 complex is internalized through endocytosis. The acidic pH of the endosome (approximately 5.5) induces the dissociation of the Tf-TfR1 complex, facilitating the release of Fe^{3+}. The receptors are recycled back to the cell membrane, and the acidic environment reduces Fe^{3+} in Fe^{2+} (Figure 1.6).

Endosomal Fe^{2+} released by the Tf-TfR1 complex is transported in the cytoplasm by the divalent metal transporter 1 (DMT1), the principal mammalian Fe^{2+} transporter responsible for iron uptake[261] (Figure 1.6). Once in the cytoplasm, Fe^{2+} can be utilized in various biochemical processes, stored as Fe^{3+} in the ferritin enzyme, or exported from the cell via the basal transporter Ferroportin 1 (FPN1) (Figure 1.6). Astrocytes modulate the activity of this transporter to maintain neuronal iron homeostasis. When iron exceeds critical concentrations, astrocytes secrete hepcidin, a key hormone in iron metabolism that negatively regulates FPN1, promoting iron storage. Hepcidin binds to FPN1 when the receptor is occupied by Fe^{2+} triggering its degradation through the ubiquitin-proteasome pathway[262]. During iron starvation, astrocytes express GPI-ceruloplasmin (Cp) which enhance the activity of FPN1, oxidizing the Fe^{2+} translocated in the transporter in Fe^{3+} that is acquired by the Tf released from oligodendrocytes or by the trivalent cation-specific transporter 1 (TCT1) expressed on the membrane of neurons[263, 264] (Figure 1.6).

Neurons acquire Fe^{2+} and Fe^{3+} from extracellular space through TfR1, DMT1 and TCT1 and release iron through FPN1 modulated by Cp and Hepcidin, reviewed in [114] (Figure 1.6). α-Syn impairs the iron homeostasis of dopaminergic neurons, increasing the expression of DMT1 transporter[265]. SH-SY5Y cells transfected with wild-type and A53T mutated form of α-syn show a higher level of DMT1, but low expression of TfR1 and FPN1 compared to the untransfected cells[265]. The expression of DMT1 is regulated at the transcription level by the iron response protein (IRP) and upregulation of this transporter contributes to iron deposition in the substantial nigra of PD models and PD patients[266]. α-Syn prevents the degradation of DMT1 enzyme,

inhibiting the E3 ubiquitin-ligase (parkin) by phosphorylation at the Ser131 residue[265].

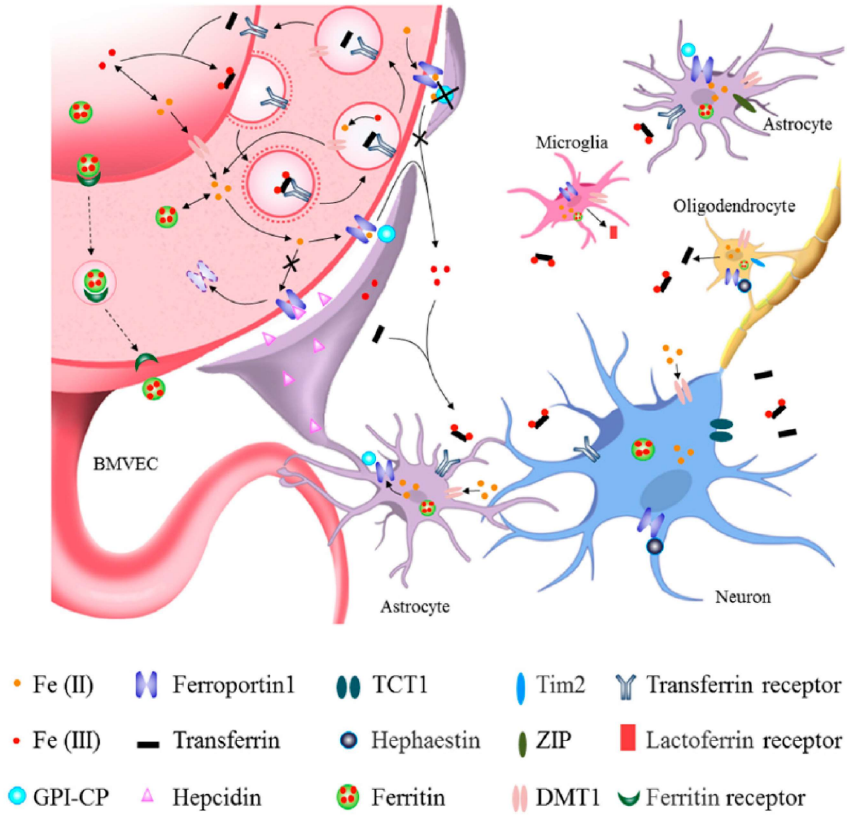

Figure 1.6: This figure is reported in the article of Gao and colleagues [114] and illustrates the main iron uptake systems present in the brain to acquire this important element from the blood vessels, which supply the brain. Iron accesses the brain interstitial compartment mostly through indirect mechanisms. In particular, it can be internalized through ferritin transcytosis across the BBB. Iron translocation can also be mediated by FPN1 and Tf-TfR1 receptors expressed on the surface of the brain microvascular epithelial cells. Moreover, astrocytes can collect iron through their extensive ramifications along the BBB and transfer to neurons. Astrocytes and oligodendrocytes coordinate iron acquisition based on its availability within the brain parenchyma.

Iron metabolism in Yeast

Yeast served as a model organism for elucidating the iron metabolism in higher-evolved eukaryotes. In yeast, the genes responsible for iron uptake are under the control of three transcription factors: Aft1, Aft2 and Yap5[267, 268, 269], whose activity seems to be coordinated by the mitochondrial

Fe-S cluster biogenesis pathway[270, 271].

Aft1/Aft2 mediate iron deficiency response.

When the iron concentrations drop in the $1\pm10\mu$M range[272], the transcription factor Aft1 translocates from the cytoplasm inside the nucleus shuttled by the PSE1 chaperone[273]. In the nucleus, Aft1/Aft2 binds to consensus sequences PyPuCACCC (Py is a pyrimidine and Pu is a purine) known as iron regulatory promoter elements (FeREs) in the upstream regions of target genes that encode for cellular iron importers[268, 269] (Figure 1.7). Despite being classified as iron-dependent transcription factors, Aft1 and Aft2 do not directly sense the iron level in the cell. Instead, this information is communicated by the monothiol glutaredoxins Grx3 and Grx4, iron-sulfur (Fe–S) cluster-binding proteins that can assemble into homodimers bridged by a [2Fe-2S] cluster[274] (Figure 1.7). The two proteins regulate the iron uptake by Aft1 inactivation[275]. In fact, studies on Δgrx3Δgrx4 strains indicate that Aft1 is constitutively active in the absence of Grx3 and Grx4[275].

In iron-optimum conditions, the cytosolic iron-sulfur cluster assembly and the iron-sulfur cluster systems synthesize [2Fe-2S] clusters in the cytoplasm and mitochondria, respectively. Mitochondrial [2Fe-2S] clusters are exported through Atm5 and once in the cytoplasm, they are transferred to Grx3 and Grx4 that assembly in a heterodimer[276]. The Grx3/Grx4 complex bind Aft1, promoting the export of this transcription factor from the nucleus to the cytoplasm[275]. A third protein, Fra2, also participates in this process facilitating the transfer of the [2Fe-2S] cluster from Grx3/Grx4 to Aft1/Aft2, which leads to their dimerization and subsequent detachment from promoter regions[276, 277]. The Aft dimer is then exported in the cytoplasm via the nuclear exportine Msn5[276].

During iron deficiency, the synthesis of iron-sulfur clusters becomes inefficient, preventing Aft1/Aft2 dimerization. The two transcription factors are retained in the nucleus, where they activate the "Iron Regulon" (reviewed in [269, 278]). When Aft1 is inhibited or it cannot translocate in the nucleus, its paralogue, Aft2, transcribes part of the genes targeted by Aft1[279]. Aft2 shared 39%

of homology with Aft1 and deletion of Aft2 in a ΔAft1 background makes the double knockout unable to grow in iron-depleted conditions and more sensitive to oxidative stress[280]. It has been shown that vacuolar and mitochondrial iron transporters, such as Smf3 and Mrs4 are specifically activated by Aft2 and not Aft1, highlighting the importance of Aft2 in enhancing the cellular response to iron starvation[280]. The genes activated by Aft1/Aft2 during iron deficiency include:

- **High-affinity iron uptake system.** On the cell surface, the ferric reductases Fre (1-4) reduce extracellular Fe^{3+} to Fe^{2+}[281], which is then reoxidized back to Fe^{3+} by the multicopper oxidase Fet3, homologous to the human ceruloplasmin. The Fe^{3+} is transported into the cell by the six-transmembrane permease Ftr1 directly in contact with Fet3 (Figure 1.7).

- **Low-affinity iron uptake system.** During hypoxia, the high-affinity iron uptake system is depleted, and the cell acquires iron through Fet4, a surface-divalent metal transporter specific for different metal ions, including Fe^{2+} and the toxic cadmium[282] (Figure 1.7).

- **Non-reductive iron import machinery** For yeast cells iron acquisition begins at the cell wall, where the mannoproteins FIT1, FIT2 and FIT3 promote the uptake of the metal and siderophores, specialized iron-chelators released by bacteria and microorganisms[283]. *S. cerevisiae* does not synthesize siderophores, but as an opportunistic living organism, it imports the ones released by neighboring microbes[284, 285]. Siderophores chelate Fe^{3+} and are internalized via endocytosis mediated by specific receptors (Arn 1-4) located in the membrane. The acidic pH of the late endosome promotes the release of iron cargo from the siderophore that is then digested by vacuole[284, 286]. In yeast, Arn proteins function similarly to the mammalian transferrin receptors[284] (Figure 1.7).

- **Vacuole transporters** In yeast, the vacuole plays an important role in maintaining physiological concentrations of divalent cations. It works as primary iron storage site in the cell, which lacks human ferritin homologs[287]. The vacuole has just one iron importer, Ccc1[288], which allows iron storage in the organelle when the cytosolic level of the metal becomes high. When the cellular iron pool is insufficient, the vacuole releases iron through a system similar to the high-affinity iron uptake. Fre6 reduces Fe^{3+} to Fe^{2+}, which is then

reoxidised to Fe^{3+} by Fet5 (a homolog of Fet3) and released in the cytosol by the Fth1 transporter. There is also a second iron export system represented by Smf3, a divalent metal ion transporter, which releases the Fe^{2+} generated by Fre6 in the cytosol[289] (Figure 1.7).

- **Mitochondria transporters** Similarly to the vacuole, mitochondria can also act as iron storage organelles in critical situations to protect the cell from iron toxicity[290]. Furthermore, mitochondria are the site of Fe-S cluster synthesis, which regulates the activation of the transcription factors Aft1/Aft2 and Yap5, involved in iron metabolism[291]. Mitochondria have two Fe^{2+} high-affinity iron importers, Mrs3 and Mrs4[292, 293] and two iron exporters Mmt1 and Mmt2[294, 295, 296] (Figure 1.7).

- **Alternative non-iron transporters** BIO genes are involved in biotin biosynthesis and, in particular, Bio2 is also involved in the last step of the Fe-S cluster assembly in the mitochondria[292]. Since biotin synthesis is an iron-demanding process, the transcription of BIO genes is downregulated under iron-deficient conditions, while biotin transporters Vht1 and BIO5 are upregulated[297, 298] (Figure 1.7).

- **Cth1 and Cth2 mRNA binding proteins**. Cth1 and Cth2 are two mRNA-binding proteins specialized in the downregulation of enzymes involved in iron-dependent processes[285, 299, 300]. They bind the target mRNAs, recruiting the helicase Dhh1 which promotes deadenylation and mRNA decay[301]. Cth1 reduces the expression of the complexes of the electron transport chain [302]. Cth2 predominantly targets enzymes of the TCA cycle, lipid metabolism, heme synthesis, amino acid biosynthesis, and the Ccc1 importer[299, 302]. Cth1 supports the cell during transient iron starvation phases, whereas Cth2 induces a metabolic shift and cellular remodeling to survive prolonged iron deficiency[302] (Figure 1.7).

.

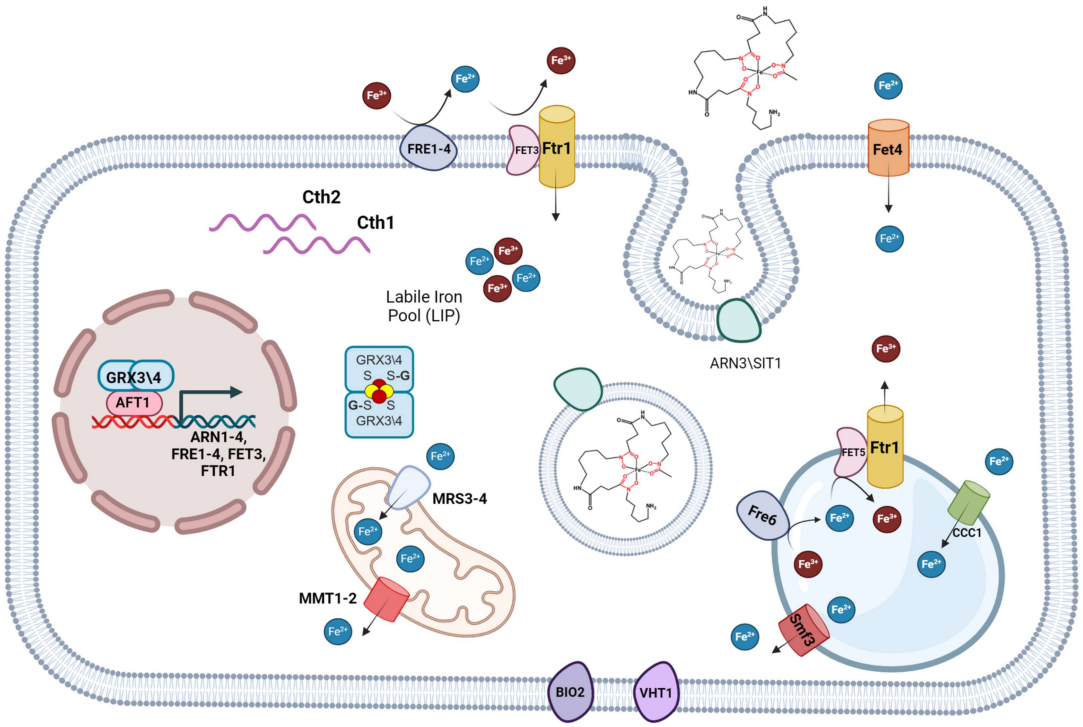

Figure 1.7: Schematic representation of the *S. cerevisiae* iron metabolism based on the article of Alonso and colleagues [278]. In response to iron deficiency, the transcription factors Aft1 and Aft2 activate the "Iron Regulon", transcribing genes involved in the uptake of extracellular iron, mobilization and recycling of intracellular iron. The cell replaces the iron-consuming processes with less iron-dependent alternatives. While the mRNA-binding proteins Cth1 and Cth2 mediate a metabolic remodeling response necessary during prolonged iron starvation.

Yap5 mediates iron overload response.

Yap 5 is a member of the Yap transcription factors (reviewed in [303]), a group of eight enzymes (Yap1-8) involved in the cellular response to various environmental stresses[304]. Yap5 is located in the nucleus, already bound to its consensus sequences through weak interactions[305]. When the cell is exposed to high iron concentrations, there is an overproduction of [2Fe-2S] clusters, which can easily translocate inside the nucleus. The binding of [2Fe-2S] cluster to the C-terminus of Yap5 induces a conformational change that tightens Yap5 to DNA, activating the genes transcription[306]. Yap5 has been identified as the transcription factor for the vacuolar iron importer Ccc1[288]. However, gene expression analysis in yeast cells cultured under iron overload conditions revealed that Yap5 also modulates the expression of Grx4, Tyw1, and Cup1[307, 308].

Grx4 is a glutaredoxin that together with Grx3 promotes the inactivation of Aft1 and its nuclear export[309]. Tyw1 encodes a [4Fe-4S]-containing enzyme, involved in the tRNA biosynthesis and that also works as a cytosolic iron scavenger, protecting the cell from toxic iron accumulation[307]. Cup1 is a metallothioprotein that can bind Cu^{+}in stable complexes[310]. Increasing the expression of Cup1 limits the Cu^{+} availability, and, consequently, inactivates the iron importer Fet3[311].

1.5 The importance of lipid metabolism in α-syn toxicity

Since the observation that lipids/vesicles influence α-syn aggregation kinetics *in vitro*[312, 313, 314] intense research focused on elucidating the nature and the pathological relevance of the α-syn affinity for phospholipid bilayers[315]. When projected onto a helical wheel the seven 11-amino-acid imperfect repeats arrange in a helix distribution[316]. Because this arrangement is characteristic of lipoproteins[317], the ability of α-syn to bind membranes phospholipids was investigated [95]. In the human brain, phosphatidylcholine (PC), phosphatidylethanolamine (PE) and phosphatidylserine (PS) account for approximately 35–40%, 35–40%, and 20% of the total phospholipids, respectively[318]. Phosphatidylinositol (PI) is just 10% of the total and it is relatively abundant compared to other tissues[319]. Davidson and colleagues demonstrated that α-syn selectively binds vesicles composed of PE, phosphatidic acid (PA) and PI[95]. This interaction induces the N-terminus of α-syn to fold in a more organized α-helix conformation[95]. These findings were also confirmed for the mutated forms of α-syn[320]. In particular, the A53T and E46K α-syn mutations increase the stability of the helical conformation, resulting in higher affinity for membranes, while the A30P has less affinity for membranes binding[320]. The studies of Lee and colleagues revealed that the interaction between α-syn and cellular membranes is initially electrostatic and involves the negatively charged acidic groups of phospholipids and the positively charged lysine residues of the protein[321]. The interaction is subsequentially stabilized by hydrophobic forces between the amphipathic helix of α-syn and the internal acyl chains of phospholipids[321]. This shift could induce as well a conformational change in the part of the protein embedded in the phospholipid bilayer, which can assume the β-sheet structure, as described by Fusco and colleagues for the type B α-syn oligomers[138, 315]. According to Lee and colleagues,

the membrane-bound fraction of α-syn works as "seeds" in the aggregation process, recruiting free α-syn, while the cytosolic fraction of the protein remains in monomeric and oligomeric forms[321]. The interaction of α-syn with the membrane is crucial for its role in assisting neurotransmission and synaptic plasticity. However, this interaction can also be harmful to the cell, as it represents the α-syn aggregation site.

1.5.1 The influence of phosphatidylinositol on α-syn aggregation

Recently, there has been significant interest in the role of PI in the pathological aggregation of α-syn. Although phosphoinositides represent just a small percentage of the cytoplasmic leaflet of all cellular membranes, they are an important signaling scaffold and proteins-recruitment platform[322]. For instance, the Akt signaling pathway, which promotes cell survival in response to extracellular signals, is activated by the phosphatidylinositide 3-kinase (PI3K), which phosphorylates PIP2 (phosphatidylinositol 4,5-bisphosphate) into PIP3[323, 324, 325]. The versatility of phosphoinositides is associated with the reversibility of their negative charge that can shift from -2 (Phosphatidylinositol, PIP) up to -5 (Phosphatidylinositol-3-phosphate, PIP3), based on the number of phosphate groups bound to the inositol head-group[326]. A recent transcriptome-wide association study links Synaptojanin 1 (SYNJ1) to SNCA[327]. SYNJ1 is the main brain lipid phosphatase responsible for the dephosphorylation of phosphoinositide. Accumulation of PIP3 in *C. elegans* and mouse PD model knock-out for SYNJ1 induces α-syn aggregation[328, 329]. Furthermore, in a recent publication, Yu and colleagues used a machine-learning approach to analyze genomic, transcriptomic, and epigenomic data from brain tissues and dopaminergic neurons, identifying candidate genes and novel pathways associated with Parkinson's disease[330]. Based on their results, four genes (IP6K2, PPIP5K2, ITPKB and INPP5F) involved in the inositol phosphate biosynthetic pathway are associated with the disease[330].

It has been reported that *in vitro*, α-syn binds to PIP2 vesicles[331], but the nature of this interaction was better investigated by Jacob and colleagues. The electrostatic attraction between the negatively charged inositol and the positively charged lysine residues at the N-terminus of α-syn promotes the protein's recruitment to the membrane, inducing the reorganization into the α-helix

structure[332]. However, because the negative charge is a phosphate group contribution, the strength of this interaction can be modulated by kinases, phosphatases and lipases activity[332]. The authors also showed that α-syn colocalized with PIP2 and PIP3 at the plasma membrane[332].

Horvath and colleagues found the molecular mechanism behind the interaction between α-syn and phosphoinositide[333]. Overexpression of α-syn monomer specifically increases the level of PI(4,5)P_2 in the membrane of hippocampal and substantial nigra neurons, but not in cortical ones. To understand how α-syn alters membrane composition, the authors analyzed the activity of PIP5K1γ, the major isoform of PI(4)P 5-kinase in the brain, which converts PI(4)P to PI(4,5)P_2[334]. PIP5K1γ is cytosolic and migrates in the membrane where it performs its function. In cells that express the A53T α-syn mutant or treated with α-syn fibrils, this enzyme predominantly localizes at the membrane due to the higher expression level of Arf6[333], the GTPase required for PIP5K1γ membrane recruitment[335]. The hyperactivation of PIP5K1γ results in elevated levels of PI(4,5)P_2, which works as a molecular scaffold for α-syn, initiating its aggregation[321]. Moreover, PI(4,5)P_2 is hydrolyzed into the corresponding diacylglycerol and inositol trisphosphate by phospholipase C[336]. Elevated levels of inositol trisphosphate contribute to cellular toxicity by promoting the release of Ca^{2+} from the ER[337].

1.5.2 Brain lipid metabolism

In the human body, the brain is second only to adipose tissue in terms of lipid content, with lipids comprising 50% of its dry weight[338]. Unlike other tissues, where fatty acids (FAs) are stored as triglycerides for energy reserves, in the brain, these biomoleculeS predominantly serve as structural components [338]. The brain requires long-chain polyunsaturated fatty acids (PUFAs), in particular arachidonic acid, eicosapentaenoic acid, and docosahexaenoic acid. Most of the PUFAs are synthesized by fatty acid synthetase and only about 8% are obtained through systemic circulation[339]. Compared to cholesterol which has to be synthesized *de novo* inside the brain, FAs can cross the blood-brain barrier[340, 341]. Astrocytes provide neurons and oligodendrocytes with lipids, cholesterol, diacylglycerol and triacylglycerol required for myelination[342] and to support their synaptic functions[343, 344] (Figure 1.8 **a**). FAs not involved in the synthesis of lipids

are stored in lipid droplets and subsequently metabolized through β-oxydation, which is not the preferential metabolic process in the brain due to the oxidative stress that it induces in the cell[345].

Lipid biosynthesis is a highly organized and compartmentalized process, occurring in specific cellular locations to ensure efficiency and regulation. The main component of the myelin layer, galactosylceramide is synthesized in the lumen of the ER starting from ceramide[346]. In the Golgi, galactosylceramides are converted into gangliosides, cerebrosides, sulfatides, and sphingomyelins. Phospholipids, triglycerides[347] and cholesterol[348] synthesis occurs as well in the ER. Another important site for lipid metabolism are the mitochondrial-associated membranes (MAMs), reviewed in [349, 350, 351] (Figure 1.8, **b**). MAM is a region of 10-80 nm in which the ER and mitochondria are in close contact and can exchange signals and biomolecules[352]. This space contains around 1052 proteins[353] involved in calcium signaling[354], autophagy[355], lipid metabolism[352], and many other biological processes reviewed in[356, 357]. Many enzymes involved in phospholipid biosynthesis reside in the MAMs such as sterol O-acyltransferase[358], phosphatidylserine synthase-1 (PSS1) and 2 (PSS2)[359], diacylglycerol acyltransferase[360], and enzymes involved in biosynthesis of glycosylphosphatidylinositol anchors[361]. Given the critical role of the biological processes occurring within MAMs, these specialized cellular domains are frequently implicated in pathological conditions, particularly neurodegenerative diseases.

1.5.3 α-syn dysregulates membrane contact sites

Molecular trafficking at the MAMs is dysregulated in Parkinson[364] and, in particular, it has been recently reported that α-syn alters the Ca^{2+} signaling[364] and *de novo* synthesis of PS[365].

De novo synthesis of phosphatidylserine at the MAMs

PS is the most abundant acidic phospholipid in the human brain and an important component of the myelin layer[318]. It is synthesized by PSS1 and PSS2, both located at the MAMs[359]. PSS1 exchanges choline of PC for serine, while PSS2 exchanges ethanolamine of PE with serine[359]. A small fraction of the PS synthesized by the two systems is transported from the ER to the plasma membrane. Most of the PS is initially transported to the mitochondria outer membrane through

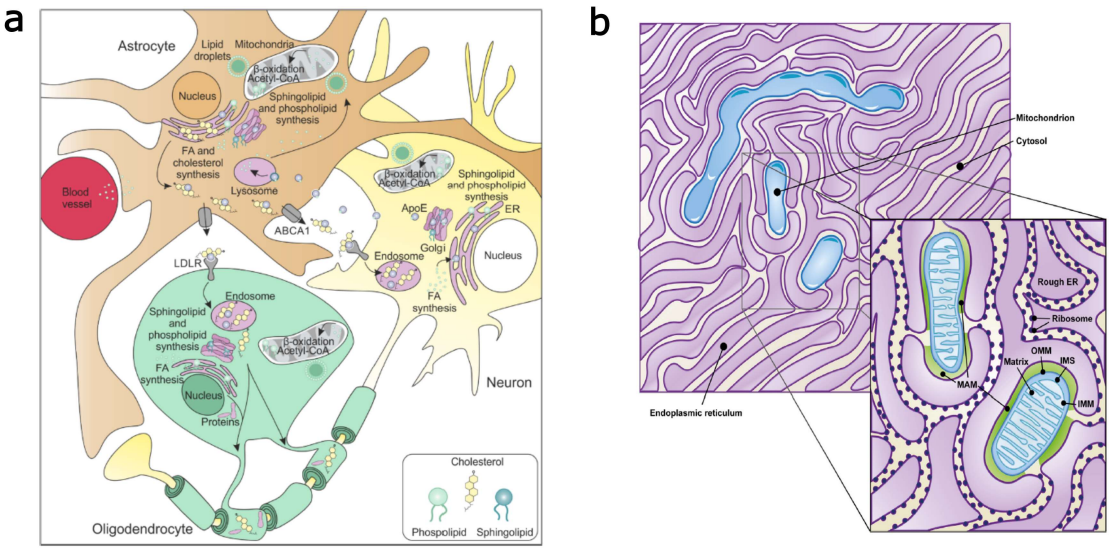

Figure 1.8: **a** In the brain most of the *de novo* synthesis of cholesterol occurs in the astrocytes which are the main supplier of this important membrane component. Cholesterol is then transported to oligodendrocyte and neurons via ApoE and ABCA1. FAs are synthesized by all the glial cells and they can be stored in lipids droplet or used as a fuel source in β-oxidation (This figure was reported in the article of Battis and colleagues [362]). **b** This figure, shown in the article by Morciano and colleagues [363], is based on the TEM imaging of the MAM compartment. This highly specialized cellular domain is generated at the interface of the ER and mitochondria.

the ER-mitochondria encounter structure (ERMES) and subsequently to the inner membrane, where PS is converted in PE by the PS decarboxylase 1 and 2 in a Ca^{2+}-dependent manner[366]. When the PE content in the mitochondria reaches a certain level, it is translocated back to the ER through ERMES where it can be converted again in PS by the PSS2[367]. The trafficking of PS at the MAMs is crucial for maintaining the correct lipid composition of both the plasma and mitochondrial membranes. Recent studies have indicated that in the context of PD and synucleinopathies, the efficiency of this system is compromised by α-syn aggregation[365]. Evidence of lipid alterations in PD patients was recently reported by Barbuti and colleagues[365]. Lipidomic profiling of postmortem PD brains revealed that SN is the most affected area, showing increased levels of cholesterol esters and reduced ceramides[365]. In particular, an increased level of PS and PE bound to long-chain unsaturated fatty acids was measured in SN and in the MAM fraction of iPSC-derived neurons able to express different levels of α-syn[365]. The authors suggested that the lipid alterations induced by α-syn impact cellular membranes and the MAMs. Since MAMs

are transient lipid rafts formed by the clustering of specific lipids, changes in their composition could affect the recruitment of resident enzymes[368, 369]. From this viewpoint, the presence of enzymes, such as phosphatidylserine synthases (PSS1 and PSS2) or long-chain fatty acid-CoA ligases, might be reduced, explaining the changes observed in the lipidomics profile.

Ca^{2+} signaling at the MAMs

Important cellular processes such as oxidative phosphorylation, ROS generation and apoptosis require Ca^{2+}. Mitochondrial Ca^{2+} homeostasis depends on the ion trafficking at the MAMs, ensured by several dynamic contact sites that overall generate a "Ca^{2+} communication currency" between the two organelles[370]. In the MAMs there are three main systems for Ca^{2+} exchange, reviewed at[356, 370]. All of them are altered by the accumulation of α-syn aggregates[371].

- The three isoforms of inositol 1,4,5-trisphosphate receptors IP3Rs on the ER membrane are in contact with the voltage-dependent anion channel 1 (VDAC1) on the mitochondrial outer membrane[372]. This interaction is bridged by the molecular chaperone glucose-regulated protein 75[373]. Through this system, mitochondria can access the Ca^{2+} reserves stored in the ER and release them only upon IP3 stimulus. In section 1.5.1 of this chapter, it was already discussed how α-syn activates IP3 inducing Ca^{2+} release from the ER. Furthermore, some publications report that VDAC1 is used by α-syn to translocate inside the mitocondria[374, 375] leading to alteration of internal processes and change to a round shape morphology.

- The interaction between the ER-resident Vesicle-associated membrane protein-associated protein B (VAPB) and the mitochondrial protein tyrosine phosphatase interacting protein 51 modulates the Ca^{2+} exchange between ER and mitochondria in the MAMs[376]. α-Syn binds to VAPB preventing the Ca^{2+} influx in the mitochondria[377], imparing important processes such as ATP synthesis and TCA cycle[377].

- When unfolded proteins accumulate in the ER, Ca^{2+} is required to support the function of chaperon enzymes. In this particular stress situation, thioredoxin transmembrane proteins, which participate in protein folding, localize in the MAMs and physically interact with the

ER calcium pump SERCA2, to transfer Ca^{2+} from the cytoplasm to the ER[378]. It has been demonstrated that α-syn aggregates interact with SERCA2 inducing an aberrant influx of Ca^{2+} in the ER[379].

1.6 Baker's yeast as a research model

Saccharomyces cerevisiae is the pioneer model organism that helped scientists to develop the current knowledge on the cellular processes and the pathogenesis of many diseases[380]. Before its advance in scientific research, yeast had a longstanding role in human culture for its unique ability to ferment alcohol and CO_2 from cereal-derived sugars[381]. Yeast is an unicellular organism with a diameter of approximately 10 μm. It possesses the typical ultrastructural features of eukaryotic cells, including a nucleus and membrane-bound organelles. The cell is isolated from the external environment by a rigid cell-wall structure 100-200 nm thick mostly composed of β-glucans and chitin. Between the cell wall and the phospholipid bilayer of the plasma membrane lies the periplasmic space, which is 35-45 Å wide. Complex sugars, like sucrose and melibiose that cannot cross the membrane, are hydrolyzed by the enzymes of periplasmic space into more permeable monosaccharides. Yeasts preferentially metabolize sugars but they can also use alternative carbon sources such as amino and organic acids, polyols, alcohols and fatty acids. Given this versatility yeast can be easily cultured in the laboratory using not expensive media. Furthermore, *S. cerevisiae* grows rapidly at 30°C in rich medium, with a doubling time of 90 minutes through an asymmetric division called budding [382]. During this process, a daughter cell (bud) outgrows from a specific site on the surface of the mother cell until it acquires a copy of the genetic content, then it detaches as a functional independent cell.

The use of yeast as a model organism became feasible when in 1978 the first successful yeast transformation with a bacteria plasmid was established and described[383]. Subsequently, two main publications described how endogenous DNA can be integrated into the yeast genome by Homology Recombination (HR)[384, 385]. HR is the error-free DNA break repair mechanism and together with the error-prone nonhomologous end joining (NHEJ) they represent the two

universal pathways for DNA break repair. In yeast, HR is the preferred DNA repair system and it has higher efficiency as it requires short homology fragments (30-50bp) and proteins that regulate and coordinate the process are constitutively expressed in the cell[386, 387, 388]. The use of HR as a tool for genome modification in combination with the development of polymerase chain reaction (PCR) drove scientists to design different strategies to study their genes of interest in a simple and comprehensive model organism like yeast.

Among the techniques developed to manipulate the yeast genome, the single-step PCR-based deletion is often used to generate gene deletions in yeast. This method requires the PCR assembling of a "deletion cassette", which includes a drug-selectable marker flanked on both the 3' and 5' ends by approximately 30-50 base pairs of homology with the target gene[389, 390]. The cassette is introduced in the yeast cell by transformation[391] and it is integrated into the genome through HR. Yeast cells that successfully integrate the cassette and replace the targeted gene with the marker are screened in the presence of a specific antibiotic. The generation of knock-out strains is quite useful for investigating the phenotypic consequences of specific gene deletion and the single-step PCR-based deletion was used to generate the yeast deletion mutant collection (`http://chemogenomics.pharmacy.ubc.ca/hiplab/GGCN_Lab/SGDP/group/yeast_deletion_project/deletions3.html`). The 20,000 knockout strains present in the collection correspond to deletions of each of 5,916 genes (including 1,159 not essential genes) and were generated using the kanamycin-resistance gene (KanMX4) flanked at the 5' and 3' ends by a 20bp unique barcode (UPTAG and the DOWNTAG), plus the homology regions[392, 393].

In yeast, gene deletion can be also performed using the auxotrophic nutritional markers: HIS3, TRP1, URA3, ADE2, LEU2 (reviewed in [394]). Following the biological advances in using yeast as a model organism, several auxotrophic strains have been generated[395] by mutating or deleting key genes involved in the synthesis of essential amino acids and nucleobases. As a result, auxotrophic strains can only grow when the missing nutrient is provided in the growth medium. By taking advantage of the genetic background of auxotrophic yeast strains, a gene of interest can be knocked out and replaced with the functional version of the gene responsible for the aux-

otrophy[396]. This genomic editing strategy is called auxotrophic complementation and can also be used for the stable expression of foreign genes. In this case, the gene of interest is first cloned in an expression vector that has in its backbone the correct version of the auxotrophy marker mutated or deleted in the host. The plasmid is linearized with a specific restriction enzyme to achieve the stable integration of the exogenous construct in the yeast genome by HR. Yeast cells that successfully integrate the gene of interest with the correct version of the previously mutated or deleted marker regain the ability to synthesize the missing nutrient without requiring its supplementation in the growth medium.

In 1996, the *Saccharomyces cerevisiae* laboratory strain S288c became the first eukaryote to have its entire genome sequenced[397]. The analyzed genome comprises ∼12.2 Mb compactly organized in 16 chromosomes. Researchers identified 6,275 open reading frames (ORFs), but only ∼ 5,800 are believed to be functional[398]. Despite humans and yeasts diverged from a common ancestor ∼ 1 billion years ago[399], 23% of yeast ORFs have a homolog in the human genome and 30% of human disease genes have a functional homolog in yeast[400]. Moreover, mammalian orthologs can often compensate for the function of genes deleted in mutant strains, as observed for the cell cycle[128], and 43% of the 547 essential genes in yeast were complemented by their human counterparts[399]. These observations suggested that several cellular mechanisms are conserved between yeasts and mammalian cells, allowing researchers to elucidate important biological pathways such as apoptosis[401], aging[402], vesicular transport[403], and protein folding, quality control and degradation[404] in this model organism.

The yeast genome is extremely compact with only 4% of genes containing introns at the beginning of their ORFs[405]. This compactness, along with the simple genome organization and the conserved PTMs, such as phosphorylation, ubiquitination[406], acetylation, and glycosylation[407], led to the development of functional genomic yeast based assays[408, 409]. A well-known example is the two-hybrid screening. This genetic yeast-based approach allows for the screening of protein-protein interactions *in vitro*. It is based on using a transcription factor composed of a DNA-binding subunit (DBS) and an activation domain (AD)[410]. In the activated conformation

DBS-AD, the transcription factor can transcribe specific genes called "reporter genes", which is generally represented by LacZ or GFP[410]. To assess if the protein A (bait) interacts with the protein B (fish), the bait is first cloned in a commercial plasmid containing the AD of the transcription factor, so that in the cell it will be expressed as a complex bait-AD[410]. Similarly, the fish is cloned in a second plasmid with the DBS of the transcription factor. Only if the bait interacts with the fish they can assemble the active form of the transcription factor (DBS-AD) that will express the reporter gene[410]. Thousands of interactions have been identified using this assay and reported in several databases and in particular BioGRID (`https://thebiogrid.org/`). Synthetic genetic array analysis is another yeast-based technique used to identify genetic interactions in yeast that could be conserved in mammalian cells. In this method, a yeast strain with the mutation of interest is crossed with a comprehensive array of viable gene deletion mutants, producing a collection of double mutants[411]. By assessing the severity of the phenotypes in the resulting strains, researchers can determine whether two genes participate in the same biological process or if one gene can compensate for the loss of function of another[412].

Given the ease of genetic manipulation in yeast and the functional conservation between yeast and humans, researchers explored the possibility of recapitulating aspects of human diseases in yeast. This approach increases the importance of yeast as a model organism, as it allows to use of this model organism in the study of significant human disorders. In this context, five different "degrees" of humanization have been established[413]:

- Degree 0) Non-humanized yeast addresses the biological processes conserved between yeast and humans in a pathological context.
- Degree 1) Expressing in yeast human proteins involved in diseases regardless of orthology to study their function and interactions in a simpler environment.
- Degree 2) Humanizing specific positions within native yeast genes to understand how small, specific differences between human and yeast genes affect protein function or interactions.
- Degree 3) Humanizing entire yeast genes by replacement with the corresponding human genes to explore their function in a simpler organism.

- Degree 4) Humanization of full pathways to study complex human biological processes (like signaling pathways or metabolic networks) within the yeast model.

In this PhD project, we will use a humanized yeast model for the study of human synucleinopathies.

1.6.1 Yeast model of human α-synuclein aggregation: the HiTox strains

In vitro cell-free studies of α-syn helped researchers to decipher important aspects relative to the behavior of this important protein in the neuropathological context with a particular focus on its structure and aggregation[414, 415]. Cellular models represent a significant advancement in understanding α-synucleinopathies as they allow researchers to examine the protein's functions under more native or physiological conditions. Furthermore, these models are a valuable platform for analyzing complex multifactorial disorders, such as neurodegenerative diseases, at the level of individual molecular events[416]. They simplify the variables present in the whole organism, leading to a precise manipulation of a single gene or consider only the effect of specific factors (e.g., environmental conditions or treatments) without the ethical issues and the costs generally associated with mammalian models or *in vivo* studies on living patients[416]. Human α-synucleinopathy cell models are generated by genetic manipulation, inducing overexpression of wild-type and mutated forms of α-syn or exploiting its prionic nature[417, 418]. This has been achieved in non-neuronal cells, primary neurons, differentiated immortalized cells and patient-derived cells (α-syn cellular models are reviewed in [416, 417]), giving important insights on the α-syn toxicity and aggregation.

The first yeast strain able to express human α-syn was generated in 2003 by Outiero and colleagues, marking a significant step forward in the α-synucleinopathy research[419]. This model is called "HiTox" and expresses α-syn at High Toxicity levels, showing growth defect and characteristic aggregates within the cytosol[419, 420]. Two copies of α-syn cDNA are integrated under the control of the inducible galactose promoter, which allows the expression of the human protein when galactose is supplemented in the cultivation media as a carbon source[419]. Furthermore, the protein is fused at the C-terminus to a GFP fluorescence tag, so it is possible to track its location *in vivo* though fluorescent microscopy[419]. The HiTox model has demonstrated that α-syn initially accumulates at the membrane level and is subsequently recruited into cytoplas-

mic inclusions, impairing the protein folding quality control system[419]. It also contributed to identifying genetic enhancers and suppressors of α-syn toxicity[421] and it represents the model organism investigated in this PhD project.

1.7 Aim of the thesis

This doctoral research is based on the previous findings in the Linster laboratory showing that cobalt, nickel, and deferoxamine can rescue the toxicity induced by the pathological aggregation of α-syn in yeast cells. After experimentally confirming the observed rescue and excluding any direct effects on protein expression levels, it became evident that these treatments activate intricate cellular mechanisms. In additional preliminary work in the host lab, it had been observed that α-syn becomes significant in hypoxia conditions but not when the cells are cultivated in aerobiosis. Given this hypoxia-dependent nature of α-syn toxicity in yeast, the model was used to further explore this interesting association.

1.7.1 Explore the mechanisms underlying α-synuclein toxicity using yeast as a model organism

Over the last 30 years, α-syn has gained a large interest in neuroscience research due to its association with PD, DLB, and multiple system atrophy (MSA). The events that trigger the anomalous α-syn aggregation and the role of a such small protein in driving the neurodegeneration, remain still open questions. This doctoral research is aimed to investigate the complexity of α-syn in an easy but comprehensive eukaryotic cell model: *S. cerevisiae*. Strains genetically engineered to overexpress the wild-type and A53T mutated form of human α-sin (α-HT) are able to partially recapitulate the proteinaceous inclusions and the toxicity described in more complex model organisms and PD patients.

The first key objective of this doctoral research consists of uncovering the mechanisms behind the potential rescue effect of cobalt, deferoxamine, and nickel on α-synuclein toxicity. Given the dose-dependent nature of α-syn aggregation, we aim to determine whether these treatments can

influence the aggregation process.

- To achieve this, we employed fluorescence microscopy to quantify the number of aggregates in the α-HT strain, both treated and untreated with cobalt, nickel, and deferoxamine. Furthermore, we study the α-syn aggregation kinetics using a microfluidic system. We monitored yeast cells growing in hypoxia conditions and in the presence of the two treatments over a period of 24 hours. The data were processed using advanced image analysis techniques to ensure accurate and robust quantification.

Secondly, we investigated the role of hypoxia in the context of α-syn toxicity.

- To explore this, we cultivated the strains under various oxygenation conditions, ranging from atmospheric oxygen levels ($O_2 \sim 20\%$) to complete anoxia (O_2 0%).

Thirdly, an important aim of this project was to understand which are the biological processes altered by α-syn toxicity and assess whether cobalt and deferoxamine can reverse these effects.

- To evaluate the toxic impact of human α-syn expression in yeast, we developed a control strain with two integrated copies of the homologous β-syn in its genome (β-HT). The strains were tested in the phenotypic high-throughput screen to confirm if the expression of human α- and β-syn in yeast have different outcomes on the cell growth.

- We performed transcriptomic profiling on β-HT, α-HT, and α-HT treated with cobalt and deferoxamine. By identifying differentially expressed genes (DEGs) in α-HT compared to β-HT, we found genes that either exacerbate or mitigate α-syn toxicity. Additionally, the DEGs in the two treatments compared to the sick untreated strain (α-HT) could pinpoint important genes involved in the toxicity rescue. The transcriptomic results were validated by quantitative PCR (qPCR) and by comparing them with independent datasets available in the literature on the same model.

- The identified DEGs were further analyzed through pathway enrichment to determine the biological processes impacted by α-syn, β-syn, and treatments with cobalt or deferoxamine. Key genes from these pathways were then selected for the generation of knock-out and

overexpression HiTox strains to investigate their specific roles in mediating toxicity and potential rescue effects.

Finally, to validate the transcriptomic findings and achieve a deeper understanding of the biological alterations in the α-HT strain, we followed a multi-omics approach, performing both targeted metabolomics and untargeted lipidomics on β-HT, α-HT, and α-HT treated with cobalt and deferoxamine. The results of this comprehensive analysis are thoroughly discussed in the final chapter of this thesis, offering insights into potential therapeutic targets for treating synucleinopathies.

Chapter 2

Materials and Methods

This chapter provides a detailed description of the techniques and experimental methodologies used in this project. This information is essential to ensure the validity and reproducibility of the research findings presented in this thesis.

2.1 Yeast strain and media

All the yeast strains used in this project were generated in the W303 MATα genetic background (MATα ura3-52 trp1Δ2 leu2-3_112 his3-11 ade2-1 can1-100), purchased from Dharcom (#YSC1059), as described by Gilter and colleagues[422, 423]. In the α-HiTox strain (α-HT), two copies of the human alpha-synuclein (α-syn) were integrated by homologous recombination into the URA3 and TRP1 loci, respectively. In the β-HiTox (β-HT) two copies of beta-synuclein (β-syn) were similarly integrated into the URA3 and TRP1 loci, respectively. In the A53T-HiTox strain (A53T-HT), two copies of α-syn point mutation A53T (A53T α-syn) were integrated into the URA3 and TRP1 loci, respectively. The empty plasmids were used for the generation of the HiTox control (HTC). The PDR5 gene was disrupted in all the strains via PCR-mediated gene replacement by the kanMX4 cassette. *ino1*Δ strains were generated via PCR-mediated gene replacement by the hphMX6 cassette[423, 424]. Two main series of thiamine strains were generated in this project. In the first series, the genes THI4, THI5, THI11, and THI12 were integrated into the HIS3 locus via homologous recombination. In the second series, the same genes (THI4, THI5,

THI11, and THI12) were expressed from a high-copy episomal vector for the HIS3 auxotrophy complementation. Strains were transformed using standard lithium acetate polyethylene glycol protocol[423, 425] and positive clones were selected on YNB (6.7 g/l yeast nitrogen base without amino acids, 5 g/l ammonium sulfate, pH 5) supplemented with 20 g/l glucose, 0.08 g/l histidine, 0.01 g/l adenine, and 0.24 g/l leucine or rich media (YPD) contained 10 g/l yeast extract, 20 g/l peptone, 20 g/l glucose and 0.2 g/l Geneticin (10131-035, Gibco) or 0.4 g/l Hygromycin B (S2908, Selleck Chemicals). Plasmid integration and gene disruption were confirmed by PCR. For all experiments, strains were cultivated in Synthetic complete (SC) medium (1.7 g/L yeast nitrogen base without amino acids, 5 g/L ammonium sulfate, 2 g/L drop-out mix, 20 g/L Raffinose/Galactose/Glucose, pH 5). The strains used in this study are listed in the Table 5.1 in the "Appendices".

2.2 Synuclein constructs

SNCA gene was amplified from SNCA-EGFP-pIRES plasmid using the primers P3 and P4 and cloned into pAG304GAL-ccdB-EGFP and pAG303GAL-ccdB-EGFP expression vectors using the Gateway cloning system[426, 427]. The A53T α-syn mutation was introduced into SNCA-EGFP-pDONR221 plasmid through site-direct mutagenesis using the QuikChange II XL Site-Directed Mutagenesis kit (#200521, Agilent) and the primers P5 and P6. The mutation was confirmed by Sanger sequencing. SNCB gene was PCR-amplified from human cDNA using the primers P1 and P2 and cloned into pAG304GAL-ccdB-EGFP and pAG303GAL-ccdB-EGFP expression vectors using the Gateway cloning system[426, 427]. In the destination vectors, all the human genes are under the control of the galactose promoter which allows the model to express the protein only when the media is supplemented with this sugar as a carbon source (Figure 2.1, **b**). Additionally, the proteins are fused to the C-terminus to a fluorescence GFP tag that makes possible the detection of the proteins in the cell through fluorescence microscopy (Figure 2.1, **c**).

2.3 Thiamine constructs

THI5, THI11 and THI12 genes were amplified from the FY4 genome using the primers P19 and P20, while THI4 was amplified with primers P21 and P22. The thiamine genes were cloned in the pAG303GAL-ccdB-HA and pAG303GPD-ccdB-HA expression vectors using the Gateway cloning system[426, 427]. The final constructs were used to generate strains in which the expression of the thiamine genes was either induced by the galactose promoter or made constitutive under the control of the glyceraldehyde-3-phosphate dehydrogenase promoter. The thiamine genes were also cloned into the pAG423GAL-ccdB-HA and pAG423GPD-ccdB-HA plasmids to achieve the constitutive or inducible expression expression of these genes through episomal vectors. In both integrative and episomal plasmids, the genes were fused at the C-terminus to an HA tag, that allows to confirm the expression of the proteins by Western blot.

all the primers and the plasmids used are listed in the Table 5.2 and Table 5.3, respectively, as presented in the "Appendices".

A scheme of the cloning strategy is represented in Figure 2.1 **a**

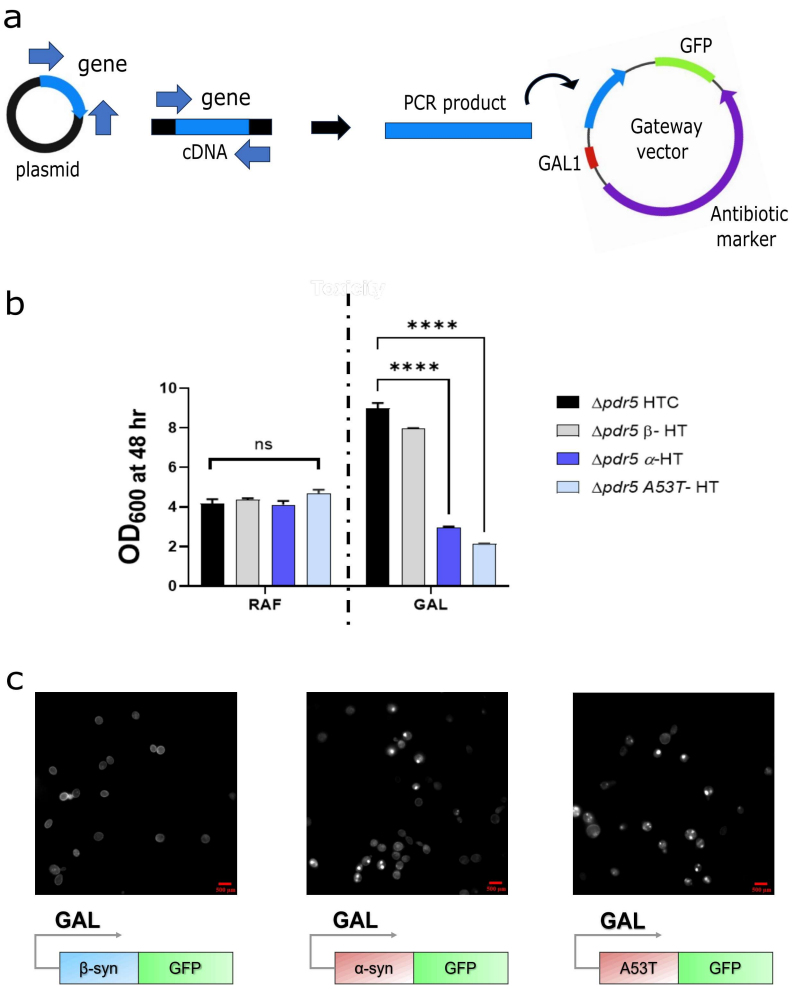

Figure 2.1: **a** Scheme of the cloning strategy performed in this study. cDNA of the genes was amplified either from a plasmid or the FY4 genome and subsequently cloned into a destination plasmid using Gateway cloning. **b** OD_{600} values measured at 48 hours for the strains: HTC, β-HT, α-HT and the A53T mutant respectively grow in SCR and SCG media. The toxicity induced by the expression of α-syn (wild-type or mutant) is appreciable only when the strain is cultivated in the presence of galactose. Each bar is the mean +/- SDs of biological triplicates cultured in 384-well plate format and measured using the Tecan Infinite 200 PRO spectrophotometer. For the statistics, a two-way ANOVA test for multiple comparisons was applied and corrected using the Dunnet statistical hypothesis. ***, adjusted p-value = 0.0002; ****, adjusted p-value < 0.0001. **c** Fluorescence microscopy imagining on β-HT, α-HT and the A53T mutant acquired with 100x objective (+ 0.5X magnification) and Xenon laser. After 16 hours of induction in hypoxia conditions, β-syn remains mostly diffuse in the cell, while α-syn and the A53T mutant form pronounced cytoplasmic aggregates.

2.4 Yeast cultivation and drug testing in yeast

Fresh single colonies from SC-glucose plates were inoculated into 5 mL SC-raffinose ("OFF"-condition, SCR) and incubated overnight with shaking (200 rpm) at 30°C. After $\sim$ 16 hours, cultivations were diluted to an OD_{600} of about 0.5. Microcultivations were performed in 384-well plate (781168, Grainer), 2 μL of cell suspension was added to 78 μL of SCR and compound condition in SC-galactose ("ON"-condition, SCG) to a final OD_{600} of 0.0125. Finally, plates were measured in a microplate reader (TECAN^{TM} In-finite M200Pro), at intervals of 10 minutes for 72 h at 30°C. Microplates were first shaken in an orbital mode with a frequency of 141.9 rpm for 480 seconds and then in linear mode with a frequency of 295.5 rpm for 120 seconds. The amplitude was set at 6 mm for the entire analysis. Yeast-grown phenotyping and data analysis were performed using GATHODE software as previously described[428]. For the cultivation in Erlenmeyer flasks, overnight culture was centrifuged at 3000g for 5 minutes and resuspended in SCG to a final 20 mL of culture 0.0125 OD_{600}. After 48h of incubation with shacking (200 rpm) at 30°C, the OD_{600} was measured with a cell density meter (WPA CO 8000 Biowave Cell Density Meter, VWR). The strains were also cultivated in the 48 well-plate (150687, Thermoscientific) to test the effect of different cultivation formats on the phenotype. A volume of 12.5 μL of a 0.5 OD_{600} culture in SCG was added to 487.5 μL of SCR, achieving a final OD_{600} of 0.0125. The plates were measured in a microplate reader (TECAN^{TM} Infinite M200Pro at 10-minute intervals for 72 hours at 30°C. The shaking protocol involved initial orbital shaking at 141.9 rpm for 120 seconds with a 6 mm amplitude, followed by linear shaking at 452.1 rpm for 120 seconds with a 3 mm amplitude. This set-up was repeated twice.

2.5 Western blotting analysis

Fresh single colonies from SC-glucose plates (SCGlu) were inoculated into 5 ml SCR and incubated overnight with shaking (200 rpm) at 30°C. To test the oxygenation effect on the α-syn expression, 1 mL of overnight culture was inoculated in 5 mL SCG and incubated with shaking (200 rpm) at 30°C. The effect of Hypoxia and treatments on the α-syn expression was tested by inoculating 1 mL of overnight culture in 5 mL SCG and 5 mL SCG supplemented with Cobalt (0.3

mM) and Deferoxamine (0.3 mM). These cultures were then incubated at 30°C without shaking. After 6 hours, 5 mL of 0.5 OD_{600} cultivation was centrifuged at 3000 x g. Yeast protein extract was prepared using a mild alkali treatment method[429]. 6 μL protein extract was loaded into a NuPAGE 4-12% Bis-Tris Gel 1.0 mm X 15 well (NP0323BOX, Invitrogen) and ran into the chamber filled up with 1X MES SDS Running Buffer (NP0002, Novex). The gel was transferred onto a Nitrocellulose 8.5 x 13.5 cm membrane (0.2 µm pore size. LC2009, Invitrogen) in 1X transfer buffer (NP0006-1, Novex) for 1 h at 35 V. The membrane was blocked for 2h in 5% BSA in Tris-Buffered Saline supplemented with 1% Tween 20. Antibodies used: 1:5000 α-Syn (Purified mouse Anti-alpha Synuclein Monoclonal Antibody, clone 4D6, Catalog number MA1-90342, ThermoFisher Scientific), 1:5000 GFP (Purified Rabbit Anti-GFP antibody, Catalog number ab6556, Abcam), 1:10000 GAPDH (Purified mouse Anti-GAPDH Monoclonal Antibody, clone GA1R, Catalog number OAEA00006, Avivasysbio), 1:5000 anti-HA tag [12CA5] (Purified mouse Anti-HA tag antibody, Catalog number ab16918, Abcam), 1:10000 anti-Rabbit IgG Secondary Antibody (IRDye 800CW Goat anti-Rabbit IgG Secondary Antibody, Catalog Number 926-32211, Licor), 1:10000 IgG anti-Mouse IgG Secondary Antibody (IRDye 680RD Goat anti-Mouse IgG Secondary Antibody, Catalog Number 926-68070, Licor).

2.6 α-Synuclein aggregates counting and time-lapse analysis

Single colonies were inoculated in 5 mL SCR and incubated at 30°C overnight. The following day, 1 mL of culture was transferred into a 1.5 mL Eppendorf tube and cells were centrifuged at 3000g for 5 minutes. Pellets were resuspended in 1 mL SCG in the presence or absence of 0.3 mM $CoCl_2$, 0.3 mM $NiCl_2$ or DFO and incubated at 30°C in a static incubator. After 24 hours, cells were visualized using the Nikon inverse Eclipse Ti2 equipped with a 100x objective (plus 1.5X extra magnification) and Xenon laser. Ten pictures for each condition were processed using ImageJ software (2.14.0/1.54f), the number of aggregates and cells was counted using the Cell Counter plugin. For all four considered conditions, the ratio of the number of aggregates over the number of cells was plotted as a boxplot using the GraphPad Prism software (9.5.1733) a one-way ANOVA test for multiple comparisons was applied. The aggregation of α-syn protein

in the cell was studied in vivo using the microscope equipped with a microfluidic yeast plate (CellASIC ONIX Y04C-02-5PK for haploid yeast cells, Merck Millipore) connected to the CellAsic ONIX2 Microfluidic System (CAX2-S0000, Merck Millipore) as illustrated in Figure 2.2. All the media used for this experiment were degassed overnight under constant nitrogen flow. The plate microfluidic chambers were first primed for 30 minutes at 6psi with SCG and compound condition in SCG according to the following scheme. To avoid cells overcrowding and start the analysis with single or few cells trapped in the chamber, 0.2 OD_{600} of HiTox strain were loaded at 24 kPa for 2 seconds. The loading was repeated until few cells colonized the chamber area of 3.5 μm height trap. The flow was maintained at 34.5 kPa during the selection of the twelve positions used in the analysis and lower to 0.1 kPa during the acquisition to ensure low media oxygenation. Three positions for each tested condition were selected based on the numbers and position references embossed in the middle of each chamber area. For the duration of the entire analysis, the microfluidic plate was vacuum sealed by the CellAsic manifold XT (CAX2-MXT20, temperature controlled) apparatus set-up to maintain a constant temperature of 30°C. Images were acquired using MetaMorph software (7.10.4.407) in multidimensional acquisition. For each position, one picture was acquired in the brightfield channel and 11 Z-stacks in the xenon channel with an interval of 7.5 minutes between each acquisition cycle. To obtain a clear visualization of the aggregate's formation\dissolution inside the cell, the focus was set using the fluorescence of xenon laser at 488 nm of excitation for 200 ms exposition and 520 nm of emission, furthermore, the autofocus function allows us to compensate the movements due to the microscope switching position that could break the fixed focus set $\pm$ 5 mm around the midplane focal position. 11 Z-stacks were acquired for all the 193 timepoints generating about 200 GB of TIF files. Considering the large amount of data, the analysis was performed on the university UL HCP supercomputer AION. 2316 files were organized in twelve folders and each series of 11 Z-slices was separately imported into ImageJ (2.14.0/1.54f; java 1.8.0_322). First, we applied the function Hyperstack to display the 193 timepoints of 32-bit 11 Z-slices TIFF images in a single window (2.3, **a**). Then we applied a Z-projection to stack the previous image based on the standard deviation through the 11 Z slices (2.3, **b**). Among the available auto-thresholding methods in ImageJ, the Yen method was the most accurate to distinguish the aggregates signal[430] (2.3, **c**). Watershed segmentation was

applied to the resulting binary image to separate clustered aggregates and avoid miscalculation in the final count[431]. Aggregates were analyzed using the Analyze Particles function with an aggregate area threshold of at least 0.19 μm^2 and a circularity between 0.70 and 1.00 to remove the not circular signals due to cells contacts (2.3, **d**). To generate a complete track over the 24h of analysis, the 193 time points of 32-bit 11 Z-slices TIFF images were processed using IMARIS software (9.9.1.61122). Aggregates were tracked over time using the autoregressive motion algorithm with a max distance and a gap size of 3 μm.

This analysis was kindly supported by the expertise of Dr. Paul Antony.

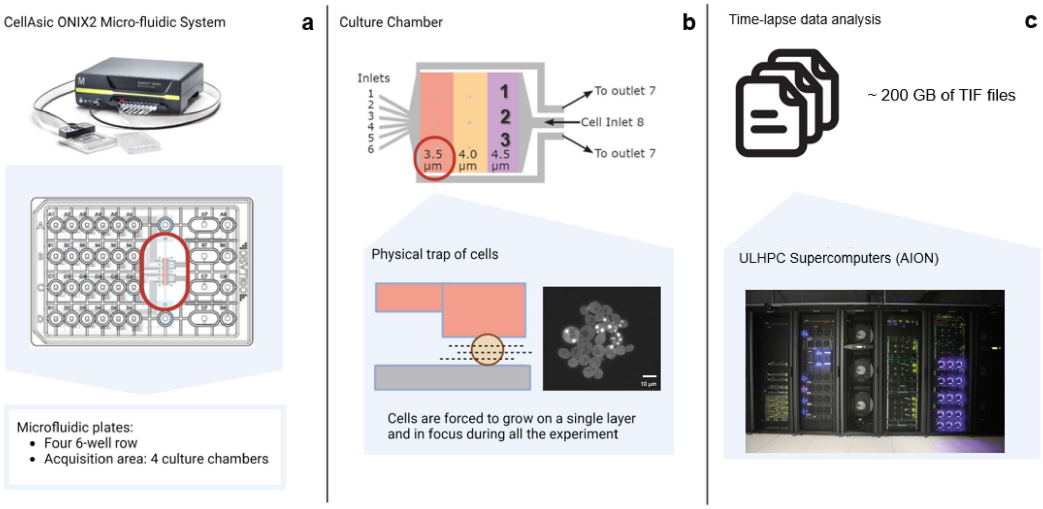

Figure 2.2: Scheme of the CellAsic ONIX2 microfluidic system used for the time-lapse analysis. **a.** The controller system keeps the temperature (30°C) and the flow rate (0.5 KPa) constant for all the analysis switching between the 4 modules of 6 hour each. The system is connected to the microfluidic plate through the manifold system which preserves the vacuum. The microfluidic plate was prepared as follow: 1-6 wells of the unit A were filled with 350 μL of SCG N_2 degassed media; 1-6 wells of the unit B were filled with 350 with 350 μL of SCG N_2 degassed media supplemented with 0.3 mM of Cobalt; 1-6 wells of the unit C were filled with 350 μL of SCG N_2 degassed media supplemented with 0.3 mM of Deferoxamine and 1-6 wells of the unit D were filled with 350 μL of SCG N_2 degassed media supplemented with 0.3 mM of Nickel. Solution inlets 1-4 were used for the analysis, but all the wells were filled as recommended in the plate's user manual. Cell inlets (A8-D8) were filled with 50 μL of 0.2 OD_{600} α-HiTox culture in SCG. **b.** The cells were forced to grow on a single layer by trapping them in the 3.5 μm height area of the culture chamber, this ensure to mantain the focus for all the experiment. **c.** The 200 GB of tif file were analyzed using the imageJ software installed in the Aion High Performance Supercomputer (HPC).

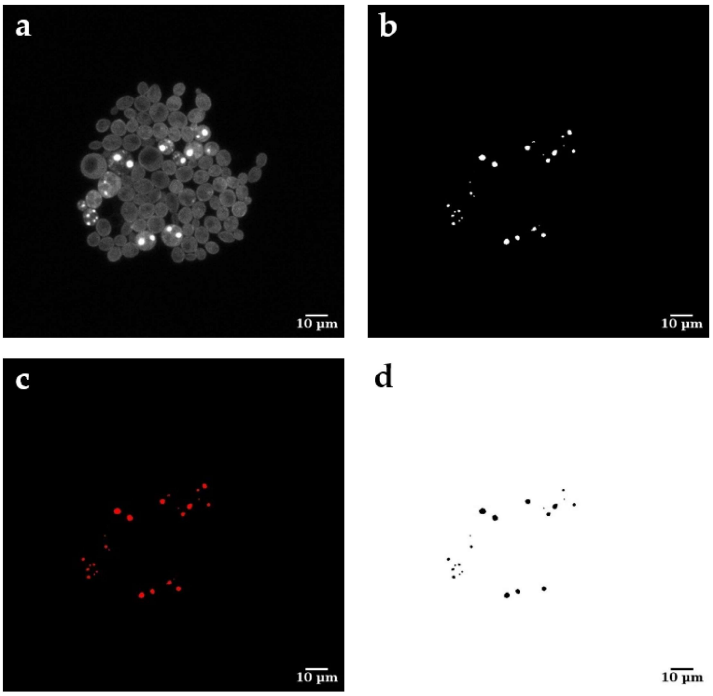

Figure 2.3: Processing workflow of an image acquired using the Xenon LED channel to extract aggregates data. cleaning and processing performed on ImageJ software (2.14.0/1.54f; java 1.8.0_322). For all the 12 positions, 193-time points of 32-bit 11 Z-slices TIFF images were acquired. **a** The 193 files were first projected (Z-projection) on the middle plane of the focus based on their standard deviation. **b** The signal of the cells was removed by applying the Yen threshold was applied and the resulting aggregates were correctly separated using the Watershed binary mask **c**. **d** The fluorescence signals due to cell contacts were cut out from the aggregates count fixing a circularity range between 0.7 and 1.00.

2.7 Rhodamine B staining

Yeast cells were stained with a 0.01% ethanol solution of Rhodamine B (C.I. 45170, Merck) following the protocol described by Nowosad and colleagues[432]. To ensure efficient dye uptake, cells were incubated overnight at 30°C in a static incubator, kept in the dark to preserve fluorescence. Cells were visualized using the Nikon inverse Eclipse Ti2 equipped with a 100x objective (plus 1.5X extra magnification). The excitation and emission wavelengths were 570 nm and 680 nm, respectively.

2.8 Transcriptomics analysis

For the RNAseq analysis, 3 independent single colonies of each strain were inoculated into 5 mL of SCR ("OFF"-condition) incubated overnight with shaking (200 rpm) at 30°C. To increase the biomass, after $\sim$ 16 hours, 3 mL of the overnight cultures was inoculated in 100 mL Erlenmeyer flasks filled with 25 mL SCR media. The flasks were incubated overnight with shaking (200 rpm) at 30°C. The 25 mL of confluent culture were transferred in sterile 50 mL falcon tubes and centrifuged at 3000xg for 5 minutes. The pellet is resuspended in 10 mL of SCG media ("ON"-condition) and diluted to a 0.5 OD_{600}, based on the measurement read on the cell density meter (WPA CO 8000 Biowave Cell Density Meter, VWR). These cultures were further diluted in SCG media and SCG supplemented with 0.3 mM Cobalt or Deferoxamine -scheme- After 6h and 12h of incubation at 30°C without shaking, the total RNA was extracted using the RNeasy Plus Mini Kit (250) (Qiagen, #REF74136) according to the manufacturer protocol for yeast samples. A mechanical cells disruption was performed using the 2 mL precellys tubes (ref) filled with 600 mg of Glass beads, acid washed (G8772, Sigma-Aldrich). To successfully achieve the mechanical lysis of the cells and the release of the genetic material, the tubes were vortex and agitated for 2 cycles at 6000rpm for 30 seconds with 30 seconds of pause in the Precellys® Evolution touch homogenizer (P000671-CLYS2-A.0, Bertin) pre-cooled to 4°C. After the extraction, genomic DNA was removed using the TURBO DNA-free Kit (#AM1907, Invitrogen). The RNA integrity number (RIN score) and the final concentration were assessed by loading the samples on the microchannels of the RNA Nano Chips (#5067-1511, Agilent Technologies) analyzed through the Agilent Bioanalyzer 2100. The RNA samples extracted at 6 and 12 hours were sequenced by the Beijing Genomics Institute (BGI) in Hong Kong, China through the DNBSEG-G400 high throughput platform. DNBSEQ Eukaryotic Strand-specific mRNA library, generated after multiple PCR cycles, was amplified with phi29 to assemble DNA nanoball (DNB) which were then loaded into nanoarrays and sequenced by Paired-ends 100 bp. It generates $\sim$20 million, paired-end 100 base pair read for sample. Raw sequencing data were filtered using SOAPnuke software to remove adaptors and low-quality sequences with more than 10% of unknown bases[433]. The read quality value was set to Phred+33. Row data were proficently trimmed and annotated by

Professor Enrico Glaab using Saccharomyces cerevisiae (S288C) as a reference genome (BioProject accession no. PRJNA128). The final dataset comprises 7,000 genes, and the PCA plot revealed distinct clustering between the groups and across the time points, highlighting the robustness of the analysis (Figure 5.2, Appendices). Differential expression analyses were performed with the R package DESeq2 (1.40.2), filtering the data by expression. The differentially expressed genes (DEGs) that satisfied the cut-off criteria log2-based fold change $|log2FC| > 1$ and P value adjusted < 0.05 were considered as significant hits. The volcano plots were generated using the R package enhancedVolcano (1.18.0). The Venn diagrams were obtained using the R package VennDiagram (1.7.3). The Pathway enrichment analysis was performed using the R package clusterProfiler (4.8.3). To overcome the problem of the missing symbol in the org.Sc.sgd.db package, Professor Enrico Glaab kindly generated an updated mapping annotation by matching gene identifiers (without the "SGD" prefix) with the corresponding gene information. Both files were sourced from the Saccharomyces Genome Database (`https://www.yeastgenome.org/`). Professor Enrico Glaab also performed a MetaCore pathway enrichment analysis on the DEGs obtained from the transcriptomic profiling to identify overlaps with human biological processes. This approach allows for a deeper understanding of the functional relevance of the DEGs in relation to human pathways.

2.9 Quantitative real-time PCR (qPCR)

The genetic hits identified in the transcriptomic analysis were confirmed by qPCR. RNA was prepared from new yeast samples independent of those used in the transcriptomic profiling. 1000 ng of RNA were converted in cDNA using the SuperScript™ III Reverse Transcriptase (18080-044, thermofisher) in combination with RNaseOUT™ Recombinant Ribonuclease Inhibitor (10154652, thermofisher), dNTP (U1515, promega) and Oligo(dT)20 Primer (18418020, Invitrogen) based on the polymerase manufacturer's instructions. cDNA was diluted 1:10, and quantification of mRNA levels was performed in the Light Cycler 480 Multiwell Plate 96 (Roche) using the Powertrack SYBR MM (A46113, thermofisher) and the primers listed in the Table 5.2 at the final concentration of 0.25 μL. Reactions were performed in duplicates in a final volume of 10μL using

the LightCycler 480 Multiwell Plate 96 (04729692001, Roche) sealed with LightCycler 480 Sealing Foil (04729757001, Roche). Cycle threshold (Ct values) and melting curves were determined using Light Cycler 480 software, version 1.5 (Roche), and results were processed using the 2-ΔΔCt method[434], with TDH3 serving as reference genes for normalization.

2.10 Metabolite Extraction and Sample Preparation for Lipids and Metabolites Analyses

GC- and LC-MS were performed to profile the metabolome of the cells after 8 and 24 h of α-synuclein expression. The analysis required a harvest culture with an OD_{600} of 2 (approximately 6 grams of dry cell weight per liter of culture) for each replicate. Similar to the transcriptomic analysis, 25 mL precultures in SCR media (OFF-conditions) were prepared and incubated overnight with shaking (200 rpm) at 30°C. After ∼24 h, the 25 mL of confluent culture was then used to prepare 100 mL of main culture in SCG media ("ON"-condition). The pellet resulting from centrifugation of the 25 mL preculture at 3000xg for 5 minutes was resuspended in 3 mL of SCG media. Based on the cell density read on the cell density meter (WPA CO 8000 Biowave Cell Density Meter, VWR), the suspension was diluted to a final OD_{600} of 0.05 in 100 mL of SCG media, and SCG media supplemented with 0.3 mM Cobalt or Deferoxamine. For the 24 h time point, the main culture was prepared using 350 mL of SCG media, instead of 100 mL and the remaining 250 mL were used for preparing the samples for the ^{31}P-NMR. 1 mL of each culture was used to measure OD_{600} and to determine biomass parameters, including biovolume and cell counts, using the Multisizer 3 Beckman Coulter Counter MS3. This information will be subsequently used for data normalization. For each condition considered three biological replicates were prepared for the 8 h time point, while four were prepared for the 24 h time points as, in the latter case, the sampling was optimized for both metabolomics and NMR analysis.

2.10.1 Metabolites extraction

100 mL of main cultures were spin down at 3000xg for 5 minutes, the resulting pellet was resuspended in 20 mL of quenching fluid composed of 60% (v/v) methanol (8388.6, Carl Roth)

and 40% (v/v) Milli-Q water. The mixture was shaken by tube inversion and vortexing until the pellet was fully resuspended, then centri-fuged at 3900xg for 3 minutes at -10°C. The pellet was washed once with 20 mL of 0.9% (w/v) NaCl solution at 4°C, and the suspension was centrifuged again at 3900xg for 3 minutes at -10°C. Intracellular metabolites were extracted from the cell pellets by adding 1 mL of extraction fluid at -20°C, which was prepared by mixing 50% (v/v) methanol (AE71.2, Carl Roth) and 50% (v/v) Milli-Q water. The mixture was transferred into 2 mL precellys tubes (P000945-LYSKO-A.0, Precellys Lysing Kit) filled with 600 mg of Glass beads, acid washed (G8772, Sigma-Aldrich). Mechanical cell disruption was performed by vortexing and agitating the tubes for 2 cycles at 6000 rpm for 30 seconds, with 30-second pauses, using the Precellys® Evolution touch homogenizer pre-cooled to 4°C. Phase separation was achieved by adding 500 μL of chloroform (7331.2, Carl Roth) and incubating the mixture in the ThermoMixer®C (Eppendorf, EP5382000066) equipped with a 2.0 mL thermoblock set at 4°C. The tubes were shaken at maximum frequency for 20 minutes, then centrifuged at maximum speed for 3 minutes at 4°C. 200 μL of the upper aqueous phase was transferred in GC-MS glass vials with microinsert (401100051, Trott) and 100 μL was transferred in 1.5 eppendorf tube for LC-MS. 200 μL of lower organic phase were transferred in amber HPLC glass vials with microinsert (451101012_E, Trott) for lipidomic analysis. Solvents were evaporated overnight in a rotary vacuum evaporator (7310031, Labconco) at -4°C. The pellet was stored at -80°C until reconstitution and analysis.

2.10.2 GC-MS anaysis

To quantify the metabolites involved in the 1C metabolism which, based on the RNA sequencing analysis, is one of the cellular metabolomic processes most affected by α-synuclein expression, polar metabolites were profiled using gas chromatography coupled to mass spectrometry (GC-MS) as reported previously with slight modifications[435]. Prior extraction, [UL-^{13}C5] Ribitol (ALD-062, Omicron Biochemicals) and Tridecanoic-d25 Acid (D-4002, Isotopes Inc.) (final concentration 5 μg/ml) and Pentanedi-oic-d6 Acid (D-5227, Isotopes Inc.) (final concentration 10 μg/ml) were added as internal standards in the extraction fluid. Dried polar extracts were derivatized in two steps using a multi-purpose sample preparation robot (Gerstel):

1. First Addition of 15 μL pyridine containing 20 mg/ml methoxyamine hydrochloride with a subsequent incubation period of 120 min at 40°C under continuous shaking.

2. Second Addition of 15 μL N-Methyl-N-trimethylsilyl-triflouroacetamide (MSTFA) with subsequent incubation at 40°C for 30 min under continuous shaking.

GC-MS analysis was performed using an Agilent 7890A GC coupled to an Agilent Mass Selective Detector (MSD; Agilent Technologies). A sample volume of 1 μL was injected into a Split/Splitless inlet operating in 1) splitless mode and 2) split 5 mode at 280°C. The gas chromatograph was equipped with a 30 m (I.D. 0.25 mm, film 0.25 μm) ZB-35 capillary column (Phenomenex) with a 5 mm guard column in front of the analytical column. Helium was used as the carrier gas with a constant flow rate of 1.2 mL/min. GC temperature program was 90°C for 1 min, then increased to 270°C at 9°C/min, further increased to 320°C at 25°C/min and held for 7 min. The total run time was 30 min. The transfer line temperature was set to 280°C. The MSD was operating under electron ionization at 70 eV. The MS source was held at 230°C and the quadrupole at 150°C. GC-MS measurements were performed in full scan mode from m/z 70 to 700 with a minimum scan rate of 4 scans/s. MetaboliteDetector (3.320200313) was used to process all GC-MS chromatograms. 24 Compounds were annotated by retention time and mass spectrum using an in-house mass spectral library (overall similarity: $>$0.80). The following deconvolution settings were applied: Peak threshold of 5; Minimum peak height of 5; 10 Bins per scan; Deconvolution width of 5 scans; No baseline adjustment; Minimum 15 peak per spectrum; No minimum required base peak intensity.

2.10.3 LC-MS analysis

Changes in the central metabolism were detected using targeting metabolomic profiling using liquid chromatography coupled to high-resolution mass spectrometry (LC-HRMS). Prior extraction, Nϵ-Trifluoroacetyl-L-lysine (53604, Sigma-aldrich), 2-Chloroquinoline-3-carboxylic acid (688517, Sigma-aldrich), 6-Chloropurine ri-boside (852481, Sigma aldrich) and U-13C U-15N Adenosine 5'- monophosphate (123603601, Silantes) were added as internal standards in the extraction fluid at the final concentration of 1 μg/mL. Dried samples were reconstituted in 50 μL of a mixture

composed of 50% of Acetonitrile (ROTISOLV® ≥99,95%, LC-MS Grade) in water supplemented with 12-[[(cyclohexylamino)-carbonyl]amino]-dodecanoic acid (CUDA, 10007923, Sanbio) to a final concentration of 100 ng/mL. The mixture was filtered using 4 mm regenerate cellulose filter (Phenex™-RC 4mm Syringe Filters 0.2μm) into an amber HPLC glass vial with microinsert. Chromatographic separation was performed on a Thermo Vanquish UHPLC. A Zic-pHILIC SeQuant column (150 x 2.1 mm, 3.5 m particle size, 100 Å pore size) connected to a Zic-pHILIC guard column (20 x 2.1 mm, 5 m particle size, Merck KgAA) was used for separation. The liquid chromatography (LC) was performed at 45°C with a constant flow rate of 0.20 mL/min. Mobile phase A consisted in 20 mM ammonium carbonate solution (pH 9.2) enriched with 5 μM of medronic acid (5191-4506, Agilent) and mobile phase B consisted in LC-MS grade. After injection of 5 µl, the following gradient was applied: 80% B for 3 min, decreasing to 20%B within 15 min, holding 20%B for 1 min before returning to starting conditions for 10 min, resulting in a total run time of 30 min. Mass spectrometric analysis was performed on a Q Exactive HF Orbitrap mass spectrometer equipped with an H-ESI electrospray ion source with the following source settings: Sheath gas - 25, Aux gas - 15, Sweep gas - 0, Spray voltage - 4.5 kV (positive) / 3.5 kV (negative), Capillary temperature - 325°C, S-Lens RF level - 50, Aux Gas Heater Temperature - 50. Mass spectrometric data were acquired in polarity switching mode in full scan mode applying the following parameters: Resolution – 60,000, AGC target – 1E6, max IT – 240 ms, Scan range – 70-1000 m/z. Data-dependent MS2 acquisition with inclusion list was performed to confirm the identity of the target compounds according to the following parameters: Resolution – 30,000, AGC target – 1E5, Max IT – 50 ms, Loop count – Top5, NCE – 30.

This analysis was kindly supported by the expertise of the Research engineer Floriane Gavotto.

2.10.4 Lipids analysis

Changes in the lipids content that affect the cellular membrane composition were assessed by LC-MS analysis using a method adapted from Cajka et al[436]. Analyses were performed on a Vanquish Flex coupled to the Exploris240 LC-MS system (Thermo Fisher). Prior extraction, EquiSPLASH™LIPIDOMIX® (330731-1EA, Avanti) was added as internal standard in the extraction fluid (5 μL per mL extraction fluid). Dried lower phase samples were reconstituted in

400 μL of methanol/toluene mixture (9:1, v/v) containing an internal standard CUDA (Cayman Chemical, Ann Arbor, MI, 150 ng/ml). After injection of 5 μL reconstituted sample (sample temperature at 4°C), lipids were separated on an Acquity UPLC CSH C18 column (100 x 2.1 mm; 1.7 μm) equipped with an Acquity UPLC CSH C18 VanGuard precolumn (5 x 2.1 mm; 1.7 μm) (Waters, Milford, MA) at a temperature of 65°C and flow rate of 0.3 mL/min. Separation was conducted using mobile phases A (10 mM ammonium formate in 60:40 acetonitrile/water with 0.1% formic acid) and B (10 mM ammonium formate in 90:10 isopropanol/acetonitrile with 0.1% formic acid) at the following gradient: 15% B for 1 min, increasing to 70% B from 1 to 9 min, increasing to 99% B from 9 to 17 min, 99% B from 17 to 25 min, decreasing to 15% B from 25 to 25.1 min, re-equilibration at 15% B from 25.1 to 30 min. After LC separation, lipid species entered the mass spectrometer with the following H-ESI source settings: Spray voltage pos – 3.5 kV, Spray voltage neg – 3 kV, Sheath gas – 45, Aux Gas – 10, Sweep Gas – 2, Ion transfer tube temperature – 320°C. The following scan settings were applied: Scan range – m/z 120-1800, Easy-IC – enabled, Mode – polarity switching, resolution – 60,000, AGC Target – Costum, Max Injection Time mode - Auto. AcquireX's interactive precursor exclusion workflow was run on pooled samples in positive and negative modes to maximize the amount of MS2 spectra for m/z detected in full scan mode.

This analysis was kindly supported by the expertise of Dr. Martin Jakubecand Dr. Lisa Schlicker.

2.10.5 Lipidomics data analysis

The chloroform phase was collected from the liquid-liquid extraction performed on four biological replicates (n = 4) of β-HT, α-HT, and α-HT incubated respectively with 0.3 mM of cobalt or deferoxamine. The resulting 16 samples were analyzed with three extraction blanks and four pool samples. The raw data obtained from each UPLC-HRMS analysis were first converted to the open-source .mzML format using MSconvert from the ProteoWizard package[437]. Data were further processed using MZmine software (version 4.1.0) with the following changes from the recommended settings: the minimum feature height was set to 1E5, and the chromatographic threshold was set to 80%. Other settings were kept at their default values using mzwizard for the UHPLC and Orbitrap pipeline[438]. Features were annotated using the inbuilt rule-based

lipidomics rules and the Mass Bank of North America database. Additionally, unknown features were assigned a chemical class using MS2Query software (version 1.5.0.) with a score cut-off of 0.6[439].

Statistics were performed using MetaboAnalyst in R (Version 4)[440]. Peak intensities were normalized to the sum of identified peaks, and missing values were imputed using the KNN algorithm. Furthermore, data were log-transformed and scaled using Pareto scaling. After Pareto scaling, a principal component analysis (PCA) was performed to visualize the sample groups and the variance Figure. After these normalization procedures, the data followed a normal distribution, and a t-test was performed to identify significant features. Features with $p < 0.05$ and a fold change higher than 2 or lower than 0.5 were filtered and transferred into ChemRich (version 4) analysis[441]. Here, features were grouped into chemical families based on their structural similarities using the Tanimoto score, and significance and fold change for these chemical groups were calculated. This analysis was kindly supported by the expertise of Dr. Martin Jakubec.

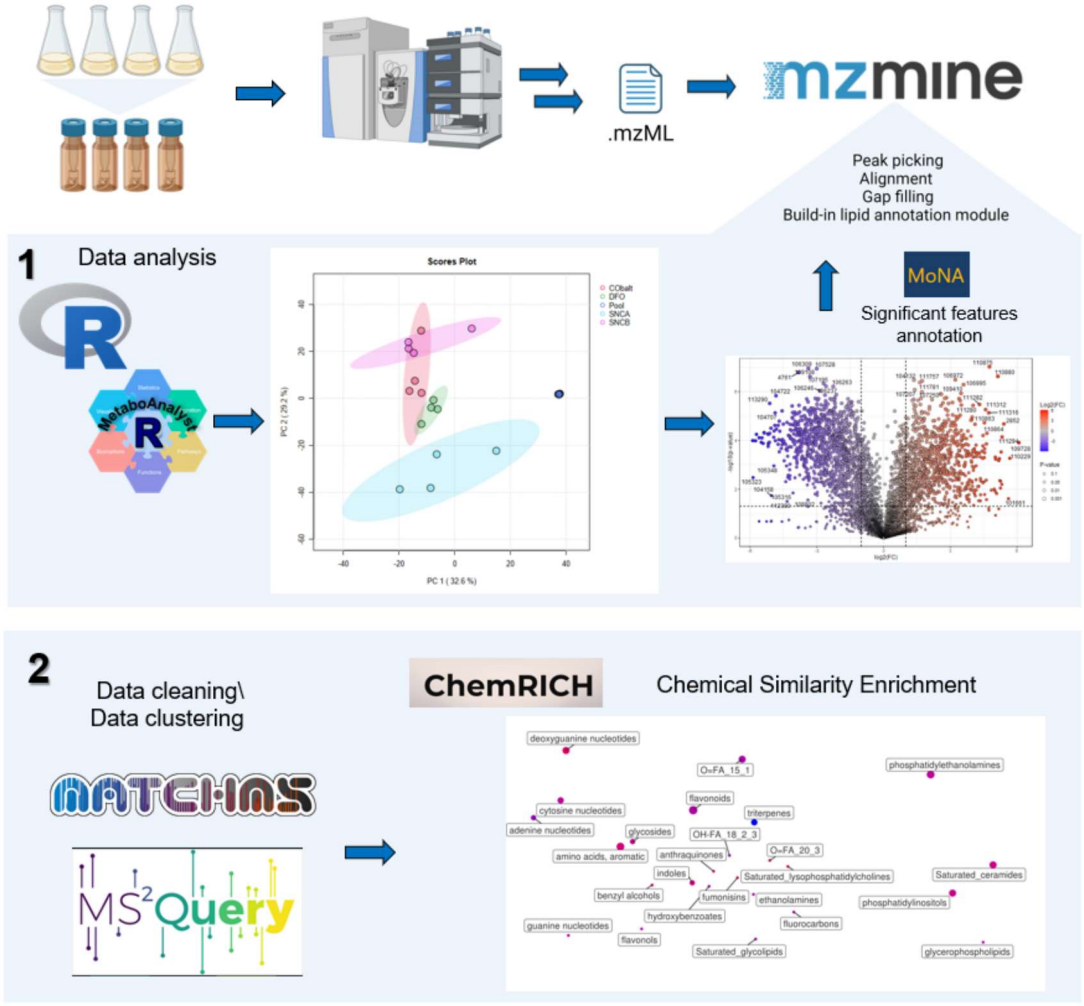

Figure 2.4: Data resulted from the untargeted lipidomic analysis performed on the β-HT, α-HT, α-HT treated with Co^{2+} or DFO was analyzed according to the workflow schematized in this figure. Data were first cleaned, processed, and normalized using MZmine software, which also allow to integrate and annotate the peaks present in the chromatogram. 1) The MZmine results were then statistically analyzed in RStudio using the MetaboAnalyst package to identify significant features. 2) The MZmine results were further analyzed using matchms and MS2Query to identify spectral similarities with compound libraries. Finally, ChemRICH was used for enrichment analysis and visualization of the major chemical classes present in the dataset.

2.11 Statistics

Plots and statistical analyses presented in this doctorate thesis were generated using GraphPad software (10.2.2.397). The plots and the statistical analysis for the transcriptomic and lipidomic data were instead performed on R studio software (version 4.1.1), using dedicated packages as outlined in this chapter.

Chapter 3

Results

This chapter presents a comprehensive summary of the experimental results obtained in this PhD research project. It describes the techniques applied to investigate the molecular processes underlying α-synuclein-induced toxicity and the protective effects observed following treatment with Cobalt, Nickel, and Deferoxamine.

3.1 Phenotypic drug assay on the HiTox model reveals Cobalt, Nickel and Deferoxamine as α-syn toxicity suppressors

Two FDA-approved drug libraries, Tocriscreen and Prestwick, were previously tested in the Linster laboratory on a yeast model of ATP13A2/PARK9 deficiency using a phenotypic high-throughput screen. This screening identified 10 drugs that effectively mitigated the increased sensitivity to zinc exposure of this yeast mutant strain[442]. Furthermore, previous studies by others in yeast and mammalian cells have demonstrated that overexpression of Ypk9, the yeast orthologue of the human ATP13A2 gene, can protect against α-syn toxicity[442, 443, 444]. The role of ATP13A2/PARK9 in the metabolism of α-syn remains unclear. However, to investigate whether these compounds could mitigate α-syn toxicity, we tested them on the α-HT strain, which expresses wild-type α-syn under the control of the galactose promoter (Ursula Heins Marroquin, unpublished data). This yeast model of human synucleinopathies was generated and analyzed in the Linster laboratory using a similar phenotypic assay. The analysis was completed with an

"ad-hoc" control strain in which two copies of human β-syn were integrated under the inducible galactose promoter (β-HT). Further details regarding the generation of these strains are provided in Section 2.1 of the Materials and Methods chapter. To induce the expression of α-syn and β-syn, we replaced the raffinose carbon source (SCR) with galactose (SCG). The inducible expression of these two human proteins is deeply explained in Section 2.1 of the Materials and Methods chapter (Figure 2.1 **b**). OD_{600} were measured after 48 hours of cultivation in the presence of manganese (Mn^{2+}), cobalt (Co^{2+}), zinc (Zn^{2+}) and nickel (Ni^{2+}), the hit compounds and the heavy metals associated to Ypk9 model[442]. As expected, the α-HT strain showed a 3-fold decreased OD_{600} compared to the HTC and β-HT controls (Figure 3.1 **a**), confirming previous results obtained by other groups[419, 421]. Interestingly, Co^{2+}, Ni^{2+}, and deferoxamine (DFO) significantly improved the growth of the α-HT strain at the concentrations tested (Figure 3.1 **b**), suggesting that these compounds could have a protective effect against the α-syn toxicity. We further investigated this observation, by testing Co^{2+}, Ni^{2+}, and DFO at different concentrations in the micromolar (μM) range. The dose-response plots of Co^{2+} and Ni^{2+} in figure 3.1 **c** and **d** revealed that these two compounds exhibited toxicity at concentrations above 0.3 mM, while deferoxamine in figure 3.1 **e** demonstrated a higher tolerance threshold, exceeding millimolar concentrations (mM). The three compounds do not have a similar beneficial effect on the growth of the A53T-HiTox strain reported in figure 3.1 **f**, suggesting their inability to overcome the toxicity of the mutated form of α-syn. Based on the dose-response plots in figure 3.1 **c-e**, we selected 0.3 mM as the optimal concentration for testing Co^{2+}, Ni^{2+} and DFO in the different experiments performed in this thesis.

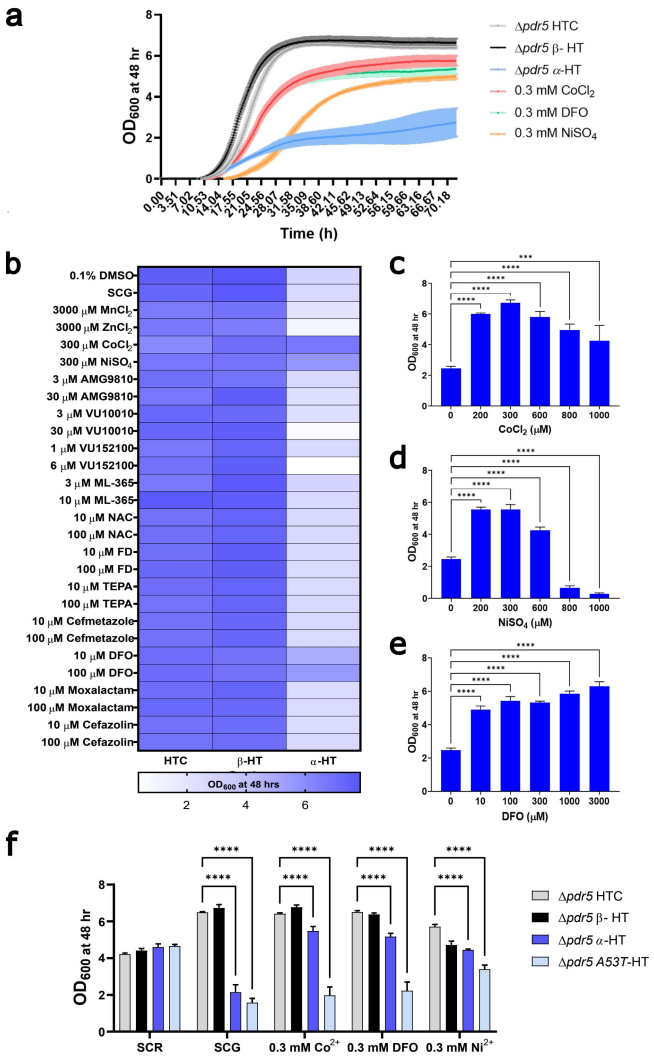

Figure 3.1: **a** Growth curves measured over 72 hours for the HTC, β-HT and α-HT strain grown in SCG media and SCG supplemented with 0.3 mM of $CoCl_2$, deferoxamine or $NiSO_4$. Each dot represents the mean +/- SDs of biological triplicates cultured in the 384-well plate format.**b** Heatmap of the phenotypic drug assays using the OD_{600} values measured at 48 hours. α-HT shows growth impairment in untreated (SCG) and in the negative control condition (1%DMSO) compared to HTC and β-HT. Dose-response assay for cobalt ($CoCl_2$) **c**, ($NiSO_4$) **d** and deferoxamine (DFO) **e**, based on the OD_{600} values measured at 48 hours. OD_{600} measured at 48 hours for the strains: HCT, β-HT, α-HT and the A53T mutant respectively grown in SCR, SCG media and SCG supplemented with 0.3 mM of $CoCl_2$, deferoxamine or $NiSO_4$ **f**. Each bar in **b**-**e** is the mean +/- SDs of biological triplicates cultured in 384-well plate format and measured using the Tecan Infinite 200 PRO spectrophotometer. For the statistics, two-way ANOVA test for multiple comparisons was applied and corrected using the Dunnet statistical hypothesis. ****, adjusted p-value $<$ 0.0001.

3.2 Hypoxia drives α-syn toxicity

The highlighted compounds, Co^{2+}, Ni^{2+} and DFO, are known to induce a hypoxia-like response by regulating hypoxia-inducible genes expression in humans and yeast[445, 446]. To investigate whether O_2 levels might interfere with the rescue mechanisms elicited by these compounds and α-syn-induced toxicity, we grew the strains in different cultivation formats that provided progressively decreasing oxygenation. In particular, we expected higher oxygenation in the Erlenmeyer flasks shaken at 200 rpm and in 48-well plates compared to the more limited oxygen availability in 384-well plates. Independently from the cultivation format, α-HT showed significantly decreased OD_{600} at 48 hours (Figure 3.2). However, toxicity was milder in the shaking flasks ($\sim$24% decrease in α-HT and $\sim$50% decrease in A53T-HT, Figure 3.2 **a, Shaking Flasks**) compared to 384 well plate ($\sim$70% decrease in α-HT and $\sim$77% decrease in A53T-HT, Figure 3.2 **b, 384-well plate**). Interestingly, the rescue effect of the three compounds was completely abolished under the normoxia condition (Figure 3.2 **a**). To confirm whether the change of the cultivation format is responsible for the alteration of the results, cells were growing in static conditions in the same flask. Similar to cultivation in 384 well-plate, cell viability was decreased by 80% in α-HT and 70% in A53T-HT. Co^{2+}, Ni^{2+} and DFO were partially able to rescue the growth defects in α-HT, but not in A53T-HT (Figure 3.2 **b**), confirming the results reported in the previous section. To further explore the importance of oxygenation in α-syn toxicity and in the effect of the drugs, the strains were grown in extreme anoxia conditions (95% of N_2 and 5% of CO_2) (Figure 3.2 **c**). Under complete absence of O_2, the OD_{600} was lower after 48 hours compared to normoxia and hypoxia conditions. However, a significant decrease in OD_{600} was appreciated in both α-syn strains. Moreover, compounds failed to rescue the growth phenotype in both strains, suggesting that certain levels of O_2 should be present for the rescue effect. Finally, we confirmed through Western blot analysis that the different growth behaviors observed in normoxic (shaking cultivation at 200 rpm) compared to hypoxic (static cultivation at 0 rpm) conditions is not due to alteration of α-syn expression levels (Figure 3.2 **e**).

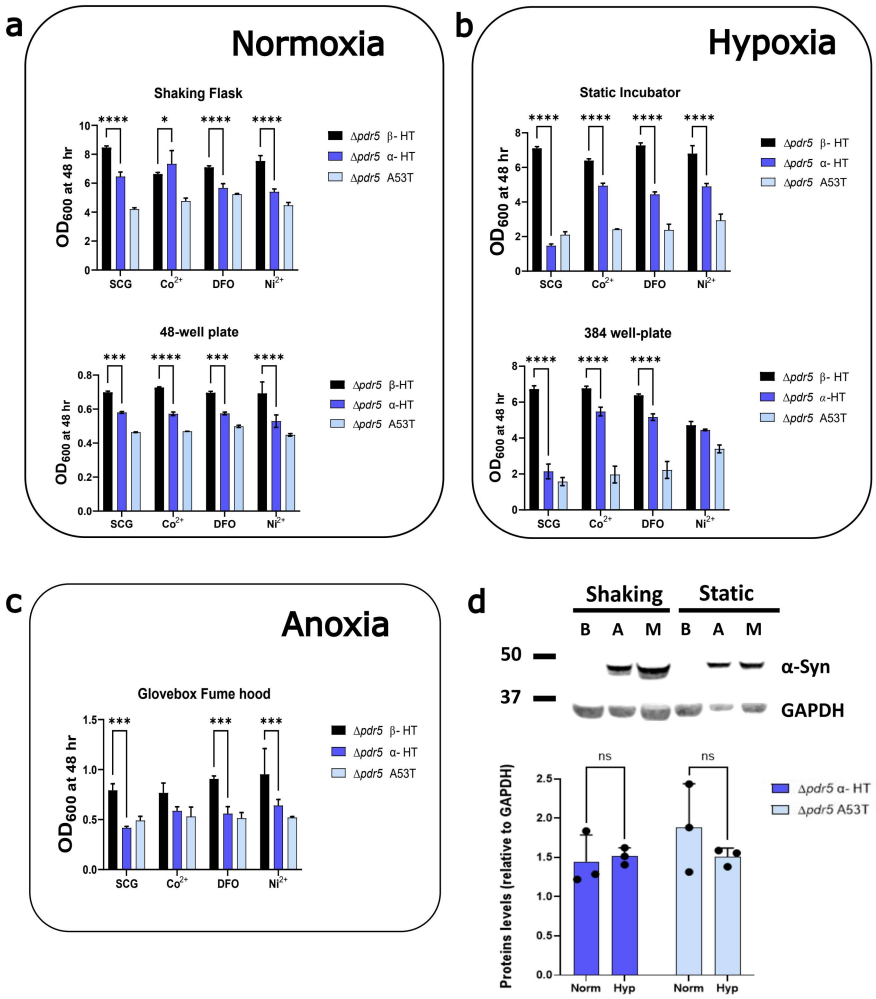

Figure 3.2: a. Yeast cultivation in Normoxia condition was performed in two different cultivation formats: shaken flasks and 48-well plate. For the shaken flasks, the β-HT, α-HT and A53T-HT strains were cultivated in Erlenmeyer flasks incubated at 30°C in a shacking incubator set at 200 rpm. For the 48 well-plate experiments, the same three strains were inoculated into a 48 well-plate and monitored using a Tecan Infinite 200 PRO spectrophotometer. **b.** Yeast cultivation in Hypoxia condition was performed as well in two different cultivation formats: Static incubator and 384 well-plate. For the static incubator, the Erlenmeyer flasks were incubated at 30°C in a static incubator (0 rpm). The 384 well-plate was monitored through Tecan Infinite 200 PRO spectrophotometer. **c.** Yeast cultivation in anoxic conditions was performed by incubation in the controlled atmosphere of the Glovebox GBoxT2 (Jacomex). **d.** Western blot analysis and relative bond intensity quantification performed at 24 hours on the protein content extracted from the β-HT, α-HT and A53T-HT strains cultured in normoxic (shaking cultivation at 200 rpm) and hypoxic (static cultivation at 0 rpm) conditions. Each bar in **d** is the mean +/- SDs of biological triplicates. For the statistics, two-way ANOVA test for multiple comparisons was applied and corrected using the Šidák statistical hypothesis.*, adjusted p-value = 0.032; ***, adjusted p-value =0.0002; ****, adjusted p-value < 0.0001.

3.3 Stable α-syn expression across treatment conditions

To test the hypothesis that Co^{2+}, Ni^{2+} and DFO directly reduce the expression level of α-syn in the cell, inducing the observed rescue effect, we performed a Western blot analysis on yeast cells after 8 hours of induction of both wild-type and A53T mutated forms of α-syn in the presence and absence of the three compounds (Figure 3.3 **a** and **b**). The quantification of α-synuclein, normalized to the GAPDH loading control, showed no significant change in α-syn levels upon treatments (Figure 3.3 **c**). Considering that Co^{2+}, Ni^{2+} and DFO do not directly affect the expression level of the protein in the cell, we next wanted to test if they reduce the number of α-syn aggregates performing fluorescence microscopy and time-lapse analysis. Exploiting the GFP tag fused at the C-terminus of the protein, we could visualize and track *in vivo* the aggregates of α-syn in the cell.

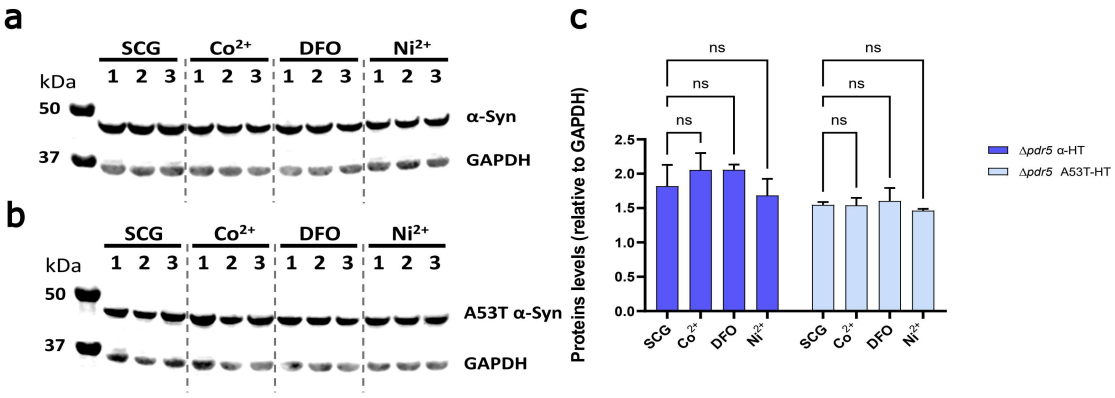

Figure 3.3: a and b. Western blot analysis performed at 8 hours of α-syn induction on the protein content extracted from the α-HT and A53T-HT strains treated and not with 0.3 mM of Co^{2+}, Ni^{2+} or DFO, respectively. **c.** Relative band intensity quantification. Each bar is the mean +/- SDs of biological triplicates. For the statistics, a two-way ANOVA test for multiple comparisons was applied and corrected using the Šidák statistical hypothesis.

3.3.1 Cobalt, Nickel and Deferoxamine significantly reduce α-syn aggregates in yeast cells

We assessed the capability of Co^{2+}, Ni^{2+} and DFO to reduce α-syn aggregation, quantifying the number of fluorescence aggregates present inside the cells. This was possible by acquiring *in vivo*

images of the α-HT cells using a fluorescence microscope set up as explained in section 2.5 of the chapter Materials and Methods. Upon inducing α-syn aggregation for $\sim$ 16 hours, in the presence and absence of the treatments, the cells show a different number of aggregates (Figure 3.4 **a** to **d**). 45% of the cells show intracellular inclusions in the untreated condition (Figure 3.4 **a**). Interestingly, when incubated with cobalt (Figure 3.4 **b**), deferoxamine (Figure 3.4 **c**), or nickel (Figure 3.4 **d**) the percentage of aggregates over the total number of cells significantly decreases to 20%. The decreased toxicity and percentage of cells with aggregates do not correlate with a reduced expression level of α-syn, as previously shown.

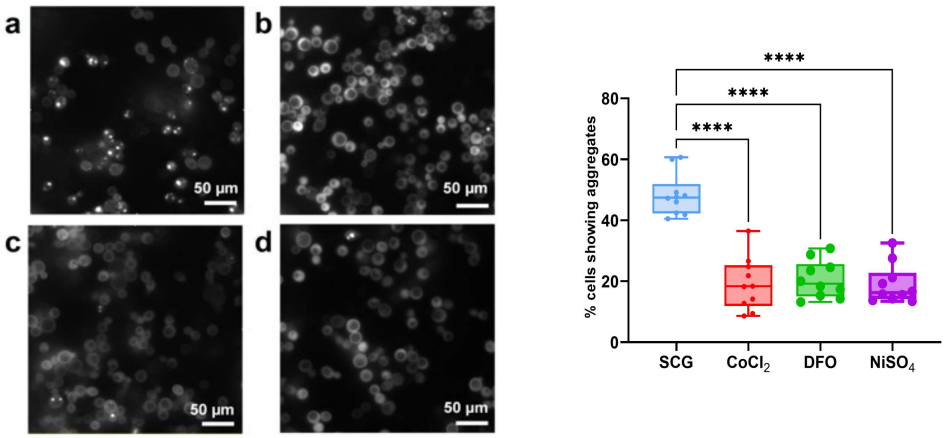

Figure 3.4: Fluorescence microscopy of yeast cells expressing αSyn-GFP acquired with 100x objective (+ 0.5X magnification) and Xenon laser. After 16 hours of induction in hypoxia conditions, the protein forms bulky aggregates in the cytoplasm (untreated) (**a**). The number of cells with protein aggregates decreased when the cells were treated with 0.3 M of Cobalt (**b**), deferoxamine (**c**) or nickel (**d**). 10 images for each condition were processed using ImageJ software. The number of aggregates and cells was counted with the Cell Counter plugin. For all four considered conditions, the ratio of the number of aggregates over the number of cells was plotted as a boxplot using the GraphPad Prism software. A one-way ANOVA test for multiple comparisons was applied. ****, P value < 0.0001

3.3.2 Time-lapse analysis

The α-syn inclusion formation and clearance in the α-HT strain untreated and treated with Co^{2+}, Ni^{2+} or DFO were quantitatively analyzed by time-lapse microfluidic experiment. A previous experiment performed on a similar yeast model engineered to express wild-type and A53T form of α-syn demonstrated that the formation of aggregations in live cells is not time-dependent, but

it is more based on a phase transition event in which the protein will start to aggregate after overcoming a specific concentration threshold[447]. The experimental set-up used in our work is slightly different as the microfluidic plate is not automated and the α-syn expression is not regulated but constantly induced during all of the experiment. The number of α-syn aggregates accumulated in the untreated α-HT were $\sim$ 20 over 24 hours (Figure 3.5 **untreated, red plot**). Treatments significantly reduced the number of aggregates to 5 at the same time point (Figure 3.5 **Co^{2+}, Ni^{2+} and DFO, red plots**). Co^{2+} and Ni^{2+} delay the formation of the aggregates which appear around 12 hours, whereas, in the untreated condition, a rapid increase in aggregates is observed after just 6 hours (Figure 3.5 **untreated, red plot**). The trends observed for the number of aggregates were also reflected in the total aggregate area. In the presence of treatments, the aggregates area (μm^2) decreased from the maximum value of 25.7 μm^2 measured in the untreated to 2.43 μm^2 in Co^{2+}, 3.89 μm^2 in DFO and 1.61 μm^2 in Ni^{2+} (Figure 3.5, **blue plots**). The plots of aggregate size showed some noise in the first 7 hours due to the merging and dissolution of aggregates and overall it was not significantly affected by the treatments. The maximum values measured at 24 hours were 0.82 μm in the untreated, 0.72 μm in cobalt, 0.48μm in deferoxamin and 0.56 μm in nickel, respectively (Fig 3.5 **black plots**).

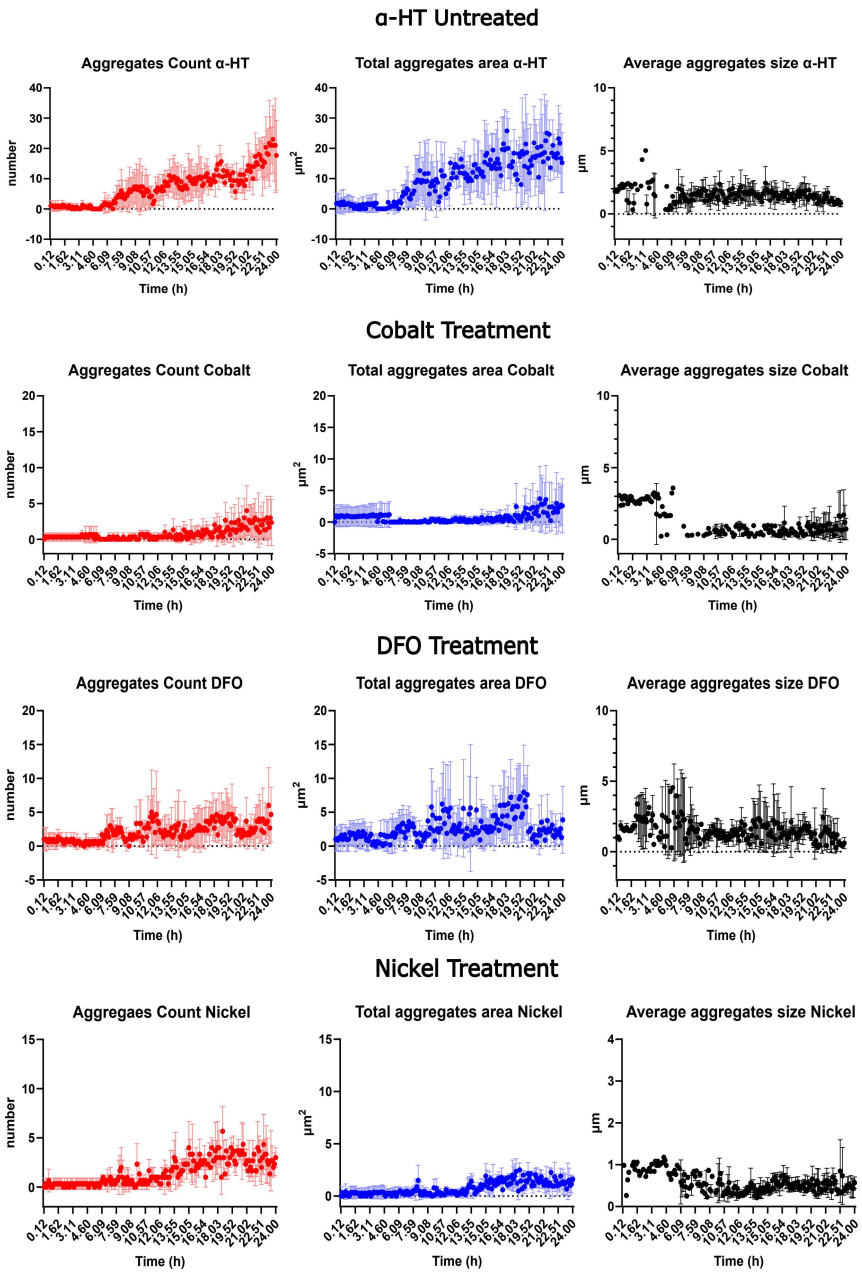

Figure 3.5: The formation and clearance of α-syn aggregates in cells, cultured both with and without the three treatments, were monitored over 24 hours. **Red plots**. Number of α-syn aggregates accumulated in the α-HT over time. In the untreated condition (α-HT untreated), a higher amount of α-syn aggregates accumulated compared to the treated strain. **Blue plots**. Total area of α-syn aggregates, which is directly proportional to the number of aggregates present in the cells. **black plots**. Average α-syn aggregates size (diameter). This value fluctuates significantly due to ongoing events of aggregate formation and fusion. Each bar represents the mean $\pm$ SDs (lighter bars) of biological triplicates.

3.3.3 Aggregates count normalization

To better understand the kinetics of aggregation and dissolution, the count values previously obtained were normalized by the number of cells. Since none of the filter masks available in ImageJ could efficiently count the cells, this value was estimated by dividing the total area occupied by cells (measured by the software) by the average area of a single cell, calculated based on the cell size (diameter) in the analyzed conditions. A time course of the cell count for each condition is provided in Figure 5.3 (Appendix). The aggregation kinetics observed in the untreated cells (Figure 3.6 **a**) follow a profile similar to that reported in α-syn seed amplification assays performed on cerebrospinal fluid samples of PD patients[448, 449]. Both the aggregate count and aggregate area plots (Figure 3.6 **a**) shown a characteristic sigmoidal pattern (Figure 3.6, **a, red dash-dot line**). The initial lag phase of the curve is partially masked by the fluorescence signal from pre-existing α-syn aggregates. This is because the protein expression was induced 6 hours before the experiment to properly set the focus during fluorescence acquisition. The lag-phase is followed by a growing phase in which α-syn monomers are rapidly incorporated in the forming inclusions. In this phase, there is an increasing number of aggregates per cell which fuse in more bigger structures that enter a stationary phase between 7 and 9 hours. In the cytoplasm, the aggregates acquire their maximum size and compromise the survival of the affected cells which died leading to the decline in the number of aggregates per cell observed after 10 hours. Around this time, the observation chamber is almost completely populated or the colony stops to divide. Co^{2+} (Figure 3.6 **b**), DFO (Figure 3.6 **c**) and Ni^{2+} (Figure 3.6 **d**), have different kinetic trends compared to the untreated strain (Figure 3.6 **a**). The sigmoidal kinetics observed in the α-HT strain is characterized by an initial rapid phase of aggregate formation followed by a phase in which the cells with aggregates die while the colony continues to divide. This pattern is not present in the kinetics of the treatments. Co^{2+} (Figure 3.6 **b**) shows its protective effect in the first 6h, clearing all the aggregates in the cells and preventing the formation of new ones. DFO (Figure 3.6 **c**) significantly reduces the number of aggregates, though it does not completely prevent their formation like cobalt. In the deferoxamine treatment, a few small aggregates appear until 12 hours. Ni^{2+} (Figure 3.6 **d**) is also effective in the first 7 hours; however, the persistent minimal fluorescence signal in both aggregate count and area suggests that α-synuclein oligomers do not

cluster into large aggregates but remain mostly diffuse within the cell. Overall all the treatments decrease the size of α-syn aggregates.

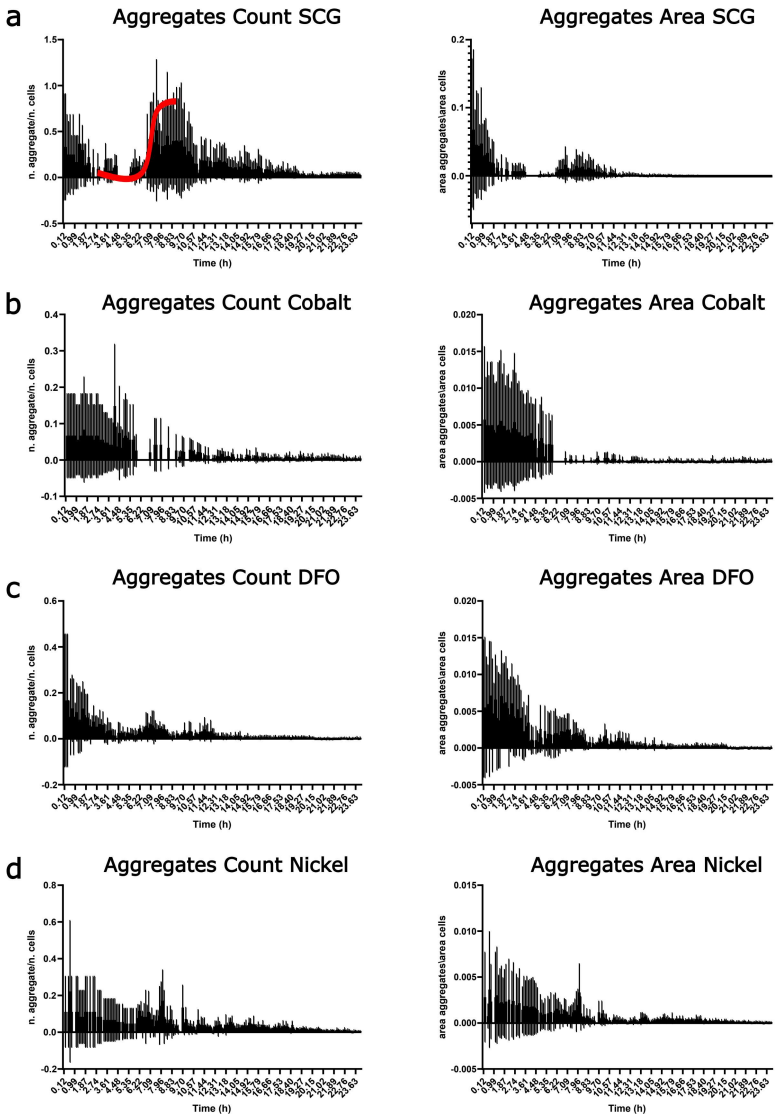

Figure 3.6: The "Aggregates Count" and "Aggregates Area" plots are obtained by normalizing the number and area of α-syn aggregates to the cells count and cell area, respectively. The normalized number of aggregates and aggregate area (black bars) for each time point are displayed for the untreated α-HT strain grown in SCG media **a** and in SCG media supplemented with 0.3 mM of Co^{2+} **b**, DFO **c**, and Ni^{2+} **d**. In the Aggregates Count plot for the untreated α-HT condition, a red dotted line represents the sigmoidal trend of α-syn aggregation. Each bar represents the mean $\pm$ SDs (dark gray bars) of biological triplicates.

3.4 Siderophores rescue α-syn toxicity

Compounds screening performed on the α-HT revealed that DFO, an iron chelator, effectively rescues the toxicity induced by α-syn expression. The protective effect of siderophores against pathological aggregation of α-syn has been reported in several PD models[450, 451, 452, 453]. Compared to the other siderophores, DFO cannot passively cross biological membranes due to its high hydrophilicity [454]. Instead, it is internalized through pinocytosis mediated by the Sit1 receptor[455]. Inside the cell, DFO is transported to the lysosome, where the acidic pH deprotonates all the three hydroxamate groups, enabling them to complex the Fe^{3+}[456, 457] (structure in Figure 3.7 **a**). In humans, the lysosomal iron content is generated from the transferrin degradation, while in yeast iron is internalized from the cytoplasm through specific vacuolar transporters. By sequestering iron inside the vacuole, DFO may reduce the metal availability in the cytosol, preventing iron from contributing to the formation of α-syn aggregates. This may justify the reduced number of α-syn aggregates and the growth rate improvement observed in the α-HT strain treated with DFO. To test this hypothesis α-HT and A53T-HT were treated with the three siderophores reported in Figure 3.7 **a**. These compounds have different cellular internalization mechanisms and they chelate iron in specific iron-ligand ratios (Figure 3.7).

- Deferiprone (DFP) is a bidentate oral iron chelator, which chelates Fe^{3+} forming stable 3:1 complexes[458, 459] (structure in Figure 3.7 **a**). Due to its small size and lipophilic nature, DFP can easily cross the cellular membranes by passive diffusion[460]. It is rapidly metabolized by the cytochrome P450 system and excreted in the urine within 2-3 hours[461]. DFP transfers iron to higher-affinity chelators such as desferrioxamine or transferrin[462].

- Desferrithiocin (DFT) is a tridentate iron chelator, which binds Fe^{3+} in a 2:1 ratio[463] (structure in Figure 3.7 **a**). DFT is larger and less lipophilic than DFP, it can cross the cellular membranes by passive diffusion but at a slow rate. Among the siderophores, it has a long half-rate of 16 hours[463] and higher toxicity as it is eliminated by the kidney where it can generate nephrotoxicity[464].

A phenotypic assay was performed to evaluate the effect of DFO, DFP and DFT on α-syn toxicity

in yeast. DFO and DFP were tested at 0.3 mM, while DFT was tested at 60 μM due to its toxicity at higher concentrations. Similarly to the experimental set-up used for the compounds screening, the expression of wild type and A53T mutant form of α-syn was induced by cultivating the cells in SCG media, with and without DFO, DFP, and DFT supplementation. According to the OD_{600} measured at 48 hours, DFO and DFT were found to rescue the growth of α-HT (Figure 3.7 **b**). Interestingly, DFT, at the low tested concentration, also demonstrated a significant positive effect on the A53T mutant, resulting in a 3-fold increase in its OD_{600} (Figure 3.7 **b**).

This result supported what is reported in the literature about the neuroprotective effect of siderophores[465], some of which are currently being evaluated in clinical trials for the treatment of PD[466].

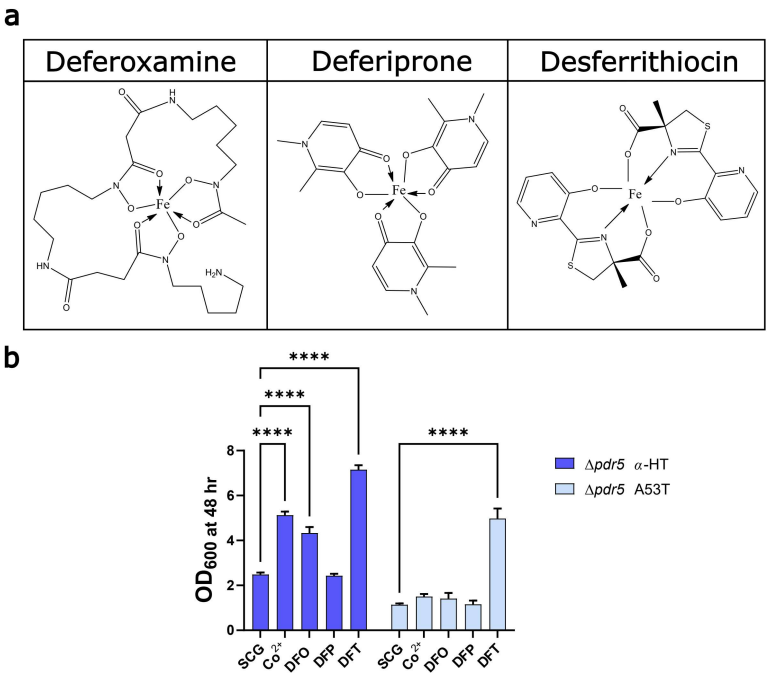

Figure 3.7: In the table, the chemical structure of the siderophores Deferoxamine (DFO), Deferiprone (DFP) and Desferrithiocin (DFT). The three molecules are represented in the Fe^{3+} chelated form as reported in the publication of Salimi et al.[467]. In DFO, the three hydroxamic groups coordinate the Fe^{3+} ion. Three molecules of DFP are required to stabilize one ion of Fe^{3+}. The amino, the hydroxy and the carbonyl group of two molecules of DFT are required to bind the Fe^{3+} ion. OD_{600} measured at 48 h for the α-HT and A53T-HT grown in SCG media supplemented with 0.3 mM of DFO and DFP, and 60 μM of DFT. Each bar is the mean +/- SDs of biological triplicates cultured in a 384-well plate. For the statistics, two-way ANOVA test for multiple comparisons was applied and corrected using the Dunnet statistical hypothesis. ****, adjusted p-value < 0.0001.

3.4.1 Effect of metal ion chelators on α-syn toxicity

The alteration of iron homeostasis in synucleinopathies has long been an interesting research topic, since the discovery of abnormal iron deposits in the *substantia nigra* of Parkinson's disease patients. The protective effect observed upon treatment with the iron chelators DFO and DFT in our yeast model highlighted the connection between iron and pathological aggregation of α-syn. Other bivalent ions have been proven responsible for the protein destabilization and aggregation[468]. To confirm that the rescue observed in this study is specific to iron chelation, different commercial metal ions chelators were considered. The selected compounds, listed in Table 3.1, have a broader or higher specificity for the metal ions that are biologically abundant. The

expression of the human proteins was induced by cultivating the cells in SCG media supplemented and not with EDTA, triglycine, TTM, TEPA and TPEN tested at nM and μM concentrations as shown in Figure 3.8. All the compounds were stable in the cultivation media and they were respectively tested on the β-HT and α-HT strains. According to the OD_{600} measured at 48 hours, triglycine and TEPA do not induce toxicity in the cells at the tested concentrations and neither alleviate the toxicity of α-syn. EDTA, TTM and TPEN do not positively affect the growth of α-HT, either. Moreover, these three compounds become toxic at certain concentrations in both β-HT and α-HT strains. In particular, TTM and TPEN show toxicity already at low μM concentrations and require to be tested in the nM range (Figure 3.8).

Iron has an important effect on α-syn, it binds to the C-terminus of the protein promoting its aggregation[109, 469]. In this perspective, α-syn could work as an iron chelator forcing the cell into iron starvation. Siderophores, which are natural iron-binding molecules with a higher affinity for iron than α-synuclein[239, 470], can effectively sequester iron from the assembling aggregates and make it available for the cell. Alternatively, DFO can improve iron availability by supplying the cell with exogenous iron, which could restore iron-dependent enzymes and processes affected by the iron deprivation induced by α-syn. To uncover the role of iron in the α-HT, we supplemented the SCG cultivation media with different concentrations of iron. To prevent the tendency of the metal to oxidize to Fe^{3+} and precipitate during the OD_{600} monitoring, cells were incubated at the same time with 100 μM ascorbate. This compound works as a reducing agent, enhancing the conversion of Fe^{3+} to Fe^{2+}, the more bioavailable form of the metal. Three concentrations of iron were tested on β-HT, α-HT and A53T-HT strains, corresponding to 50 μM (low), 100μM (optimal), 200μM and 300μM(high) in the presence of 100μM ascorbate (Figure 3.8), as previously reported for yeast[471]. The same strains were also cultivated with 100 μM ascorbate alone to exclude any potential contributions induced by this iron reductant (Figure 5.4, Appendices). Furthermore, to test the ability of DFO to sequester iron from α-syn aggregates or to provide the cell with exogenous iron, we cultivated the strains in the presence of DFO alone and DFO chelated with 100 μM Fe^{3+} (Figure 3.8). In this case, it was not require to add ascorbate as DFO binds to the metal ion preventing its precipitation in the cultivatium media. Decreasing in

OD_{600} measurements at 48 hours for high iron concentrations indicates that iron supplementation is harmful for α-HT and A53T-HT compared to β-HT control. Interestingly, the protective effect of DFO is completely lost when chelated with 100μM iron. While microorganisms synthesized siderophores to acquire iron from the external environment, an increase in iron influx appears to be toxic for α-HT and A53T-HT (Figure 3.8). These results may suggest that the chelating activity of DFO primarily occurs within the cell.

Chelator	Ion specificity
Ethylenediaminetetraacetic acid (EDTA)	EDTA is a versatile chemical reagent extensively used across various fields. It is a cell wall and membrane permeabilizing agent used in solvent and buffer preparation due to its remarkable ability to chelate a wide range of divalent cations (EDTA applications are reviewed in [472]). It forms stable complexes with numerous metal ions[473, 474]: (Fe^{2+}/Fe^{3+}), magnesium (Mg^{2+}), copper (Cu^{2+}), cobalt (Co^{3+}), zinc (Zn^{2+}) and lead (Pb^{2+}). More information regarding the EDTA binding affinity at [472, 473, 474]
Triglycine (Gly-Gly-Gly)	Tripeptide of the amino acid glycine that can bind Mg^{2+}[475]
Ammonium tetrathiomolybdate (TTM)	TTM is a Cu^{2+} chelator used for the treatment of Wilson's disease[476]. It prevents copper absorption, forming with the metal a tripartite complex excreted in the urine[477]
Tetraethylenepentamine pentahydrochloride (TEPA)	It is a cell-permeable chelating agent that has a stronger ability to bind Cu^{2+} in water solutions[478, 479].
(N,N,N',N'-tetrakis(2-pyridinylmethyl)-1,2-ethanediamine (TPEN)	TPEN is a cell-permeable Zn^{2+} chelator used in biological studies to limit the availability of this metal ion in the cellular medium[458, 480]

Table 3.1: Metal ions chelators stable in synthetic complete media

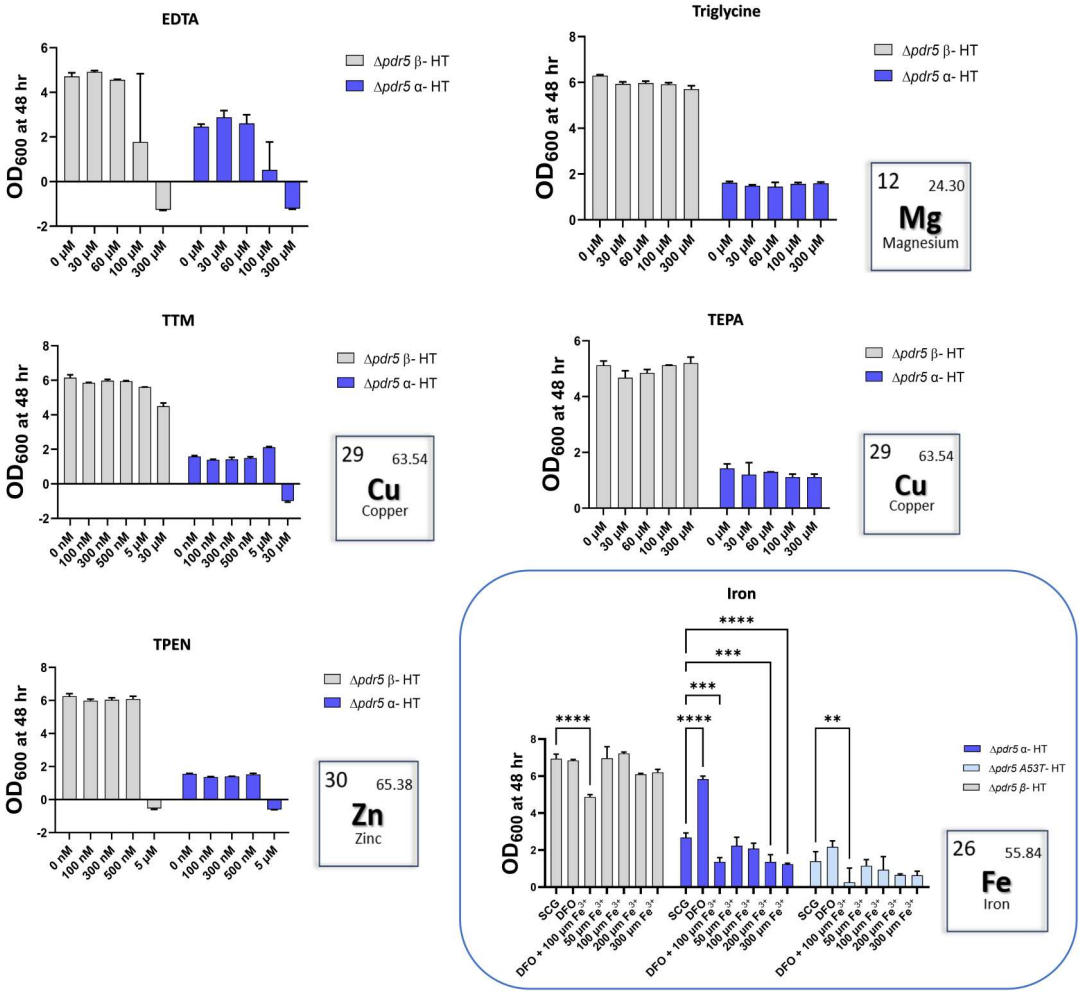

Figure 3.8: Dose response curves obtained incubating the α-HT strain with different concentration of metal ion chelators. The tested compounds are listed in Table 3.1 and reported in the title of each bar plot. The metal ion was reported for all the tested chelators except for EDTA, which complexes a wide range of metal ions. EDTA, Triglycine and TEPA were tested in μM concentrations range, while because of their toxicity, TTM and TPEN were tested at nM range. Fe^{3+} was tested at 0 (SCG), 50, 100, 200 and 300 μM concentration in the presence of 100 μM ascorbate. The chelated form of Fe^{3+} with DFO was also tested, revealing an increase in toxicity compared to the rescue induced by the unchelated molecule (100 μM ascorbate was not supplemented in the presence of DFO). Each bar is the mean +/- SDs of biological triplicates. For the statistics, a two-way ANOVA test for multiple comparisons was applied and corrected using the Dunnet statistical hypothesis. **, adjusted p-value 0.001; ***, adjusted p-value = 0.0002; ****, adjusted p-value < 0.0001.

3.4.2 Alteration of iron homeostasis in the α-HT strain

The α-syn ability to complex iron within its aggregates was assessed by staining the cell with Rhodamine B (C.I. 45170). This fluorescence dye was reported to be efficient for the iron content staining in yeast cells[432]. The expression of the human proteins was induced by cultivating in SCG media and before the microscopy image acquisition, the cells were stained as reported in section 2.7 of the Materials and Methods chapter. Aggregates of the GFP-tagged α-syn emitted green fluorescence under 488 nm excitation, while Rhodamine B exhibited orange fluorescence when excited at 578 nm. In the β-HT, GFP and Rhodamine B fluorescence signals are mostly diffuse inside the cell and no aggregates are detected (Figure 3.9 **a**). In the α-HT, the rhodamine B staining overlaps the GFP signal of the α-syn aggregates, suggesting that iron is trapped in the protein aggregates (Figure 3.9 **b**).

Our experimental results support the iron contribution to the toxicity of α-syn, but do not clarify to which extent the pathological aggregation of the protein affects the iron metabolism of the cell and if it induces an iron starvation response. The transcriptomic profiling performed in this study on the α-HT compared to the β-HT can clarify these doubts and give some hints regarding the protective mechanism activated by DFO. In yeast, "iron deficiency response" is mediated by Aft1 and Aft2 transcription factors, which activate the expression of iron transporters on the membrane, promoting the metal uptake (Figure 3.9 **c**). The expression levels of these two transcription factors remained unaffected in α-HT. Interestingly, YAP5 the transcription factor of the genes involved in the "iron overload response" is downregulated in the α-HT strain compared to the β-HT control at 12 hours (a more detailed explanation of the genes deregulated in the α-HT strain will be provided in section 3.5.2). To understand which genes involved in iron metabolism are affected by DFO treatment, we performed a gene association analysis on the 50 genes specifically upregulated by DFO compared to the β-HT control at 12 hours using the open-source tool GeneMANIA (https://genemania.org/). We identify an interesting cluster around Yap5 (Figure 3.9 **d**), which includes proteins involved in DNA Repair (Cmr1, Smc5, Mms4, Cdc13, Dal4 and Tah11); protoporphyrin and heme transport (Pug1); dolichol biosynthesis (Sec59); protein sorting (Syg1) and degradation (Apj1); meiotic recombination (Mei5). These results suggest that the

DFO rescue is mostly due to the activation of DNA repair proteins which seem to interact with the Yap5 transcription factor.

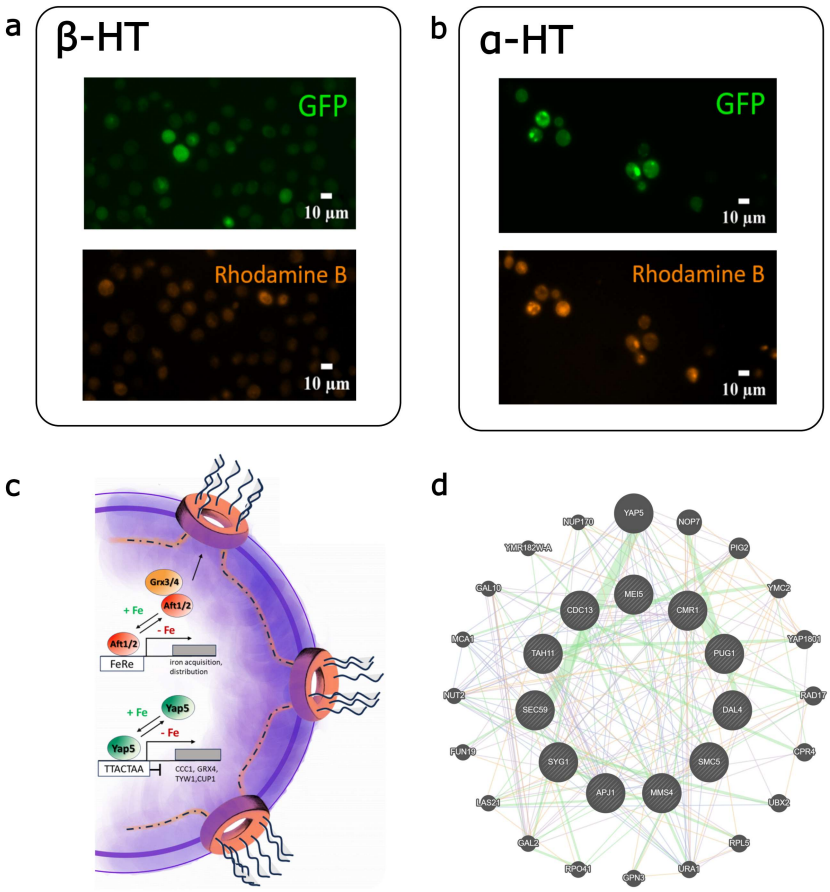

Figure 3.9: **a** Fluorescence microscopy images of β-HT: The top panels display the green fluorescence of the GFP tag fused to the C-terminus of the β-syn protein, while the bottom panels show the orange staining from rhodamine B. In both cases, the signals appear mostly diffuse inside the cell. **b** Fluorescence microscopy images of α-HT: The top panels show the green fluorescence of the GFP tag fused to the C-terminus of the α-syn protein, with the bottom panels illustrating the orange rhodamine B staining. In both images, the protein aggregates exhibit overlapping signals. **c** In the nucleus, the transcription factors Aft1 and Aft2 initiate the "iron deficiency response", leading to the transcription of membrane iron importers. On the opposite, the transcription factor Yap5 triggers the "iron overload response" which induces the metal storage in the vacuole. **d** Gene interaction network generated by GeneMANIA for the 50 genes specifically upregulated by DFO treatment compared to the β-HT control at 12 hours. Key genes involved in DNA repair mechanisms, such as MR1, SMC5, MMS4, CDC13, DAL4, and TAH11, seem to interact to Yap5.

3.5 Transcriptomics analysis in the HiTox Strains

In this study, we examined the differences at the transcriptomic level in 15 yeast samples, including two control groups: HTC and β-HT, one disease group represented by the α-HT strain, and two treatment groups, respectively exposed to 0.3 mM Co^{2+} and DFO. Each considered group consists of 3 independent biological samples (n = 3). All the details regarding strain cultivation, RNA extraction, and data processing are reported in the chapter Materials and Methods of this thesis.

3.5.1 β-HT vs HTC

RNA-seq analysis was performed in R studio software (version 4.1.1), using the DeSEQ2 package to identify the differentially expressed genes (DEGs), based on the following thresholds: log2-based fold change $|log2FC| > 1$ and adjusted P-value < 0.05. We first compared the two control strains: β-HT and HTC Figure 3.11. The β-HT was generated by the heterologous expression of human β-syn, the α-syn homolog devoided of the NAC hydrophobic core and so less prone to aggregate. This analysis elucidates to which extent the expression of the human protein affects yeast cell biology and if β-HT can be used as a valid control in the experimental part of this study.

28 and 328 significant DEGs were identified after 6 and 12 hours of β-syn overexpression, respectively (Figure 3.11 **a**). Pathway enrichment analysis indicated that the biological processes most affected in the β-HT were relative to ER (GO:0005789), DNA binding (GO:0003677), protein transportation (GO:0015031) and cell cycle (GO:0007049) (Figure 3.11 **b**). To explore which genes involved in the highlighted biological processes are affected by the expression of β-syn, we first generated a volcano plot at 12 hours (Figure 3.11 **c**). The gene expression profile is mostly dominated by the auxotrophic selection markers: URA1, URA2, URA3 and TRP1. In particular, the most up and down-regulated genes are URA1 and TRP1, involved in the uracil and tryptophan biosynthesis, respectively. This result is probably due to the "position effect" consequential to the integration of a GFP-tagged recombinant transcript in a host genomic region with a high density of essential genes [481]. At 12 hours, the number of DEGs upregulated is 279 while the downregulated DEGs are 49 (Figure 3.11 **a**). The huge discrepancy suggested that the expression

of β-syn induces more gene expression than downregulation in the cell. We restricted the pathway enrichment to the upregulated genes (Figure 3.11 **d**), finding that the main activated function in the cell is oxidoreductase activity (GO:0016491). Among the members of this large group, various dehydrogenases, particularly IMD1-2, TDH1, and MAN2, are the most significantly upregulated at 12 hours (a complete Table with all the genes associated with the oxidoreductase activity is reported in the Appendices, see Table 5.10). We conclude that the expression of the human GFP-tagged protein in yeast cells activates oxidative stress, however, it does not affect vital biological processes such as DNA duplication, chaperone-mediated protein folding and the secretory pathway. The cell activates the cellular response mechanism to oxidative stress, upregulating genes such as Hsp30, Hsp12, Hsp26, Hsp104, Ddr2 and Gpx1.

The DEGs mentioned in this chapter are reported in the Table 3.2.

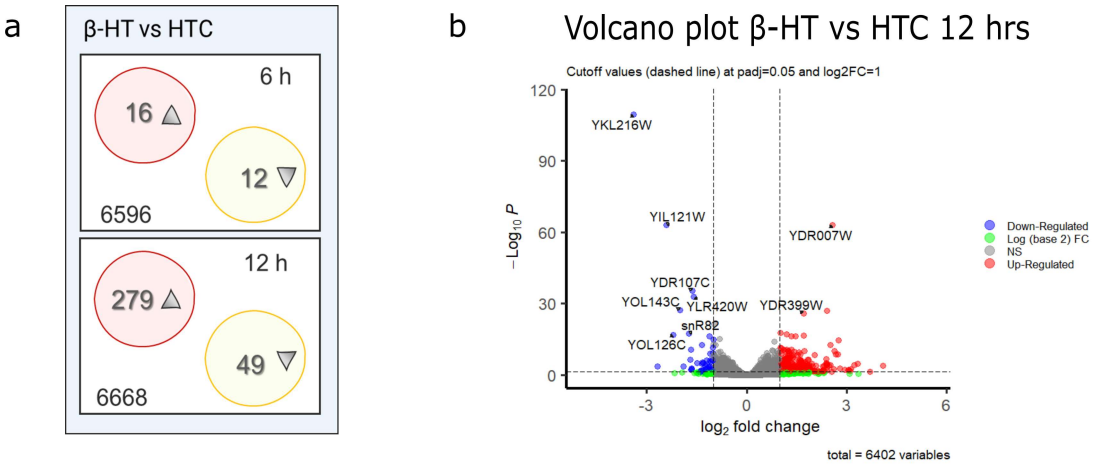

Figure 3.10: **a** Venn diagram showing the significantly differentially expressed genes up-regulated (red) and down-regulated (yellow) at 6 and 12 hours time points. **b** Volcano plot of the DEGs measured for the 12 hours time point in the binomial comparison β-HT vs HTC. The transverse axis represents the log2-based fold change (log2FoldChange), while on the vertical axis is reported the negative log10-based p-adjusted value ($-Log10P$). Red, upregulated genes with a log2FoldChange > 1; blue, downregulated genes with a log2FoldChange < -1.Green, not significant genes up- and downregulated. DEG, differentially expressed gene.

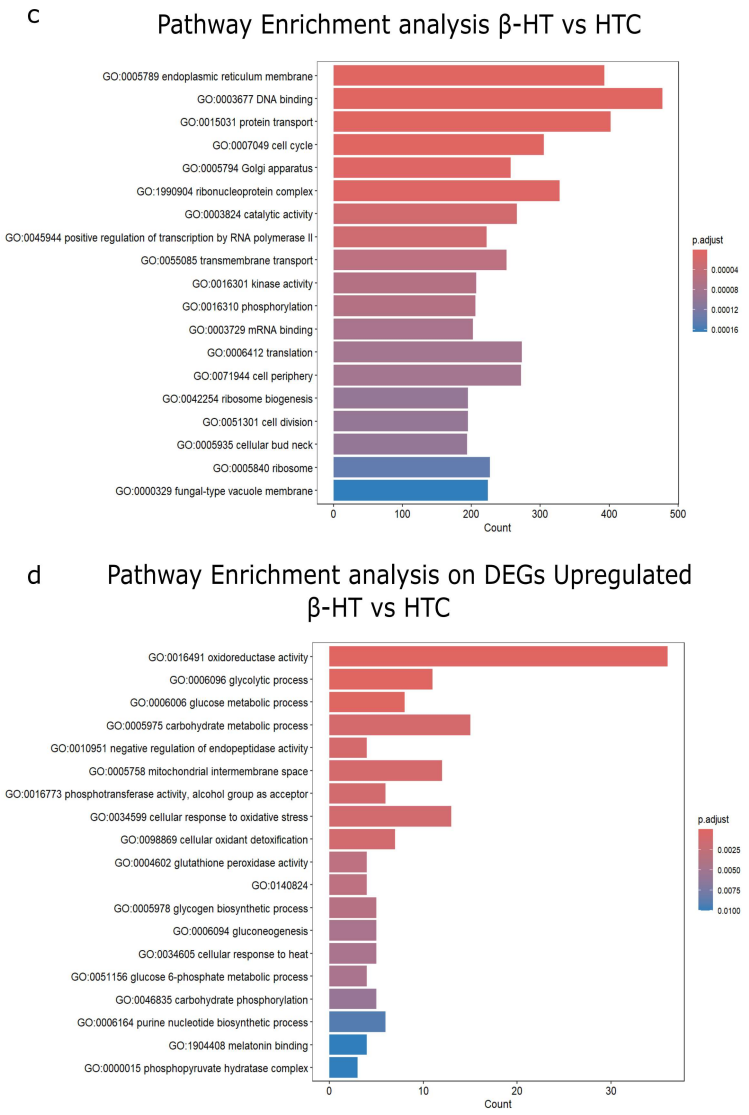

Figure 3.11: Bar plots showing Gene Ontology analysis results of **c** DEGs with a p-adjust < 0.05; **d** upregulated DEGs with a p-adjust < 0.05. The color of each bar represents the p-adjust of each term involved in the analysis. The size of each bar represents the gene counts of this term involved in the analysis.

Table 3.2: DEGs in the β-HT strain compared to the HTC control at 12 hours.

β-HT vs HTC			
Gene	Enzyme	Log2FoldChange	padj
YKL216W	URA1	-3.38	4.10E-110
YJL130C	URA2	-1.67	0.005
YEL021W	URA3	2.41	1.13E-27
YDR007W	TRP1	2.57	1.04E-63
YAR073W	IMD1	2.62	5.57E-11
YHR216W	IMD2	2.74	2.32E-15
YNR073C	MAN2	2.38	7.86E-06
YJL052W	TDH1	2.41	0.0008
YCR021C	HSP30	3.12	0.002
YCR021C	HSP30	3.12	0.002
YFL014W	HSP12	1.36	0.004
YBR072W	HSP26	2.38	4.25E-05
YLL026W	HSP104	1.08	0.003
YOL052C-A	DDR2	1.41	0.0002
YKL026C	GPX1	1.95	2.19E-05

3.5.2 Impact of α-syn expression on the Transcriptome

The differential expression analysis between α-HT and β-HT leads to different results compared to the previous one between the two control groups. Based on the predefined cut-off criteria established for this analysis (log2-based fold change $|log2FC| > 1$ and adjusted P-value < 0.05), 43 and 728 significant DEGs were identified after 6 and 12 hours of α-syn expression. At 6 hours, the DEGs significantly upregulated in α-HT compared to β-HT control are 20 while the downregulated are 23 (Figure 3.12 **a**). At 12 hours, the list of genes affected by α-syn overexpression increased to 259 upregulated and 523 downregulated (Figure 3.12 **a**). The pathway enrichment analysis reveals the alteration of the same biological processes observed for the β-HT vs HTC comparison with the main difference of the DNA repair response (GO:0006281) activated in the α-HT, suggesting the presence of important DNA damages completely absent in the β-HT strain (Figure 3.12 **b**).

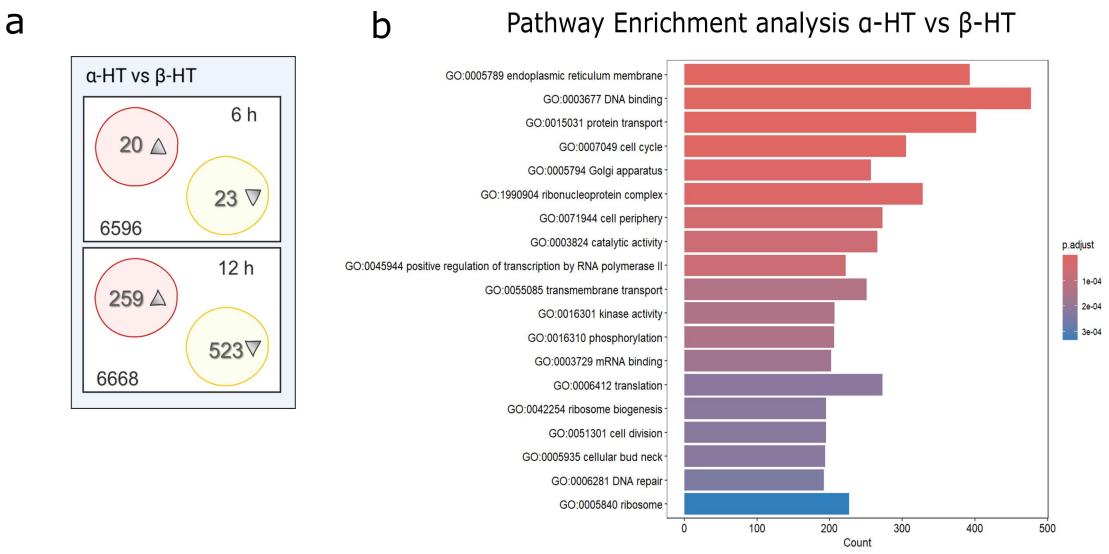

Figure 3.12: **a** Venn diagram showing the significantly differentially expressed genes up-regulated (red) and down-regulated (yellow) at 6 and 12 hours time points. **b** Bar plots showing Gene Ontology analysis results of DEGs at 12 hours with a p-adjust < 0.05 in the comparison α-HT vs β-HT.

To understand which genes dominate the transcriptional differences we generated volcano plots at 6 and 12 hours (Figure 3.13 **a** and **b**). At 6 hours, genes involved in misfolding protein re-

sponse (ULI1 and KAR2), cell wall remodeling and stability (NCW2), and iron uptake (FIT3) are upregulated. Moreover, genes triggered by low oxygen and heme levels (RTA1 and PAU5) are also more highly expressed. In contrast, key genes of 1C metabolism (MET6, MET17 and SAM1) and ergosterol biosynthesis (ERG5) are downregulated. Unexpectedly, we observed that INO1 is one of the DEGs significantly upregulated in the α-HT already after 6 hours. This gene encodes for inositol-3-phosphate synthase[482], the enzyme that catalyzes the rate-limiting step of phosphoinositide biosynthesis in eukaryotes[483]. INO1 expression is highly regulated by two positive modulators, INO2 and INO4, and one negative represented by OPI3[484]. During the lag phase, INO1 is repressed as the cell relies on inositol 1-phosphate available in the medium[484]. Considering the canonical expression profile of this gene and the importance of its activity for membrane stability, it was interesting to find it upregulated when the cell is still in the lag phase. The DEGs respectively up and downregulated at 6 hours are listed with the relative functions in Table 5.4 and Table 5.5 reported in the Appendices section.

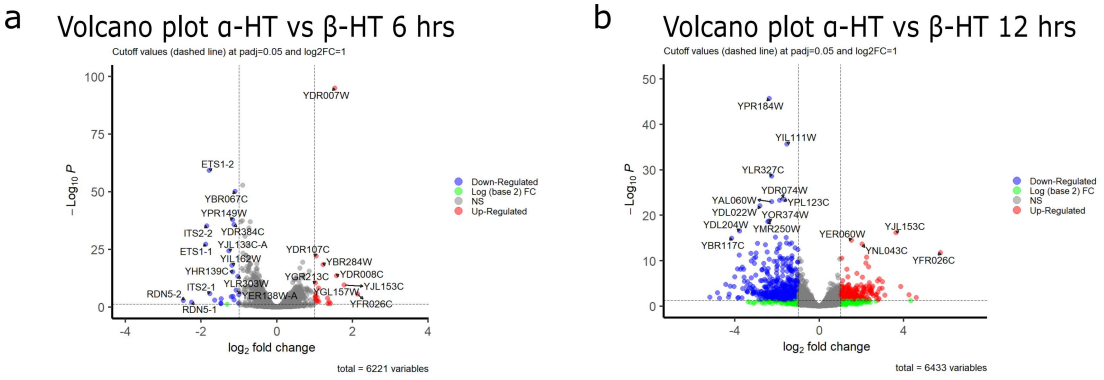

Figure 3.13: Volcano plot of the DEGs measured for the 6 **a** and 12 hours **b** in the binomial comparison α-HT vs β-HT. The transverse axis represents the log2-based fold change (log2FoldChange), while on the vertical axis is reported the negative log10-based p-adjusted value ($-Log10P$). Red, upregulated genes with a log2FoldChange > 1; blue, downregulated genes with a log2FoldChange < -1.Green, not significant genes up- and downregulated. DEG, differentially expressed gene.

After 12 hours, the number of DEGs increased significantly (Figure 3.12 **a**). To better understand the biological processes these genes are involved in, we performed a pathway enrichment analysis on both upregulated and downregulated genes at 12 hours time point (Figure 3.14 **a** and **b**). The most significantly upregulated process is thiamine biosynthesis (GO:0009228 and

GO:0009229) (Figure 3.14 **b**), while the most significantly downregulated pathways include cellular amino acid biosynthesis (GO:0008652) and oxidoreductase activity (GO:0016491) (Figure 3.14 **b**). This result shows an opposite trend to the previous comparison (β-HT vs HCT), where the cell response to oxidative stress was among the most upregulated processes (see the previous Figure 3.12 **d**). Besides the upregulation of thiamine genes, we found other important gene clusters; in particular, the hexoses transporters HXT11, HXT12, HXT14, HXT15, HXT16, HXT2, HXT4 and HXT9, supporting recent literature on the ability of α-syn to regulate the glucose transporters[485]. Members of the IMA isomaltase family, IMA2, IMA3, IMA4, IMA5 were also upregulated. The observed enhancement in carbohydrate uptake and utilization is in line with the evidence that hyperglycemia, a non-motor symptom, affects more than 50% of PD patients[486], and further supports the well-established association between diabetes and risk of PD[487].

Most of the genes downregulated at 12 hours are involved in the biosynthesis of amino acids (GO:008652) (Figure 3.14 **b**). However, we noticed interesting clusters such as:

- genes involved in ergosterol synthesis: ERG11, ERG2, ERG24, ERG28, ERG3, and ERG4. Ergosterol is the yeast equivalent of mammalian cholesterol and, similarly, it is essential for membranes stabilization[488]. Ergosterol is also a component of the lipid drafts required for signaling and vesicle trafficking.

- Genes encoding proteins with unknown functions located at the mitochondria–ER contact sites, such as FMP16, FMP23, FMP27, FMP33, FMP45 and FMP48, as well at the ER-plasma membrane site, as TCB1.

- Autophagy genes ATG1, ATG36, ATG41.

- Vacuolar genes APE3, COT1, CPS1, MSB3, VBA3, VBA4, VBA5, VFA1, RTC2, RTC3, RTC4, VMR1, YCK3, RNY1.

- Genes involved in iron metabolism like CAD1, CIA2, ISU1, FET3, FET4, NAR1, FRA1, FRE7, GRX2, GRX4, YAP5, VHT1, SMF3, MRS4, IBA57.

- Genes involved in lipid metabolism and lipid-related processes, like FAA1, FAA3, CAB1, CEM1, CWP1, NCP2, POX1, PRY1, SUT1, DPP1, MGL2, EHT1, HFD1, YPC1, UPS1 and FAT3.

- genes involved in the energetic metabolism CAT2, CIT1, CIT2, COA2, COQ11, COQ5, COX26, COX5B, CRC1, CYB2, CYC1, CYC7, ERC1, ERR1, ERR2, ERR3, GUT1, GUT2, ICL1, IDH1, IDH2, IDP1, IDP2, MPC2, MPC3, PDH1, PYC2, SHH4, and SUE1.

The DEGs mentioned in this chapter are reported in the table below (Table 3.3). The complete lists of up- and down-regulated DEGs in the comparison α-HT vs β-HT at 12 hours are quite extensive, so only the most significant hits are discussed in detail in this thesis. For these key genes, their expression data, including log fold change and adjusted p-values, are provided in the text.

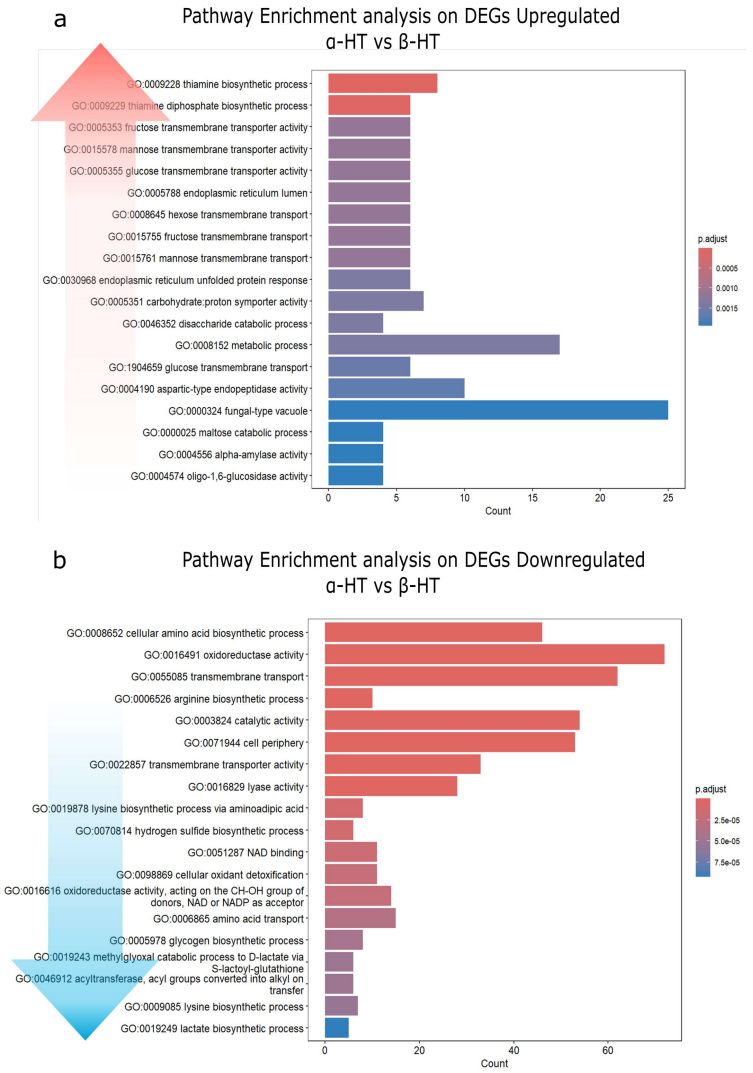

Figure 3.14: Bar plots showing Gene Ontology analysis results of **b** DEGs at 12 hours with a p-adjust < 0.05; **c** upregulated DEGs at 12 hours with a p-adjust < 0.05; **d** downregulated DEGs at 12 hours with a p-adjust < 0.05

Table 3.3: DEGs in the α-HT strain β-HT control at 12 hours.

Enzyme	LFC	padj	Enzyme	LFC	padj	Enzyme	LFC	padj
APE3	-1.32	4.00E-11	FAA1	-1.56	1.97E-02	IMA3	1.50	4.80E-03
ATG1	-1.47	1.68E-02	FAA3	-1.02	1.22E-07	IMA4	1.37	5.10E-03
ATG36	-1.04	3.39E-06	FAT3	-1.25	2.07E-03	IMA5	1.20	2.99E-03
ATG41	-3.86	1.43E-02	FET3	-1.71	1.73E-02	ISU1	-1.69	4.25E-03
CAB1	-2.27	7.73E-04	FET4	-1.22	3.30E-04	MGL2	-1.08	6.34E-03
CAD1	-1.13	3.80E-03	FMP16	-1.94	5.48E-04	MPC2	-1.87	1.13E-02
CAT2	-2.36	4.89E-11	FMP23	-4.03	4.87E-05	MPC3	-3.72	8.02E-09
CEM1	-1.13	3.22E-06	FMP27	-1.04	6.16E-04	MRS4	-1.57	2.90E-04
CIA2	-1.74	3.14E-02	FMP33	-1.04	2.22E-04	MSB3	-1.29	1.44E-03
CIT1	-1.74	1.87E-05	FMP45	-3.79	6.45E-12	NAR1	-1.62	5.56E-04
COA2	-1.06	2.58E-05	FMP48	-2.16	8.82E-04	PDH1	-1.13	3.07E-02
COQ11	-1.20	3.88E-03	FRA1	-1.12	1.34E-03	POX1	-2.15	1.49E-03
COQ5	-1.02	2.08E-10	FRE7	-1.68	3.54E-02	PRY1	-1.34	3.31E-10
COT1	-1.04	1.42E-03	GRX2	-1.35	1.92E-09	PYC2	-1.62	1.16E-02
COX26	-1.59	4.28E-05	GRX4	-1.71	3.14E-02	RNY1	-1.64	3.95E-24
COX5B	-1.53	2.06E-36	GUT1	-1.38	1.97E-06	RTC2	-3.01	1.40E-07
CPS1	-2.22	1.06E-03	GUT2	-1.48	7.40E-04	RTC3	-2.04	6.86E-05
CRC1	-2.22	3.47E-05	HFD1	-1.01	1.09E-04	RTC4	-1.60	4.73E-03
CWP1	-3.56	4.40E-07	HXT11	1.98	2.11E-05	SHH4	-2.46	4.01E-08
CYB2	-1.30	1.39E-02	HXT12	2.04	4.01E-07	SHH4	-2.46	4.01E-08
CYC1	-1.08	6.72E-03	HXT14	2.38	1.41E-03	SMF3	-1.66	2.37E-03
CYC7	-2.37	1.27E-05	HXT15	1.44	1.89E-03	SUT1	-2.04	6.47E-05
DPP1	-1.27	5.47E-03	HXT16	1.28	1.93E-02	TCB1	-1.15	1.47E-13
EHT1	-1.28	3.28E-02	HXT2	1.59	4.31E-03	UPS1	-1.07	1.13E-04
ERC1	-1.20	4.14E-03	HXT4	2.03	6.14E-04	VBA3	-3.41	6.76E-04
ERG11	-1.06	1.37E-02	HXT9	1.56	2.78E-03	VBA4	-1.11	4.07E-02
ERG2	-1.03	4.03E-02	IBA57	-1.35	6.20E-06	VBA5	-1.96	1.72E-02
ERG24	-1.41	2.20E-09	ICL1	-1.12	2.81E-02	VFA1	-1.27	2.18E-02
ERG28	-1.73	2.15E-09	IDH1	-1.13	9.34E-06	VHT1	-2.74	5.44E-04
ERG3	-1.70	3.04E-03	IDH2	-1.40	2.20E-14	VMR1	-2.53	5.30E-05
ERG4	-1.70	7.94E-05	IDP1	-2.53	2.22E-03	YAP5	-1.18	4.92E-02
ERR1	-2.72	1.20E-08	IDP2	-0.40	2.65E-01	YCK3	-1.04	2.91E-02
ERR2	-2.63	3.69E-10	IMA2	1.09	2.04E-03	YPC1	-1.74	3.57E-03
ERR3	-2.54	5.43E-05						

3.5.3 Cobalt and Deferoxamine treatments

The comparison between the HTC and β-HT indicates that the galactose inducible expression of human β-syn in yeast does not compromise essential cellular pathways and suggests that β-HT can be used as a control strain. To uncover the genes specifically targeted by the Co^{2+} or DFO, we inferred the differences between the DEGs among the three groups, each compared to the β-HT control. The DEGs of α-HT untreated, α-HT treated with 0.3 mM Co^{2+}, and α-HT treated with 0.3 mM DFO identified at both time points (6 and 12 hours) are summarized in the Venn diagrams shown in Figure 3.15 and Figure 3.16. After 6 hours of α-syn expression, α-HT and the two treatments share $\sim$20% of up- and down-regulated genes (Figure 3.15 **a** and **b**). Co^{2+} treatment upregulates 19 unique genes and downregulates 12 unique genes (Figure 3.15). Among the upregulated genes, Co^{2+} activates TIR and PAU, which are important families of proteins involved in the stress response (Cobalt list in Figure 3.15). In contrast, it downregulates CHO1 (LFC - 1.08, padj 2.10E-25) and OPT2 (LFC - 1.07, padj 1.24E-15), key genes involved in the synthesis of phospholipids (Cobalt list in Figure 3.15). DFO treatment specifically upregulated 3 genes and downregulated 25 (Figure 3.15). Among the downregulated genes, ERG25 (LFC - 1.20, padj 1.57E-06), ERG11 (LFC - 1.08, padj 2.19E-06), and ERG3 (LFC - 1.03, padj 1.26E-05) are involved in ergosterol biosynthesis (Deferoxamine list in Figure 3.15).

After 12 hours of α-syn expression, the percentage of shared DEGs among the three groups increased up to 221 for upregulated genes and 428 for downregulated genes (Figure 3.16 **a** and **b**). Co^{2+} treatment resulted in the upregulation of 25 unique genes, mostly involved in the cell cycle, and the downregulation of 23 unique genes, including those related to the TCA cycle, lipid metabolism, and heme synthesis (Cobalt list in Figure 3.16). DFO treatment led to the upregulation of 50 unique genes, mainly associated with DNA repair, lipid metabolism, and heme biosynthesis, and the downregulation of 23 unique genes involved in ribosomal function, DNA processes, and mitochondrial activities (DFO list in Figure 3.16).

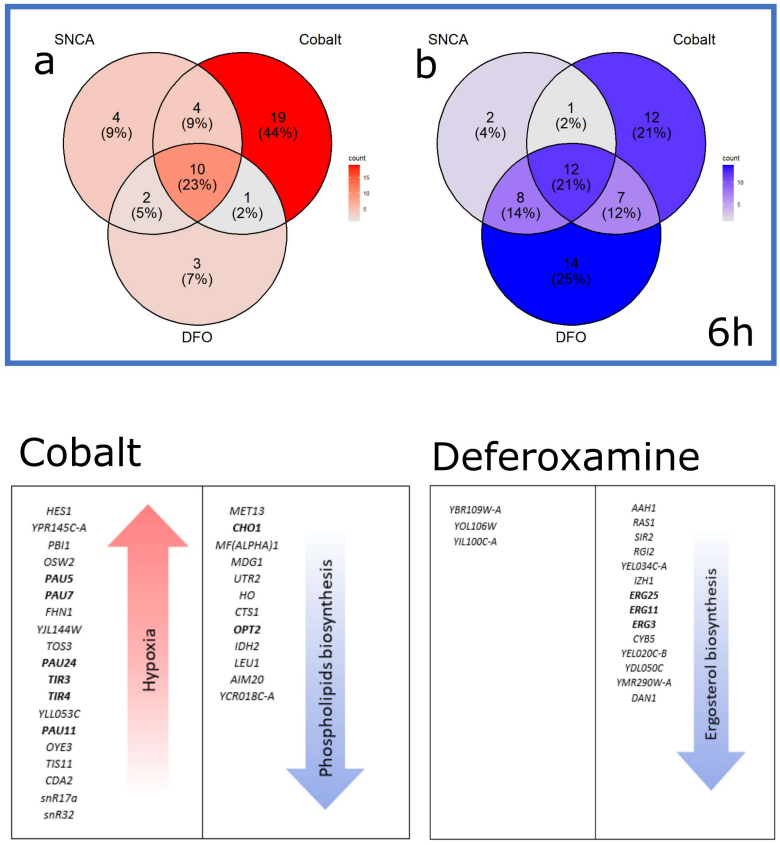

Figure 3.15: a. Venn diagram showing the overlap in DEGs between the α-HT untreated and α-HT treated with cobalt 0.3 mM and deferoxamine 0.3 mM. The diagram highlights shared and unique gene expression profiles across the three conditions, based on the transcriptomic analysis performed after 6 hours of α-syn expression. The genes distinctly affected by the two treatments are listed in the tables below the plots. The first column highlights the upregulated genes, while the second column focuses on the downregulated ones. Based on the identified genes, we indicated in the arrows the cellular processes potentially affected by each treatment.

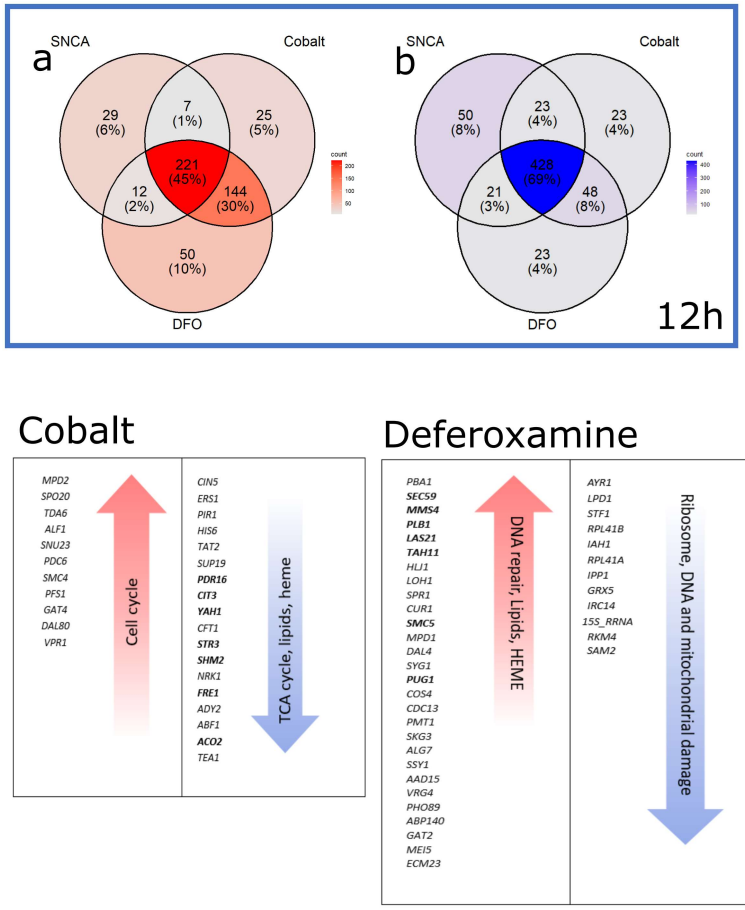

Figure 3.16: **a.** Venn diagram showing the overlap in DEGs between the α-HT untreated and α-HT treated with cobalt 0.3 mM and deferoxamine 0.3 mM. The diagram highlights shared and unique gene expression profiles across the three conditions, based on the transcriptomic analysis performed after 12 hours of α-syn expression. The genes distinctly affected by the two treatments are listed in the tables below the plots. The first column highlights the upregulated genes, while the second column focuses on the downregulated ones. Based on the identified genes, we indicated in the arrows the cellular processes potentially affected by each treatment.

3.5.4 DEGs affected by Cobalt treatment

The DEGs between the α-HT treated with 0.3 mM Cobalt and the untreated strain could indicates the genes responsible for the observed rescue phenotype. Unfortunately, no significant hits were identified in the comparison between DFO treatment and the untreated α-HT strain. Therefore, this chapter will primarily focus on the effect of Co^{2+} on the gene expression. Based on the predefined cut-off criteria established for this analysis (log2-based fold change $|log2FC| > 1$ and adjusted P-value < 0.05), 12 and 5 significant DEGs were identified at 6 and 12 hours time points, respectively. At 6 hours, the DEGs significantly upregulated are 9, while the downregulated are 3 (Figure 3.17 **a**). At 12 hours, the DEGs significantly upregulated are 2, while the downregulated are 3 (Figure 3.17 **b**).

The DEGs respectively up and downregulated at 6 and 12 hours time points are listed with the relative functions in Table 5.6, 5.7, 5.8, 5.9 reported in the Appendices.

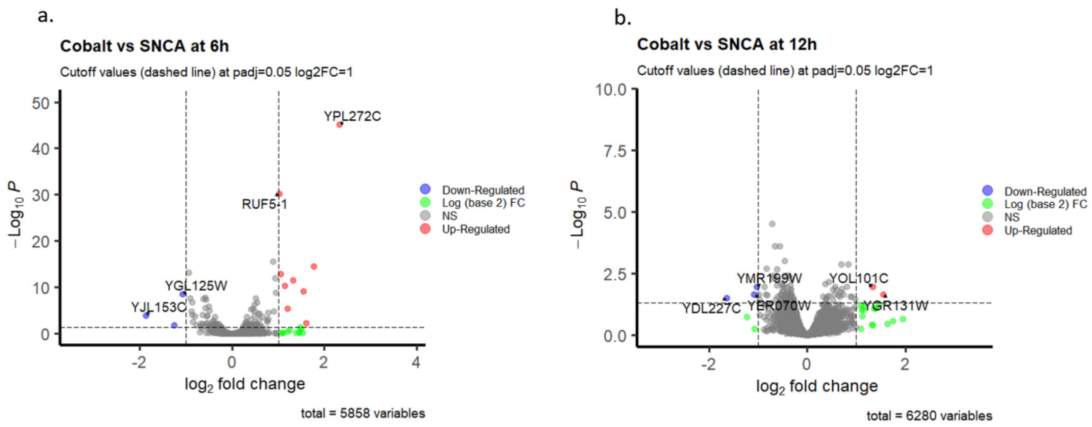

Figure 3.17: Volcano plot of the DEGs measured in the binomial comparison between the α-HT treated with 0.3 mM Cobalt and the untreated strain at 6 hours **a** and 12 hours **b**. The transverse axis represents the log2-based fold change (log2FoldChange), while on the vertical axis is reported the negative log10-based p-adjusted value ($-Log10P$). The line parallel to the x-axis is y = 1.30 (log_{10} 0.05). Red, upregulated genes with a log2FoldChange > 1; blue, downregulated genes with a log2FoldChange < -1; Green, not significant genes up- and downregulated. DEG, differentially expressed gene.

After 6 hours, the most significant upregulated gene in the α-HT strain treated with Co^{2+} 0.3 mM is YPL272C. This gene encodes for PBI1, an enzyme whose function is still unknown, that seems

to be involved in the transportation machinery responsible for the phosphatidylserine translocation from the ER to the endosome, where it is converted in phosphatidylethanolamine[489]. PBI1 was initially identified as one of the transcripts highly upregulated in yeast exposed to ketoconazole, an ergosterol biosynthesis inhibitor[490], inferring a possible role also in the detoxification of toxic ergosterol intermediates accumulated upon the antifungal treatment[491]. Alteration of the ergosterol pathway is also supported by the upregulation of HES1 (YOR237W), one of the seven oxysterol-binding proteins [492] conserved in humans [493, 494]. This protein family shares a common essential role in the cell, related to ergosterol homeostasis. The knockout of all seven members leads to a lethal phenotype[495]. Among the up-regulated genes, YFL020C and YER011W show a strong association with hypoxia response. These genes encode respectively for PAU5 and TIR1. As explained in the Introduction chapter of this thesis, PAU and TIR are heme-repressed genes that encode for mannoproteins that contribute to the cell membrane during hypoxic stress.[204, 205, 206]. Among the genes upregulated by the Co^{2+} treatment, there is also YDR453C, which encodes for TSA2, one of the members of the peroxiredoxins antioxidant[496]. A family of proteins well conserved among all organisms involved in the detoxification of reactive nitrogen species[497].

After 12 hours, only two of the genes upregulated at 6 hours are still significant: YOL101C and YGR131W which encode respectively for the IZH4 and FHN1 enzymes. IZH4 is a member of the "Implicated in Zinc Homeostasis family" which also includes IZH1, IZH2 and IZH3[498]. The expression of these genes depends on the cellular zinc level: IZH1 and IZH2 are expressed in zinc-limitation conditions, while IZH3 and IZH4 are expressed in high zinc concentrations. Furthermore, the presence of the low-oxygen response element in the promoter region allows speculation of a possible IZH4 role in the hypoxic response as it can be recognized and targeted by the hypoxia sensor Mga2p[498]. FNH1 is a protein of unknown function and similarly to PBI1 was highlighted among the upregulated transcripts after ketoconazole exposure[490].

The three DEGs downregulated at 6 hours are INO1 (YJL153C), MET13 (YGL125W) and MET6 (YER091C) (Figure 3.17 **a**). MET13 is one of the two yeast methylenetetrahydrofolate reductases

isozymes, the second is MET12[499]. It catalyzes the reduction of 5,10-methylene tetrahydrofolate (CH_2-THF) to 5-methyl-tetrahydrofolate (CH_3-THF), the methyl donor for the conversion of homocysteine in methionine[500], which in a subsequent step of the one-carbon (C1) metabolism is converted in S-adenosylmethionine (AdoMet), the preferred cofactor for biological methyl group transfers (Figure 3.18). Similarly to the mammalian homolog, MET13 is NADPH-dependent and negatively regulated by AdoMet[501]. MET6 encodes for the cobalamine independent 5-methyl-tetrahydrofolate homocysteine methyltransferase[502, 503, 504] which catalyzes the conversion of homocysteine into methionine. Cobalamine-independent methyl transferases were first characterized in bacteria[505] and plants[506, 507] and generally use zinc as a cofactor[508] to promote the transfer of the methyl group carried by the CH_3-THF[509]. The activities of these two enzymes are critical for the balance of homocysteine levels and for the regulation of phospholipids biosynthesis[510].Interestingly INO1, which was upregulated in the α-HT strain compared to the β-HT control, is significantly downregulated in the presence of Co^{2+}.

After 12 hours, the DEGs downregulated by Co^{2+} treatment are CNL1 (YMR199W), RNR1 (YER070W) and HO (YDL227C). CNL1 encodes for the homonym cyclin-dependent kinases and together with CNL2 and CLN3, it regulates the transition G1 to S in the cell cycle[511]. RNR1 encodes for the ribonucleotide reductase, which is essential in DNA replication and repair as it catalyzes the rate-limiting step in *de novo* deoxyribonucleotide biosynthesis, converting nucleotides to deoxynucleotides.

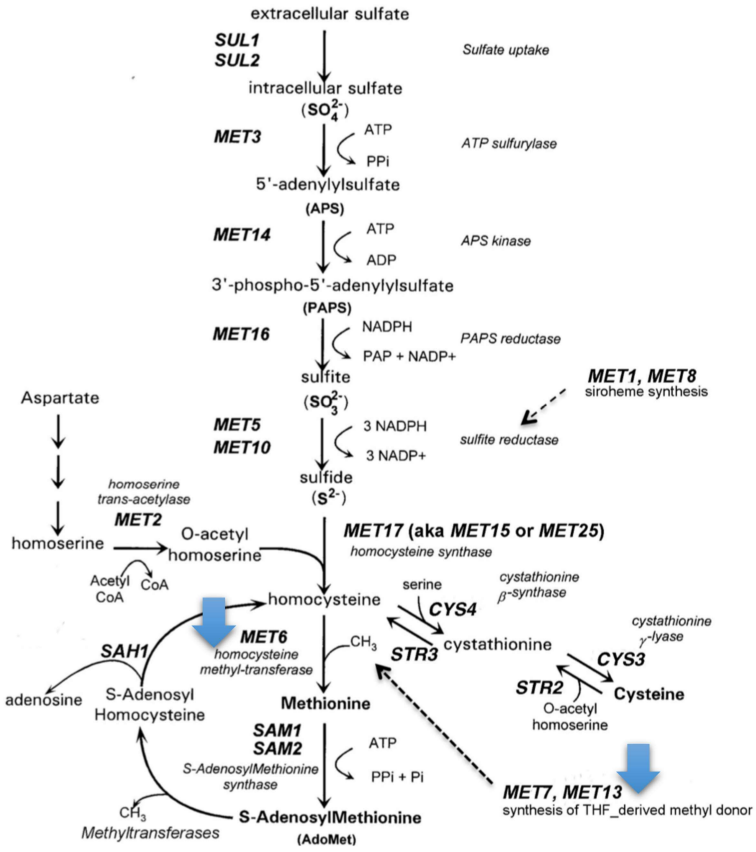

Figure 3.18: In yeast, structural genes encoding components of sulfur amino acid metabolism are called MET, as they were initially identified through mutations causing methionine auxotrophy. This schematic, adapted from Thomas et al.[512], illustrates the reaction cascade responsible for extracellular sulfate assimilation into cysteine and methionine. In particular, MET6 catalyzes the conversion of homocysteine in methionine, using the methyl group transferred by MET13. The blue arrows highlighted that these genes are downregulated in the α-HT strain.

3.6 INO1 knock-out

The transcriptomic analysis showed that MET genes are downregulated in the α-HT strain, suggesting that sulfur amino acid biosynthesis is among the affected biological processes. Based on this hypothesis, α-syn overexpression is expected to result in altered levels of metabolites involved in this pathway, particularly leading to homocysteine accumulation and reduced levels of methionine and AdoMet. In this thesis, we tried to validate the transcriptomic result and the relative

hypothesis by performing a targeted gas chromatography-mass spectrometry analysis on the β-HT strain, untreated α-HT and α-HT treated with 0.3 mM Co^{2+} and 0.3 mM DFO. Unfortunately, the analysis failed to detect the metabolites of interest. However, using liquid chromatography-mass spectrometry, we measured the levels of myo-inositol-1P, the product of the enzyme encoded by INO1. This gene is upregulated in the α-HT strain at 12 hours, but it becomes significantly downregulated upon the treatment with Co^{2+} (Figure 3.19 **a**) already at 6 hours. Myo-inositol-1P levels are increased by about 21% in the α-HT strain compared to the β-HT control. In the presence of Co^{2+}, its levels decrease by about 55%, and by approximately 45% upon DFO treatment (Figure 3.19 **b**). Finally, to verify the role of INO1, we generated Δino1 strains, replacing the gene with the hygromycin resistance marker (more information on the strategy used to generate this strain is reported in section 2.1 of the Materials and Method chapter). Because yeast relies on the inositol available in the media during the initial stages of growth, we cultivated the strains using a commercial medium lacking this supplement to exclude this contribution. It is important to note that the absence of inositol supplementation is not lethal for the Δino1 strains, as the severity of this auxotrophy depends on which gene of the inositol metabolism is mutated[513]. However, it does induce a mild phenotype, making the strains more susceptible to cell death during growth ("inositol-less death")[514, 515] (The viability of the δino1 in the media without inositol is shown in Figure 5.5 of the Appendices, where the growth of the knock-out strains is compared to that of the wild-type in the same cultivation media). Knocking out the INO1 gene in the α-HT strain did not produce any beneficial effects, nor did it compromise the rescue effects induced by Co^{2+} and DFO treatments (Figure 3.19 **c**). However, this genetic modification is lethal in the A53T-HT strain, which failed to grow even in the presence of inositol (Figure 3.19 **c**). A more complete version of the plot reported in Figure 3.19 **c** considering also the WT strains is reported Figure 5.5 in the Appendices.

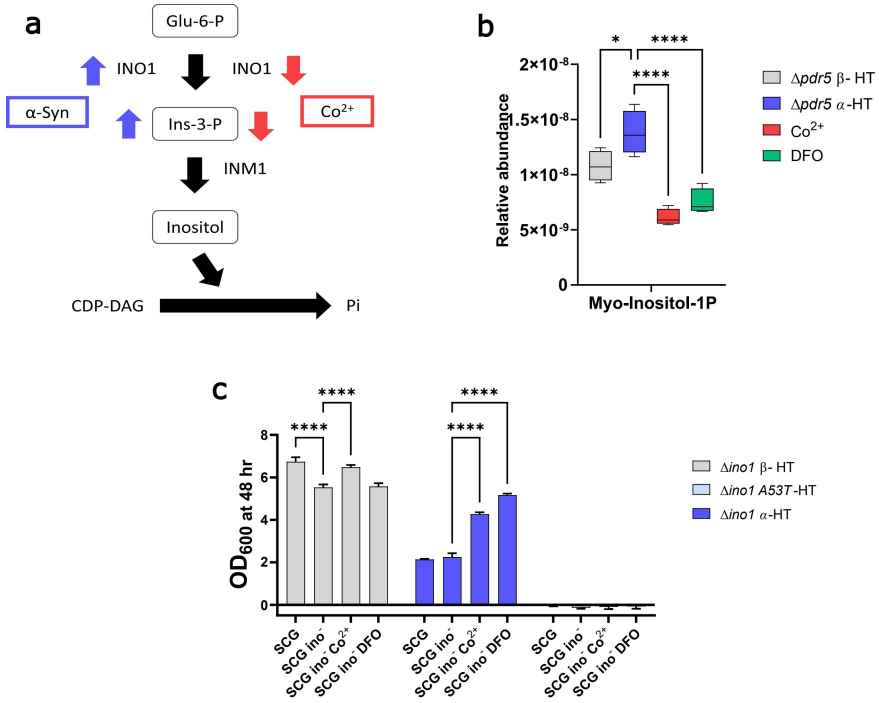

Figure 3.19: **a** Scheme of the inositol synthesis in *S. cerevisiae* with the key enzymes INO1 and INM1 highlighted. The arrows blue and red indicate the effect of α-syn and Co^{2+}, respectively, on the expression levels of the two genes according to our transcriptomic data. **b** Level of myoinositol detected by targeted metabolomic analysis performed as explained in the section of Materials and Methods. We reported the relative abundance normalized for the cell concentration. Each box is the mean +/- SDs of four biological replicates (n = 4). For the statistics, a two-way ANOVA test for multiple comparisons was applied and corrected using the Dunnet statistical hypothesis. *, adjusted p-value = 0.024; ****, adjusted p-value < 0.0001. **c** OD_{600} measured at 48 hours for the Δino1 strains generated in the β-HT, α-HT and A53T-HT background. The strains were cultured in SCG media, with and without inositol, and with or without the addition of 0.3 mM Co^{2+} and DFO. Each bar is the mean +/- SDs of biological triplicates cultured in a 384-well plate. For the statistics, two-way ANOVA test for multiple comparisons was applied and corrected using the Dunnet statistical hypothesis. ****, adjusted p-value < 0.0001.

3.7 Alteration central carbon metabolism

The first association between neurodegenerative diseases and alteration of cellular metabolism arose with the discovery of an acute form of Parkinsonism in individuals addicted to the synthetic drug MPTP (1-methyl-4-phenyl-1,2,3,6-tetrahydropyridine)[516, 517]. In the brain, MPTP is metabolized into the ionic form MPP^+ which explicates a neurotoxic effect, leading to loss of

dopaminergic neurons[518]. MPP^+ acts at the very beginning of the electron transport chain, inhibiting the NADH-ubiquinone oxidoreductase (Complex I).

Despite the absence of Complex I in the respiratory chain of S. cerevisiae [519], our model suggests that the expression of α-syn affects mitochondrial respiration efficiency, particularly in the later stages of the electron transport chain (Figure 3.20). Under low-oxygen conditions, the cell expresses the hypoxic isoforms of cytochrome C oxidase (COX5b) and cytochrome C (CYC7). COX5b exhibits a higher catalytic constant compared to its aerobic counterpart, COX5a, while CYC7 has a longer half-life than CYC1, as it is not degraded via proteasome[520]. Cox5 is a component of the complex IV which transfers electrons to oxygen, generating the membrane H^+ gradient. CYC7 shuttles electrons from complex III to complex IV and then to oxygen, the final electron acceptor. COX5b and CYC7 are not the only components of the electron transport chain significantly downregulated in the α-HT strain. Additionally, COQ5, a methyltransferase, and COQ11, a dehydrogenase, both involved in the synthesis of Coenzyme Q, are similarly downregulated[521]. In *S. cerevisiae* when the mitochondrial respiratory capacity is reduced or limited, the cell has to ensure sufficient production of glutamate. It has been reported that in this critical situation the expression of the genes encoding the first three steps of the TCA cycle: CIT1, ACO1, IDH1, and IDH2 switches between dependence on the HAP genes in cells with efficient respiration to the RTG genes in cells with lower mitochondrial respiratory activity[522]. In the α-HT strain, the genes YNR001C (CIT1), YLR304C (ACO1), YNL037C (IDH1), YOR136W (IDH2), YBL103C (IDP2), YNL009W (IDP3) and YBL103C (RTG3) are all downregulated. These results suggest this glutamate generating branch of the TCA cycle is less efficient in the α-HT strain in hypoxia conditions. In this study, we further investigated the impact of impaired oxidative phosphorylation on cellular metabolism by performing a targeted metabolomics analysis on the β-HT control, the α-HT strain, and the effects of Co^{2+} and DFO treatments. We extracted the total metabolites from four independent biological replicates ($n = 4$) as reported in section 2.7.1 of the chapter Materials and Methods (Figure 3.20).

The α-HT strain shows a significant accumulation of glycolysis intermediates, as shown in Fig-

ure 3.20. In particular, 3-phosphoglycerate (3PG) and pyruvate levels increase by 47% and 72% respectively, when compared to the β-HT. Interestingly, Co^{2+} treatment restores pyruvate to the control level. DFO also reduces pyruvate levels, though it is less effective than Co^{2+}. Fructose 1,6 bisphosphatase (F1.6BP) level increases by 11% in the presence of DFO, while Co^{2+} treatment increases phosphoenolpyruvate (PEP) level by $\sim$ 40%. These results are consistent with the downregulation of the gene YOR347C in the α-HT strain which encodes for the pyruvate kinase enzyme (Pyk2).

Once glucose is converted into pyruvate at the end of glycolysis, it translocates inside the mitochondria using the carriers MPC2 (YHR162W) and MPC3 (YGR243W), both downregulated in the α-HT strain. Canonically, pyruvate is converted into acetyl-CoA by the pyruvate dehydrogenase (PDH) complex and fuels into the TCA cycle. Alternatively, acetyl-CoA can be generated in the cytosol bypassing the activity of the PDH enzyme, through the multistep conversion of acetaldehyde[523]. Our findings suggest that α-syn expression impacts both of these key metabolic pathways. The synthesis of cytosolic acetyl-CoA is catalyzed by acetaldehyde dehydrogenases (ALD2, ALD3, ALD4) and acetyl-CoA synthetase (ACS1), which genes are all downregulated in the α-HT strain. Acetyl-CoA is subsequently converted to citrate by the CIT1 (YNR001C) and CIT2 (YCR005C) enzymes[523]. Despite the lower expression of these enzymes in α-HT, citrate accumulates two times more in α-HT compared to controls and decreases in the presence of DFO. In mitochondria, citrate is converted first into α-ketoglutarate and then into succinate. Otherwise, citrate can be exported to the cytoplasm via the antiporters Ctp1 and Yhm2, entering the glyoxylate cycle, where it is converted to succinate[524]. The level of succinate is twice as high in α-HT compared to β-HT controls and, although not significantly, both Co^{2+} and DFO treatments reduce the succinate levels (Figure 3.20). Furthermore, since ornithine and glutamate can contribute to the TCA cycle, we also measured their levels. We observed a 60% decrease in ornithine in α-HT, which is restored by Co^{2+} and DFO treatments (Figure 3.20). The accumulation of pyruvate in the α-HT strain could consequently lead to increased levels of acetyl-CoA (not measured in this study), the main precursor of fatty acids. This could potentially alter the biosynthesis of long-chain fatty acids in the α-HT strain[523]. In this context, an important aspect must be

considered: the acetyl moieties translocate within the organelles bound to an L-carnitine molecule shuttled through different transporters. The three main yeast acetylcarnitine transferases: CRC1 (YOR100C), CAT2 (YML042W) and YAT1 (YAR035W) are downregulated in the α-HT strain. Furthermore, yeast cannot synthesize L-carnitine *de novo*, they rely on the exogenous L-carnitine imported via the Hnm1 transporter, whose expression is regulated by AGP2 (YBR132C) also downregulated in the α-HT strain. The alteration in metabolite levels was observed specifically in the untreated α-HT strain, suggesting that the disruption of energy metabolism in cells subjected to hypoxic stress could be a key factor underlying the toxicity induced by α-syn accumulation in yeast. In the next chapter, a more in-depth examination of lipid metabolism will be addressed. The enzymes mentioned in this chapter are reported in the following Table with the expression information of the relative genes (Table 3.20)

Table 3.4: DEGs in the α-HT strain compared to the β-HT control at 12 hours involved in the cellular metabolism.

β-HT vs HTC		
Enzyme	Log2FoldChange	padj
ACO1	-1.16	5.39E-04
ACS1	-2.33	3.85E-07
AGP2	-2.08	6.91E-16
ALD2	-1.29	1.02E-07
ALD3	-1.50	1.79E-09
ALD4	-2.38	1.90E-19
CAT2	-2.36	4.89E-11
CIT1	-1.74	1.87E-05
CIT2	-2.27	1.62E-03
COQ11	-1.20	3.88E-03
COQ5	-1.02	2.08E-10
COX5b	-1.53	2.06E-36
CRC1	-2.22	3.47E-05
CYC7	-2.37	1.27E-05
IDH1	-1.13	9.34E-06
IDH2	-1.40	2.20E-14
IDP2	-0.40	2.65E-01
IDP3	-1.21	2.18E-03
MPC2	-1.87	1.13E-02
MPC3	-3.72	8.02E-09
PYK2	-1.18	1.49E-03
RTG3	-1.19	4.57E-02
YAT1	-1.64	8.39E-05

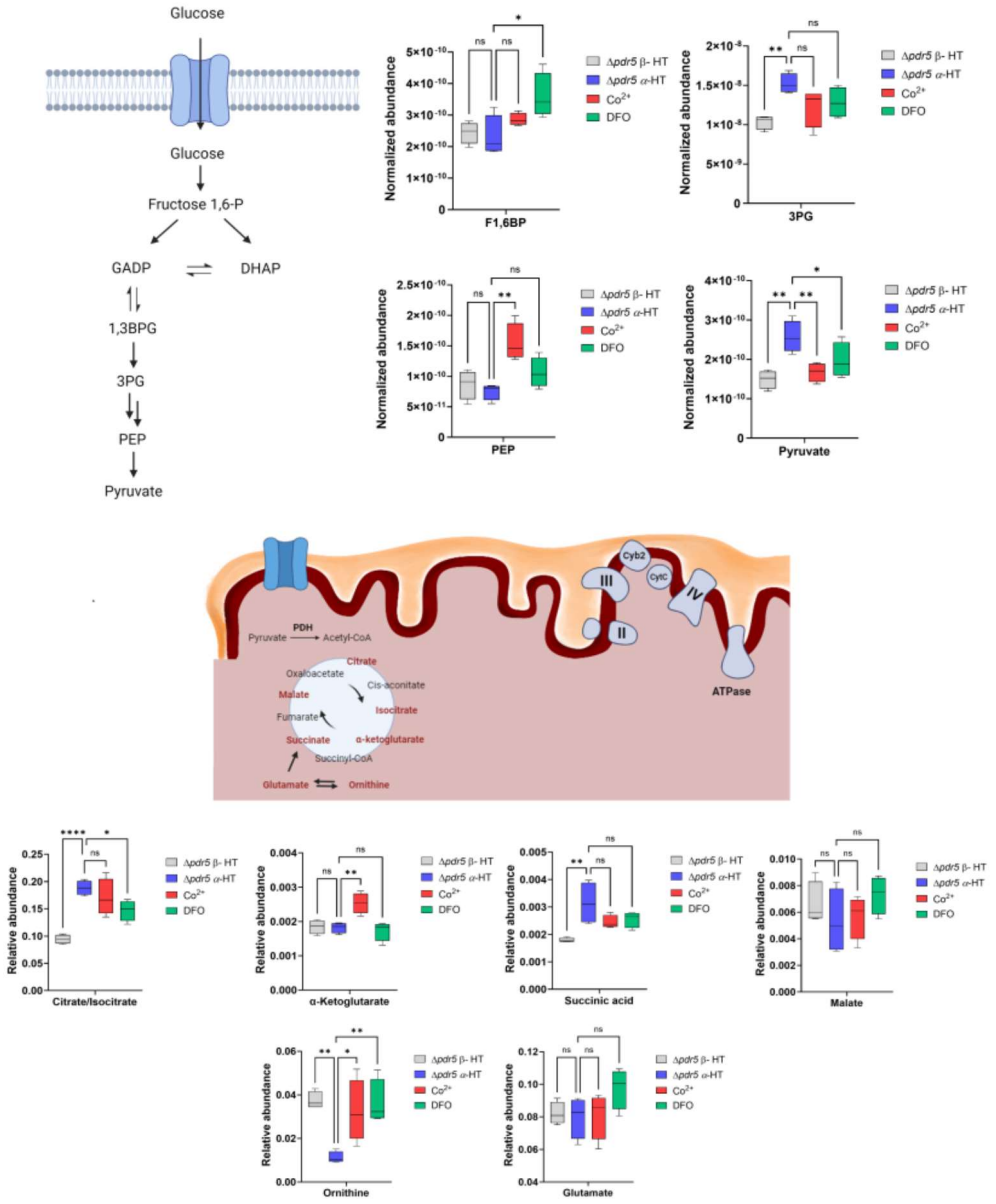

Figure 3.20: The transcriptomic analysis performed in this study suggested a dysregulation of the last complexes of the electron transport chain. The reported metabolites (in red) were detected by the targeted metabolomic analysis performed as explained in the section of Materials and Methods. For each of them, we reported the relative abundance normalized for the cell concentration. Each box is the mean +/- SDs of four biological replicates (n = 4). For the statistics, a two-way ANOVA test for multiple comparisons was applied and corrected using the Dunnet statistical hypothesis.*, adjusted p-value = 0.024;**, adjusted p-value = 0.001; ****, adjusted p-value < 0.0001.

3.8 Alteration of lipid metabolism

The lipidomic data resulted from four biological replicates (n = 4) of β-HT, α-HT, and α-HT incubated respectively with 0.3 mM Co^{2+} or DFO were analyzed in R studio software (version 4.1.1), using the MetaboAnalystR package (4.0.0). Differences in lipidic compositions among the groups were identified according to the following thresholds: log2-based fold change $|log2FC| > 2$ and P-value < 0.05. The significant hits were then annotated through MZmine software as reported in section 2.7.5 of the Materials and Methods chapter. The volcano plot reveals 2022 differential features between the α-HT strain and β-HT control; 2784 between α-HT and Co^{2+} treatment; 2094 between α-HT and DFO treatment (Figure 3.21 **a,b** and **c**). MZmine software is based on public and private libraries (MassBank, GNPS, MoNA, HMDB, NIST, LipidBlast and Public Repositories), but it does not provide coverage for all living organisms, such as *S. cerevisiae*. For this reason, over a large number of significant features identified, we were able to annotate: 16 lipids for the binomial comparison β-HT vs α-HT (Figure 3.21 **a**); 13 lipids for the α-HT untreated vs Co^{2+} treatment (Figure 3.21 **b**); 12 lipids for the α-HT untreated vs DFO treatment (Figure 3.21 **c**). The identified features are listed in Tables 3.5, 3.6 and 3.7, below in this section. Among the lipids significantly decreased in the α-HT compared to β-HT we found mostly phosphatidylcholine species (Figure 3.21 **a**). In contrast, four lipids were found to be increased: phosphatidylinositol (PI 16:1_18:1) (Figure 3.21 **a**), squalene, lysophosphatidylcholine (LPC 12:0), and phosphatidylcholine (PC 30:1, which likely corresponds to PC 14:0_16:1 or 16:0_14:1). As LPC 12:0 and PC 30:1 are typically not abundant in yeast, their presence may be associated to the expression of human α-syn. In particular, accumulation of LPC 12:0 is associated with defective hydrolysis of PC, already reported in models of α-syn[525]. Furthermore, the presence of the PI 16:1_18:1 and squalene is consistent with the altered expression of INO1 and ERG genes observed in the transcriptomic profiling of the α-HT strain compared to the β-HT control at 12 hours (see Table 3.3 for an overview of the key genes differentially regulated in α-HT versus β-HT at 12 hours). However, the presence of phosphatidylcholines was unexpected, as no genes involved in the biosynthesis of this crucial phospholipid were identified among the DEGs in the α-HT for the same comparison (α-HT vs β-HT) at both time points (6 and 12 hours). Co^{2+} and DFO

show an opposite result compared to α-HT. In particular, Co^{2+} decreases phosphatidylinositol (PI 26:0_18:1) and PC 30:1 (Figure 3.21 **b**). This result is in line with the downregulation of INO1 observed in the α-HT strain treated with Co^{2+} when compared to the untreated strain at 6 hours. Deferoxamine increases both phosphatidylcholine and phosphatidylserine, decreasing squalene and LPC 12:0 (Figure 3.21 **c**). Lowered squalene matches the downregulation of the ERG genes observed for the DFO treatment when compared to the β-HT control at 6 hours (Figure 3.15).

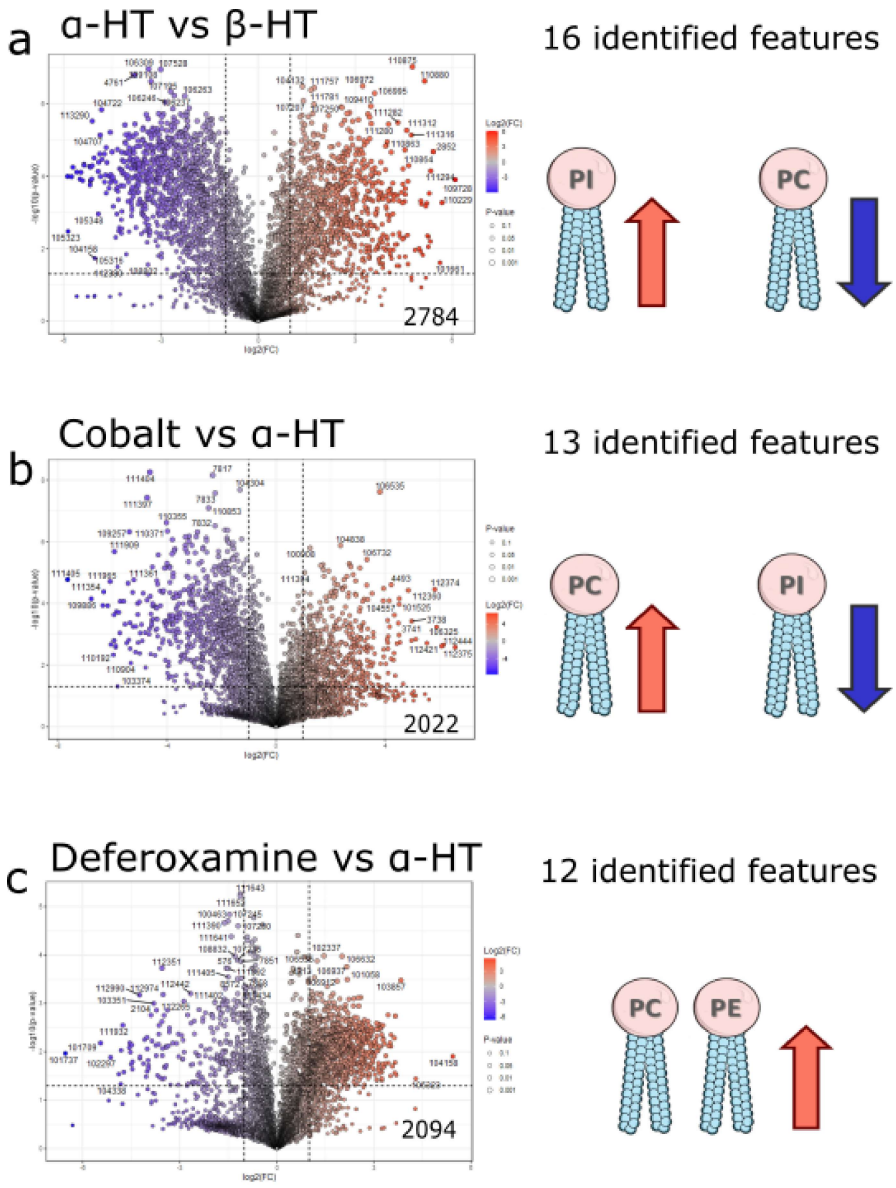

Figure 3.21: Volcano plots showing lipids differentially increased and decreased between **a** α-HT and β-HT control, **b** α-HT treated with 0.3 mM of Co^{2+} and α-HT untreated, **c** α-HT treated with 0.3 mM of DFO and α-HT untreated. Each dot represents one specific lipid. The x-axis represents log_2 Fold change, and the y-axis represents $-log_{10}$ P-value. The two lines parallel to the y-axis are x $= -2$ and x $= 2.0$. The line parallel to the x-axis is y $= 1.30$ (log_{10} 0.05). Dots above the broken line indicate lipids significantly changed. Purple, lipids significantly decreased with a log2FoldChange < -2; orange, lipids significantly increased with a log2FoldChange > 2. The lipids schemes to the right of the identified features in MZmine are based on what is reported in Tables 3.5, 3.6 and 3.7, below in this section. The arrows indicate the trends followed by the indicated lipids class.

Table 3.5: Lipidomic results at 24 hours for α-HT vs β-HT

16 Lipids identified at 24 hours in α-HT vs β-HT		
Compound name	**Log2FoldChange**	**p-value**
PC 24:1	-3.322	1.36E-05
PC 28:1	-2.8199	0.0004
α-TOCHOPHERYL ACETATE	-2.5661	0.001
PC 36:1, PC 18:0-18:1	-2.2913	7.20E-06
PC 30:2	-2.0128	7.91E-05
PE 26:0	-1.6323	3.77E-06
PE 28:1	-1.5341	0.0009
PC 18:1 20:1	-1.204	6.30E-06
PC 24:0	-1.1485	6.73E-05
PC 32:1, PC 16:0_16:1	-1.1083	0.001
NCGC00178646-02!2,4-dihydroxyheptadecyl acetate	-1.0444	0.0003
PI 34:2, PI 16:1_18:1	1.0599	0.0001
Squalene	2.2259	0.0069
LPC 12:0	2.87	0.007
PC 30:1	2.877	9.15E-06

Table 3.6: Lipidomic results at 24 hours for α-HT treated with 0.3 mM Co^{2+} vs α-HT untreated

13 Lipids identified at 24 hours in Cobalt treatment vs α-HT		
Compound name	**Log2FoldChange**	**p-value**
PC 28:1	3.08	0.003
PC 24:1	2.9298	0.0144
PC 32:1, PC 16:0_16:1	2.0329	0.001

Continued on next page

Table 3.6 – continued from previous page

Compound name	Log2FoldChange	p-value
Dioctyl Phthalate	1.9988	0.045
PC 30:2	1.9739	0.002
PE 28:1	1.8134	0.013
PE 18:0_18:1	1.7237	0.002
PC 36:1, PC 18:0_18:1	1.6326	0.045
PI 42:1, PI 26:0_16:1	1.2368	0.044
PE 26:0	-1.0226	0.001
NCGC00178646-02!2,4-dihydroxyheptadecyl acetate	-1.5587	0.001
PC 30:1	-1.7564	0.0002
PI 44:1, PI 26:0_18:1	-2.0982	0.014

Table 3.7: Lipidomic results at 24 hours for α-HT treated with 0.3 mM DFO vs α-HT untreated

12 Lipids identified at 24 hours in DFO treatment vs α-HT		
Compound name	**Log2FoldChange**	**p-value**
PC 24:1	2.4832	0.0029
PE 18:0_18:1	2.123	0.010
PE 28:1	1.9146	0.006
PC 32:1, PC 16:0_16:1	1.7439	0.003
PE 28:1	1.638	0.004
PC 30:2	1.5598	0.002
PC 36:1, PC 18:0_18:1	1.3428	0.013
PC 30:0	1.3118	0.012
Dioctyl Phthalate	1.1683	0.011

Continued on next page

Table 3.7 – continued from previous page

Compound name	Log2FoldChange	p-value
NCGC00178646-02!2,4-dihydroxyheptadecyl acetate	1.001	0.004
Squalene	-3.041	0.004
LPC 12:0	-3.096	0.006

3.8.1 OLE1 activity

Ole1 is the yeast homolog of the human Stearoyl-CoA desaturase. It is an iron and oxygen-dependent enzyme that catalyzes the biosynthesis of palmitoleic (16:1) and oleic (18:1) fatty acids[526]. A previous lipidomics analysis performed by Fanning and colleagues on different α-syn expression models, including yeasts, revealed an accumulated level of oleic acid (18:1)[527]. Furthermore, pharmacological inhibition of the stearoyl-CoA-desaturase, the mammalian enzyme responsible for the synthesis of oleic acid, alleviates the toxicity induced by α-syn[528]. Based on this evidence, we expected to find upregulation of OLE1 in the α-HT strain transcriptomic profile. Unexpectedly, not only the expression level of OLE1 was unaffected in the DEGs identified in the α-HT strain, but even qPCR analysis failed to detect any increase in the expression of this enzyme (Figure 3.22 **b**). Further studies on the OLE1 have shown that cobalt and nickel increase the mRNA level of this enzyme due to the presence of low-oxygen response element in its promoter region[529]. Consistently our qPCR analysis confirmed that Co^{2+} increases the expression of OLE1(Figure 3.22 **b**). Instead, DFO does not have the same effect (Figure 3.22 **b**), despite the proven efficiency of 1,10-phenanthroline, another iron chelator, to induce OLE1[446].

In this study, we used the data from the untargeted lipidomic analysis to investigate the activity of this key enzyme in the α-HT strain (Figure 3.22 **a**). We observed that α-HT strain accumulates 1.8-fold more palmitic acid (C16:0) and 4-fold more stearic acid (C18:0) compared to the β-HT control stain (Figure 3.22 **c** and **e**). Treatment with Co^{2+} and DFO reduces this accumulation almost to the control level for both fatty acids (Figure 3.22 **c** and **e**). Similar results were observed

for the unsaturated version of these fatty acids, resulting from the catalytic activity of Ole1. α-HT strain accumulates 4-fold more palmitoleic acid (C16:1) and 10-fold more oleic acid (C18:1) compared to the β-HT control strain (Figure 3.22 **d** and **f**). Co^{2+} and DFO significantly decrease the levels of unsaturated fatty acids. α-HT treated with Co^{2+} shown only 2-fold higher levels of palmitoleic acid (C16:1) and oleic acid (C18:1) compared to the β-HT control strain (Figure 3.22 **d** and **f**). Similarly, the same strain treated with DFO has a 2-fold increased level of palmitoleic acid (C16:1) and $\sim$ 4-fold more oleic acid (C18:1) compared to the β-HT control strain (Figure 3.22 **d** and **f**). These findings indicate that Ole1 activity is increased in the α-HT strain, as these measurements more reliably reflect Ole1 activity than gene expression. α-Syn expression leads to a significant increase in unsaturated fatty acids, while both Co^{2+} and DFO treatments restore their level to the ones observed for the control. The ability of Co^{2+} and DFO to prevent the accumulation of FAs in the cells affected by α-syn toxicity could be part of their protective mechanism.

The ratios between saturated and unsaturated FAs estimated from the untargeted lipidomics analysis may reflect the activity of Ole1 enzyme (Figure 3.23). For the conversion of palmitic acid (C16:0) into palmitoleic acid (16:1), the ratio 16:1/16:0 was 8 in the β-HT strain and it increased up to 18.5 in α-HT, 11.4 in the presence of $Co_2{}^{+}$ and 15.7 of DFO (Figure 3.23). For the stearic acid conversion (18:0) into oleic acid (18:1), the conversion (18:1/18:0) ratio was 6.4 in the β-HT strain and increased up to 15.4 in α-HT, 9.5 in the presence of $Co_2{}^{+}$ and 17.5 of DFO (Figure 3.23).

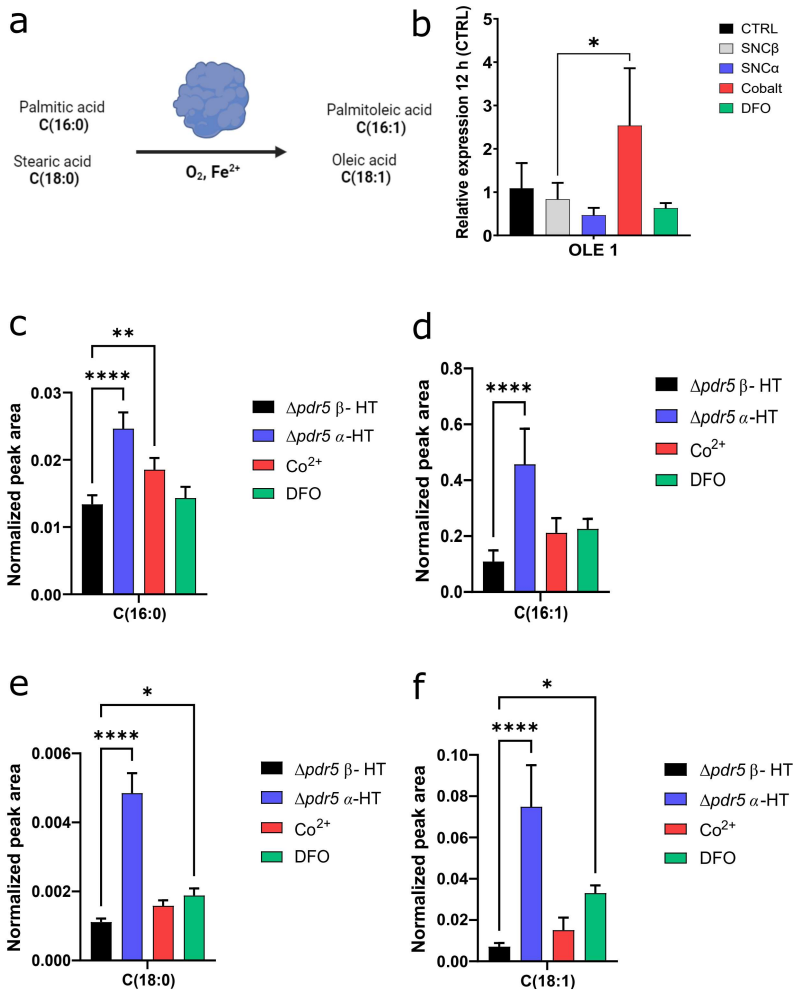

Figure 3.22: **a** Scheme of the enzymatic activity of Ole1 enzyme: palmitic acid (16:0) and staric acid (18:0) are converted in palmitoleic (16:1) and oleic acid (18:1), respectively. This reaction requires oxygen and iron as cofactors. **b** Validation of the expression level of Ole1 enzyme by RT-qPCR analysis. The relative expression of Ole1 at 12 hours is significant in α-HT treated with Co^{2+} 0.3 mM. The analysis was not performed at 6 hours, because the gene was missing in the DEGs list at this time point. Each bar is the mean +/- SDs of three biological replicates (n = 3). For the statistics, a one-way ANOVA test for multiple comparisons was applied and corrected using the Dunnet statistical hypothesis. ***, adjusted P Value = 0.0002;****, adjusted P Value < 0.0001. The levels of palmitic acid (16:0) **c**, stearic acid (18:0) **e**, palmitoleic acid (16:1) **d** and oleic acid (18:1) **f** shown in the figure are estimated normalizing the values obtained from the result of the untargeting lipidomic analysis for the cell concentration. All the measured lipids are significantly increased in the α-HT. Each bar is the mean +/- SDs of three biological replicates (n = 4). For the statistics, a one-way ANOVA test for multiple comparisons was applied and corrected using the Dunnet statistical hypothesis. ***, adjusted P Value = 0.0002;****, adjusted P Value < 0.0001.

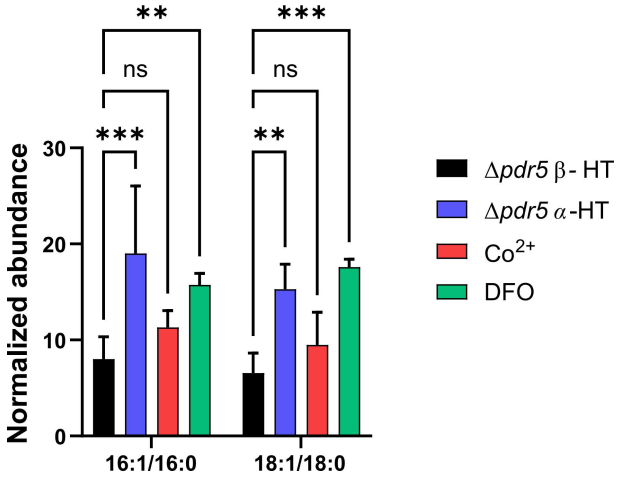

Figure 3.23: The ratios 16:1/16:0 and 18:1/18:0 are calculated based on the levels of saturated and unsaturated FAs measured in the untargeted lipidomic analysis performed in this study. The conversion of both FAs incread significantly in hte α-HT strain untreated and treated with DFO, while Co^{2+} treatments does not show difference compared to the β-HT control strain. All the measured lipids are significantly increased in the α-HT. Each bar is the mean +/- SDs of three biological replicates (n = 4). For the statistics, a one-way ANOVA test for multiple comparisons was applied and corrected using the Sidak statistical hypothesis. **, adjusted p-value = 0.002; ***, adjusted p-value = 0.0002; ****, adjusted p-value < 0.0001.

3.8.2 Diglycerides and Triglycerides

According to Fanning and colleagues pathological expression of α-syn induces an extensive synthesis of FAs in the cell. This excess is stored in diglycerides (DG) and triglycerides (TGs) that in a short time crowd the ER, compromising the secretory pathway, proteins folding and vesicles cycling with severe consequences for the cell homeostasis[527]. Using the results obtained from the untargeted lipidomics profiling performed on the yeast model used in this study, we estimated as well the level of di- and triglycerides. Among the annotated DG and TGs identified in the analysis, we focused on the more abundant ones. In particular, we noticed that DG (18:0\18:1) is the most accumulated DG, whose level is 10-fold higher in the α-HT compared to the β-HT control. Co^{2+} restores this DG (18:0\18:1) to the control level, while DFO halves it (Figure 3.24, **Diglyceride**). This finding is in line with the trend previously estimated for the stearic and oleic acid levels in the

α-HT strain. Similarly, the TGs species identified in the analysis are significantly accumulated in the α-HT strain compared to the β-HT control (Figure 3.24, **Triglycerides)**. In this case, Co^{2+} is more efficient than DFO in reducing the level of these lipids (Figure 3.24, **Triglycerides)**.

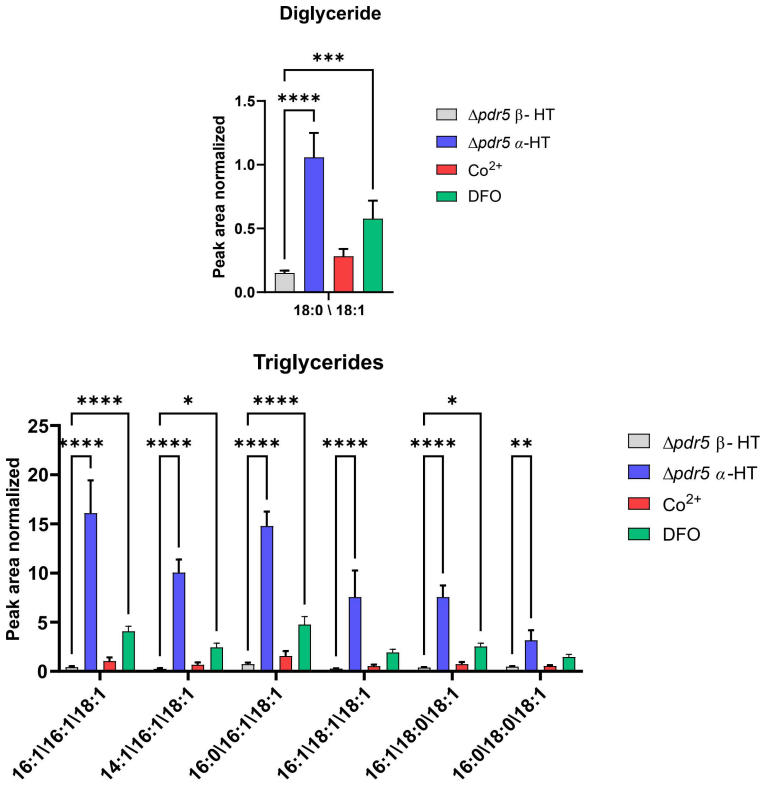

Figure 3.24: The levels of DG (18:0\18:1) (upper part) and TGs (bottom part) shown in the figure are estimated normalizing the values obtained from the untargeted lipidomic analysis for the cell concentration. All the measured lipids are significantly increased in the α-HT and in the same strain treated with DFO 0.3 mM. Each bar is the mean +/- SDs of three biological replicates (n = 4). For the statistics, a one-way ANOVA test for multiple comparisons was applied and corrected using the Dunnet statistical hypothesis. ***, adjusted p-value = 0.0002;****, adjusted p-value < 0.0001

3.9 The thiamine genes

Based on the pathway enrichment analysis of the DEGs upregulated in the α-HT strain compared to the β-HT control at 12 hours, the most affected biological processes were the thiamine biosynthetic process (GO:0009228) and the thiamine diphosphate biosynthetic process (GO:0009229)

(see Figure 3.14 **a**). Thiamine, also known as vitamin B1, is a molecule composed of a methyl thiazole ring and a methyl pyrimidine ring bound together by a methylene bridge[530] (Figure 3.25, **a**). This molecule is the precursor of an important cofactor: thiamine pyrophosphate[531]. Bacteria, plants, and fungi can synthesize thiamine *de novo*, while mammals acquire this supplement from the diet[532]. In yeast, thiamine biosynthesis is organized into two main branches corresponding to the two main structural moieties present in its structure[533] (Figure 3.25 **c**). The "THI genes" encode for the enzymes involved in this biosynthetic process and some of them were identified in the transcriptomic analysis performed in this study. In particular, THI5 (YFL058W), THI12 (YNL332W), THI13 (YDL244W), THI20 (YOL055C) and THI21 (YPL258C) were upregulated in the α-HT strain at 12 hours (Figure 3.25 **b** and Table 3.8). THI5\11\12\and 13 share high sequence homology and catalyze the first reaction of the pyrimidine ring assembly[534] (Figure 3.25 **c**). They convert histidine and pyridoxal 5'-phosphate into the pyrimidine structure through a mechanism that is still poorly understood [535]. It has been reported that this conversion requires iron, and THI5 is a single-turnover enzyme [536] able to bind iron in its active site [537]. THI20\21 are mostly involved in the second step of the same synthetic branch[538] (Figure 3.25 **c**).

Table 3.8: THI genes upregulated in the α-HT strain vs β-HT control at 12 hours.

α-HT vs β-HT at 12 hours			
Gene	Enzyme	Log2FoldChange	padj
YFL058W	THI5	3.87	4.80E-05
YJR156C	THI11	1.06	0.044
YNL332W	THI12	2.98	0.0001
YDL244W	THI13	1.82	0.005
YOL055C	THI20	1.50	0.0001
YPL258C	THI21	1.08	0.002
YPL258C	THI21	1.08	0.002

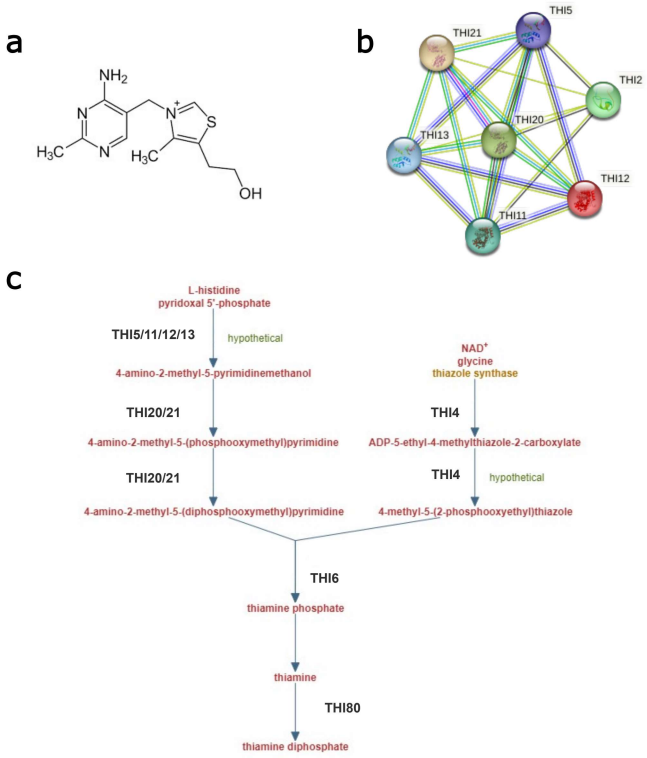

Figure 3.25: **a** Chemical structure of Thiamine. **b** Protein cluster obtained on STRING website (`https://string-db.org/`) with THI genes identified in the transcriptomic profiling of the α-HT strain. **c** Scheme of the thiamine pyrophosphate synthesis pathway in*S. cerevisiae* as reported on the SGD website (`https://pathway.yeastgenome.org/`) with all the genes.

The upregulation of these genes was confirmed by quantitative PCR (Figure 3.26). In the same analysis, we checked the expression of other THI genes (THI4 and THI80) to understand to which extent the pathway was active in the α-HT strain. At 6 hours, the accumulation of THI5\11\12\13 and THI4 was 5-fold and 4-fold higher in the α-HT compared to the β-HT control, respectively (Figure 3.26 **a**). Co^{2+} treatment resulted in a 4-fold increase in THI5\11\12\13 expression compared to the control (Figure 3.26 **a**). THI4 seems also to follow an increasing trend in its expression level in the presence of Co^{2+} (Figure 3.26 **a**). DFO treatment led to a 3-fold increase in THI5\11\12\13 and 4-fold in THI4 expression (Figure 3.26 **a**). At 12 hours, the expression of THI5\11\12\13 increases in α-HT up to 10-fold compared to the β-HT control, 30-fold upon treatment with Co^{2+} and 20-fold with DFO (Figure 3.26 **b**). Co^{2+} also increases the THI20

expression almost 10-fold compared to the β-HT control (Figure 3.26 **b**).

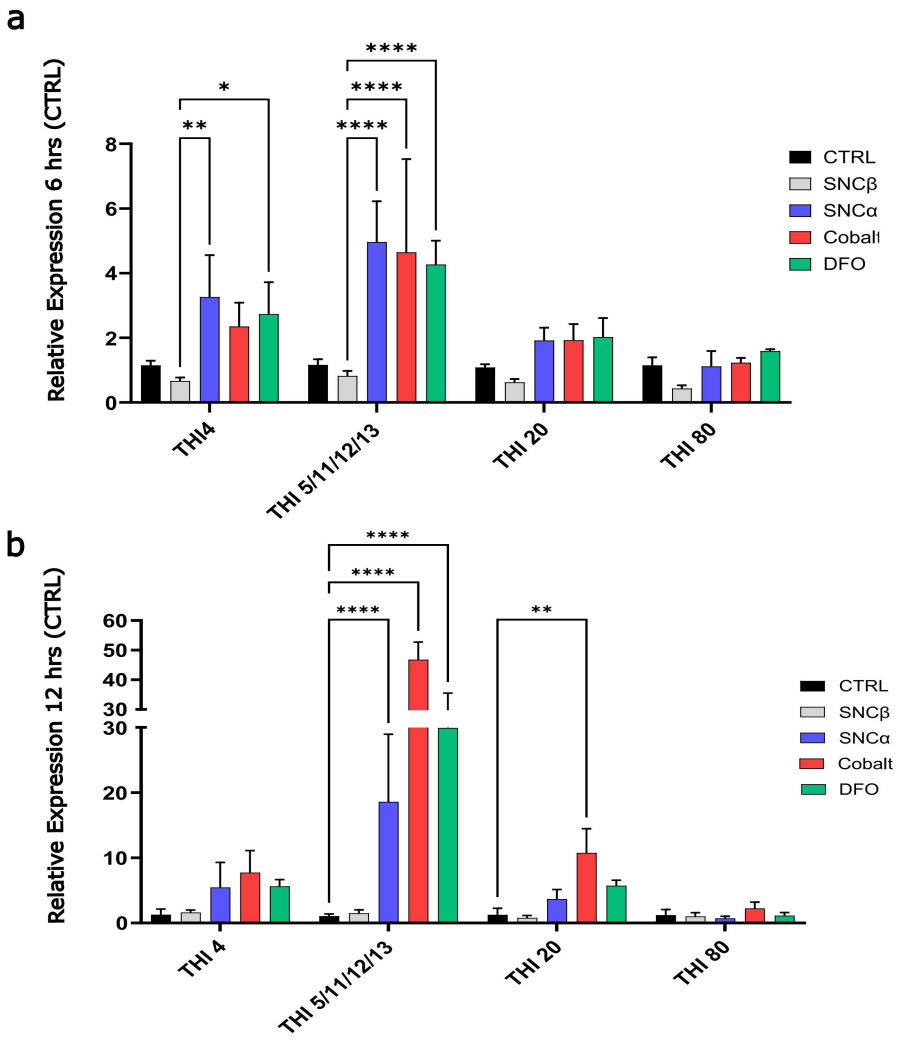

Figure 3.26: Validation of the expression level of THI enzymes by RT-qPCR analysis. Due to the high sequence homology among THI5, THI11, THI12, and THI13, it is not possible to measure the expression of these genes individually. The relative expression of the genes at 6 hours **a** and 12 hours **b** is significantly increased in the α-HT strain untreated and treated with Co^{2+} and DFO 0.3 mM. Each bar is the mean +/- SDs of three biological replicates (n = 3). For the statistics, a one-way ANOVA test for multiple comparisons was applied and corrected using the Dunnet statistical hypothesis. *, adjusted p-value = 0.024; **, adjusted p-value = 0.001; ****, adjusted p-value < 0.0001.

3.9.1 Generation of thiamine overexpression strain

The finding that THI4 and THI5\11\12\13 were confirmed upregulated in the α-HT strain treated with Co^{2+} and DFO led to a further investigation of thiamine biosynthesis. Initially, we cultivated the strain in increasing concentrations of thiamine to boost the synthesis of thiamine pyrophosphate in the cells (Figure 5.6, Appendices). However, we found that simply supplementing the α-HT strain with thiamine did not produce a positive effect on its phenotype (Figure 5.6, Appendices). Consequently, we decided to generate α-HT and β-HT strains able to overexpress the upregulated thiamine genes, following the idea that strong overexpression of those genes may have protective effects against the toxicity induced by α-syn. In fact, it has been reported that thiamine has a beneficial effect in PD patients and PD mouse models promoting dopamine release and reverting some of the disease symptoms[539, 540]. Furthermore, the isoform redundancy made it complicated to adopt the reverse, knockout strategy. We performed a phenotypic assay on the α-HT and β-HT strains engineered to overexpress thiamine synthesis genes (Figure 3.27).

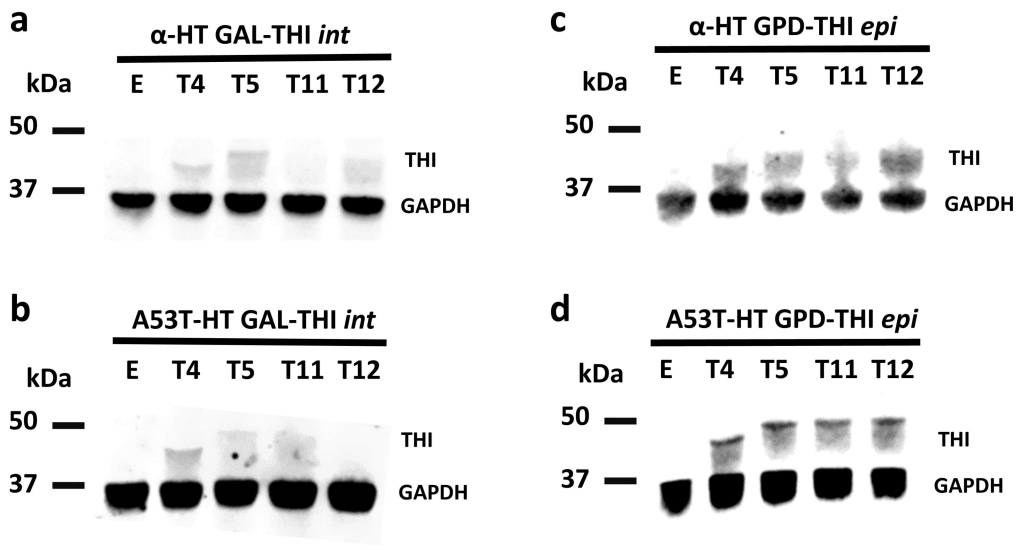

Figure 3.27: In this study, Western blot analysis was used to validate the expression of THI4, THI5, THI11, and THI12, each tagged with an HA epitope at the C-terminus for detection, as reported in the section of the Materials and Methods. The THI4 (T4), THI5 (T5), THI11 (T11), and THI12 (T12) proteins were detected using an antibody specific to the HA tag. This was done after 6 hours of induction in SCG media (**a** and **b**) or under constitutive expression conditions (**c** and **d**). As expected, the bands corresponding to T4, T5, T11, and T12 were less intense under the inducible expression conditions (**a** and **b**) compared to the constitutive expression conditions (**c** and **d**). This suggests that inducible systems lead to lower expression levels compared to constitutive systems, which aligns with standard expectations for these two modes of gene expression. In all conditions, the control strain containing the empty plasmid (E) did not show any bands, confirming the specificity of the HA antibody for the tagged THI proteins. THI4 (T4) had a lower molecular weight compared to the other thiamine-related proteins (T5, T11, T12), which explains why the T4 band was detected at a different level or position on the blot. These results demonstrate that the expression of THI4, THI5, THI11, and THI12 was successfully induced and detected in the experimental conditions, with clear differences in expression levels between the inducible and constitutive systems. The absence of bands in the control (empty plasmid) reinforces the validity of the detection method.

We considered two main series of strain, in one the THI genes were integrated inside the genome (Figure 3.28) and in the second series of strain the THI genes were inserted in an episomal vector (Figure 3.29). The genes are under the control of either the galactose promoter (GAL-THI) to achieve an inducible expression similar to the synuclein proteins, or under the GPD promoter (GPD-THI) for constitutive expression (Figures 3.28 and 3.29). The inducible expression of THI4 and THI5 seems to have a mild positive effect on the growth of the α-HT strain and the A53T-HT mutant strain (when treated with DFO) (Figures 3.28 **a** and **c**). The constitutive expression of

THI11 has a positive effect on the growth of the A53T-HT mostly in the presence of Co^{2+} and DFO, but not on the α-HT strain (Figures 3.28 **b** and **d**). When the THI genes were expressed through episomal vector (Figures 3.29) no positive effect was observed, except for THI12, which seems to improve the phenotype of the A53T-HT strain when it is induced by galactose (Figures 3.29 **c**).

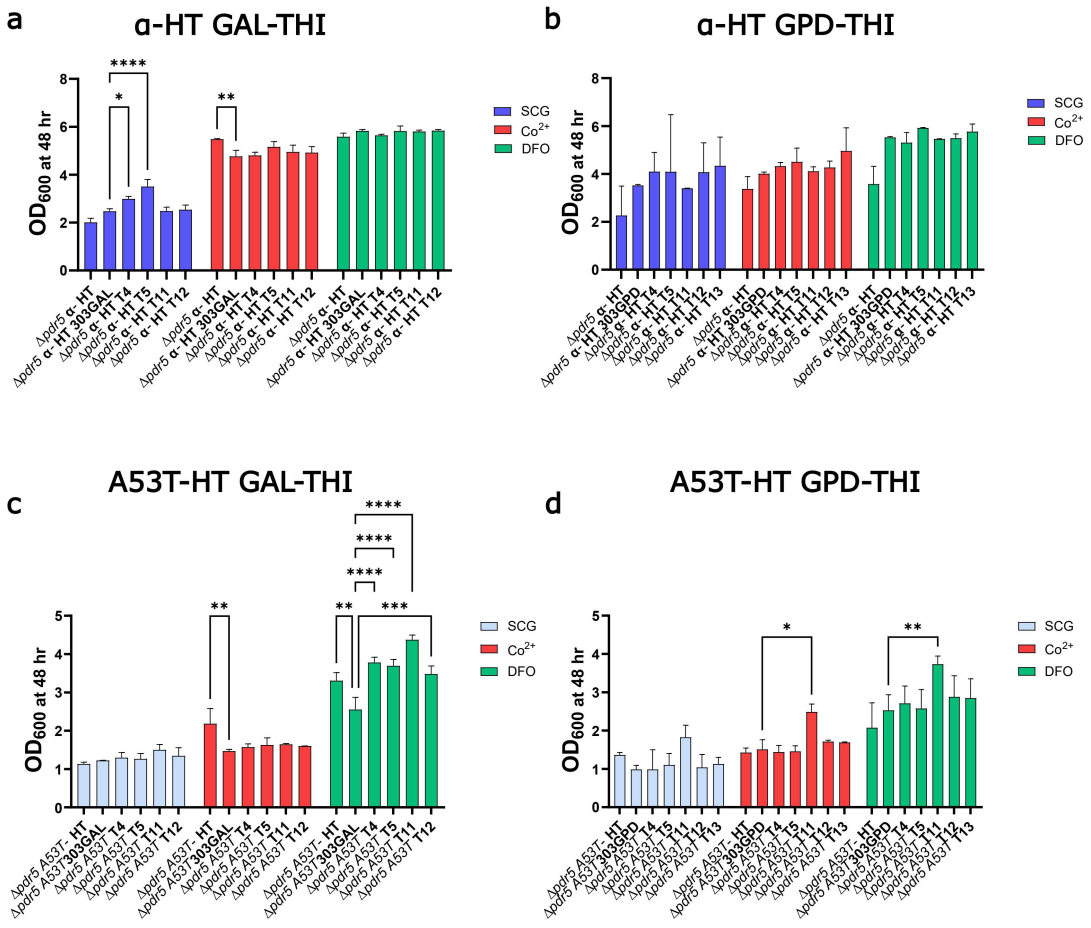

Figure 3.28: OD_{600} measured at 48 hours for the thiamine overexpression strains generated in both genetic backgrounds (α-HT, A53T-HT) by THI4 and THI5\11\12\13 episomial expression. The genes are under the control of inducible promoter in **a** and **c**, under constitutive GDP promoter in **b** and **d**. Each bar is the mean +/- SDs of biological triplicates cultured in a 384-well plate. For the statistics, a two-way ANOVA test for multiple comparisons was applied and corrected using the Dunnet statistical hypothesis. *, adjusted p-value = 0.024; **, adjusted p-value = 0.001; ***, adjusted p-value =0.0002; ****, adjusted p-value < 0.0001.

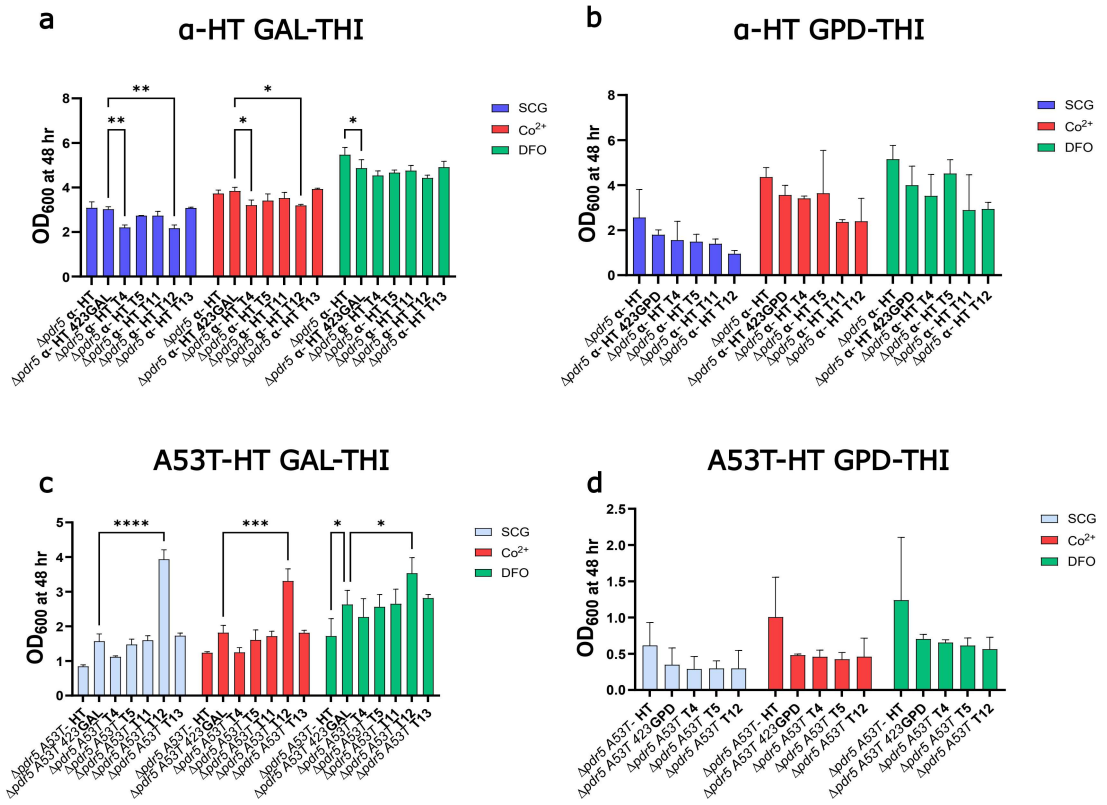

Figure 3.29: OD_{600} measured at 48 hours for the thiamine overexpression strains generated in both genetic backgrounds (α-HT, A53T-HT) by THI4 and THI5\11\12\13 episomial expression. The genes are under the control of inducible promoter in **a** and **c**, under constitutive promoter in **b** and **d**. Each bar is the mean +/- SDs of biological triplicates cultured in a 384-well plate. For the statistics, a two-way ANOVA test for multiple comparisons was applied and corrected using the Dunnet statistical hypothesis. *, adjusted P-value = 0.024; **, adjusted p-value = 0.001; ***, adjusted p-value =0.0002; ****, adjusted p-value < 0.0001.

3.9.2 Validation of thiamine overexpression strains

To confirm if the integration of the THI4 and THI5\11\12\13 in the genome of α-HT and A53T-HT strains enhanced the level of thiamine, we performed a targeted metabolomic analysis, focusing on the level of thiamine, thiamine monophosphate (TMP) and thiamine pyrophosphate (TPP). Interestingly, we were able to detect thiamine in the α-HT strain, but not TMP or TPP. In particular, A53T-HT has a thiamine level 10-fold higher than α-HT (Figure 3.31 **b**). Surprisingly, in both strains, thiamine level is significantly reduced when the THI4, THI5 and THI11 are overex-

pressed (Figure 3.31). We noticed that the inducible expression of THI5 integrated in the genome of α-HT led to an increased level of TPP(Figure 3.31 **a**). A similar, though much milder, effect was noted with THI11 in the A53T strain (Figure 3.31 **b**). This result may explain the positive effect previously observed in the phenotype of the same strains.

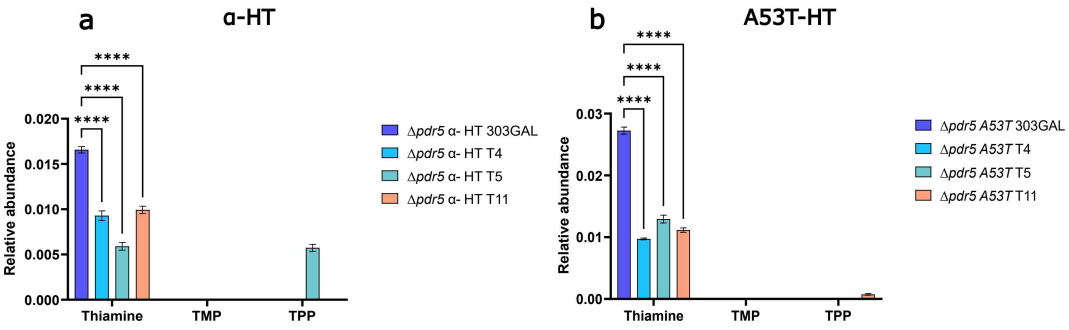

Figure 3.30: Levels of thiamine, TMP, and TPP measured at 24 hours for **a** α-HT, **b** A53T-HT and overexpressing the thiamine biosynthesis genes THI4 and THI5 and THI11 integrative expression. The genes are under the control of the inducible GAL promoter. Each bar is the mean +/- SDs of four biological replicates (n = 4). For the statistics, a two-way ANOVA test for multiple comparisons was applied and corrected using the Dunnet statistical hypothesis. *, adjusted p-value = 0.024, ****, adjusted p-value $<$ 0.0001.

Thiamine, TMP and TPP were also measured also in the β-HT, α-HT and α-HT treated with Co^{2+} and DFO after 24 hours of synuclein proteins induction. The level of these metabolites is lowered compared to the previous analysis as in this case the relative abundance was normalized for the cell concentration. However, consistent with earlier results, α-HT accumulated more thiamine than the β-HT and the treated strains. Additionally, TPP was undetectable in the α-HT strain, while both β-HT and α-HT treated with Co^{2+} and DFO exhibited detectable levels of this metabolite.

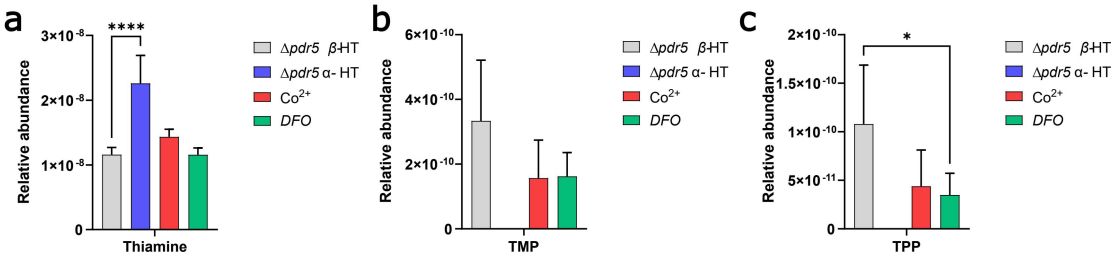

Figure 3.31: Levels of thiamine **a**, TMP **b**, and TPP **c** measured for the β-HT, α-HT and A53T-HT after 24 hours of *alpha*- and β-syn expression. Each bar is the mean +/- SDs of four biological replicates (n = 4). For the statistics, a two-way ANOVA test for multiple comparisons was applied and corrected using the Dunnet statistical hypothesis. ***, adjusted P Value = 0.0002;****, adjusted P Value $<$ 0.0001.

Although the absence of measurements of TMP and TPP in the α-HT strain is interesting and consistent for two different measurements (thiamine strains and HiTox strains), it is important to recognize that this measurement does not prove a suppression of the biosynthesis of TPP in the α-HT strain. The measurements may be influenced by the low cell concentrations of the α-HT strain, which shows a lower growth compared to the β-HT control and the two rescued treatments.

Chapter 4

Discussion and Perspectives

α-Syn is a key protein in the context of PD. Despite the important discoveries made since the first sequencing of the SNCA gene thirty years ago, the link between this important neurodegenerative disease and the molecular mechanisms at the base of the toxicity induced by the pathological aggregation of this protein remains unclear. The research project presented in this PhD thesis starts from the observation that Co^{2+}, Ni^{2+} and DFO can alleviate the α-syn toxicity in a yeast model of human synucleinopathies.

4.1 The Biological Role of Cobalt, Nickel and Deferoxamine

Cobalt[541] and Nickel[542] are elements from groups 9 and 10 of the periodic table respectively, classified as members of the "Iron Triad" due to their magnetic properties similar to those described for iron[543]. At the biological level, they work as co-factors of enzymes involved in important processes conserved among all the phyla of life[544].

Cobalt is ion-coordinated in the corrinoid ring structure of vitamin B12[545, 546] where it binds and activates the methyl group facilitating its transfer between different biological substrates. Cobalt can bind to a methyl group or a 5'-deoxyadenosyl group, forming methylcobalamin, and adenosylcobalamin, respectively. Methylcobalamin is an essential coenzyme in methyltransferase reactions[547], specifically catalyzing the transmethylation of homocysteine to methionine in the cytosol[548, 549]. Adenosylcobalamin, on the other hand, is required for the isomerization of

methylmalonyl CoA in the mitochondria.

The use of Nickel as an enzyme cofactor is mostly confined to bacteria, plants, archaea, and primitive eucaryotes more experienced with highly reducing environmental conditions of our planet at the beginning of life[550, 551]. Only a restricted group of eight enzymes (listed in Table 4.1) uses nickel as a cofactor. For this reason, they are called "nickel-enzymes" and are specialized in the processing of CO, CO_2, H_2, NH_3, O_2, CH_4[552].

Enzyme	Complete name	Function
CODH	[NiFe]-carbon monoxide dehydrogenase[553] (**Redox Enzyme**)	It catalyzes the oxidation of CO into CO_2[554]
ACS	Acetyl-CoA decarbonylase/synthase (**Redox Enzyme**)	It condenses the CO_2 produced by CODH enzyme with a methyl group and a coenzyme A to form acetyl-CoA[555].
MCR	[NiFe]-hydrogenase methyl-CoM reductase[553] (**Redox Enzyme**)	It catalyzes the reduction of methyl-S-coenzyme M $CH_3-S-CoM$ by coenzyme B (CoB) to yield CH_4.
NiSOD	Ni-superoxide dismutase (**Redox Enzyme**)	It is a unique member of the SOD family able to carry out the superoxide dismutation in water[556, 557].
LarA	lactate racemase	It uses Ni^{2+} to catalyze the interconversion of lactic acid in L- and D-isomers[558, 559].
GlxI	glyoxalase I (**Nonredox Enzyme**)	It represents the main cellular detoxification system of toxic glycolysis side-product α-ketoaldehyde in lactate.
ARD	acireductone dioxygenase (**Nonredox Enzyme**)	It is involved in the methionine salvage pathway[560, 561] and based on the metal present in its active site, it can convert the same substrate in different products[562]. In presence of nickel, the enzyme forms 3-methylthiopropionate, formate and CO[563].
Urease	urease (**Nonredox Enzyme**)	Urease active side has two Ni^{2+} that bind and decompose urea, excreted by vertebrates, in ammonia and bicarbonate[564].

Table 4.1: Nickel dependent enzymes

Deferoxamine[565], also known as desferrioxamine B, is a siderophore originally discovered in the soil bacterium *Streptomyces pilosus*, which plays an important role in the iron metabolism of mi-

croorganisms[566]. Similarly to the other iron donors involved in the process of host-mediated iron sequestration (nutritional immunity)[567], DFO is able to stabilize ferric iron Fe^{3+} and many transition metal ions in neutral coordination complexes. The three hydroxamic functional groups present in its structure replace the aqueous molecules surrounding the Fe^{3+} in 1:1 complex[456, 568, 569] (DFO structure reported in Figure 3.7, in the Results chapter). Due to its natural ability to chelate Fe^{3+}, DFO and other siderophores were approved as therapy in the wide spectrum of hemato-disorders that lead to toxic iron accumulation in liver and heart[570, 571].

Cobalt, nickel and DFO share the ability to induce an "hypoxia-like" response in mammalian cells[572] and in yeast[573]. For this property, they are frequently used in molecular biology as a tool to mimic hypoxia[574, 575]. While iron chelators induce hypoxia by sequestering iron from heme proteins, which work as cellular oxygen sensors, the mechanism by which transition metals like cobalt and nickel trigger a similar cellular response remains unclear. It has been suggested that cobalt and other metals can replace iron in the heme groups inhibiting the cellular oxygen sensing[576], but this hypothesis is still under debate. Several studies have demonstrated that cobalt, nickel, and iron chelators upregulate the expression of yeast hypoxic genes containing a specific LORE (Low-Oxygen Response Element) sequence in their promoter regions[446, 529]. This short region (ACTCAACAA) is essential for the activation of yeast genes implicated in various cellular processes, including lipid and ergosterol biosynthesis (OLE1, ERG3, ERG11, ERG25), iron-starvation response (FTR1), and energy metabolism (COX5b and CYC7)[446, 575] (Figure 4.1). One of the objectives of this thesis is to investigate whether the protective effects of these three compounds are mediated against α-syn toxicity through the modulation of a specific cellular pathway associated with these processes under hypoxic conditions.

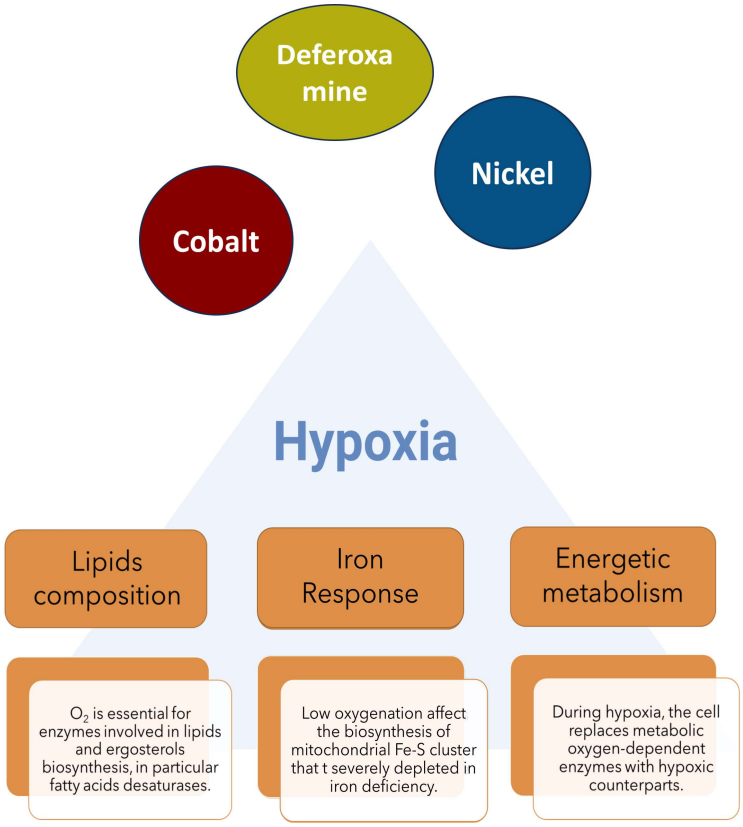

Figure 4.1: This scheme outlines the main hypothesis of this thesis. α-Syn alters critical biological processes in yeast cells, particularly under hypoxic conditions. In this context, Co^{2+}, Ni^{2+}, and DFO can alleviate the toxicity induced by α-syn by modulating the affected processes, which include lipid biosynthesis, iron response, and energy metabolism.

4.2 Hypoxia drives α-syn toxicity via ceramides synthesis

Evidence that hypoxia may positively contribute to PD pathology, exacerbating the toxicity of α-syn was recently confirmed by Li and colleagues. The authors found that exposition to hypoxia conditions (13% of O_2) induces hippocampal neurodegeneration and cognitive deficits in mouse[183]. During chronic hypoxia, extensive activation of HIF-2α increases the expression of alkaline ceramidase, which converts ceramide into free fatty acids and sphingosine[577]. Ceramides are involved in a broad range of pathologies and specifically activate protein phosphatase 2A (PP2A)[578, 579], the phosphatase of α-syn[580]. Decreasing the level of ceramides inhibits

PP2A increasing the pool of Ser129 phosphorylated α-syn, which is more prone to aggregation compared to its dephosphorylated form[183].

In this PhD thesis, we confirmed that hypoxia is an essential condition to induce the toxicity of α-syn also in yeast cells. Based on our transcriptomics results, hypoxia does not lead to a direct downregulation of the PPH22 phosphatase, the yeast orthologous of human PP2A. Nevertheless, similarly on what was reported for the mouse model, cultivation in hypoxic conditions seems to alter the ceramide synthesis pathway in the the α-HiTox strain. In yeast, the enzyme YPC1 canonically deacetylates phytoceramide in sphingosine and free fatty acids, but it has also an important reverse activity. YPC1 synthesizes phytoceramide from palmitic acid and phytosphingosine in a *salvage pathway*, when the principal ceramide synthesis system is inhibited[581, 582]. Our transcriptomic analysis reveals that after 12 hours of α-syn expression, YPC1 is significantly downregulated in the α-HiTox (LOG -1.74 and padj 0.003). There is no evidence in the literature that the expression of this can be modulated under hypoxia stress. Nevertheless, we noticed the presence of a potential upc2 consensus sequence (-487bp upstream of the starting codon) and two mot3 consensus sequences (-394bp and -891bp upstream of the starting codon) upstream of the YPC1 coding sequence. These observations suggest that during hypoxia, cells may increase the synthesis of ceramides and sphingosines to stabilize the membranes under low-oxygen conditions. In the α-HT strain, the downregulation of key genes involved in the biosynthesis of these lipids could lead to a decrease in ceramide levels, potentially resulting in fatal consequences for cell survival during hypoxia.

4.3 Targeting α-syn toxicity through its aggregation

There is strong genetic evidence that increased expression of α-synuclein leads to the pathogenesis in synucleinopathies. For instance, duplications and triplications of the SNCA locus lead to an autosomal dominant form of PD[583, 584] and single nucleotide polymorphisms (SNPs) in the SNCA gene increase the risk of PD[585, 586, 587]. Therapeutic strategies based on the use of antisense oligonucleotides (ASOs) to target α-syn transcription have shown promising results in the treatment of PD. Reducing α-syn expression in mice prevents the formation of aggregates and

motor deficit[588, 589]. Considering the strong correlation between the expression level of α-syn and its toxicity, we considered the hypothesis that Co^{2+}, Ni^{2+}, and DFO might directly influence the expression of the human SNCA gene in the yeast model used in this study. To test this hypothesis, we performed Western blot analysis on protein extracts from treated and untreated cells. Our results demonstrated that none of the treatments significantly altered α-syn expression levels in the cells.

Besides the expression level, α-syn induces toxicity in a dose-dependent manner[590]. The possibility that the accumulation of misfolding protein exacerbates the aggregation process in a pathological loop, is still an open debate[591]. Nevertheless, the prion-like propagation of α-syn[175] and the correlation between protein aggregation and autophagic dysfunction[592], strengthen the opinion that α-syn aggregation should be reconsidered as gain-of-toxic-function[117]. Co^{2+}, Ni^{2+}, and DFO do not modulate the expression of the SNCA gene under the conditions tested, but they may interfere directly or indirectly with the aggregation process of the protein. Exploiting the GFP fluorescence tag present at the C-terminus of the human protein, we were able to visualize and quantify the α-syn aggregates present in the cell. The percentage of cells with aggregates measured in this thesis for the untreated condition (40%) was consistent with already published data on yeast model carrying two copies of human wild-type SNCA gene[593]. The treatments significantly reduced the number of α-syn aggregates, altering the kinetics of the process. According to the data by the time-lapse analysis performed in this thesis:

- Co^{2+} rescues the toxicity of α-synuclein by preventing the formation of new aggregates.
- DFO reduces the number of α-syn aggregates per cell but does not revert their formation.
- Ni^{2+} rapidly disassembles the α-syn aggregates forcing the protein to remain diffuse in the cell.

According to these results, the three compounds do not prevent the expression of α-syn protein in the cell. They rather alter the aggregation kinetic acting on biological processes associated with the hypoxia response as proposed in the scheme shown in Figure 4.1.

4.4 DFO alleviates α-syn toxicity acting on genes regulated by YAP5

In this research thesis, we bring evidence that overexpression of human α-syn in yeast induces *iron dyshomeostasis*. The identification of DFO, an iron chelator, among the compounds able to alleviate the α-syn toxicity, strengthens the important role of iron homeostasis in neurodegenerative diseases. We confirmed that iron rather than other biologically abundant metal ions, contributes to the α-syn toxicity, checking the effect of different metal ion chelators with different degrees of specificity. All the compounds tested, with the exception of DFT, another iron chelator, failed in rescuing the growth phenotype of the α-HT strain. Furthermore, the rhodamine B staining indicates that iron is present in the aggregates, suggesting that the metal may be sequestered in the cytoplasm during the α-syn aggregation. Considering that siderophore compounds ensure the acquisition of environmental Fe^{3+}, we initially evaluated the hypothesis that α-syn was driving the cell to iron starvation and DFO treatment compensates for the lack of metal. This hypothesis was challenged by incubating the cell with different concentrations of iron and DFO complexed with Fe^{3+} (Fe^{3+}-DFO). Increasing Fe^{3+} concentrations, in the presence of the reducing agent ascorbate, led to increased toxicity in the α-HT strain.

In yeast, the response to iron deficiency is mediated by the transcription factors Aft1 and Aft2, which activate the expression of iron transporters on the membrane, promoting iron import in the cell. The transcriptomic profiling of the α-HT compared to the β-HT does not reveal significant changes in the expression level of the two transcription factors. Nevertheless, several important downstream genes were significantly downregulated. The mannoprotein Fit2 (YOR382W), the high-affinity iron importer complex Ftr1/Fet3 (YMR058W), the siderophore uptake receptors as Sit1 (YEL065W) and Enb1 (YOL158C), both mitochondrial iron importers Mrs3 (YJL133W) and Mrs4 (YKR052C), the biotin intermediates importers Bio5 (YNR056C) and Vht1 (YGR065C), the iron vacuolar exporter Smf3 (YLR034C) and the Aft1/Aft2 regulator Grx4 (YER174C) are all downregulated in the α-HT strain. Interestingly, YAP5, the transcription factor of the genes involved in the iron overload response was also downregulated in the α-HT. Yap5, Aft1/Aft2 are all regulated by the intracellular level of Fe-S clusters synthesized by the mitochondrial iron-sulfur

cluster assembly machinery. We wondered if the alteration of iron metabolism in the α-HT was due to an impairment of de denovo Fe-S assembly. We found that Isu1 and Iba57 are downregulated in α-HT. Isu1 serves as a scaffold for the recruitment of all the members of the assembly machinery[594] and its downregulation in parallel with one of the Mrs transporters decreases the rate of Fe-S clusters. Iba57 is involved in the latest steps of the synthesis, it incorporates iron-sulfur clusters into apo-proteins. Finally, the gene association analysis on the 50 genes specifically upregulated by DFO compared to the β-HT control at 12 hours indicated that this siderophore activates the DNA repair process, protoporphyrin and heme transport, protein sorting and degradation. These important cellular mechanisms are highly affected in the α-HT strain.
The enzymes mentioned in this chapter are reported in the following Table with the expression information of the relative genes (Table 4.2)

Table 4.2: DEGs downregulated in the α-HT strain compared to the β-HT control at 12 hours.

β-HT vs HTC		
Protein	Log2FoldChange	padj
FIT2	-1.09	5.39E-04
FET3	-1.71	3.85E-07
FTR1	-0.90	6.91E-16
SIT1	-2.90	1.02E-07
ENB1	-2.01	1.79E-09
MRS3	-1.05	1.90E-19
MRS4	-1.57	4.89E-11
VHT1	-2.74	1.87E-05
SMF3	-1.66	1.62E-03
BIO5	-1.83	3.88E-03
GRX4	-1.71	2.08E-10
YAP5	-1.18	2.06E-36
IBA57	-1.35	3.47E-05
ISU1	-1.69	1.27E-05

4.5 Cobalt mitigates α-syn induced toxicity via lipids metabolism and hypoxic genes regulation

One of the aims of this study consisted in the identification of the molecular mechanisms at the base of the toxicity induced by α-syn through transcriptomic analysis. For this purpose, we designed an experimental essay considering two control groups (HTC and β-HT), one disease group (α-HT) and two treatment groups, respectively exposed to 0.3 mM of Co^{2+} and DFO. We selected two different time points, earlier (6 hours) and later (12 hours) in the lag phase to avoid the intense transcriptomic activity generally associated with the exponential growth phase and gene expression changes due to acute α-syn toxicity. The transcriptomic analysis performed in this study suggested that the heterologous expression of human β-syn in *S. cerevisiae* does not compromise essential cellular processes but instead induces oxidative stress. As highlighted by the pathway enrichment analysis performed on DEGs identified in the binomial comparison β-HT vs HCT, the cell activates oxidative detoxification mechanisms and restores homeostasis, as also evident in the growth curve of the β-HT strain that resembles the one of the HCT control. The results represent one of the first evidence that yeast strains overexpressing human β-syn are valid controls in the studies of α-syn toxicity in yeast.
We obtained different results when we compared the α-HT strain with the β-HT. One of the main changes compared to the previous comparison between the two controls was the presence of DNA repair in the processes highlighted by the pathway enrichment analysis. There is strong evidence that DNA damage is involved in the neurodegeneration in PD, as patients have higher levels of oxidative DNA damage products in the cerebrospinal fluid and peripheral serum[595].

Focusing on the genes mostly affected by α-syn expression, after 6 hours our analysis identified INO1 as the most upregulated gene in α-HT. This unexpected finding contrasts with the transcriptomic regulation reported for INO1 which should be repressed during the lag phase[596]. INO1 encodes the inositol-3-phosphate synthase which catalyzes the cyclization reaction of glucose 6-phosphate into inositol 3-phosphate (myo-inositol-1-phosphate)[482, 597], the first, irreversible, rate-limiting step in the biosynthesis of all inositol-containing compounds[598] (Figure 3.19 **a**).

Inositol is the precursor of phosphoinositides and inositol-sphingolipids, important constituents of the cellular membrane that can work as secondary messengers in signal-transduction pathways. For this reason, the percentage of phosphoinositides in the cellular membranes is relatively low compared to the other lipid classes.

In the transcriptomic profiling of the α-HT strain treated with 0.3 mM Co^{2+}, INO1 emerged as one of the most significantly downregulated differentially expressed genes (DEGs). This opposite trend in the INO1 expression compared to the α-HT strain leads us to propose the importance of this gene in the context of α-syn toxicity. For this purpose, we knocked out INO1 in the α-HT and we tested the resulting strain in a phenotyping assay performed using cultivation media without inositol in the formulation. Although we were unable to ameliorate the α-syn toxicity-associated sick phenotype, we observed increased lethality in the A53T-HT strain upon deletion of INO1.

4.6 α-syn expression changes the membranes lipid composition

The transcriptomic analysis performed in this study suggests that α-syn overexpression should increase the percentage of phosphoinositol in the membrane. To confirm this observation and analyze the general effect of α-syn on the membrane composition we performed an untargeted lipidomics analysis on the β-HT, α-HT untreated and treated with 0.3 mM of Co^{2+} and DFO. Considering the stability of lipids compared to the mRNA, the samples for this analysis were collected at 24 hours of α-syn expression (i.e. later in the growth curve). Treatment with Co^{2+} not only decreased phosphoinositol, consistent with the transcriptomic findings, but also led to an increase in phosphatidylcholine levels. Similarly, DFO treatment also resulted in an increase in phosphatidylcholine. These results strongly suggest that α-syn overexpression induces a shift in the membrane lipid composition through higher levels of phosphoinositol.

4.6.1 Accumulation of Oleic Acid in α-syn models

S. cerevisiae has a simple fatty acid composition mostly based on C16 and C18 FAs[599, 600]. 80% of total FAs are monounsaturated by Ole1, the essential Δ9 desaturase resident in the ER[601].

Ole1 is an iron and oxygen-dependent enzyme that catalyzes the biosynthesis of palmitoleic (16:1) and oleic (18:1) acids[526]. Based on the untargeted lipidomic data, we estimated the levels of palmitic acid (C16:0), stearic acid (C18:0), palmitoleic acid (C16:1), and oleic acid (C18:1), which were consistent with the fatty acid ratios reported previously for yeast strains grown under standard conditions[600]. We wanted to investigate whether α-syn expression in our model leads to the accumulation of oleic acid (C18:1), potentially due to alteration of Ole1 activity, validating observations from a similar yeast model[527]. We observed a significant accumulation of the four analyzed fatty acids (FAs) in the α-HT strain with the unsaturated FAs showing more important increases than the corresponding saturated FAs. Additionally, both Co^{2+} and DFO treatments were found to decrease the levels of these FAs, bringing them nearly to control levels. Based on the unsaturated to saturated fatty acids (16:1/16:0 and 18:1/18:0) Ole1 efficiency was significantly higher in the α-HT strain compared to the β-HT strain, likely due to the accumulation of its substrates (C16:0 and C18:0). DFO and even more importantly Co^{2+} strikingly antagonize the effects on saturated and unsaturated FAs levels induced by high α-syn expression, strongly suggesting an important role of the FA saturation index in the mechanism underlying the protective effects of these compounds.

The untargeted metabolomic analysis conducted in this study confirms that the elevated levels of oleic acid (C18:1), observed in various α-syn toxicity models[527] and in the yeast strains used in this project, could be linked to the accumulation of the Ole1 enzyme substrates (C16:0 and C18:0). This results could be justified in different ways taking into account not just the functionality of this enzyme to convert C16:0 and C18:0 in the respective unsaturated counterparts but also its cellular localization, its access to the substrates, the efficiency of the β-oxydation process. All these factors can be affected in the α-HT strain and contribute to the observed accumulation of FAs. Co^{2+} and DFO treatments effectively prevent this fatty acid accumulation, as the levels of the enzyme's precursors closely resemble those of the control in the presence of these two treatments.

To counteract the accumulation of fatty acids (FAs) and prevent the release of free FAs into

the cytoplasm, the cell enhances the synthesis of diacylglycerols (DGs) and triacylglycerols (TGs) [527]. To test this hypothesis, we measured the levels of these two lipid classes using the same methodology. We observed indeed as high accumulation of DGs and TGs in the α-HT strain, which was significantly reduced after Co^{2+} and DFO treatments. The evidence that these lipids primarily contained unsaturated C16:1 and C18:1 species, further supports the presence of a compensatory mechanism.

4.7 Alteration ATP metabolism

The evidence that synthetic inhibitors of the first complex of the electron transport chain can induce neurodegeneration and parkinsonism in healthy individuals has been largely consolidated[516, 517]. The transcriptomic profile performed in this study provides the first evidence that α-syn overexpression affects the electron transport chain in yeast, a model organism that lacks complex I, specifically at the level of the final components (Figure 4.2 **a**). Our findings show that Cyc7 and Cox5b, the "hypoxic isoforms" of cytochrome C and cytochrome C oxidase, respectively, were downregulated in the α-HT strain. Moreover, ATP metabolism was identified as the most significantly altered pathway among the top 10 pathways affected in the α-HT DEGs homologous to humans (Figure 4.2 **b**). Generally, reduced ATP production drives an increased glycolytic flux, and our transcriptomic and metabolomic analyses reveal that glycolysis is indeed altered in the α-HT strain. The glycolytic intermediates phosphoenolpyruvate and pyruvate accumulate differently in the α-HT strain compared to the β-HT control (Figure 4.2 **c**). While studies in mammalian cells suggest that α-syn may physically interact with glycolytic enzymes, reducing their efficiency [602, 603], we observed downregulation of these genes in the α-HT strain.

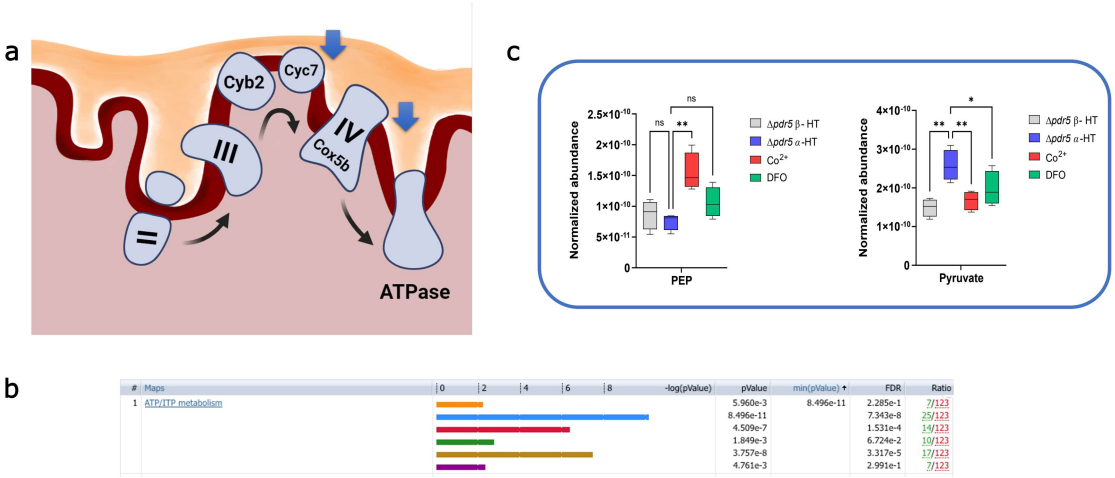

Figure 4.2: **a** Scheme of the mitochondrial respiratory chain of *S.cerevisiae*. The blue arrows indicate downregulation of the expression of the Cyc7 and Cox5b, the two cytochrome C and cytochrome C oxidase isoforms expressed in hypoxic conditions in teh α-HT strain. **b** ATP metabolism emerged as the most significantly altered pathway in the α-HT strain when considering DEGs homologous to human genes. The bar colors in the figure correspond to different comparisons: orange represents the α-HT vs. HTC comparison at 6 hours; blue for α-HT vs. HTC at 12 hours; red for DFO treatment vs. α-HT at 6 hours; green for DFO treatment vs. α-HT at 12 hours; brown for cobalt treatment vs. α-HT at 6 hours; and purple for cobalt treatment vs. α-HT at 12 hours. The ratio indicates the number of ATP metabolism-related genes, present in both yeast and humans, that are significantly differentially expressed in these comparisons. The two treatments (DFO and cobalt) reduce the number of differentially expressed genes between the two-time points, while α-HT shows an opposite trend. **c** Relative abundance of phosphoenolpyruvate and pyruvate at 24 hours. Each box is the mean +/- SDs of four biological replicates (n = 4). For the statistics, a two-way ANOVA test for multiple comparisons was applied and corrected using the Dunnet statistical hypothesis. *, adjusted p-value = 0.024; **, adjusted p-value = 0.001.

4.7.1 Pyruvate accumulation at the center of α-syn toxicity

Bringing together all the findings from the three different omics approaches applied in this study to a yeast model of human synucleinopathies, it seems that changes in the levels of pyruvate may play a role in the toxic phenotype observed in the α-HT strain. Part of this metabolite accesses the mitochondria through the pyruvate carriers and is converted into acetyl-CoA by the PDH complex (Figure 4.3). However, because in the α-HT strain key components of these carriers (MPC2 and MPC3) are downregulated, more pyruvate may be converted into cytosolic acetyl-CoA by the PDH bypassing system (Figure 4.3).

Mitochondrial acetyl-CoA flows in the TCA cycle, where it is converted into citrate (Figure 4.3). This intermediate is significantly accumulated in the α-HT strain, possibly due to the downregulation of both isoforms of the isocitrate dehydrogenases (IDH1 and IDH2), an effect that in yeast seems to be associated with a reduced respiratory function[522]. The excess citrate is exported from the mitochondria to the cytosol, where it can enter the glyoxalate cycle and increase the pool of succinate (Figure 4.3). The elevated levels of succinate in the α-HT strain would support this hypothesis.

When acetyl-CoA levels increase in the mitochondria, it can be converted into acetate by acetyl-carnitine and exported to the cytoplasm through Ach1 [604] (Figure 4.3). This process allows mitochondrial acetyl-CoA to contribute to the synthesis of its cytosolic counterpart. In the α-HT strain, the downregulation of mitochondrial acetyl-carnitine translocase Crc1 (LFC -2.21 padj 3.47E-05) may complicate this transfer, further contributing to the accumulation of citrate.

Cytosolic acetyl-CoA is used as a precursor by the type I FA synthetases (reviewed at [605]). Higher levels of pyruvate and acetyl-CoA can explain the accumulation of palmitic acid (C16:0), stearic acid (C18:0), palmitoleic acid (C16:1), and oleic acid (C18:1) observed here in the α-HT strain, contributing to the lipidic dyshomeostasis induced by α-syn.

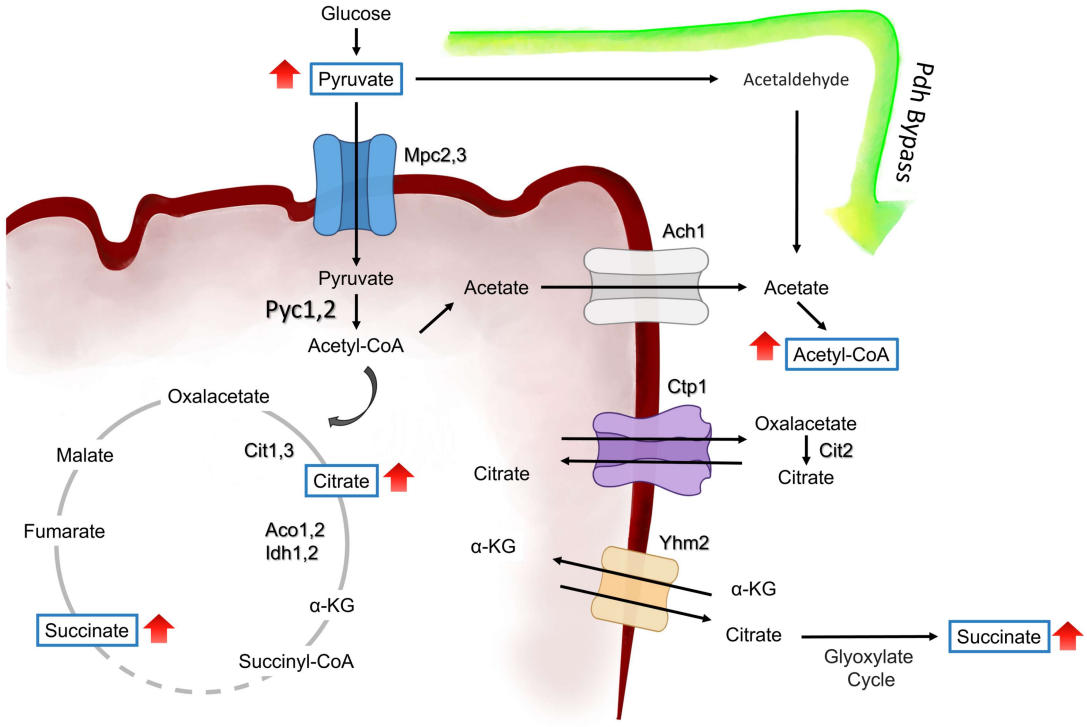

Figure 4.3: A schematic representation of the alternative reactions at the interface of glycolysis and the TCA cycle, inspired by the publication of Rossum and colleagues (2016)[523]. Red arrows highlight the metabolites identified as accumulating in the α-HT strain through metabolomics analysis. Although acetyl-CoA was not directly measured, its accumulation is hypothesized due to observed disruptions in the TCA cycle and electron transport chain.

4.8 Thiamine beneficial effect

In this study, we observed significant upregulation of genes involved in thiamine biosynthesis in the α-HT strain. Although this biosynthetic pathway has been lost in mammalian cells over the course of evolution, several studies on PD models and PD patients have demonstrated the beneficial effects of thiamine in alleviating some disease symptoms[539]. Thiamine is the precursor of thiamine pyrophosphate (TPP), the required cofactor for performing the decarboxylation of aα-keto organic acids in the cell[606]. TPP is, in fact, involved in pyruvate decarboxylase, pyruvate dehydrogenase, alpha-ketoglutarate dehydrogenase, branched-chain amino acid dehydrogenase,

2-hydroxyphytanoyl-CoA lyase and transketolase[607]. Among the THI genes, the members identified in our analysis were THI5\11\12\13 and THI4. These genes encode the enzymes responsible for the initial steps in thiamine biosynthesis for the formation of the pyrimidine and thiazole rings, respectively[538, 608]. To explore if thiamine was part of the rescue mechanism observed when the α-HT strain is cultivated in the presence of Co^{2+} and DFO, we generated yeast strains able to overexpress α-syn and THI5, THI 11, THI 12, THI 13 and THI4. We found that THI5 overexpression had a beneficial effect on the growth phenotype of the α-HT strain, while THI11 improved the growth of the A53T-HT mutant strain in the presence of the two treatments (Co^{2+} and DFO). To validate the functionality of these engineered strains, we also measured the intracellular levels of thiamine, thiamine monophosphate (TMP), and thiamine pyrophosphate (TPP). Both strains α-HT and A53T accumulate thiamine compared to the same strains overexpressing the thiamine genes. Unexpectedly, none of the strains produced detectable levels of TMP or TPP, except for the α-HT strain overexpressing the THI5 gene, which exhibited very low levels of TPP, aligning with the results observed in the phenotyping assays of this strain. The beneficial effect of THI11 in the A53T strain is more pronounced when the gene is expressed under a constitutive promoter, such as GPD.

As previously mentioned, TPP is a crucial cofactor for several key enzymes involved in cellular metabolism. In the α-HT strain, the synthesis of this vital cofactor appears to be inhibited at the early stages, as neither TMP nor TPP is detectable. Restoring TPP levels in cells affected by α-syn toxicity could improve the efficiency of pyruvate decarboxylase and alpha-ketoglutarate dehydrogenase and contribute to reducing the elevated levels of pyruvate observed in this strain.

Bibliography

[1] Michael A Lodato et al. "Aging and neurodegeneration are associated with increased mutations in single human neurons". In: *Science* 359.6375 (2018), pp. 555–559.

[2] Shofiul Azam et al. "The ageing brain: molecular and cellular basis of neurodegeneration". In: *Frontiers in cell and developmental biology* 9 (2021), p. 683459.

[3] Pasko Rakic. "Neurons in rhesus monkey visual cortex: systematic relation between time of origin and eventual disposition". In: *Science* 183.4123 (1974), pp. 425–427.

[4] Pasko Rakic. "No more cortical neurons for you". In: *Science* 313.5789 (2006), pp. 928–929.

[5] David M Wilson et al. "Hallmarks of neurodegenerative diseases". In: *Cell* 186.4 (2023), pp. 693–714.

[6] Claudio Soto. "Unfolding the role of protein misfolding in neurodegenerative diseases". In: *Nature Reviews Neuroscience* 4.1 (2003), pp. 49–60.

[7] Leticia Lemus and Veit Goder. "Regulation of endoplasmic reticulum-associated protein degradation (ERAD) by ubiquitin". In: *Cells* 3.3 (2014), pp. 824–847.

[8] Ralph A Nixon. "The role of autophagy in neurodegenerative disease". In: *Nature medicine* 19.8 (2013), pp. 983–997.

[9] Georgia Minakaki et al. "Autophagy inhibition promotes SNCA/alpha-synuclein release and transfer via extracellular vesicles with a hybrid autophagosome-exosome-like phenotype". In: *Autophagy* 14.1 (2018), pp. 98–119.

[10] Shu Yuan et al. "Rethinking of Alzheimer's disease: Lysosomal overloading and dietary therapy". In: *Frontiers in Aging Neuroscience* 15 (2023), p. 1130658.

[11] J Paul Taylor, John Hardy, and Kenneth H Fischbeck. "Toxic proteins in neurodegenerative disease". In: *science* 296.5575 (2002), pp. 1991–1995.

[12] Aaron Ciechanover. "The ubiquitin-proteasome proteolytic pathway". In: *Cell* 79.1 (1994), pp. 13–21.

[13] James E Galvin et al. "Axon pathology in Parkinson's disease and Lewy body dementia hippocampus contains α-, β-, and γ-synuclein". In: *Proceedings of the National Academy of Sciences* 96.23 (1999), pp. 13450–13455.

[14] Michel Goedert and Maria Grazia Spillantini. "Synucleinopathies and tauopathies". In: *Basic Neurochemistry*. Elsevier, 2012, pp. 829–843.

[15] Christian Lavedan et al. "Identification, localization and characterization of the human γ-synuclein gene". In: *Human genetics* 103 (1998), pp. 106–112.

[16] Ross Jakes, Maria Grazia Spillantini, and Michel Goedert. "Identification of two distinct synucleins from human brain". In: *FEBS letters* 345.1 (1994), pp. 27–32.

[17] Zhong-Zong Pan et al. "γ-Synuclein promotes cancer cell survival and inhibits stress-and chemotherapy drug-induced apoptosis by modulating MAPK pathways". In: *Journal of Biological Chemistry* 277.38 (2002), pp. 35050–35060.

[18] Luc Maroteaux, James T Campanelli, and Richard H Scheller. "Synuclein: a neuron-specific protein localized to the nucleus and presynaptic nerve terminal". In: *Journal of Neuroscience* 8.8 (1988), pp. 2804–2815.

[19] James E Galvin et al. "Differential expression and distribution of α-, β-, and γ-synuclein in the developing human substantia nigra". In: *Experimental neurology* 168.2 (2001), pp. 347–355.

[20] Manish Kumar Jain et al. "Comparative analysis of the conformation, aggregation, interaction, and fibril morphologies of human α-, β-, and γ-synuclein proteins". In: *Biochemistry* 57.26 (2018), pp. 3830–3848.

[21] Michel Goedert. "Alpha-synuclein and neurodegenerative diseases". In: *Nature reviews neuroscience* 2.7 (2001), pp. 492–501.

[22] Vladimir N Uversky et al. "Biophysical properties of the synucleins and their propensities to fibrillate: inhibition of α-synuclein assembly by β-and γ-synucleins". In: *Journal of Biological Chemistry* 277.14 (2002), pp. 11970–11978.

[23] Carlos W Bertoncini et al. "Release of long-range tertiary interactions potentiates aggregation of natively unstructured α-synuclein". In: *Proceedings of the National Academy of Sciences* 102.5 (2005), pp. 1430–1435.

[24] Atsushi Iwata et al. "α-Synuclein forms a complex with transcription factor Elk-1". In: *Journal of neurochemistry* 77.1 (2001), pp. 239–252.

[25] Makoto Hashimoto et al. "β-Synuclein inhibits α-synuclein aggregation: a possible role as an anti-parkinsonian factor". In: *Neuron* 32.2 (2001), pp. 213–223.

[26] Yuxin Fan et al. "β-synuclein modulates α-synuclein neurotoxicity by reducing α-synuclein protein expression". In: *Human molecular genetics* 15.20 (2006), pp. 3002–3011.

[27] Igor F Tsigelny et al. "Dynamics of α-synuclein aggregation and inhibition of pore-like oligomer development by β-synuclein". In: *The FEBS journal* 274.7 (2007), pp. 1862–1877.

[28] James WP Brown et al. "β-Synuclein suppresses both the initiation and amplification steps of α-synuclein aggregation via competitive binding to surfaces". In: *Scientific reports* 6.1 (2016), p. 36010.

[29] Andre Leitao et al. "Unveiling a Selective Mechanism for the Inhibition of -Synuclein Aggregation by -Synuclein". In: *International Journal of Molecular Sciences* 19.2 (2018). ISSN: 1422-0067. URL: https://www.mdpi.com/1422-0067/19/2/334.

[30] Evelien Van de Vondel et al. "Vibrational circular dichroism sheds new light on the competitive effects of crowding and β-synuclein on the fibrillation process of α-synuclein". In: *Biochemistry* 57.41 (2018), pp. 5989–5995.

[31] Junna Hayashi and John A Carver. "β-Synuclein: An enigmatic protein with diverse functionality". In: *Biomolecules* 12.1 (2022), p. 142.

[32] Hongjun Ji et al. "Identification of a breast cancer-specific gene, BCSG1, by direct differential cDNA sequencing". In: *Cancer research* 57.4 (1997), pp. 759–764.

[33] Yangfu Jiang et al. "γ synuclein, a novel heat-shock protein-associated chaperone, stimulates ligand-dependent estrogen receptor α signaling and mammary tumorigenesis". In: *Cancer research* 64.13 (2004), pp. 4539–4546.

[34] Airy Sanjeev and Venkata SK Mattaparthi. "Computational Study on the Role of γ-Synuclein in Inhibiting the α-Synuclein Aggregation". In: *Central Nervous System Agents in Medicinal Chemistry (Formerly Current Medicinal Chemistry-Central Nervous System Agents)* 19.1 (2019), pp. 24–30.

[35] Natalia Ninkina et al. "γ-Synucleinopathy: neurodegeneration associated with overexpression of the mouse protein". In: *Human molecular genetics* 18.10 (2009), pp. 1779–1794.

[36] Andrei Surguchov et al. "Synoretin—a new protein belonging to the synuclein family". In: *Molecular and Cellular Neuroscience* 13.2 (1999), pp. 95–103.

[37] E Dorsey et al. "The emerging evidence of the Parkinson pandemic". In: *Journal of Parkinson's disease* 8.s1 (2018), S3–S8.

[38] N Maserejian, L Vinikoor-Imler, and A Dilley. "Estimation of the 2020 global population of Parkinson's disease (PD)". In: *Movement Disorders*. Vol. 35. WILEY 111 RIVER ST, HOBOKEN 07030-5774, NJ USA. 2020, S79–S80.

[39] MC de De Rijk et al. "Prevalence of Parkinson's disease in Europe: A collaborative study of population-based cohorts. Neurologic Diseases in the Elderly Research Group." In: *Neurology* 54.11 Suppl 5 (2000), S21–3.

[40] James Parkinson. "An essay on the shaking palsy". In: *The Journal of neuropsychiatry and clinical neurosciences* 14.2 (2002), pp. 223–236.

[41] Oleh Hornykiewicz. "Dopamine (3-hydroxytyramine) and brain function". In: *Pharmacological reviews* 18.2 (1966), pp. 925–964.

[42] Matthew M McGregor and Alexandra B Nelson. "Circuit mechanisms of Parkinson's disease". In: *Neuron* 101.6 (2019), pp. 1042–1056.

[43] Sairam Ramesh and Arosh S Perera Molligoda Arachchige. "Depletion of dopamine in Parkinson's disease and relevant therapeutic options: A review of the literature". In: *AIMS neuroscience* 10.3 (2023), p. 200.

[44] Roger L Albin, Anne B Young, and John B Penney. "The functional anatomy of basal ganglia disorders". In: *Trends in neurosciences* 12.10 (1989), pp. 366–375.

[45] Eisaku Ohama and Fusahiro Ikuta. "Parkinson's disease: distribution of Lewy bodies and monoamine neuron system". In: *Acta neuropathologica* 34 (1976), pp. 311–319.

[46] Lysia S Forno. "The Neuropathology Of Parkinson'S Disease: The Lewy body as a clue to the nerve cell degeneration". In: *Progress in Parkinson research* (1988), pp. 11–21.

[47] Haruo Okazaki, Lewis E Lipkin, and Stanley M Aronson. "Diffuse intracytoplasmic ganglionic inclusions (Lewy type) associated with progressive dementia and quadriparesis in flexion". In: *Journal of neuropathology and experimental neurology* 20.2 (1961), pp. 237–244.

[48] FH Lewy and M Lewandowsky. "Handbuch der Neurologie". In: *Berlin: Julius Springer* (1912).

[49] WRG Gibb, T Scott, and AJ Lees. "Neuronal inclusions of Parkinson's disease". In: *Movement disorders: official journal of the Movement Disorder Society* 6.1 (1991), pp. 2–11.

[50] Clifford W Shults. "Lewy bodies". In: *Proceedings of the National Academy of Sciences* 103.6 (2006), pp. 1661–1668.

[51] Michael S Pollanen, Dennis W Dickson, and Catherine Bergeron. "Pathology and biology of the Lewy body". In: *Journal of Neuropathology & Experimental Neurology* 52.3 (1993), pp. 183–191.

[52] Maria Grazia Spillantini et al. "α-Synuclein in Lewy bodies". In: *Nature* 388.6645 (1997), pp. 839–840.

[53] Michael S Pollanen, Catherine Bergeron, and Luitgard Weyer. "Detergent-Insoluble Cortical Lewy Body Fibrils Share Epitopes with Neurofilament and τ". In: *Journal of neurochemistry* 58.5 (1992), pp. 1953–1956.

[54] Takeshi Iwatsubo et al. "Purification and characterization of Lewy bodies from the brains of patients with diffuse Lewy body disease." In: *The American journal of pathology* 148.5 (1996), p. 1517.

[55] Hilal A Lashuel. "Do Lewy bodies contain alpha-synuclein fibrils? and Does it matter? A brief history and critical analysis of recent reports". In: *Neurobiology of disease* 141 (2020), p. 104876.

[56] Maria Grazia Spillantini et al. "Filamentous α-synuclein inclusions link multiple system atrophy with Parkinson's disease and dementia with Lewy bodies". In: *Neuroscience letters* 251.3 (1998), pp. 205–208.

[57] Minami Baba et al. "Aggregation of alpha-synuclein in Lewy bodies of sporadic Parkinson's disease and dementia with Lewy bodies." In: *The American journal of pathology* 152.4 (1998), p. 879.

[58] Omar MA El-Agnaf et al. "Effects of the mutations Ala30 to Pro and Ala53 to Thr on the physical and morphological properties of α-synuclein protein implicated in Parkinson's disease". In: *FEBS letters* 440.1-2 (1998), pp. 67–70.

[59] R Anthony Crowther, Susan E Daniel, and Michel Goedert. "Characterisation of isolated α-synuclein filaments from substantia nigra of Parkinson's disease brain". In: *Neuroscience letters* 292.2 (2000), pp. 128–130.

[60] Sarah H Shahmoradian et al. "Lewy pathology in Parkinson's disease consists of crowded organelles and lipid membranes". In: *Nature neuroscience* 22.7 (2019), pp. 1099–1109.

[61] Walter J Schulz-Schaeffer. "The synaptic pathology of α-synuclein aggregation in dementia with Lewy bodies, Parkinson's disease and Parkinson's disease dementia". In: *Acta neuropathologica* 120 (2010), pp. 131–143.

[62] L Hansen et al. "The Lewy body variant of Alzheimer's disease: a clinical and pathologic entity". In: *Neurology* 40.1 (1990), pp. 1–1.

[63] Kondi Wong et al. "Neuropathology provides clues to the pathophysiology of Gaucher disease". In: *Molecular genetics and metabolism* 82.3 (2004), pp. 192–207.

[64] WRG Gibb, MM Esiri, and AJ Lees. "Clinical and pathological features of diffuse cortical Lewy body disease (Lewy body dementia)". In: *Brain* 110.5 (1987), pp. 1131–1153.

[65] WRG Gibb. "Idiopathic Parkinson's disease and the Lewy body disorders". In: *Neuropathology and applied neurobiology* 12.3 (1986), pp. 223–234.

[66] Margaret M Tompkins and William D Hill. "Contribution of somal Lewy bodies to neuronal death". In: *Brain research* 775.1-2 (1997), pp. 24–29.

[67] Koichi Wakabayashi et al. "The Lewy body in Parkinson's disease: molecules implicated in the formation and degradation of α-synuclein aggregates". In: *Neuropathology* 27.5 (2007), pp. 494–506.

[68] James B Leverenz et al. "Proteomic identification of novel proteins in cortical lewy bodies". In: *Brain Pathology* 17.2 (2007), pp. 139–145.

[69] John HT Power, Olivia L Barnes, and Fariba Chegini. "L ewy Bodies and the Mechanisms of Neuronal Cell Death in P arkinson's Disease and Dementia with L ewy Bodies". In: *Brain Pathology* 27.1 (2017), pp. 3–12.

[70] Carrie K Jones et al. "Discovery, synthesis, and structure–activity relationship development of a series of N-4-(2, 5-dioxopyrrolidin-1-yl) phenylpicolinamides (VU0400195, ML182): characterization of a novel positive allosteric modulator of the metabotropic glutamate receptor 4 (mGlu4) with oral efficacy in an antiparkinsonian animal model". In: *Journal of medicinal chemistry* 54.21 (2011), pp. 7639–7647.

[71] Arvid Carlsson, Margit Lindqvist, and TOR Magnusson. "3, 4-Dihydroxyphenylalanine and 5-hydroxytryptophan as reserpine antagonists". In: *Nature* 180.4596 (1957), pp. 1200–1200.

[72] PL McGeer and LR Zeldowicz. "Administration of dihydroxyphenylalanine to parkinsonian patients". In: *Canadian Medical Association Journal* 90.7 (1964), p. 463.

[73] George C Cotzias, Paul S Papavasiliou, and Rosemary Gellene. "Modification of Parkinsonism—chronic treatment with L-dopa". In: *New England Journal of Medicine* 280.7 (1969), pp. 337–345.

[74] Paul S Papavasiliou et al. "Levodopa in Parkinsonism: potentiation of central effects with a peripheral inhibitor". In: *New England Journal of Medicine* 286.1 (1972), pp. 8–14.

[75] MD Yahr et al. "Modification of L-dopa therapy of Parkinsonism by alpha-methyldopa hydrazine (MK-486)." In: *Transactions of the American Neurological Association* 96 (1971), pp. 55–58.

[76] AJ Lees, KM Shaw, and GM Stern. "" Off period" dystonia and" on period" choreoathetosis in levodopa-treated patients with Parkinson's disease". In: *The Lancet* 310.8046 (1977), p. 1034.

[77] H Baas et al. "Catechol-O-methyltransferase inhibition with tolcapone reduces the" wearing off" phenomenon and levodopa requirements in fluctuating parkinsonian patients". In: *Neurology* 50.5suppl5 (1998), S46–S53.

[78] Gennaro Pagano et al. "Prasinezumab slows motor progression in rapidly progressing early-stage Parkinson's disease". In: *Nature medicine* (2024), pp. 1–8.

[79] Joseph Jankovic et al. "Safety and tolerability of multiple ascending doses of PRX002/RG7935, an anti–α-synuclein monoclonal antibody, in patients with Parkinson disease: a randomized clinical trial". In: *JAMA neurology* 75.10 (2018), pp. 1206–1214.

[80] Maria Grazia Spillantini, M Goedert, and A Divane. "Assignment of human {alpha}-synuclein (SNCA) and {beta}-synuclein (SNCB) genes to chromosomes 4q21 and 5q35". In: *Genomics* 27.2 (1995).

[81] Robert L Nussbaum. "The identification of alpha-synuclein as the first Parkinson disease gene". In: *Journal of Parkinson's disease* 7.s1 (2017), S43–S49.

[82] Mihael H Polymeropoulos et al. "Mutation in the α-synuclein gene identified in families with Parkinson's disease". In: *science* 276.5321 (1997), pp. 2045–2047.

[83] Michel Goedert. "The awakening of α-synuclein". In: *Nature* 388.6639 (1997), pp. 232–233.

[84] Javier Simon-Sanchez et al. "Genome-wide association study reveals genetic risk underlying Parkinson's disease". In: *Nature genetics* 41.12 (2009), pp. 1308–1312.

[85] "Dissection of the genetics of Parkinson's disease identifies an additional association 5 of SNCA and multiple associated haplotypes at 17q21". In: *Human molecular genetics* 20.2 (2011), pp. 345–353.

[86] Todd L Edwards et al. "Genome-wide association study confirms SNPs in SNCA and the MAPT region as common risk factors for Parkinson disease". In: *Annals of human genetics* 74.2 (2010), pp. 97–109.

[87] Nathan Pankratz et al. "Genomewide association study for susceptibility genes contributing to familial Parkinson disease". In: *Human genetics* 124 (2009), pp. 593–605.

[88] International Parkinson Disease Genomics Consortium et al. "Imputation of sequence variants for identification of genetic risks for Parkinson's disease: a meta-analysis of genome-wide association studies". In: *The Lancet* 377.9766 (2011), pp. 641–649.

[89] Marc D Binder, Nobutaka Hirokawa, Uwe Windhorst, et al. *Encyclopedia of neuroscience*. Vol. 3166. Springer Berlin, Germany, 2009.

[90] Paul H Weinreb et al. "NACP, a protein implicated in Alzheimer's disease and learning, is natively unfolded". In: *Biochemistry* 35.43 (1996), pp. 13709–13715.

[91] Leonid Breydo, Jessica W Wu, and Vladimir N Uversky. "α-Synuclein misfolding and Parkinson's disease". In: *Biochimica et Biophysica Acta (BBA)-Molecular Basis of Disease* 1822.2 (2012), pp. 261–285.

[92] Do-Hyoung Kim et al. "Salient features of monomeric alpha-synuclein revealed by NMR spectroscopy". In: *Biomolecules* 10.3 (2020), p. 428.

[93] Do-Hyoung Kim and Kyou-Hoon Han. "PreSMo target-binding signatures in intrinsically disordered proteins". In: *Molecules and cells* 41.10 (2018), pp. 889–899.

[94] Peter E Wright and H Jane Dyson. "Intrinsically unstructured proteins: re-assessing the protein structure-function paradigm". In: *Journal of molecular biology* 293.2 (1999), pp. 321–331.

[95] W Sean Davidson et al. "Stabilization of α-synuclein secondary structure upon binding to synthetic membranes". In: *Journal of Biological Chemistry* 273.16 (1998), pp. 9443–9449.

[96] Julia M George et al. "Characterization of a novel protein regulated during the critical period for song learning in the zebra finch". In: *Neuron* 15.2 (1995), pp. 361–372.

[97] Robert Bussell Jr and David Eliezer. "A structural and functional role for 11-mer repeats in α-synuclein and other exchangeable lipid binding proteins". In: *Journal of molecular biology* 329.4 (2003), pp. 763–778.

[98] Sreeganga Chandra et al. "A broken α-helix in folded α-synuclein". In: *Journal of Biological Chemistry* 278.17 (2003), pp. 15313–15318.

[99] Allan Chris M Ferreon et al. "Interplay of α-synuclein binding and conformational switching probed by single-molecule fluorescence". In: *Proceedings of the National Academy of Sciences* 106.14 (2009), pp. 5645–5650.

[100] Kenji Ueda et al. "Molecular cloning of cDNA encoding an unrecognized component of amyloid in Alzheimer disease." In: *Proceedings of the National Academy of Sciences* 90.23 (1993), pp. 11282–11286.

[101] Katherina Vamvaca, Michael J Volles, and Peter T Lansbury Jr. "The first N-terminal amino acids of α-synuclein are essential for α-helical structure formation in vitro and membrane binding in yeast". In: *Journal of molecular biology* 389.2 (2009), pp. 413–424.

[102] Wolfgang Hoyer et al. "Impact of the acidic C-terminal region comprising amino acids 109- 140 on α-synuclein aggregation in vitro". In: *Biochemistry* 43.51 (2004), pp. 16233–16242.

[103] Sang Myun Park et al. "Distinct roles of the N-terminal-binding domain and the C-terminal-solubilizing domain of α-synuclein, a molecular chaperone". In: *Journal of Biological Chemistry* 277.32 (2002), pp. 28512–28520.

[104] Chang-Wei Liu et al. "A precipitating role for truncated α-synuclein and the proteasome in α-synuclein aggregation: implications for pathogenesis of Parkinson disease". In: *Journal of Biological Chemistry* 280.24 (2005), pp. 22670–22678.

[105] Jacqueline Burré et al. "α-Synuclein promotes SNARE-complex assembly in vivo and in vitro". In: *Science* 329.5999 (2010), pp. 1663–1667.

[106] Anvesh KR Dasari et al. "Tau interacts with the C-terminal region of α-synuclein, promoting formation of toxic aggregates with distinct molecular conformations". In: *Biochemistry* 58.25 (2019), pp. 2814–2821.

[107] Morten Schallburg Nielsen et al. "Ca2+ binding to α-synuclein regulates ligand binding and oligomerization". In: *Journal of Biological Chemistry* 276.25 (2001), pp. 22680–22684.

[108] Rani Moons et al. "Metal ions shape α-synuclein". In: *Scientific reports* 10.1 (2020), p. 16293.

[109] Andrés Binolfi et al. "Interaction of α-synuclein with divalent metal ions reveals key differences: A link between structure, binding specificity and fibrillation enhancement". In: *Journal of the American Chemical Society* 128.30 (2006), pp. 9893–9901.

[110] Yu Lu et al. "Phosphorylation of α-synuclein at Y125 and S129 alters its metal binding properties: implications for understanding the role of α-synuclein in the pathogenesis of Parkinson's disease and related disorders". In: *ACS chemical neuroscience* 2.11 (2011), pp. 667–675.

[111] Daniel Twohig and Henrietta M Nielsen. "α-synuclein in the pathophysiology of Alzheimer's disease". In: *Molecular neurodegeneration* 14.1 (2019), p. 23.

[112] Tobias S Ulmer et al. "Structure and dynamics of micelle-bound human α-synuclein". In: *Journal of Biological Chemistry* 280.10 (2005), pp. 9595–9603.

[113] Ricardo Guerrero-Ferreira et al. "Cryo-EM structure of alpha-synuclein fibrils". In: *elife* 7 (2018), e36402.

[114] Guofen Gao et al. "Brain iron metabolism, redox balance and neurological diseases". In: *Antioxidants* 12.6 (2023), p. 1289.

[115] Reinhard Jahn, David C Cafiso, and Lukas K Tamm. "Mechanisms of SNARE proteins in membrane fusion". In: *Nature Reviews Molecular Cell Biology* 25.2 (2024), pp. 101–118.

[116] Jacqueline Burré, Manu Sharma, and Thomas C Südhof. "α-Synuclein assembles into higher-order multimers upon membrane binding to promote SNARE complex formation". In: *Proceedings of the National Academy of Sciences* 111.40 (2014), E4274–E4283.

[117] Manu Sharma and Jacqueline Burré. "α-Synuclein in synaptic function and dysfunction". In: *Trends in neurosciences* 46.2 (2023), pp. 153–166.

[118] Jichao Sun et al. "Functional cooperation of α-synuclein and VAMP2 in synaptic vesicle recycling". In: *Proceedings of the National Academy of Sciences* 116.23 (2019), pp. 11113–11115.

[119] Vincent A Pieribone et al. "Distinct pools of synaptic vesicles in neurotransmitter release". In: *Nature* 375.6531 (1995), pp. 493–497.

[120] Minchuan Zhang and George J Augustine. "Synapsins and the synaptic vesicle reserve pool: floats or anchors?" In: *Cells* 10.3 (2021), p. 658.

[121] Jiajie Diao et al. "Native α-synuclein induces clustering of synaptic-vesicle mimics via binding to phospholipids and synaptobrevin-2/VAMP2". In: *elife* 2 (2013), e00592.

[122] Antonio Alcaro, Robert Huber, and Jaak Panksepp. "Behavioral functions of the mesolimbic dopaminergic system: an affective neuroethological perspective". In: *Brain research reviews* 56.2 (2007), pp. 283–321.

[123] LL Iversen. "Role of transmitter uptake mechanisms in synaptic neurotransmission." In: *British journal of pharmacology* 41.4 (1971), p. 571.

[124] Gary Rudnick. "Mechanisms of biogenic amine neurotransmitter transporters". In: *Neurotransmitter transporters: structure, function, and regulation*. Springer, 2002, pp. 25–52.

[125] Peter Henricus Maria Franciscus Van Domburg et al. *The human substantia nigra and ventral tegmental area*. Springer, 1991.

[126] George R Uhl et al. "Dopamine transporter messenger RNA in Parkinson's disease and control substantia nigra neurons". In: *Annals of Neurology: Official Journal of the American Neurological Association and the Child Neurology Society* 35.4 (1994), pp. 494–498.

[127] Mohamed Jaber et al. "The dopamine transporter: a crucial component regulating dopamine transmission". In: *Movement disorders: official journal of the Movement Disorder Society* 12.5 (1997), pp. 629–633.

[128] Melanie G Lee and Paul Nurse. "Complementation used to clone a human homologue of the fission yeast cell cycle control gene cdc2". In: *Nature* 327.6117 (1987), pp. 31–35.

[129] Jarod Swant et al. "α-Synuclein stimulates a dopamine transporter-dependent chloride current and modulates the activity of the transporter". In: *Journal of Biological Chemistry* 286.51 (2011), pp. 43933–43943.

[130] Christophe Wersinger et al. "Modulation of dopamine transporter function by α-synuclein is altered by impairment of cell adhesion and by induction of oxidative stress". In: *The FASEB journal* 17.14 (2003), pp. 1–30.

[131] Brittany Butler et al. "Dopamine transporter activity is modulated by α-synuclein". In: *Journal of Biological Chemistry* 290.49 (2015), pp. 29542–29554.

[132] Christophe Wersinger, Milan Rusnak, and Anita Sidhu. "Modulation of the trafficking of the human serotonin transporter by human alpha-synuclein". In: *European Journal of Neuroscience* 24.1 (2006), pp. 55–64.

[133] Lluis Miquel-Rio et al. "Human α-synuclein overexpression in mouse serotonin neurons triggers a depressive-like phenotype. Rescue by oligonucleotide therapy". In: *Translational Psychiatry* 12.1 (2022), p. 79.

[134] Diana Alarcón-Arís et al. "Selective α-synuclein knockdown in monoamine neurons by intranasal oligonucleotide delivery: potential therapy for Parkinson's disease". In: *Molecular Therapy* 26.2 (2018), pp. 550–567.

[135] Stephen J Wood et al. "α-Synuclein fibrillogenesis is nucleation-dependent: implications for the pathogenesis of Parkinson s disease". In: *Journal of Biological Chemistry* 274.28 (1999), pp. 19509–19512.

[136] Marthe HR Ludtmann et al. "α-synuclein oligomers interact with ATP synthase and open the permeability transition pore in Parkinson's disease". In: *Nature communications* 9.1 (2018), p. 2293.

[137] Bart D van Rooijen, Mireille MAE Claessens, and Vinod Subramaniam. "Membrane permeabilization by oligomeric α-synuclein: in search of the mechanism". In: *PLoS One* 5.12 (2010), e14292.

[138] Giuliana Fusco et al. "Structural basis of membrane disruption and cellular toxicity by α-synuclein oligomers". In: *Science* 358.6369 (2017), pp. 1440–1443.

[139] Plamena R Angelova et al. "Ca2+ is a key factor in α-synuclein-induced neurotoxicity". In: *Journal of cell science* 129.9 (2016), pp. 1792–1801.

[140] Emma Deas et al. "Alpha-synuclein oligomers interact with metal ions to induce oxidative stress and neuronal death in Parkinson's disease". In: *Antioxidants & redox signaling* 24.7 (2016), pp. 376–391.

[141] Je Min Yoo et al. "Polymorphism in alpha-synuclein oligomers and its implications in toxicity under disease conditions". In: *Frontiers in Molecular Biosciences* 9 (2022), p. 959425.

[142] Guilherme AP de Oliveira and Jerson L Silva. "Alpha-synuclein stepwise aggregation reveals features of an early onset mutation in Parkinson's disease". In: *Communications biology* 2.1 (2019), p. 374.

[143] Karin M Danzer et al. "Different species of α-synuclein oligomers induce calcium influx and seeding". In: *Journal of Neuroscience* 27.34 (2007), pp. 9220–9232.

[144] Stefan Auer, Christopher M Dobson, and Michele Vendruscolo. "Characterization of the nucleation barriers for protein aggregation and amyloid formation". In: *HFSP journal* 1.2 (2007), pp. 137–146.

[145] Laxmikant Gadhe et al. "Intermediates of α-synuclein aggregation: Implications in Parkinson's disease pathogenesis". In: *Biophysical Chemistry* 281 (2022), p. 106736.

[146] VS Mangipudi and AFSHIN FALSAFI. "Direct estimation of the adhesion of solid polymers". In: *Adhesion Science and Engineering*. Elsevier, 2002, pp. 75–138.

[147] Xi Li et al. "Early stages of aggregation of engineered α-synuclein monomers and oligomers in solution". In: *Scientific Reports* 9.1 (2019), p. 1734.

[148] Dhiman Ghosh et al. "Structure based aggregation studies reveal the presence of helix-rich intermediate during α-Synuclein aggregation". In: *Scientific reports* 5.1 (2015), p. 9228.

[149] Mihaela M Apetri et al. "Secondary structure of α-synuclein oligomers: characterization by raman and atomic force microscopy". In: *Journal of molecular biology* 355.1 (2006), pp. 63–71.

[150] Fabiana Miraglia et al. "Subcellular localization of alpha-synuclein aggregates and their interaction with membranes". In: *Neural Regeneration Research* 13.7 (2018), pp. 1136–1144.

[151] Pablo Gracia et al. "Multiplicity of α-synuclein aggregated species and their possible roles in disease". In: *International journal of molecular sciences* 21.21 (2020), p. 8043.

[152] Siddhartha Banerjee et al. "A novel pathway for amyloids self-assembly in aggregates at nanomolar concentration mediated by the interaction with surfaces". In: *Scientific reports* 7.1 (2017), p. 45592.

[153] Natalie Landeck et al. "Two C-terminal sequence variations determine differential neurotoxicity between human and mouse α-synuclein". In: *Molecular neurodegeneration* 15 (2020), pp. 1–23.

[154] Salman F Banani et al. "Biomolecular condensates: organizers of cellular biochemistry". In: *Nature reviews Molecular cell biology* 18.5 (2017), pp. 285–298.

[155] Clifford P Brangwynne et al. "Germline P granules are liquid droplets that localize by controlled dissolution/condensation". In: *Science* 324.5935 (2009), pp. 1729–1732.

[156] Clifford P Brangwynne, Timothy J Mitchison, and Anthony A Hyman. "Active liquid-like behavior of nucleoli determines their size and shape in Xenopus laevis oocytes". In: *Proceedings of the National Academy of Sciences* 108.11 (2011), pp. 4334–4339.

[157] Trish E Kaiser, Robert V Intine, and Miroslav Dundr. "De novo formation of a subnuclear body". In: *Science* 322.5908 (2008), pp. 1713–1717.

[158] Armelle Corpet et al. "PML nuclear bodies and chromatin dynamics: catch me if you can!" In: *Nucleic Acids Research* 48.21 (2020), pp. 11890–11912.

[159] Amandine Molliex et al. "Phase separation by low complexity domains promotes stress granule assembly and drives pathological fibrillization". In: *Cell* 163.1 (2015), pp. 123–133.

[160] Soumik Ray et al. "α-Synuclein aggregation nucleates through liquid–liquid phase separation". In: *Nature chemistry* 12.8 (2020), pp. 705–716.

[161] Alexander K Buell et al. "Solution conditions determine the relative importance of nucleation and growth processes in α-synuclein aggregation". In: *Proceedings of the National Academy of Sciences* 111.21 (2014), pp. 7671–7676.

[162] Ricardo Gaspar et al. "Secondary nucleation of monomers on fibril surface dominates α-synuclein aggregation and provides autocatalytic amyloid amplification". In: *Quarterly reviews of biophysics* 50 (2017), e6.

[163] Pratibha Kumari et al. "Structural insights into α-synuclein monomer–fibril interactions". In: *Proceedings of the National Academy of Sciences* 118.10 (2021), e2012171118.

[164] Samuel IA Cohen et al. "Proliferation of amyloid-β42 aggregates occurs through a secondary nucleation mechanism". In: *Proceedings of the National Academy of Sciences* 110.24 (2013), pp. 9758–9763.

[165] Volodymyr V Shvadchak, Mireille MAE Claessens, and Vinod Subramaniam. "Fibril breaking accelerates α-synuclein fibrillization". In: *Biophysical Journal* 108.2 (2015), 63a.

[166] Mattias Törnquist et al. "Secondary nucleation in amyloid formation". In: *Chemical communications* 54.63 (2018), pp. 8667–8684.

[167] Roberta Cascella et al. "The release of toxic oligomers from α-synuclein fibrils induces dysfunction in neuronal cells". In: *Nature communications* 12.1 (2021), p. 1814.

[168] Stanley B Prusiner. "Prions". In: *Proceedings of the National Academy of Sciences* 95.23 (1998), pp. 13363–13383.

[169] Stanley B Prusiner. "Neurodegenerative diseases and prions". In: *New England Journal of Medicine* 344.20 (2001), pp. 1516–1526.

[170] C Warren Olanow and Patrik Brundin. "Parkinson's disease and alpha synuclein: is Parkinson's disease a prion-like disorder?" In: *Movement Disorders* 28.1 (2013), pp. 31–40.

[171] Jeffrey H Kordower et al. "Lewy body–like pathology in long-term embryonic nigral transplants in Parkinson's disease". In: *Nature medicine* 14.5 (2008), pp. 504–506.

[172] Jia-Yi Li et al. "Lewy bodies in grafted neurons in subjects with Parkinson's disease suggest host-to-graft disease propagation". In: *Nature medicine* 14.5 (2008), pp. 501–503.

[173] Masami Masuda-Suzukake et al. "Prion-like spreading of pathological α-synuclein in brain". In: *Brain* 136.4 (2013), pp. 1128–1138.

[174] Paula Desplats et al. "Inclusion formation and neuronal cell death through neuron-to-neuron transmission of α-synuclein". In: *Proceedings of the National Academy of Sciences* 106.31 (2009), pp. 13010–13015.

[175] Heiko Braak et al. "Staging of brain pathology related to sporadic Parkinson's disease". In: *Neurobiology of aging* 24.2 (2003), pp. 197–211.

[176] Kelvin C Luk et al. "Pathological α-synuclein transmission initiates Parkinson-like neurodegeneration in nontransgenic mice". In: *Science* 338.6109 (2012), pp. 949–953.

[177] Jessica M Froula et al. "Defining α-synuclein species responsible for Parkinson's disease phenotypes in mice". In: *Journal of Biological Chemistry* 294.27 (2019), pp. 10392–10406.

[178] L Eric Huang et al. "Activation of hypoxia-inducible transcription factor depends primarily upon redox-sensitive stabilization of its α subunit". In: *Journal of Biological Chemistry* 271.50 (1996), pp. 32253–32259.

[179] Johannes Burtscher et al. "Fatal attraction–The role of hypoxia when alpha-synuclein gets intimate with mitochondria". In: *Neurobiology of Aging* 107 (2021), pp. 128–141.

[180] Johannes Burtscher et al. "Hypoxia and brain aging: Neurodegeneration or neuroprotection?" In: *Ageing research reviews* 68 (2021), p. 101343.

[181] Jean-Paul Janssens. "Aging of the respiratory system: impact on pulmonary function tests and adaptation to exertion". In: *Clinics in chest medicine* 26.3 (2005), pp. 469–484.

[182] Dörthe M Katschinski. "Is there a molecular connection between hypoxia and aging?" In: *Experimental gerontology* 41.5 (2006), pp. 482–484.

[183] Gaifen Li et al. "Chronic hypoxia leads to cognitive impairment by promoting HIF-2α-mediated ceramide catabolism and alpha-synuclein hyperphosphorylation". In: *Cell Death Discovery* 8.1 (2022), p. 473.

[184] Hideo Fujiwara et al. "α-Synuclein is phosphorylated in synucleinopathy lesions". In: *Nature cell biology* 4.2 (2002), pp. 160–164.

[185] Natali D'Aiuto et al. "Hypoxia, acidification and oxidative stress in cells cultured at large distances from an oxygen source". In: *Scientific Reports* 12.1 (2022), p. 21699.

[186] Satish Srinivasan and Narayan G Avadhani. "Cytochrome c oxidase dysfunction in oxidative stress". In: *Free Radical Biology and Medicine* 53.6 (2012), pp. 1252–1263.

[187] Giuseppe Paradies et al. "The effect of reactive oxygen species generated from the mitochondrial electron transport chain on the cytochrome c oxidase activity and on the cardiolipin content in bovine heart submitochondrial particles". In: *FEBS letters* 466.2-3 (2000), pp. 323–326.

[188] Marta Robotta et al. "Locally resolved membrane binding affinity of the N-terminus of α-synuclein". In: *Biochemistry* 51.19 (2012), pp. 3960–3962.

[189] Stephanie Ghio et al. "Cardiolipin promotes pore-forming activity of alpha-synuclein oligomers in mitochondrial membranes". In: *ACS chemical neuroscience* 10.8 (2019), pp. 3815–3829.

[190] Erika Ponzini et al. "Methionine oxidation in α-synuclein inhibits its propensity for ordered secondary structure". In: *Journal of Biological Chemistry* 294.14 (2019), pp. 5657–5665.

[191] R Labbe-Bois. "The ferrochelatase from Saccharomyces cerevisiae. Sequence, disruption, and expression of its structural gene HEM15." In: *Journal of Biological Chemistry* 265.13 (1990), pp. 7278–7283.

[192] Li Zhang and L Guarente. "Heme binds to a short sequence that serves a regulatory function in diverse proteins." In: *The EMBO journal* 14.2 (1995), pp. 313–320.

[193] Thomas Hon et al. "A mechanism of oxygen sensing in yeast: multiple oxygen-responsive steps in the heme biosynthetic pathway affect Hap1 activity". In: *Journal of Biological Chemistry* 278.50 (2003), pp. 50771–50780.

[194] Richard S Zitomer and CHARLES V Lowry. "Regulation of gene expression by oxygen in Saccharomyces cerevisiae". In: *Microbiological reviews* 56.1 (1992), pp. 1–11.

[195] L Zhang and A Hach. "Molecular mechanism of heme signaling in yeast: the transcriptional activator Hap1 serves as the key mediator". In: *Cellular and Molecular Life Sciences CMLS* 56 (1999), pp. 415–426.

[196] Jutta Deckert et al. "Mutational analysis of Rox1, a DNA-bending repressor of hypoxic genes in Saccharomyces cerevisiae". In: *Molecular and cellular biology* (1995).

[197] Tania M Malave and Sharon YR Dent. "Transcriptional repression by Tup1–Ssn6". In: *Biochemistry and Cell Biology* 84.4 (2006), pp. 437–443.

[198] Lee G Klinkenberg et al. "Combinatorial repression of the hypoxic genes of Saccharomyces cerevisiae by DNA binding proteins Rox1 and Mot3". In: *Eukaryotic cell* 4.4 (2005), pp. 649–660.

[199] Larry A Allen et al. "Isoforms of Yeast Cytochrome c Oxidase Subunit V Affect the Binuclear Reaction Center and Alter the Kinetics of Interaction with the Isoforms of Yeast Cytochrome c ()". In: *Journal of Biological Chemistry* 270.1 (1995), pp. 110–118.

[200] RA Waterland et al. "The isoforms of yeast cytochrome c oxidase subunit V alter the in vivo kinetic properties of the holoenzyme". In: *Journal of Biological Chemistry* 266.7 (1991), pp. 4180–4186.

[201] Rrichard S Zitomer, Pauline Carrico, and Jutta Deckert. "Regulation of hypoxic gene expression in yeast". In: *Kidney international* 51.2 (1997), pp. 507–513.

[202] Odeniel Sertil et al. "The DAN1 gene of S. cerevisiae is regulated in parallel with the hypoxic genes, but by a different mechanism". In: *Gene* 192.2 (1997), pp. 199–205.

[203] Odeniel Sertil et al. "Synergistic repression of anaerobic genes by Mot3 and Rox1 in Saccharomyces cerevisiae". In: *Nucleic acids research* 31.20 (2003), pp. 5831–5837.

[204] J MARCEL van der Vaart et al. "Identification of three mannoproteins in the cell wall of Saccharomyces cerevisiae". In: *Journal of bacteriology* 177.11 (1995), pp. 3104–3110.

[205] L Heleen P Caro et al. "Transcription of multiple cell wall protein-encoding genes in Saccharomyces cerevisiae is differentially regulated during the cell cycle". In: *FEMS microbiology letters* 161.2 (1998), pp. 345–349.

[206] Natalia Abramova et al. "Reciprocal regulation of anaerobic and aerobic cell wall mannoprotein gene expression in Saccharomyces cerevisiae". In: *Journal of bacteriology* 183.9 (2001), pp. 2881–2887.

[207] Natalia E Abramova et al. "Regulatory mechanisms controlling expression of the DAN/TIR mannoprotein genes during anaerobic remodeling of the cell wall in Saccharomyces cerevisiae". In: *Genetics* 157.3 (2001), pp. 1169–1177.

[208] Brian D Cohen et al. "Induction and repression of DAN1 and the family of anaerobic mannoprotein genes in Saccharomyces cerevisiae occurs through a complex array of regulatory sites". In: *Nucleic Acids Research* 29.3 (2001), pp. 799–808.

[209] Melody Germann et al. "Characterizing sterol defect suppressors uncovers a novel transcriptional signaling pathway regulating zymosterol biosynthesis". In: *Journal of Biological Chemistry* 280.43 (2005), pp. 35904–35913.

[210] shild Vik and Jasper Rine. "Upc2p and Ecm22p, dual regulators of sterol biosynthesis in Saccharomyces cerevisiae". In: *Molecular and cellular biology* (2001).

[211] Parissa Alimardani et al. "SUT1-promoted sterol uptake involves the ABC transporter Aus1 and the mannoprotein Dan1 whose synergistic action is sufficient for this process". In: *Biochemical Journal* 381.1 (2004), pp. 195–202.

[212] Manickam Viswanathan et al. "Seripauperins of Saccharomyces cerevisiae: a new multigene family encoding serine-poor relatives of serine-rich proteins". In: *Gene* 148.1 (1994), pp. 149–153.

[213] Masafumi Iwami. "Bombyxin: an insect brain peptide that belongs to the insulin family". In: *Zoological science* 17.8 (2000), pp. 1035–1044.

[214] Yuko Kawabe, Hannah Waterson, and Akira Mizoguchi. "Bombyxin (Bombyx insulin-like peptide) increases the respiration rate through facilitation of carbohydrate catabolism in Bombyx mori". In: *Frontiers in Endocrinology* 10 (2019), p. 150.

[215] Mariel Donzeau, Jean-Paul Bourdineaud, and Guy J-M Lauquin. "Regulation by low temperatures and anaerobiosis of a yeast gene specifying a putative GPI-anchored plasma membrane". In: *Molecular microbiology* 20.2 (1996), pp. 449–459.

[216] Leslie RZ Kowalski, Keiji Kondo, and Masayori Inouye. "Cold-shock induction of a family of TIP1-related proteins associated with the membrane in Saccharomyces cerevisiae". In: *Molecular microbiology* 15.2 (1995), pp. 341–353.

[217] Tristan Rossignol et al. "Genome-wide monitoring of wine yeast gene expression during alcoholic fermentation". In: *Yeast* 20.16 (2003), pp. 1369–1385.

[218] Najma Rachidi et al. "Saccharomyces cerevisiae PAU genes are induced by anaerobiosis". In: *Molecular microbiology* 35.6 (2000), pp. 1421–1430.

[219] Jason R Cannon and J Timothy Greenamyre. "The role of environmental exposures in neurodegeneration and neurodegenerative diseases". In: *Toxicological Sciences* 124.2 (2011), pp. 225–250.

[220] Caroline M Tanner. "The role of environmental toxins in the etiology of Parkinson's disease". In: *Trends in neurosciences* 12.2 (1989), pp. 49–54.

[221] JM Gorell et al. "Occupational exposures to metals as risk factors for Parkinson's disease". In: *Neurology* 48.3 (1997), pp. 650–658.

[222] EC Hirsch et al. "Iron and aluminum increase in the substantia nigra of patients with Parkinson's disease: an X-ray microanalysis". In: *Journal of neurochemistry* 56.2 (1991), pp. 446–451.

[223] DT Dexter et al. "Alterations in the levels of iron, ferritin and other trace metals in Parkinson's disease and other neurodegenerative diseases affecting the basal ganglia". In: *Brain* 114.4 (1991), pp. 1953–1975.

[224] Peter Riederer et al. "Transition metals, ferritin, glutathione, and ascorbic acid in parkinsonian brains". In: *Journal of neurochemistry* 52.2 (1989), pp. 515–520.

[225] Anna Wypijewska et al. "Iron and reactive oxygen species activity in parkinsonian substantia nigra". In: *Parkinsonism & related disorders* 16.5 (2010), pp. 329–333.

[226] Stephen H Banyard, David K Stammers, and Pauline M Harrison. "Electron density map of apoferritin at 2.8-Å resolution". In: *Nature* 271.5642 (1978), pp. 282–284.

[227] Robert R Crichton. "Structure and function of ferritin". In: *Angewandte Chemie International Edition in English* 12.1 (1973), pp. 57–65.

[228] Kay L Double et al. "Iron-binding characteristics of neuromelanin of the human substantia nigra". In: *Biochemical pharmacology* 66.3 (2003), pp. 489–494.

[229] Toshihide Shima et al. "Binding of iron to neuromelanin of human substantia nigra and synthetic melanin: an electron paramagnetic resonance spectroscopy study". In: *Free Radical Biology and Medicine* 23.1 (1997), pp. 110–119.

[230] Dariusz Koziorowski et al. "ELISA reveals a difference in the structure of substantia nigra ferritin in Parkinson's disease and incidental Lewy body compared to control". In: *Parkinsonism & related disorders* 13.4 (2007), pp. 214–218.

[231] F Bolzoni et al. "Magnetic investigations of human mesencephalic neuromelanin". In: *Biochimica et Biophysica Acta (BBA)-Molecular Basis of Disease* 1586.2 (2002), pp. 210–218.

[232] Manfred Gerlach et al. "The Role of Iron in the Pathogenesis of Parkinson's Disease". In: *Neurodegenerative diseases and metal ions* 1 (2006), pp. 125–149.

[233] Henry John Horstman Fenton. "LXXIII.—Oxidation of tartaric acid in presence of iron". In: *Journal of the Chemical Society, Transactions* 65 (1894), pp. 899–910.

[234] Karina Joppe et al. "The contribution of iron to protein aggregation disorders in the central nervous system". In: *Frontiers in Neuroscience* 13 (2019), p. 15.

[235] Natalie Golts et al. "Magnesium inhibits spontaneous and iron-induced aggregation of α-synuclein". In: *Journal of Biological Chemistry* 277.18 (2002), pp. 16116–16123.

[236] Marcus Kostka et al. "Single particle characterization of iron-induced pore-forming α-synuclein oligomers". In: *Journal of Biological Chemistry* 283.16 (2008), pp. 10992–11003.

[237] Natalie Ostrerova-Golts et al. "The A53T α-synuclein mutation increases iron-dependent aggregation and toxicity". In: *Journal of Neuroscience* 20.16 (2000), pp. 6048–6054.

[238] Indi SS Bharathi, KS Rao, et al. "Copper-and iron-induced differential fibril formation in alpha-synuclein: TEM study". In: *Neurosci Lett* 424.2 (2007), pp. 78–82.

[239] Yong Peng et al. "Binding of α-synuclein with Fe (III) and with Fe (II) and biological implications of the resultant complexes". In: *Journal of inorganic biochemistry* 104.4 (2010), pp. 365–370.

[240] Paul Davies, Dima Moualla, and David R Brown. "Alpha-synuclein is a cellular ferrireductase". In: *PloS one* 6.1 (2011), e15814.

[241] Dinendra L Abeyawardhane et al. "Iron redox chemistry promotes antiparallel oligomerization of α-synuclein". In: *Journal of the American Chemical Society* 140.15 (2018), pp. 5028–5032.

[242] AL Friedlich, RE Tanzi, and JT Rogers. "The 5-untranslated region of Parkinson's disease α-synuclein messengerRNA contains a predicted iron responsive element". In: *Molecular psychiatry* 12.3 (2007), pp. 222–223.

[243] David Olivares et al. "Physiological and pathological role of alpha-synuclein in Parkinson's disease through iron mediated oxidative stress; the role of a putative iron-responsive element". In: *International journal of molecular sciences* 10.3 (2009), pp. 1226–1260.

[244] Nadja Straumann et al. "Visualizing alpha-synuclein and iron deposition in M83 mouse model of Parkinson's disease in vivo". In: *bioRxiv* (2023).

[245] Francesco Agostini et al. "α-Synuclein toxicity in Drosophila melanogaster is enhanced by the presence of Iron: implications for Parkinson's disease". In: *Antioxidants* 12.2 (2023), p. 261.

[246] Upasana Ganguly et al. "Interaction of α-synuclein and Parkin in iron toxicity on SH-SY5Y cells: implications in the pathogenesis of Parkinson's disease". In: *Biochemical Journal* 477.6 (2020), pp. 1109–1122.

[247] Julia Chifman, Reinhard Laubenbacher, and Suzy V Torti. "A systems biology approach to iron metabolism". In: *A Systems Biology Approach to Blood* (2014), pp. 201–225.

[248] F Wayne Outten and Elizabeth C Theil. "Iron-based redox switches in biology". In: *Antioxidants & redox signaling* 11.5 (2009), pp. 1029–1046.

[249] Daniel Lundin et al. "The origin and evolution of ribonucleotide reduction". In: *Life* 5.1 (2015), pp. 604–636.

[250] Marianne Ilbert and Violaine Bonnefoy. "Insight into the evolution of the iron oxidation pathways". In: *Biochimica et Biophysica Acta (BBA)-Bioenergetics* 1827.2 (2013), pp. 161–175.

[251] Zhongwei Zhao. "Iron and oxidizing species in oxidative stress and Alzheimer's disease". In: *Aging Medicine* 2.2 (2019), pp. 82–87.

[252] Scott J Dixon et al. "Ferroptosis: an iron-dependent form of nonapoptotic cell death". In: *cell* 149.5 (2012), pp. 1060–1072.

[253] Xuejun Jiang, Brent R Stockwell, and Marcus Conrad. "Ferroptosis: mechanisms, biology and role in disease". In: *Nature reviews Molecular cell biology* 22.4 (2021), pp. 266–282.

[254] Kai-Jung Lin et al. "Iron brain menace: the involvement of ferroptosis in Parkinson disease". In: *Cells* 11.23 (2022), p. 3829.

[255] Tobias M Seibt, Bettina Proneth, and Marcus Conrad. "Role of GPX4 in ferroptosis and its pharmacological implication". In: *Free Radical Biology and Medicine* 133 (2019), pp. 144–152.

[256] Shihui Hao et al. "Cysteine dioxygenase 1 mediates erastin-induced ferroptosis in human gastric cancer cells". In: *Neoplasia* 19.12 (2017), pp. 1022–1032.

[257] Lohans Pedrera et al. "Ferroptotic pores induce Ca2+ fluxes and ESCRT-III activation to modulate cell death kinetics". In: *Cell Death & Differentiation* 28.5 (2021), pp. 1644–1657.

[258] Luana L Scheffer et al. "Mechanism of Ca2+-triggered ESCRT assembly and regulation of cell membrane repair". In: *Nature communications* 5.1 (2014), p. 5646.

[259] Nikhlesh K Singh and Gadiparthi N Rao. "Emerging role of 12/15-Lipoxygenase (ALOX15) in human pathologies". In: *Progress in lipid research* 73 (2019), pp. 28–45.

[260] Sally E Wenzel et al. "PEBP1 wardens ferroptosis by enabling lipoxygenase generation of lipid death signals". In: *Cell* 171.3 (2017), pp. 628–641.

[261] Mitchell D Knutson. "Non-transferrin-bound iron transporters". In: *Free Radical Biology and Medicine* 133 (2019), pp. 101–111.

[262] Ivana De Domenico et al. "Hepcidin-induced internalization of ferroportin requires binding and cooperative interaction with Jak2". In: *Proceedings of the National Academy of Sciences* 106.10 (2009), pp. 3800–3805.

[263] Ivana De Domenico et al. "Ferroxidase activity is required for the stability of cell surface ferroportin in cells expressing GPI-ceruloplasmin". In: *The EMBO journal* 26.12 (2007), pp. 2823–2831.

[264] Zouhair K Attieh et al. "Ceruloplasmin ferroxidase activity stimulates cellular iron uptake by a trivalent cation-specific transport mechanism". In: *Journal of Biological Chemistry* 274.2 (1999), pp. 1116–1123.

[265] Mingxia Bi et al. "α-Synuclein regulates iron homeostasis via preventing parkin-mediated DMT1 ubiquitylation in Parkinson's disease models". In: *ACS Chemical Neuroscience* 11.11 (2020), pp. 1682–1691.

[266] Hong Jiang et al. "Up-regulation of divalent metal transporter 1 in 6-hydroxydopamine intoxication is IRE/IRP dependent". In: *Cell research* 20.3 (2010), pp. 345–356.

[267] Yuko Yamaguchi-Iwai, Andrew Dancis, and Richard D Klausner. "AFT1: a mediator of iron regulated transcriptional control in Saccharomyces cerevisiae." In: *The EMBO journal* 14.6 (1995), pp. 1231–1239.

[268] Y Yamaguchi-Iwai et al. "Iron-regulated DNA binding by the AFT1 protein controls the iron regulon in yeast." In: *The EMBO journal* 15.13 (1996), pp. 3377–3384.

[269] Caroline C Philpott and Olga Protchenko. "Response to iron deprivation in Saccharomyces cerevisiae". In: *Eukaryotic cell* 7.1 (2008), pp. 20–27.

[270] Julian C Rutherford et al. "Activation of the iron regulon by the yeast Aft1/Aft2 transcription factors depends on mitochondrial but not cytosolic iron-sulfur protein biogenesis". In: *Journal of Biological Chemistry* 280.11 (2005), pp. 10135–10140.

[271] Opal S Chen et al. "Transcription of the yeast iron regulon does not respond directly to iron but rather to iron-sulfur cluster biosynthesis". In: *Journal of Biological Chemistry* 279.28 (2004), pp. 29513–29518.

[272] Richard F Hassett, Annette M Romeo, and Daniel J Kosman. "Regulation of High Affinity Iron Uptake in the YeastSaccharomyces cerevisiae: ROLE OF DIOXYGEN AND Fe (II)". In: *Journal of Biological Chemistry* 273.13 (1998), pp. 7628–7636.

[273] Ryo Ueta, Ayako Fukunaka, and Yuko Yamaguchi-Iwai. "Pse1p mediates the nuclear import of the iron-responsive transcription factor Aft1p in Saccharomyces cerevisiae". In: *Journal of Biological Chemistry* 278.50 (2003), pp. 50120–50127.

[274] Angela-Nadia Albetel and Caryn E Outten. "Characterization of Glutaredoxin Fe–S Cluster-Binding Interactions Using Circular Dichroism Spectroscopy". In: *Methods in enzymology*. Vol. 599. Elsevier, 2018, pp. 327–353.

[275] Luis Ojeda et al. "Role of glutaredoxin-3 and glutaredoxin-4 in the iron regulation of the Aft1 transcriptional activator in Saccharomyces cerevisiae". In: *Journal of Biological Chemistry* 281.26 (2006), pp. 17661–17669.

[276] Catherine B Poor et al. "Molecular mechanism and structure of the Saccharomyces cerevisiae iron regulator Aft2". In: *Proceedings of the National Academy of Sciences* 111.11 (2014), pp. 4043–4048.

[277] Attila Kumánovics et al. "Identification of FRA1 and FRA2 as genes involved in regulating the yeast iron regulon in response to decreased mitochondrial iron-sulfur cluster synthesis". In: *Journal of Biological Chemistry* 283.16 (2008), pp. 10276–10286.

[278] Lucía Ramos-Alonso et al. "Iron regulatory mechanisms in Saccharomyces cerevisiae". In: *Frontiers in Microbiology* 11 (2020), p. 582830.

[279] Pierre-Louis Blaiseau, Emmanuel Lesuisse, and Jean-Michel Camadro. "Aft2p, a novel iron-regulated transcription activator that modulates, with Aft1p, intracellular iron use and resistance to oxidative stress in yeast". In: *Journal of Biological Chemistry* 276.36 (2001), pp. 34221–34226.

[280] Maïté Courel et al. "Direct activation of genes involved in intracellular iron use by the yeast iron-responsive transcription factor Aft2 without its paralog Aft1". In: *Molecular and cellular biology* 25.15 (2005), pp. 6760–6771.

[281] Andrew Dancis et al. "Genetic evidence that ferric reductase is required for iron uptake in Saccharomyces cerevisiae". In: *Molecular and cellular biology* 10.5 (1990), pp. 2294–2301.

[282] Laran T Jensen and Valeria Cizewski Culotta. "Regulation of Saccharomyces cerevisiae FET4 by oxygen and iron". In: *Journal of molecular biology* 318.2 (2002), pp. 251–260.

[283] Olga Protchenko et al. "Three cell wall mannoproteins facilitate the uptake of iron in Saccharomyces cerevisiae". In: *Journal of Biological Chemistry* 276.52 (2001), pp. 49244–49250.

[284] Cheol-Won Yun et al. "Siderophore-iron uptake in Saccharomyces cerevisiae: identification of ferrichrome and fusarinine transporters". In: *Journal of Biological Chemistry* 275.21 (2000), pp. 16354–16359.

[285] Emmanuel Lesuisse et al. "Siderophore uptake and use by the yeast Saccharomyces cerevisiae". In: *Microbiology* 147.2 (2001), pp. 289–298.

[286] Cheol-Won Yun et al. "Desferrioxamine-mediated iron uptake in Saccharomyces cerevisiae: evidence for two pathways of iron uptake". In: *Journal of Biological Chemistry* 275.14 (2000), pp. 10709–10715.

[287] Fabio Raguzzi, Emmanuel Lesuisse, and Robert R Crichton. "Iron storage in Saccharomyces cerevisiae". In: *FEBS letters* 231.1 (1988), pp. 253–258.

[288] Liangtao Li et al. "CCC1 is a transporter that mediates vacuolar iron storage in yeast". In: *Journal of Biological Chemistry* 276.31 (2001), pp. 29515–29519.

[289] Arvinder Singh, Navjot Kaur, and Daniel J Kosman. "The metalloreductase Fre6p in Fe-efflux from the yeast vacuole". In: *Journal of Biological Chemistry* 282.39 (2007), pp. 28619–28626.

[290] Huilan Lin et al. "Genetic and biochemical analysis of high iron toxicity in yeast: iron toxicity is due to the accumulation of cytosolic iron and occurs under both aerobic and anaerobic conditions". In: *Journal of Biological Chemistry* 286.5 (2011), pp. 3851–3862.

[291] Liangtao Li et al. "The mitochondrial iron exporter genes MMT1 and MMT2 in yeast are transcriptionally regulated by Aft1 and Yap1". In: *Journal of Biological Chemistry* 295.6 (2020), pp. 1716–1726.

[292] Ulrich Muhlenhoff et al. "A specific role of the yeast mitochondrial carriers MRS3/4p in mitochondrial iron acquisition under iron-limiting conditions". In: *Journal of Biological Chemistry* 278.42 (2003), pp. 40612–40620.

[293] Elisabeth M Froschauer, Rudolf J Schweyen, and Gerlinde Wiesenberger. "The yeast mitochondrial carrier proteins Mrs3p/Mrs4p mediate iron transport across the inner mito-

chondrial membrane". In: *Biochimica et Biophysica Acta (BBA)-Biomembranes* 1788.5 (2009), pp. 1044–1050.

[294] Liangtao Li and Jerry Kaplan. "Characterization of two homologous yeast genes that encode mitochondrial iron transporters". In: *Journal of Biological Chemistry* 272.45 (1997), pp. 28485–28493.

[295] Liangtao Li et al. "Expression of the yeast cation diffusion facilitators Mmt1 and Mmt2 affects mitochondrial and cellular iron homeostasis: evidence for mitochondrial iron export". In: *Journal of Biological Chemistry* 289.24 (2014), pp. 17132–17141.

[296] Olga Kolaj-Robin et al. "Cation diffusion facilitator family: structure and function". In: *FEBS letters* 589.12 (2015), pp. 1283–1295.

[297] Caroline C Philpott, Sébastien Leidgens, and Avery G Frey. "Metabolic remodeling in iron-deficient fungi". In: *Biochimica et Biophysica Acta (BBA)-Molecular Cell Research* 1823.9 (2012), pp. 1509–1520.

[298] Matthias Weider et al. "Vhr1p, a new transcription factor from budding yeast, regulates biotin-dependent expression of VHT1 and BIO5". In: *Journal of Biological Chemistry* 281.19 (2006), pp. 13513–13524.

[299] Sergi Puig, Eric Askeland, and Dennis J Thiele. "Coordinated remodeling of cellular metabolism during iron deficiency through targeted mRNA degradation". In: *Cell* 120.1 (2005), pp. 99–110.

[300] Mar Martínez-Pastor et al. "Negative feedback regulation of the yeast CTH1 and CTH2 mRNA binding proteins is required for adaptation to iron deficiency and iron supplementation". In: *Molecular and cellular biology* (2013).

[301] Elisa Pedro-Segura et al. "The Cth2 ARE-binding protein recruits the Dhh1 helicase to promote the decay of succinate dehydrogenase SDH4 mRNA in response to iron deficiency". In: *Journal of Biological Chemistry* 283.42 (2008), pp. 28527–28535.

[302] Sergi Puig, Sandra V Vergara, and Dennis J Thiele. "Cooperation of two mRNA-binding proteins drives metabolic adaptation to iron deficiency". In: *Cell metabolism* 7.6 (2008), pp. 555–564.

[303] María Teresa Martínez-Pastor, Ana Perea-García, and Sergi Puig. "Mechanisms of iron sensing and regulation in the yeast Saccharomyces cerevisiae". In: *World Journal of Microbiology and Biotechnology* 33.4 (2017), p. 75.

[304] Claudina Rodrigues-Pousada, Regina A Menezes, and Catarina Pimentel. "The Yap family and its role in stress response". In: *Yeast* 27.5 (2010), pp. 245–258.

[305] Liangtao Li et al. "Yap5 is an iron-responsive transcriptional activator that regulates vacuolar iron storage in yeast". In: *Molecular and cellular biology* (2008).

[306] Nicole Rietzschel et al. "The basic leucine zipper stress response regulator Yap5 senses high-iron conditions by coordination of [2Fe-2S] clusters". In: *Molecular and cellular biology* (2015).

[307] Liangtao Li et al. "Yap5 protein-regulated transcription of the TYW1 gene protects yeast from high iron toxicity". In: *Journal of Biological Chemistry* 286.44 (2011), pp. 38488–38497.

[308] Catarina Pimentel et al. "The role of the Yap5 transcription factor in remodeling gene expression in response to Fe bioavailability". In: *PloS one* 7.5 (2012), e37434.

[309] Nuria Pujol-Carrion et al. "Glutaredoxins Grx3 and Grx4 regulate nuclear localisation of Aft1 and the oxidative stress response in Saccharomyces cerevisiae". In: *Journal of cell science* 119.21 (2006), pp. 4554–4564.

[310] Jenifer Calvo, Hunmin Jung, and Gabriele Meloni. "Copper metallothioneins". In: *Iubmb Life* 69.4 (2017), pp. 236–245.

[311] Paul A Cobine et al. "Yeast contain a non-proteinaceous pool of copper in the mitochondrial matrix". In: *Journal of Biological Chemistry* 279.14 (2004), pp. 14447–14455.

[312] Jacqueline Burré, Manu Sharma, and Thomas C Südhof. "Definition of a molecular pathway mediating α-synuclein neurotoxicity". In: *Journal of Neuroscience* 35.13 (2015), pp. 5221–5232.

[313] Min Zhu, Jie Li, and Anthony L Fink. "The association of α-synuclein with membranes affects bilayer structure, stability, and fibril formation". In: *Journal of Biological Chemistry* 278.41 (2003), pp. 40186–40197.

[314] Céline Galvagnion et al. "Lipid vesicles trigger α-synuclein aggregation by stimulating primary nucleation". In: *Nature chemical biology* 11.3 (2015), pp. 229–234.

[315] Bryan A Killinger et al. "Endogenous alpha-synuclein monomers, oligomers and resulting pathology: let's talk about the lipids in the room". In: *npj Parkinson's Disease* 5.1 (2019), p. 23.

[316] Christine C Jao et al. "Structure of membrane-bound α-synuclein studied by site-directed spin labeling". In: *Proceedings of the National Academy of Sciences* 101.22 (2004), pp. 8331–8336.

[317] Marianne Schiffer and Allen B Edmundson. "Use of helical wheels to represent the structures of proteins and to identify segments with helical potential". In: *Biophysical journal* 7.2 (1967), pp. 121–135.

[318] Lars Svennerholm. "Distribution and fatty acid composition of phosphoglycerides in normal human brain". In: *Journal of lipid research* 9.5 (1968), pp. 570–579.

[319] Lucia E Rameh et al. "A new pathway for synthesis of phosphatidylinositol-4, 5-bisphosphate". In: *Nature* 390.6656 (1997), pp. 192–196.

[320] Jason D Perlmutter, Anthony R Braun, and Jonathan N Sachs. "Curvature dynamics of α-synuclein familial parkinson disease mutants". In: *Journal of Biological Chemistry* 284.11 (2009), pp. 7177–7189.

[321] He-Jin Lee, Chan Choi, and Seung-Jae Lee. "Membrane-bound α-synuclein has a high aggregation propensity and the ability to seed the aggregation of the cytosolic form". In: *Journal of Biological Chemistry* 277.1 (2002), pp. 671–678.

[322] Stuart McLaughlin and Diana Murray. "Plasma membrane phosphoinositide organization by protein electrostatics". In: *Nature* 438.7068 (2005), pp. 605–611.

[323] Sandeep Robert Datta, Anne Brunet, and Michael E Greenberg. "Cellular survival: a play in three Akts". In: *Genes & development* 13.22 (1999), pp. 2905–2927.

[324] Igor Vivanco and Charles L Sawyers. "The phosphatidylinositol 3-kinase–AKT pathway in human cancer". In: *Nature Reviews Cancer* 2.7 (2002), pp. 489–501.

[325] Jong-Ho Lee et al. "EGFR-phosphorylated platelet isoform of phosphofructokinase 1 promotes PI3K activation". In: *Molecular cell* 70.2 (2018), pp. 197–210.

[326] Edgar E Kooijman et al. "Ionization properties of phosphatidylinositol polyphosphates in mixed model membranes". In: *Biochemistry* 48.40 (2009), pp. 9360–9371.

[327] Yang I Li et al. "Prioritizing Parkinson's disease genes using population-scale transcriptomic data". In: *Nature communications* 10.1 (2019), p. 994.

[328] Chi-Jing Choong et al. "Phosphatidylinositol-3, 4, 5-trisphosphate interacts with alpha-synuclein and initiates its aggregation and formation of Parkinson's disease-related fibril polymorphism". In: *Acta Neuropathologica* 145.5 (2023), pp. 573–595.

[329] Ping-Yue Pan et al. "Synj1 haploinsufficiency causes dopamine neuron vulnerability and alpha-synuclein accumulation in mice". In: *Human molecular genetics* 29.14 (2020), pp. 2300–2312.

[330] Eric Yu et al. "Machine learning nominates the inositol pathway and novel genes in Parkinson's disease". In: *Brain* 147.3 (2024), pp. 887–899.

[331] Vijaya Narayanan and Suzanne Scarlata. "Membrane binding and self-association of α-synucleins". In: *Biochemistry* 40.33 (2001), pp. 9927–9934.

[332] Reeba Susan Jacob et al. "α-Synuclein plasma membrane localization correlates with cellular phosphatidylinositol polyphosphate levels". In: *Elife* 10 (2021), e61951.

[333] Jonathan D Horvath et al. "α-Synuclein-dependent increases in PIP5K1γ drive inositol signaling to promote neurotoxicity". In: *Cell reports* 42.10 (2023).

[334] Markus R Wenk et al. "PIP kinase Iγ is the major PI (4, 5) P2 synthesizing enzyme at the synapse". In: *Neuron* 32.1 (2001), pp. 79–88.

[335] Michael Krauss et al. "ARF6 stimulates clathrin/AP-2 recruitment to synaptic membranes by activating phosphatidylinositol phosphate kinase type Iγ". In: *The Journal of cell biology* 162.1 (2003), pp. 113–124.

[336] Joseph J Baldassare, Patricia A Henderson, and Gary J Fisher. "Isolation and characterization of one soluble and two membrane-associated forms of phosphoinositide-specific phospholipase C from human platelets". In: *Biochemistry* 28.14 (1989), pp. 6010–6016.

[337] Eamonn J Dickson, Björn H Falkenburger, and Bertil Hille. "Quantitative properties and receptor reserve of the IP3 and calcium branch of Gq-coupled receptor signaling". In: *Journal of General Physiology* 141.5 (2013), pp. 521–535.

[338] PTAD Morell and AD Toews. "Biochemistry of lipids". In: *Handbook of clinical neurology* 66.1 (1996), pp. 33–50.

[339] Stanley I Rapoport, Michael CJ Chang, and Arthur A Spector. "Delivery and turnover of plasma-derived essential PUFAs in mammalian brain". In: *Journal of lipid research* 42.5 (2001), pp. 678–685.

[340] Reynold Spector. "Fatty acid transport through the blood-brain barrier". In: *Journal of neurochemistry* 50.2 (1988), pp. 639–643.

[341] Helga Jurevics and Pierre Morell. "Cholesterol for synthesis of myelin is made locally, not imported into brain". In: *Journal of neurochemistry* 64.2 (1995), pp. 895–901.

[342] Nutabi Camargo et al. "Oligodendroglial myelination requires astrocyte-derived lipids". In: *PLoS biology* 15.5 (2017), e1002605.

[343] Kristina Hofmann et al. "Astrocytes and oligodendrocytes in grey and white matter regions of the brain metabolize fatty acids". In: *Scientific reports* 7.1 (2017), p. 10779.

[344] Anne-Lieke F van Deijk et al. "Astrocyte lipid metabolism is critical for synapse development and function in vivo". In: *Glia* 65.4 (2017), pp. 670–682.

[345] Peter Schönfeld and Georg Reiser. "Why does brain metabolism not favor burning of fatty acids to provide energy?-Reflections on disadvantages of the use of free fatty acids as fuel for brain". In: *Journal of Cerebral Blood Flow & Metabolism* 33.10 (2013), pp. 1493–1499.

[346] Hein Sprong et al. "UDP-galactose: ceramide galactosyltransferase is a class I integral membrane protein of the endoplasmic reticulum". In: *Journal of Biological Chemistry* 273.40 (1998), pp. 25880–25888.

[347] Jean E Vance. "Phospholipid synthesis and transport in mammalian cells". In: *Traffic* 16.1 (2015), pp. 1–18.

[348] Qingyang Shi et al. "Intracellular cholesterol synthesis and transport". In: *Frontiers in Cell and Developmental Biology* 10 (2022), p. 819281.

[349] Sonia Missiroli et al. "Mitochondria-associated membranes (MAMs) and inflammation". In: *Cell death & disease* 9.3 (2018), p. 329.

[350] Thomas Simmen and Maria Sol Herrera-Cruz. "Plastic mitochondria-endoplasmic reticulum (ER) contacts use chaperones and tethers to mould their structure and signaling". In: *Current opinion in cell biology* 53 (2018), pp. 61–69.

[351] Peng Gao, Zhencheng Yan, and Zhiming Zhu. "Mitochondria-associated endoplasmic reticulum membranes in cardiovascular diseases". In: *Frontiers in cell and developmental biology* 8 (2020), p. 604240.

[352] Marçal Vilar et al. "The fold of α-synuclein fibrils". In: *Proceedings of the National Academy of Sciences* 105.25 (2008), pp. 8637–8642.

[353] Aleix Sala-Vila et al. "Interplay between hepatic mitochondria-associated membranes, lipid metabolism and caveolin-1 in mice". In: *Scientific reports* 6.1 (2016), p. 27351.

[354] Gyorgy Szabadkai et al. "Chaperone-mediated coupling of endoplasmic reticulum and mitochondrial Ca2+ channels". In: *The Journal of cell biology* 175.6 (2006), pp. 901–911.

[355] Yan G Zhao et al. "The ER contact proteins VAPA/B interact with multiple autophagy proteins to modulate autophagosome biogenesis". In: *Current Biology* 28.8 (2018), pp. 1234–1245.

[356] William A Prinz, Alexandre Toulmay, and Tamas Balla. "The functional universe of membrane contact sites". In: *Nature reviews Molecular cell biology* 21.1 (2020), pp. 7–24.

[357] Haoxi Wu, Pedro Carvalho, and Gia K Voeltz. "Here, there, and everywhere: The importance of ER membrane contact sites". In: *Science* 361.6401 (2018), eaan5835.

[358] Teruo Hayashi et al. "MAM: more than just a housekeeper". In: *Trends in cell biology* 19.2 (2009), pp. 81–88.

[359] Scot J Stone and Jean E Vance. "Phosphatidylserine synthase-1 and-2 are localized to mitochondria-associated membranes". In: *Journal of Biological Chemistry* 275.44 (2000), pp. 34534–34540.

[360] Antonio E Rusinol et al. "A unique mitochondria-associated membrane fraction from rat liver has a high capacity for lipid synthesis and contains pre-Golgi secretory proteins including nascent lipoproteins." In: *Journal of Biological Chemistry* 269.44 (1994), pp. 27494–27502.

[361] Jolanta Vidugiriene et al. "Segregation of glycosylphosphatidylinositol biosynthetic reactions in a subcompartment of the endoplasmic reticulum". In: *Journal of Biological Chemistry* 274.21 (1999), pp. 15203–15212.

[362] Kristina Battis, Wei Xiang, and Jürgen Winkler. "The bidirectional interplay of α-Synuclein with lipids in the central nervous system and its implications for the pathogenesis of Parkinson's disease". In: *International journal of molecular sciences* 24.17 (2023), p. 13270.

[363] Giampaolo Morciano et al. "Role of mitochondria-associated ER membranes in calcium regulation in cancer-specific settings". In: *Neoplasia* 20.5 (2018), pp. 510–523.

[364] Adolfo Garcia Erustes et al. "α-Synuclein Interactions in Mitochondria-ER Contacts: A Possible Role in Parkinson's Disease". In: *Contact* 5 (2022), p. 25152564221119347.

[365] Peter A Barbuti et al. "The Role of Alpha Synuclein in Synucleinopathy: Impact on Lipid Regulation at Mitochondria ER Membranes". In: *bioRxiv* (2024), pp. 2024–06.

[366] Federica Gibellini and Terry K Smith. "The Kennedy pathway—de novo synthesis of phosphatidylethanolamine and phosphatidylcholine". In: *IUBMB life* 62.6 (2010), pp. 414–428.

[367] Michael J Glade and Kyl Smith. "Phosphatidylserine and the human brain". In: *Nutrition* 31.6 (2015), pp. 781–786.

[368] Daniel Lingwood and Kai Simons. "Lipid rafts as a membrane-organizing principle". In: *science* 327.5961 (2010), pp. 46–50.

[369] Héctor A Lucero and Phillips W Robbins. "Lipid rafts–protein association and the regulation of protein activity". In: *Archives of biochemistry and biophysics* 426.2 (2004), pp. 208–224.

[370] Nutan Sharma et al. "Pathophysiological significance of calcium signaling at mitochondria-associated endoplasmic reticulum membranes (MAMs)". In: *Current Opinion in Physiology* 17 (2020), pp. 234–242.

[371] Cristina Guardia-Laguarta et al. "α-Synuclein is localized to mitochondria-associated ER membranes". In: *Journal of Neuroscience* 34.1 (2014), pp. 249–259.

[372] Rosario Rizzuto et al. "Close contacts with the endoplasmic reticulum as determinants of mitochondrial Ca2+ responses". In: *Science* 280.5370 (1998), pp. 1763–1766.

[373] Han Xu et al. "IP 3 R-Grp75-VDAC1-MCU calcium regulation axis antagonists protect podocytes from apoptosis and decrease proteinuria in an adriamycin nephropathy rat model". In: *BMC nephrology* 19 (2018), pp. 1–11.

[374] Amandine Rovini et al. "Molecular mechanism of olesoxime-mediated neuroprotection through targeting α-synuclein interaction with mitochondrial VDAC". In: *Cellular and Molecular Life Sciences* 77 (2020), pp. 3611–3626.

[375] Tatiana K Rostovtseva et al. "α-Synuclein shows high affinity interaction with voltage-dependent anion channel, suggesting mechanisms of mitochondrial regulation and toxicity in Parkinson disease". In: *Journal of Biological Chemistry* 290.30 (2015), pp. 18467–18477.

[376] Kurt J De Vos et al. "VAPB interacts with the mitochondrial protein PTPIP51 to regulate calcium homeostasis". In: *Human molecular genetics* 21.6 (2012), pp. 1299–1311.

[377] Sébastien Paillusson et al. "α-Synuclein binds to the ER–mitochondria tethering protein VAPB to disrupt Ca 2+ homeostasis and mitochondrial ATP production". In: *Acta neuropathologica* 134 (2017), pp. 129–149.

[378] Laura V Vandervore et al. "TMX2 is a crucial regulator of cellular redox state, and its dysfunction causes severe brain developmental abnormalities". In: *The American Journal of Human Genetics* 105.6 (2019), pp. 1126–1147.

[379] Cristine Betzer et al. "Alpha-synuclein aggregates activate calcium pump SERCA leading to calcium dysregulation". In: *EMBO reports* 19.5 (2018), e44617.

[380] David Botstein and Gerald R Fink. "Yeast: an experimental organism for 21st century biology". In: *Genetics* 189.3 (2011), pp. 695–704.

[381] Louis Pasteur. *Etudes sur la bière*. Books on Demand, 1876.

[382] Andrea A Duina, Mary E Miller, and Jill B Keeney. "Budding yeast for budding geneticists: a primer on the Saccharomyces cerevisiae model system". In: *Genetics* 197.1 (2014), pp. 33–48.

[383] Albert Hinnen, James B Hicks, and Gerald R Fink. "Transformation of yeast." In: *Proceedings of the National Academy of Sciences* 75.4 (1978), pp. 1929–1933.

[384] Terry L Orr-Weaver, Jack W Szostak, and Rodney J Rothstein. "Yeast transformation: a model system for the study of recombination." In: *Proceedings of the national Academy of Sciences* 78.10 (1981), pp. 6354–6358.

[385] Jack W Szostak et al. "The double-strand-break repair model for recombination". In: *Cell* 33.1 (1983), pp. 25–35.

[386] Michael C Lorenz et al. "Gene disruption with PCR products in Saccharomyces cerevisiae". In: *Gene* 158.1 (1995), pp. 113–117.

[387] Marcin G Fraczek, Samina Naseeb, and Daniela Delneri. "History of genome editing in yeast". In: *Yeast* 35.5 (2018), pp. 361–368.

[388] Nadine Eckert-Boulet, Rodney Rothstein, and Michael Lisby. "Cell biology of homologous recombination in yeast". In: *DNA Recombination: Methods and Protocols* (2011), pp. 523–536.

[389] Rodney Rothstein. "[19] Targeting, disruption, replacement, and allele rescue: Integrative DNA transformation in yeast". In: *Methods in enzymology*. Vol. 194. Elsevier, 1991, pp. 281–301.

[390] Marie E Petracek and Mark S Longtine. "PCR-based engineering of yeast genome". In: *Methods in enzymology*. Vol. 350. Elsevier, 2002, pp. 445–469.

[391] Shigeyuki Kawai, Wataru Hashimoto, and Kousaku Murata. "Transformation of Saccharomyces cerevisiae and other fungi: methods and possible underlying mechanism". In: *Bioengineered bugs* 1.6 (2010), pp. 395–403.

[392] Bart Scherens and Andre Goffeau. "The uses of genome-wide yeast mutant collections". In: *Genome biology* 5 (2004), pp. 1–8.

[393] Guri Giaever and Corey Nislow. "The yeast deletion collection: a decade of functional genomics". In: *Genetics* 197.2 (2014), pp. 451–465.

[394] Jack T Pronk. "Auxotrophic yeast strains in fundamental and applied research". In: *Applied and environmental microbiology* 68.5 (2002), pp. 2095–2100.

[395] S Russo, G Poli, et al. "Yeasts: from genetics to biotechnology." In: *Journal of Environmental Pathology, Toxicology and Oncology: Official Organ of the International Society for Environmental Toxicology and Cancer* 14.3-4 (1995), pp. 133–157.

[396] D Botstein and RW Davis. "Principles and practice of recombinant DNA research with yeast". In: *The molecular biology of the yeast Saccharomyces: metabolism and gene expression. Cold Spring Harbor Laboratory, Cold Spring Harbor, NY* (1982), pp. 607–636.

[397] Douglas E Bassett Jr et al. "Exploiting the complete yeast genome sequence". In: *Current opinion in genetics & development* 6.6 (1996), pp. 763–766.

[398] André Goffeau et al. "Life with 6000 genes". In: *Science* 274.5287 (1996), pp. 546–567.

[399] Aashiq H Kachroo et al. "Systematic humanization of yeast genes reveals conserved functions and genetic modularity". In: *Science* 348.6237 (2015), pp. 921–925.

[400] Edward M Marcotte et al. "Detecting protein function and protein-protein interactions from genome sequences". In: *Science* 285.5428 (1999), pp. 751–753.

[401] Ana Joyce Munoz et al. "Systems biology of yeast cell death". In: *FEMS yeast research* 12.2 (2012), pp. 249–265.

[402] Andreas Zimmermann et al. "Yeast as a tool to identify anti-aging compounds". In: *FEMS yeast research* 18.6 (2018), foy020.

[403] Juan S Bonifacino and Benjamin S Glick. "The mechanisms of vesicle budding and fusion". In: *cell* 116.2 (2004), pp. 153–166.

[404] Mariusz Karbowski and Richard J Youle. "Regulating mitochondrial outer membrane proteins by ubiquitination and proteasomal degradation". In: *Current opinion in cell biology* 23.4 (2011), pp. 476–482.

[405] Geoffrey M Cooper and RE Hausman. "The complexity of eukaryotic genomes". In: *The Cell: A Molecular Approach* 2 (2000).

[406] Engin Ozkaynak et al. "The yeast ubiquitin genes: a family of natural gene fusions." In: *The EMBO journal* 6.5 (1987), pp. 1429–1439.

[407] Steven Bates et al. "Outer chain N-glycans are required for cell wall integrity and virulence of Candida albicans". In: *Journal of Biological Chemistry* 281.1 (2006), pp. 90–98.

[408] Wei Liu et al. "From Saccharomyces cerevisiae to human: The important gene co-expression modules". In: *Biomedical reports* 7.2 (2017), pp. 153–158.

[409] Florent Laval et al. "Homo cerevisiae—Leveraging Yeast for Investigating Protein–Protein Interactions and Their Role in Human Disease". In: *International Journal of Molecular Sciences* 24.11 (2023), p. 9179.

[410] Peter Uetz et al. "A comprehensive analysis of protein–protein interactions in Saccharomyces cerevisiae". In: *Nature* 403.6770 (2000), pp. 623–627.

[411] Amy Hin Yan Tong et al. "Systematic genetic analysis with ordered arrays of yeast deletion mutants". In: *Science* 294.5550 (2001), pp. 2364–2368.

[412] John L Hartman IV, Barbara Garvik, and Lee Hartwell. "Principles for the buffering of genetic variation". In: *Science* 291.5506 (2001), pp. 1001–1004.

[413] Jon M Laurent et al. "Efforts to make and apply humanized yeast". In: *Briefings in functional genomics* 15.2 (2016), pp. 155–163.

[414] Kelly A Conway, James D Harper, and Peter T Lansbury. "Fibrils formed in vitro from α-synuclein and two mutant forms linked to Parkinson's disease are typical amyloid". In: *Biochemistry* 39.10 (2000), pp. 2552–2563.

[415] Joanna Narkiewicz, Gabriele Giachin, and Giuseppe Legname. "In vitro aggregation assays for the characterization of α-synuclein prion-like properties". In: *Prion* 8.1 (2014), pp. 19–32.

[416] Diana F Lázaro, Maria Angeliki S Pavlou, and Tiago Fleming Outeiro. "Cellular models as tools for the study of the role of alpha-synuclein in Parkinson's disease". In: *Experimental neurology* 298 (2017), pp. 162–171.

[417] Marion Delenclos et al. "Cellular models of alpha-synuclein toxicity and aggregation". In: *Journal of neurochemistry* 150.5 (2019), pp. 566–576.

[418] Katrina Albert et al. "Cellular Models of Alpha-Synuclein Aggregation: What Have We Learned and Implications for Future Study". In: *Biomedicines* 10.10 (2022), p. 2649.

[419] Tiago Fleming Outeiro and Susan Lindquist. "Yeast cells provide insight into alpha-synuclein biology and pathobiology". In: *Science* 302.5651 (2003), pp. 1772–1775.

[420] Vikram Khurana and Susan Lindquist. "Modelling neurodegeneration in Saccharomyces cerevisiae: why cook with baker's yeast?" In: *Nature Reviews Neuroscience* 11.6 (2010), pp. 436–449.

[421] Esti Yeger-Lotem et al. "Bridging high-throughput genetic and transcriptional data reveals cellular responses to alpha-synuclein toxicity". In: *Nature genetics* 41.3 (2009), pp. 316–323.

[422] Aaron D Gitler et al. "α-Synuclein is part of a diverse and highly conserved interaction network that includes PARK9 and manganese toxicity". In: *Nature genetics* 41.3 (2009), pp. 308–315.

[423] Achim Wach. "PCR-synthesis of marker cassettes with long flanking homology regions for gene disruptions in S. cerevisiae". In: *Yeast* 12.3 (1996), pp. 259–265.

[424] Pierre Hentges et al. "Three novel antibiotic marker cassettes for gene disruption and marker switching in Schizosaccharomyces pombe". In: *Yeast* 22.13 (2005), pp. 1013–1019.

[425] Daniel Gietz et al. "Improved method for high efficiency transformation of intact yeast cells." In: *Nucleic acids research* 20.6 (1992), p. 1425.

[426] James L Hartley, Gary F Temple, and Michael A Brasch. "DNA cloning using in vitro site-specific recombination". In: *Genome research* 10.11 (2000), pp. 1788–1795.

[427] Xiquan Liang et al. "Single step BP/LR combined Gateway reactions". In: *Biotechniques* 55.5 (2018).

[428] Paul P Jung et al. "Protocols and programs for high-throughput growth and aging phenotyping in yeast". In: *PloS one* 10.3 (2015), e0119807.

[429] Vitaly V Kushnirov. "Rapid and reliable protein extraction from yeast". In: *Yeast* 16.9 (2000), pp. 857–860.

[430] Jui-Cheng Yen, Fu-Juay Chang, and Shyang Chang. "A new criterion for automatic multilevel thresholding". In: *IEEE Transactions on Image Processing* 4.3 (1995), pp. 370–378.

[431] Zhang Xiao-Jing, Sun Wan-Rong, and Zhong Zheng-Hui. "A new algorithm for watershed segmentation of cells in marrow". In: *2005 IEEE Engineering in Medicine and Biology 27th Annual Conference*. IEEE. 2006, pp. 6456–6459.

[432] Karolina Nowosad et al. "Pulsed electric field (Pef) enhances iron uptake by the yeast saccharomyces cerevisiae". In: *Biomolecules* 11.6 (2021), p. 850.

[433] Yuxin Chen et al. "SOAPnuke: a MapReduce acceleration-supported software for integrated quality control and preprocessing of high-throughput sequencing data". In: *Gigascience* 7.1 (2018), gix120.

[434] Kenneth J Livak and Thomas D Schmittgen. "Analysis of relative gene expression data using real-time quantitative PCR and the 2- $\Delta\Delta$CT method". In: *methods* 25.4 (2001), pp. 402–408.

[435] Jean-Pierre Trezzi et al. "Metabolic profiling of body fluids and multivariate data analysis". In: *MethodsX* 4 (2017), pp. 95–103.

[436] Tomas Cajka, Jennifer T Smilowitz, and Oliver Fiehn. "Validating quantitative untargeted lipidomics across nine liquid chromatography–high-resolution mass spectrometry platforms". In: *Analytical chemistry* 89.22 (2017), pp. 12360–12368.

[437] Matthew C Chambers et al. "A cross-platform toolkit for mass spectrometry and proteomics". In: *Nature biotechnology* 30.10 (2012), pp. 918–920.

[438] Robin Schmid et al. "Integrative analysis of multimodal mass spectrometry data in MZmine 3". In: *Nature biotechnology* 41.4 (2023), pp. 447–449.

[439] Niek F de Jonge et al. "MS2Query: reliable and scalable MS2 mass spectra-based analogue search". In: *Nature Communications* 14.1 (2023), p. 1752.

[440] Zhiqiang Pang et al. "MetaboAnalystR 4.0: a unified LC-MS workflow for global metabolomics". In: *Nature Communications* 15.1 (2024), p. 3675.

[441] Dinesh Kumar Barupal and Oliver Fiehn. "Chemical Similarity Enrichment Analysis (ChemRICH) as alternative to biochemical pathway mapping for metabolomic datasets". In: *Scientific reports* 7.1 (2017), p. 14567.

[442] Ursula Heins-Marroquin et al. "Phenotypic assays in yeast and zebrafish reveal drugs that rescue ATP13A2 deficiency". In: *Brain Communications* 1.1 (2019), fcz019.

[443] Alessandra Chesi et al. "The role of the Parkinson's disease gene PARK9 in essential cellular pathways and the manganese homeostasis network in yeast". In: *PloS one* 7.3 (2012), e34178.

[444] Jason P Covy, Elisa A Waxman, and Benoit I Giasson. "Characterization of cellular protective effects of ATP13A2/PARK9 expression and alterations resulting from pathogenic mutants". In: *Journal of neuroscience research* 90.12 (2012), pp. 2306–2316.

[445] Qingdong Ke, Thomas Kluz, and Max Costa. "Down-regulation of the expression of the FIH-1 and ARD-1 genes at the transcriptional level by nickel and cobalt in the human lung adenocarcinoma A549 cell line". In: *International journal of environmental research and public health* 2.1 (2005), pp. 10–13.

[446] Michael J Vasconcelles et al. "Identification and Characterization of a Low Oxygen Response Element Involved in the Hypoxic Induction of a Family ofSaccharomyces cerevisiae Genes: IMPLICATIONS FOR THE CONSERVATION OF OXYGEN SENSING IN EUKARYOTES". In: *Journal of Biological Chemistry* 276.17 (2001), pp. 14374–14384.

[447] Giansimone Perrino et al. "Quantitative characterization of α-synuclein aggregation in living cells through automated microfluidics feedback control". In: *Cell reports* 27.3 (2019), pp. 916–927.

[448] Luis Concha-Marambio et al. "Seed amplification assay for the detection of pathologic alpha-synuclein aggregates in cerebrospinal fluid". In: *Nature protocols* 18.4 (2023), pp. 1179–1196.

[449] Stefan Bräuer et al. "Kinetic parameters of alpha-synuclein seed amplification assay correlate with cognitive impairment in patients with Lewy body disorders". In: *Acta Neuropathologica Communications* 11.1 (2023), p. 162.

[450] Fabia Febbraro et al. "Chronic intranasal deferoxamine ameliorates motor defects and pathology in the α-synuclein rAAV Parkinson's model". In: *Experimental neurology* 247 (2013), pp. 45–58.

[451] Donna W Lee et al. "Inhibition of prolyl hydroxylase protects against 1-methyl-4-phenyl-1, 2, 3, 6-tetrahydropyridine-induced neurotoxicity: model for the potential involvement of the hypoxia-inducible factor pathway in Parkinson disease". In: *Journal of Biological Chemistry* 284.42 (2009), pp. 29065–29076.

[452] Eleonora Carboni et al. "Deferiprone rescues behavioral deficits induced by mild iron exposure in a mouse model of alpha-synuclein aggregation". In: *NeuroMolecular Medicine* 19 (2017), pp. 309–321.

[453] Qi Xu, Anumantha G Kanthasamy, and Manju B Reddy. "Neuroprotective effect of the natural iron chelator, phytic acid in a cell culture model of Parkinson's disease". In: *Toxicology* 245.1-2 (2008), pp. 101–108.

[454] John B Lloyd, Hazel Cable, and Catherine Rice-Evans. "Evidence that desferrioxamine cannot enter cells by passive diffusion". In: *Biochemical pharmacology* 41.9 (1991), pp. 1361–1363.

[455] Emmanuel Lesuisse, Monique Simon-Casteras, and Pierre Labbe. "Siderophore-mediated iron uptake in Saccharomyces cerevisiae: the SIT1 gene encodes a ferrioxamine B permease that belongs to the major facilitator superfamily". In: *Microbiology* 144.12 (1998), pp. 3455–3462.

[456] Denise Bellotti and Maurizio Remelli. "Deferoxamine B: A natural, excellent and versatile metal chelator". In: *Molecules* 26.11 (2021), p. 3255.

[457] Sarina Entezari et al. "Iron chelators in treatment of iron overload". In: *Journal of Toxicology* 2022.1 (2022), p. 4911205.

[458] Des Richardson, Prem Ponka, and Erica Baker. "The effect of the iron (III) chelator, desferrioxamine, on iron and transferrin uptake by the human malignant melanoma cell". In: *Cancer research* 54.3 (1994), pp. 685–689.

[459] Robert C Hider and A Victor Hoffbrand. "The role of deferiprone in iron chelation". In: *New England Journal of Medicine* 379.22 (2018), pp. 2140–2150.

[460] Katherine P Hoyes and John B Porter. "Subcellular distribution of desferrioxamine and hydroxypyridin-4-one chelators in K562 cells affects chelation of intracellular iron pools". In: *British journal of haematology* 85.2 (1993), pp. 393–400.

[461] Michael Spino et al. "Deferiprone pharmacokinetics with and without iron overload and in special patient populations". In: *Blood* 126.23 (2015), p. 3365.

[462] William Breuer et al. "Desferrioxamine-chelatable iron, a component of serum non–transferrin-bound iron, used for assessing chelation therapy: Presented in preliminary form at the 10th International Conference on Oral Chelators symposium on iron chelators held in Limassol, Cyprus, March 2000 (Transfusion Science, in press)." In: *Blood, The Journal of the American Society of Hematology* 97.3 (2001), pp. 792–798.

[463] Raymond J Bergeron et al. "Desferrithiocin: a search for clinically effective iron chelators". In: *Journal of Medicinal Chemistry* 57.22 (2014), pp. 9259–9291.

[464] Hossein Heli, Siamak Mirtorabi, and Khashayar Karimian. "Advances in iron chelation: an update". In: *Expert opinion on therapeutic patents* 21.6 (2011), pp. 819–856.

[465] Amy Corbin Farr and May P Xiong. "Challenges and opportunities of deferoxamine delivery for treatment of Alzheimer's disease, Parkinson's disease, and intracerebral hemorrhage". In: *Molecular pharmaceutics* 18.2 (2020), pp. 593–609.

[466] Ahmed Negida et al. "Efficacy of the iron-chelating agent, deferiprone, in patients with Parkinson's disease: A systematic review and meta-analysis". In: *CNS Neuroscience & Therapeutics* 30.2 (2024), e14607.

[467] Zohreh Salimi et al. "Iron chelators: as therapeutic agents in diseases". In: *Annals of Medicine and Surgery* 86.5 (2024), pp. 2759–2776.

[468] Deyhim Atarod et al. "Bivalent metal ions induce formation of α-synuclein fibril polymorphs with different cytotoxicities". In: *Scientific Reports* 12.1 (2022), p. 11898.

[469] Vladimir N Uversky, Jie Li, and Anthony L Fink. "Metal-triggered structural transformations, aggregation, and fibrillation of human α-synuclein: a possible molecular link between Parkinson s disease and heavy metal exposure". In: *Journal of Biological Chemistry* 276.47 (2001), pp. 44284–44296.

[470] Robert C Hider and Xiaole Kong. "Chemistry and biology of siderophores". In: *Natural product reports* 27.5 (2010), pp. 637–657.

[471] Minoo Shakoury-Elizeh et al. "Metabolic response to iron deficiency in Saccharomyces cerevisiae". In: *Journal of Biological Chemistry* 285.19 (2010), pp. 14823–14833.

[472] Claudia Oviedo and Jaime Rodríguez. "EDTA: the chelating agent under environmental scrutiny". In: *Quimica Nova* 26 (2003), pp. 901–905.

[473] Serafina Corsello et al. "The usefulness of chelation therapy for the remission of symptoms caused by previous treatment with mercury-containing pharmaceuticals: a case report". In: *Cases Journal* 2 (2009), pp. 1–5.

[474] Attila Kovács, Dénes S Nemcsok, and Tamás Kocsis. "Bonding interactions in EDTA complexes". In: *Journal of Molecular Structure: THEOCHEM* 950.1-3 (2010), pp. 93–97.

[475] S Blażejak and Wanda Duszkiewicz-Reinhard. "Yeast cell biomass as a potential source of magnesium bioplexes-a review." In: *Polish journal of food and nutrition sciences* (2004).

[476] George J Brewer et al. "Treatment of Wilson's disease with ammonium tetrathiomolybdate: I. Initial therapy in 17 neurologically affected patients". In: *Archives of Neurology* 51.6 (1994), pp. 545–554.

[477] Tiantian Fang et al. "Tetrathiomolybdate induces dimerization of the metal-binding domain of ATPase and inhibits platination of the protein". In: *Nature communications* 10.1 (2019), p. 186.

[478] Yankai Zhao et al. "Performance and mechanism of copper removal from wastewater by sodium tetraethylenepentamine-N, N, N, N, N-pentadithiocarboxylic acid". In: *Journal of Molecular Structure* 1242 (2021), p. 130727.

[479] Susan S Percival and Meri Layden-Patrice. "HL-60 cells can be made copper deficient by incubating with tetraethylenepentamine". In: *The Journal of nutrition* 122.12 (1992), pp. 2424–2429.

[480] Young-Eun Cho et al. "Cellular Zn depletion by metal ion chelators (TPEN, DTPA and chelex resin) and its application to osteoblastic MC3T3-E1 cells". In: *Nutrition research and practice* 1.1 (2007), pp. 29–35.

[481] Qian Gui et al. "Transcriptome analysis in yeast reveals the externality of position effects". In: *Molecular Biology and Evolution* 38.8 (2021), pp. 3294–3307.

[482] TF Donahue and SA Henry. "myo-Inositol-1-phosphate synthase. Characteristics of the enzyme and identification of its structural gene in yeast." In: *Journal of Biological Chemistry* 256.13 (1981), pp. 7077–7085.

[483] Lisa S Klig and Susan A Henry. "Isolation of the yeast INO1 gene: located on an autonomously replicating plasmid, the gene is fully regulated." In: *Proceedings of the National Academy of Sciences* 81.12 (1984), pp. 3816–3820.

[484] Vladimir Jiranek, J Anthony Graves, and Susan A Henry. "Pleiotropic effects of the opi1 regulatory mutation of yeast: its effects on growth and on phospholipid and inositol metabolism". In: *Microbiology* 144.10 (1998), pp. 2739–2748.

[485] Nadeeja Wijesekara et al. "α-Synuclein regulates peripheral insulin secretion and glucose transport". In: *Frontiers in Aging Neuroscience* 13 (2021), p. 665348.

[486] Ana Marques et al. "Glucose dysregulation in Parkinson's disease: Too much glucose or not enough insulin?" In: *Parkinsonism & related disorders* 55 (2018), pp. 122–127.

[487] Wei Liu and Jianfeng Tang. "Association between diabetes mellitus and risk of Parkinson's disease: a prisma-compliant meta-analysis". In: *Brain and behavior* 11.8 (2021), e02082.

[488] M Veen and C Lang. *Interactions of the ergosterol biosynthetic pathway with other lipid pathways*. 2005.

[489] Wayne R Riekhof et al. "An assembly of proteins and lipid domains regulates transport of phosphatidylserine to phosphatidylserine decarboxylase 2 in Saccharomyces cerevisiae". In: *Journal of Biological Chemistry* 289.9 (2014), pp. 5809–5819.

[490] Ameeta K Agarwal et al. "Genome-wide expression profiling of the response to polyene, pyrimidine, azole, and echinocandin antifungal agents in Saccharomyces cerevisiae". In: *Journal of Biological Chemistry* 278.37 (2003), pp. 34998–35015.

[491] Muthukumar Kannan, Wayne R Riekhof, and Dennis R Voelker. "Transport of phosphatidylserine from the endoplasmic reticulum to the site of phosphatidylserine decarboxylase2 in yeast". In: *Traffic* 16.2 (2015), pp. 123–134.

[492] Bo Jiang et al. "A new family of yeast genes implicated in ergosterol synthesis is related to the human oxysterol binding protein". In: *Yeast* 10.3 (1994), pp. 341–353.

[493] Saara Laitinen et al. "Family of human oxysterol binding protein (OSBP) homologues: a novel member implicated in brain sterol metabolism". In: *Journal of lipid research* 40.12 (1999), pp. 2204–2211.

[494] Wolfgang A Schmalix and Wolfhard Bandlow. "SWH1 from yeast encodes a candidate nuclear factor containing ankyrin repeats and showing homology to mammalian oxysterol-binding protein". In: *Biochimica et Biophysica Acta (BBA)-Gene Structure and Expression* 1219.1 (1994), pp. 205–210.

[495] Christopher T Beh et al. "Overlapping functions of the yeast oxysterol-binding protein homologues". In: *Genetics* 157.3 (2001), pp. 1117–1140.

[496] Jin Sook Jeong et al. "Purification and characterization of a second type thioredoxin peroxidase (type II TPx) from Saccharomyces cerevisiae". In: *Biochemistry* 38.2 (1999), pp. 776–783.

[497] Chi-Ming Wong et al. "Cooperation of yeast peroxiredoxins Tsa1p and Tsa2p in the cellular defense against oxidative and nitrosative stress". In: *Journal of Biological Chemistry* 277.7 (2002), pp. 5385–5394.

[498] Thomas J Lyons et al. "Metalloregulation of yeast membrane steroid receptor homologs". In: *Proceedings of the National Academy of Sciences* 101.15 (2004), pp. 5506–5511.

[499] Rhonda K Raymond, Evdokia K Kastanos, and Dean R Appling. "Saccharomyces cerevisiae expresses two genes encoding isozymes of methylenetetrahydrofolate reductase". In: *Archives of Biochemistry and Biophysics* 372.2 (1999), pp. 300–308.

[500] Philippe Goyette et al. "Human methylenetetrahydrofolate reductase: isolation of cDNA, mapping and mutation identification". In: *Nature genetics* 7.2 (1994), pp. 195–200.

[501] Sanja Roje et al. "Metabolic engineering in yeast demonstrates thats-adenosylmethionine controls flux through the methylenetetrahydrofolate reductase reaction in vivo". In: *Journal of Biological Chemistry* 277.6 (2002), pp. 4056–4061.

[502] Ulrike Csaikl and Franz Csaikl. "Molecular cloning and characterization of the MET6 gene of Saccharomyces cerevisiae". In: *Gene* 46.2-3 (1986), pp. 207–214.

[503] Huda S Suliman, Dean R Appling, and Jon D Robertus. "The gene for cobalamin-independent methionine synthase is essential in Candida albicans: a potential antifungal target". In: *Archives of biochemistry and biophysics* 467.2 (2007), pp. 218–226.

[504] Johannes Eichel et al. "Vitamin-B12-Independent Methionine Synthase from a Higher Plant (Catharanthus Roseus) Molecular Characterization, Regulation, Heterologous Expression, and Enzyme Properties". In: *European Journal of Biochemistry* 230.3 (1995), pp. 1053–1058.

[505] Carolyn D Whitfield, Edward J Steers Jr, and Herbert Weissbach. "Purification and properties of 5-methyltetrahydropteroyltriglutamate-homocysteine transmethylase". In: *Journal of Biological Chemistry* 245.2 (1970), pp. 390–401.

[506] Jean-Luc Ferrer et al. "Crystal Structures of Cobalamin-independent Methionine Synthase Complexed with Zinc, Homocysteine, and Methyltetrahydrofolate*". In: *Journal of Biological Chemistry* 279.43 (2004), pp. 44235–44238.

[507] Robert Pejchal and Martha L Ludwig. "Cobalamin-independent methionine synthase (MetE): a face-to-face double barrel that evolved by gene duplication". In: *PLoS biology* 3.2 (2005), e31.

[508] Huda S Suliman et al. "Purification and properties of cobalamin-independent methionine synthase from Candida albicans and Saccharomyces cerevisiae". In: *Archives of Biochemistry and Biophysics* 441.1 (2005), pp. 56–63.

[509] Katrina Peariso et al. "Characterization of the zinc binding site in methionine synthase enzymes of Escherichia coli: the role of zinc in the methylation of homocysteine". In: *Journal of the American Chemical Society* 120.33 (1998), pp. 8410–8416.

[510] Myriam Visram et al. "Homocysteine regulates fatty acid and lipid metabolism in yeast". In: *Journal of Biological Chemistry* 293.15 (2018), pp. 5544–5555.

[511] Jeffrey A Hadwiger et al. "A family of cyclin homologs that control the G1 phase in yeast." In: *Proceedings of the National Academy of Sciences* 86.16 (1989), pp. 6255–6259.

[512] Dominique Thomas and Yolande Surdin-Kerjan. "Metabolism of sulfur amino acids in Saccharomyces cerevisiae". In: *Microbiology and Molecular Biology Reviews* 61.4 (1997), pp. 503–532.

[513] J Anthony Graves and Susan A Henry. "Regulation of the yeast INO1 gene: The products of the INO2, INO4 and OPI1 regulatory genes are not required for repression in response to inositol". In: *Genetics* 154.4 (2000), pp. 1485–1495.

[514] Susan A Henry, Maria L Gaspar, and Stephen A Jesch. "The response to inositol: regulation of glycerolipid metabolism and stress response signaling in yeast". In: *Chemistry and physics of lipids* 180 (2014), pp. 23–43.

[515] Anna D Frej et al. "The inositol-3-phosphate synthase biosynthetic enzyme has distinct catalytic and metabolic roles". In: *Molecular and cellular biology* 36.10 (2016), pp. 1464–1479.

[516] Glenn C Davis et al. "Chronic Parkinsonism secondary to intravenous injection of meperidine analogues". In: *Psychiatry research* 1.3 (1979), pp. 249–254.

[517] J William Langston et al. "Chronic Parkinsonism in humans due to a product of meperidine-analog synthesis". In: *Science* 219.4587 (1983), pp. 979–980.

[518] Solomon H Snyder and Robert J D'Amato. "MPTP: A neurotoxin relevant to the pathophysiology of Parkinson's disease: The 1985 George C. Cotzias Lecture". In: *Neurology* 36.2 (1986), pp. 250–250.

[519] Toni Gabaldón, Daphne Rainey, and Martijn A Huynen. "Tracing the evolution of a large protein complex in the eukaryotes, NADH: ubiquinone oxidoreductase (Complex I)". In: *Journal of molecular biology* 348.4 (2005), pp. 857–870.

[520] David A Pearce and Fred Sherman. "Differential ubiquitin-dependent degradation of the yeast apo-cytochrome c isozymes". In: *Journal of Biological Chemistry* 272.50 (1997), pp. 31829–31836.

[521] Christopher M Allan et al. "Identification of Coq11, a new coenzyme Q biosynthetic protein in the CoQ-synthome in Saccharomyces cerevisiae". In: *Journal of Biological Chemistry* 290.12 (2015), pp. 7517–7534.

[522] Zhengchang Liu and Ronald A Butow. "A transcriptional switch in the expression of yeast tricarboxylic acid cycle genes in response to a reduction or loss of respiratory function". In: *Molecular and cellular biology* 19.10 (1999), pp. 6720–6728.

[523] Harmen M van Rossum et al. "Alternative reactions at the interface of glycolysis and citric acid cycle in Saccharomyces cerevisiae". In: *FEMS yeast research* 16.3 (2016), fow017.

[524] Graziana Assalve et al. "Ctp1 and Yhm2: two mitochondrial citrate transporters to support metabolic flexibility of Saccharomyces cerevisiae". In: *International Journal of Molecular Sciences* 25.3 (2024), p. 1870.

[525] Hila Avisar et al. "Lipid level alteration in human and cellular models of alpha synuclein mutations". In: *npj Parkinson's Disease* 8.1 (2022), p. 52.

[526] Antonia María Romero et al. "Regulation of yeast fatty acid desaturase in response to iron deficiency". In: *Biochimica et Biophysica Acta (BBA)-Molecular and Cell Biology of Lipids* 1863.6 (2018), pp. 657–668.

[527] Saranna Fanning et al. "Lipidomic analysis of α-synuclein neurotoxicity identifies stearoyl CoA desaturase as a target for Parkinson treatment". In: *Molecular cell* 73.5 (2019), pp. 1001–1014.

[528] Benjamin M Vincent et al. "Inhibiting stearoyl-CoA desaturase ameliorates α-synuclein cytotoxicity". In: *Cell reports* 25.10 (2018), pp. 2742–2754.

[529] Kurt E Kwast et al. "Oxygen sensing in yeast: evidence for the involvement of the respiratory chain in regulating the transcription of a subset of hypoxic genes". In: *Proceedings of the National Academy of Sciences* 96.10 (1999), pp. 5446–5451.

[530] Julie A Maupin-Furlow. "Vitamin B1 (thiamine) metabolism and regulation in Archaea". In: *B Group Vitamins-Current Uses and Perspectives* (2018), pp. 9–31.

[531] Michel Frederich et al. "Thiaminylated adenine nucleotides. Chemical synthesis, structural characterization and natural occurrence". In: *The FEBS Journal* 276.12 (2009), pp. 3256–3268.

[532] Qinglin Du, Honghai Wang, and Jianping Xie. "Thiamin (vitamin B1) biosynthesis and regulation: a rich source of antimicrobial drug targets?" In: *International journal of biological sciences* 7.1 (2011), p. 41.

[533] Christopher T Jurgenson, Tadhg P Begley, and Steven E Ealick. "The structural and biochemical foundations of thiamin biosynthesis". In: *Annual review of biochemistry* 78.1 (2009), pp. 569–603.

[534] Raymond Wightman and Peter A Meacock. "The THI5 gene family of Saccharomyces cerevisiae: distribution of homologues among the hemiascomycetes and functional redundancy in the aerobic biosynthesis of thiamin from pyridoxine". In: *Microbiology* 149.6 (2003), pp. 1447–1460.

[535] Anushree Mondal et al. "Oxidative Dearomatization of PLP in Thiamin Pyrimidine Biosynthesis in Candida albicans". In: *Journal of the American Chemical Society* 145.8 (2023), pp. 4421–4430.

[536] Rung-Yi Lai et al. "Mechanistic Studies on the Single-Turnover Yeast Thiamin Pyrimidine Synthase: Characterization of the Inactive Enzyme". In: *Journal of the American Chemical Society* 144.24 (2022), pp. 10711–10717.

[537] Rung-Yi Lai et al. "Thiamin pyrimidine biosynthesis in Candida albicans: a remarkable reaction between histidine and pyridoxal phosphate". In: *Journal of the American Chemical Society* 134.22 (2012), pp. 9157–9159.

[538] Yuko Kawasaki et al. "Biosynthesis of hydroxymethylpyrimidine pyrophosphate in Saccharomyces cerevisiae". In: *Current genetics* 47 (2005), pp. 156–162.

[539] Khanh vq Lng and Lan TH Nguyn. "The beneficial role of thiamine in Parkinson disease". In: *CNS neuroscience & therapeutics* 19.7 (2013), pp. 461–468.

[540] Antonio Costantini et al. "Long-term treatment with high-dose thiamine in Parkinson disease: an open-label pilot study". In: *The Journal of Alternative and Complementary Medicine* 21.12 (2015), pp. 740–747.

[541] DOMINIQUE LISON. "CHAPTER 25 - Cobalt". In: *Handbook on the Toxicology of Metals (Third Edition)*. Ed. by Gunnar F. Nordberg et al. Third Edition. Burlington: Academic Press, 2007, pp. 511–528. ISBN: 978-0-12-369413-3. DOI: https://doi.org/10.1016/B978-012369413-3/50080-X. URL: https://www.sciencedirect.com/science/article/pii/B978012369413350080X.

[542] JRDE Laeter. "Atomic weights of the elements: Review 2000". In: *Pure Appl. Chem.* 75 (2003), pp. 683–800.

[543] Wei Zhou and Lin Guo. "Iron triad (Fe, Co, Ni) nanomaterials: structural design, functionalization and their applications". In: *Chemical Society Reviews* 44.19 (2015), pp. 6697–6707.

[544] Stéphane L. Benoit and Robert J. Maier. "Nickel Ions in Biological Systems". In: *Encyclopedia of Metalloproteins*. Ed. by Robert H. Kretsinger, Vladimir N. Uversky, and Eugene A. Permyakov. New York, NY: Springer New York, 2013, pp. 1501–1505. ISBN: 978-1-4614-1533-6. DOI: 10.1007/978-1-4614-1533-6_75. URL: https://doi.org/10.1007/978-1-4614-1533-6_75.

[545] E Lester Smith. "Presence of cobalt in the anti-pernicious anaemia factor". In: *Nature* 162.4108 (1948), pp. 144–145.

[546] Edward L Rickes et al. "Vitamin B12, a cobalt complex". In: *Science* 108.2797 (1948), pp. 134–134.

[547] JR Guest et al. "A methyl analogue of cobamide coenzyme in relation to methionine synthesis by bacteria". In: *Nature* 195.4839 (1962), pp. 340–342.

[548] Miriam Rossi et al. "The structure of a B12 coenzyme: methylcobalamin studies by X-ray and NMR methods". In: *Journal of the American Chemical Society* 107.6 (1985), pp. 1729–1738.

[549] D Leclerc et al. "Cloning and mapping of a cDNA for methionine synthase reductase, a flavoprotein defective in patients with homocystinuria". In: *Proceedings of the National Academy of Sciences* 95.6 (1998), pp. 3059–3064.

[550] Kurt O Konhauser et al. "Oceanic nickel depletion and a methanogen famine before the Great Oxidation Event". In: *Nature* 458.7239 (2009), pp. 750–753.

[551] Marila Alfano and Christine Cavazza. "Structure, function, and biosynthesis of nickel-dependent enzymes". In: *Protein Science* 29.5 (2020), pp. 1071–1089.

[552] Stephen W Ragsdale. "Nickel and the carbon cycle". In: *Journal of inorganic biochemistry* 101.11-12 (2007), pp. 1657–1666.

[553] Juan C Fontecilla-Camps et al. "Structure–function relationships of anaerobic gas-processing metalloenzymes". In: *Nature* 460.7257 (2009), pp. 814–822.

[554] Frank T Robb and Stephen M Techtmann. "Life on the fringe: microbial adaptation to growth on carbon monoxide". In: *F1000Research* 7 (2018).

[555] Panagiotis S Adam, Guillaume Borrel, and Simonetta Gribaldo. "Evolutionary history of carbon monoxide dehydrogenase/acetyl-CoA synthase, one of the oldest enzymatic complexes". In: *Proceedings of the National Academy of Sciences* 115.6 (2018), E1166–E1173.

[556] Bernard Meunier et al. *Biomimetic oxidations catalyzed by transition metal complexes*. World Scientific, 2000.

[557] Merle Uudsemaa and Toomas Tamm. "Density-functional theory calculations of aqueous redox potentials of fourth-period transition metals". In: *The Journal of Physical Chemistry A* 107.46 (2003), pp. 9997–10003.

[558] Shramana Chatterjee et al. "Unveiling the mechanisms and biosynthesis of a novel nickel-pincer enzyme". In: *Biochemical Society Transactions* 50.4 (2022), pp. 1187–1196.

[559] Robert P Hausinger, Jian Hu, and Benoît Desguin. "The nickel-pincer coenzyme of lactate racemase: A case study of uncovering cofactor structure and biosynthesis". In: *Methods in enzymology*. Vol. 685. Elsevier, 2023, pp. 341–371.

[560] Agnieszka Sekowska and Antoine Danchin. "The methionine salvage pathway in Bacillus subtilis". In: *BMC microbiology* 2 (2002), pp. 1–14.

[561] Agnieszka Sekowska et al. "Bacterial variations on the methionine salvage pathway". In: *BMC microbiology* 4 (2004), pp. 1–17.

[562] Yong Dai, Pieter C Wensink, and Robert H Abeles. "One protein, two enzymes". In: *Journal of Biological Chemistry* 274.3 (1999), pp. 1193–1195.

[563] Yong Dai, Thomas C Pochapsky, and Robert H Abeles. "Mechanistic studies of two dioxygenases in the methionine salvage pathway of Klebsiella pneumoniae". In: *Biochemistry* 40.21 (2001), pp. 6379–6387.

[564] Luca Mazzei, Francesco Musiani, and Stefano Ciurli. "The structure-based reaction mechanism of urease, a nickel dependent enzyme: Tale of a long debate". In: *JBIC Journal of Biological Inorganic Chemistry* 25.6 (2020), pp. 829–845.

[565] J Velasquez and AA Wray. *Deferoxamine In StatPearls*. 2023.

[566] H Keberle. "The biochemistry of desferrioxamine and its relation to iron metabolism". In: *Annals of the New York Academy of Sciences* 119.2 (1964), pp. 758–768.

[567] M Indriati Hood and Eric P Skaar. "Nutritional immunity: transition metals at the pathogen–host interface". In: *Nature Reviews Microbiology* 10.8 (2012), pp. 525–537.

[568] Marcus Miethke and Mohamed A Marahiel. "Siderophore-based iron acquisition and pathogen control". In: *Microbiology and molecular biology reviews* 71.3 (2007), pp. 413–451.

[569] D.J. Raines et al. "Siderophores". In: Dec. 2015. ISBN: 9780124095472. DOI: 10.1016/B978-0-12-409547-2.11040-6.

[570] Sujit Sheth. "Iron chelation: an update". In: *Current opinion in hematology* 21.3 (2014), pp. 179–185.

[571] Samir K Ballas et al. "The effect of iron chelation therapy on overall survival in sickle cell disease and β-thalassemia: A systematic review". In: *American Journal of Hematology* 93.7 (2018), pp. 943–952.

[572] Yong Yuan et al. "Cobalt inhibits the interaction between hypoxia-inducible factor-α and von Hippel-Lindau protein by direct binding to hypoxia-inducible factor-α". In: *Journal of Biological Chemistry* 278.18 (2003), pp. 15911–15916.

[573] Julie E Gleason et al. "Analysis of hypoxia and hypoxia-like states through metabolite profiling". In: *PloS one* 6.9 (2011), e24741.

[574] Ximena Borenstein et al. "Functional changes in murine mammary cancer cells elicited by CoCl2-induced hypoxia". In: *Nitric Oxide* 23.3 (2010), pp. 234–241.

[575] Yide Jiang et al. "MGA2 is involved in the low-oxygen response element-dependent hypoxic induction of genes in Saccharomyces cerevisiae". In: *Molecular and cellular biology* 21.18 (2001), pp. 6161–6169.

[576] Mark A Goldberg, Susan P Dunning, and H Franklin Bunn. "Regulation of the erythropoietin gene: evidence that the oxygen sensor is a heme protein". In: *Science* 242.4884 (1988), pp. 1412–1415.

[577] Mariana Nikolova-Karakashian and Alfred H Merrill Jr. "[22] Ceramidases". In: *Methods in enzymology*. Vol. 311. Elsevier, 2000, pp. 194–201.

[578] Rick T Dobrowsky et al. "Ceramide activates heterotrimeric protein phosphatase 2A". In: *Journal of Biological Chemistry* 268.21 (1993), pp. 15523–15530.

[579] Charles E Chalfant et al. "The structural requirements for ceramide activation of serine-threonine protein phosphatases". In: *Journal of lipid research* 45.3 (2004), pp. 496–506.

[580] Kang-Woo Lee et al. "Enhanced phosphatase activity attenuates α-synucleinopathy in a mouse model". In: *Journal of Neuroscience* 31.19 (2011), pp. 6963–6971.

[581] Cungui Mao et al. "Cloning of an alkaline ceramidase from Saccharomyces cerevisiae: an enzyme with reverse (CoA-independent) ceramide synthase activity". In: *Journal of Biological Chemistry* 275.10 (2000), pp. 6876–6884.

[582] Cungui Mao et al. "Cloning and characterization of a Saccharomyces cerevisiae alkaline ceramidase with specificity for dihydroceramide". In: *Journal of Biological Chemistry* 275.40 (2000), pp. 31369–31378.

[583] AB Singleton et al. "α-Synuclein locus triplication causes Parkinson's disease". In: *science* 302.5646 (2003), pp. 841–841.

[584] Marie-Christine Chartier-Harlin et al. "α-synuclein locus duplication as a cause of familial Parkinson's disease". In: *The Lancet* 364.9440 (2004), pp. 1167–1169.

[585] Wataru Satake et al. "Genome-wide association study identifies common variants at four loci as genetic risk factors for Parkinson's disease". In: *Nature genetics* 41.12 (2009), pp. 1303–1307.

[586] Ignacio F Mata et al. "SNCA variant associated with Parkinson disease and plasma α-synuclein level". In: *Archives of neurology* 67.11 (2010), pp. 1350–1356.

[587] Julia Fuchs et al. "Genetic variability in the SNCA gene influences α-synuclein levels in the blood and brain". In: *The FASEB journal* 22.5 (2008), pp. 1327–1334.

[588] Tracy A Cole et al. "α-Synuclein antisense oligonucleotides as a disease-modifying therapy for Parkinson's disease". In: *JCI insight* 6.5 (2021).

[589] Alevtina D Zharikov et al. "shRNA targeting α-synuclein prevents neurodegeneration in a Parkinson's disease model". In: *The Journal of clinical investigation* 125.7 (2015), pp. 2721–2735.

[590] Marusela Oliveras-Salvá et al. "rAAV2/7 vector-mediated overexpression of alpha-synuclein in mouse substantia nigra induces protein aggregation and progressive dose-dependent neurodegeneration". In: *Molecular neurodegeneration* 8 (2013), pp. 1–14.

[591] Justus C Dächsel et al. "The ups and downs of α-synuclein mRNA expression". In: *Movement disorders: official journal of the Movement Disorder Society* 22.2 (2007), pp. 293–295.

[592] Giovanni Bellomo et al. "The vicious cycle between α-synuclein aggregation and autophagic-lysosomal dysfunction". In: *Movement Disorders* 35.1 (2020), pp. 34–44.

[593] Doris Petroi et al. "Aggregate clearance of α-synuclein in Saccharomyces cerevisiae depends more on autophagosome and vacuole function than on the proteasome". In: *Journal of Biological Chemistry* 287.33 (2012), pp. 27567–27579.

[594] Jana Gerber et al. "The yeast scaffold proteins Isu1p and Isu2p are required inside mitochondria for maturation of cytosolic Fe/S proteins". In: *Molecular and cellular biology* 24.11 (2004), pp. 4848–4857.

[595] Akio Kikuchi et al. "Systemic increase of oxidative nucleic acid damage in Parkinson's disease and multiple system atrophy". In: *Neurobiology of disease* 9.2 (2002), pp. 244–248.

[596] Maria Laura Gaspar et al. "Phosphatidic acid species 34: 1 mediates expression of the myo-inositol 3-phosphate synthase gene INO1 for lipid synthesis in yeast". In: *Journal of Biological Chemistry* 298.7 (2022).

[597] HOL Fischer. "Chemical and biological relationships between hexoses and inositols". In: *Harvey Lect., Ser* 40 (1944), pp. 156–178.

[598] Arun Lahiri Majumder, Margaret D Johnson, and Susan A Henry. "1L-myo-inositol-1-phosphate synthase". In: *Biochimica et Biophysica Acta (BBA)-Lipids and Lipid Metabolism* 1348.1-2 (1997), pp. 245–256.

[599] BC Viljoen, JLF Kock, and PM Lategan. "Long-chain fatty acid composition of selected genera of yeasts belonging to the Endomycetales". In: *Antonie van leeuwenhoek* 52 (1986), pp. 45–51.

[600] Gabriele Tuller et al. "Lipid composition of subcellular membranes of an FY1679-derived haploid yeast wild-type strain grown on different carbon sources". In: *Yeast* 15.14 (1999), pp. 1555–1564.

[601] Andrew G Mitchell and Charles E Martin. "A novel cytochrome b5-like domain is linked to the carboxyl terminus of the Saccharomyces cerevisiae δ-9 fatty acid desaturase ()". In: *Journal of Biological Chemistry* 270.50 (1995), pp. 29766–29772.

[602] A Melnikova et al. "α-Synuclein overexpression in SH-SY5Y human neuroblastoma cells leads to the accumulation of thioflavin S-positive aggregates and impairment of glycolysis". In: *Biochemistry (Moscow)* 85 (2020), pp. 604–613.

[603] Hongfei Qiao et al. "Alpha-synuclein induces microglial migration via PKM2-dependent glycolysis". In: *International journal of biological macromolecules* 129 (2019), pp. 601–607.

[604] Yun Chen et al. "Ach1 is involved in shuttling mitochondrial acetyl units for cytosolic C2 provision in Saccharomyces cerevisiae lacking pyruvate decarboxylase". In: *FEMS Yeast Research* 15.3 (2015), fov015.

[605] Yating Hu et al. "Engineering Saccharomyces cerevisiae cells for production of fatty acid-derived biofuels and chemicals". In: *Open biology* 9.5 (2019), p. 190049.

[606] Frank Jordan. "Current mechanistic understanding of thiamin diphosphate-dependent enzymatic reactions". In: *Natural product reports* 20.2 (2003), pp. 184–201.

[607] Derrick Lonsdale and Chandler Marrs. *Thiamine deficiency disease, dysautonomia, and high calorie malnutrition*. Academic Press, 2017.

[608] Ewa Kowalska and Andrzej Kozik. "The genes and enzymes involved in the biosynthesis of thiamin and thiamin diphosphate in yeasts". In: *Cellular & molecular biology letters* 13 (2008), pp. 271–282.

[609] Romain Froquet et al. "Control of cellular physiology by TM9 proteins in yeast and Dictyostelium". In: *Journal of Biological Chemistry* 283.11 (2008), pp. 6764–6772.

[610] Marcin Kolaczkowski et al. "Differential regulation of ceramide synthase components LAC1 and LAG1 in Saccharomyces cerevisiae". In: *Eukaryotic cell* 3.4 (2004), pp. 880–892.

[611] Z Lewis Liu and Jaewoong Moon. "A novel NADPH-dependent aldehyde reductase gene from Saccharomyces cerevisiae NRRL Y-12632 involved in the detoxification of aldehyde inhibitors derived from lignocellulosic biomass conversion". In: *Gene* 446.1 (2009), pp. 1–10.

[612] Maise Gomes Queiroz et al. "The Saccharomyces cerevisiae Ncw2 protein works on the chitin/β-glucan organisation of the cell wall". In: *Antonie van Leeuwenhoek* 114.7 (2021), pp. 1141–1153.

[613] CC Philpott et al. "The response to iron deprivation in Saccharomyces cerevisiae: expression of siderophore-based systems of iron uptake". In: *Biochemical Society Transactions* 30.4 (2002), pp. 698–702.

[614] Taki Nishimura et al. "Inhibition of cholesterol biosynthesis by 25-hydroxycholesterol is independent of OSBP". In: *Genes to Cells* 10.8 (2005), pp. 793–801.

[615] Vesa M Olkkonen and Elina Ikonen. "Getting to Grips with the Oxysterol-Binding Protein Family–a Forty Year Perspective". In: *Contact* 7 (2024), p. 25152564241273598.

[616] Katarina Vaskovicova et al. "Plasma membrane protein Nce102 modulates morphology and function of the yeast vacuole". In: *Biomolecules* 10.11 (2020), p. 1476.

[617] Fumiyoshi Abe. "Induction of DAN/TIR yeast cell wall mannoprotein genes in response to high hydrostatic pressure and low temperature". In: *FEBS letters* 581.25 (2007), pp. 4993–4998.

[618] Jie Ge et al. "Why multiple small subunits (Y2 and Y4) for yeast ribonucleotide reductase? Toward understanding the role of Y4". In: *Proceedings of the National Academy of Sciences* 98.18 (2001), pp. 10067–10072.

[619] Aisling Y Coughlan et al. "The yeast mating-type switching endonuclease HO is a domesticated member of an unorthodox homing genetic element family". In: *Elife* 9 (2020), e55336.

Chapter 5

Appendices

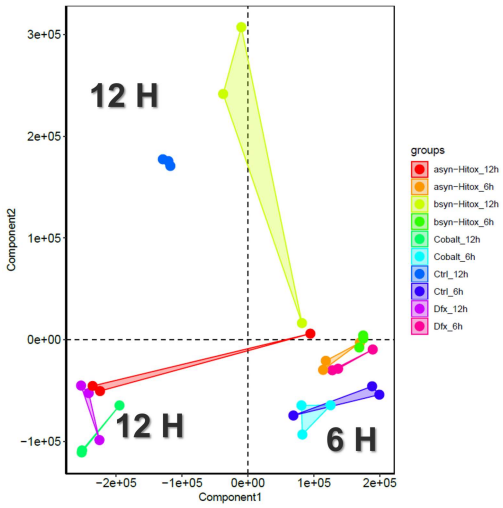

Figure 5.1: Principal components analysis of HTC (CTRL), β-HT, α-HT and α-HT strain treated with 0.3 mM Co^{2+} or DFO at 6 and 12 hours time point. At 6 hours, there are two main clusters: the HCT and the α-HT strain treated with 0.3 mM Co^{2+} show a clear separation compared to the other groups. At 12 hours there is a clear distinction between the two control groups (HTC and β-HT) compared to the α-HT strain treated and not. This picture was kindly provided by Professor Enrico Glaab

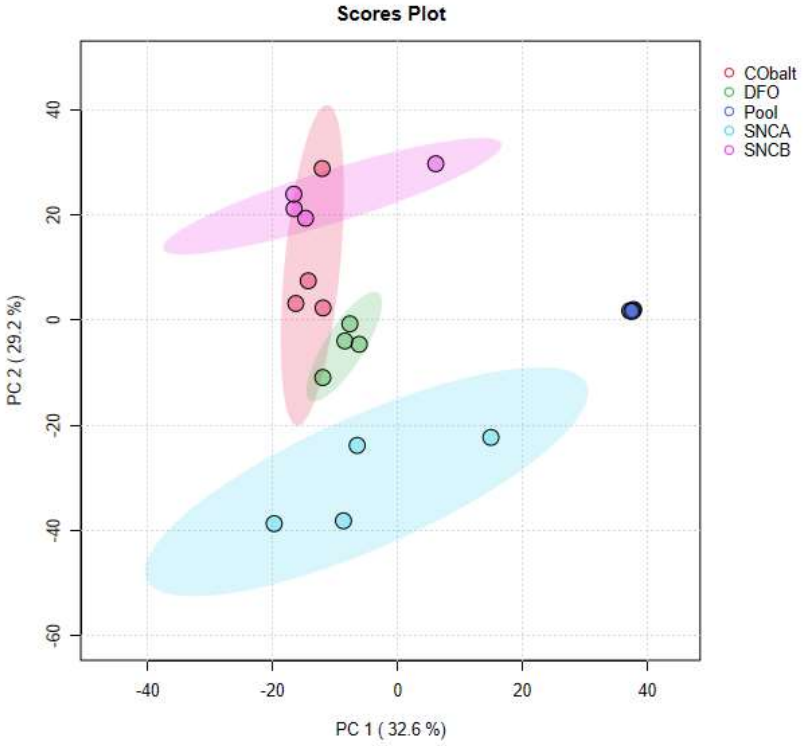

Figure 5.2: Principal component analysis of the results obtained from the untargeted lipidomic analysis performed on β-HT, α-HT, α-HT treated with Co^{2+} or DFO. Samples were analyzed after 24 hours of induction of both synuclein proteins, revealing distinct clusters. The α-HT strains (both treated and untreated) are separated from the β-HT cluster and clearly demonstrate a distinction between treated and untreated samples, highlighting the differences between these conditions. Additionally, a fifth group represents pooled samples, prepared by pooling together an aliquot from every analyzed sample. The tight clustering of these pooled samples indicates the robustness of the analysis. PC1 (32.6%) captures biological variation among the samples more efficiently compared to PC2 (29.2%).

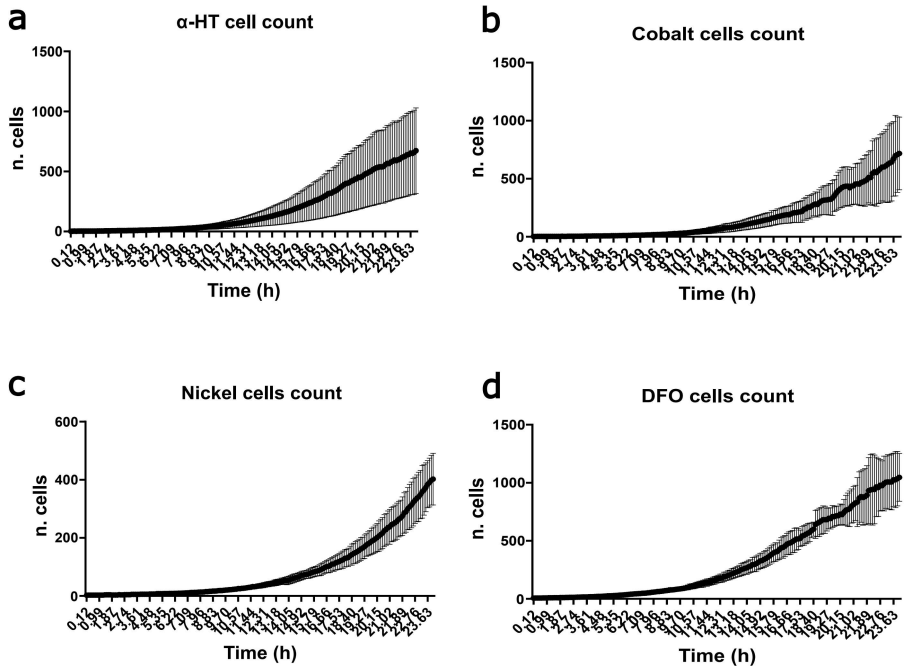

Figure 5.3: The number of cells was estimated for the α-HT strain untreated **a** and treated with Co^{2+} **b**, DFO **c** and Ni^{2+} **d** for each frame acquired during the time-lapse.

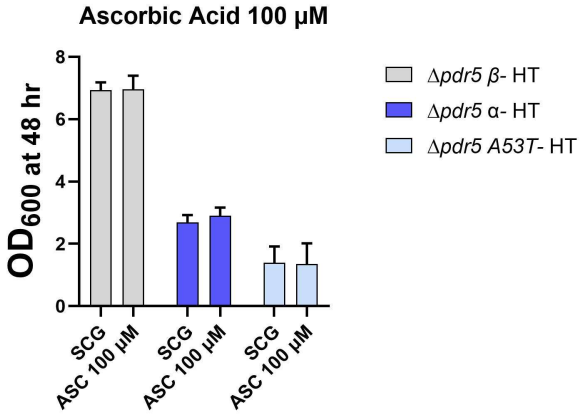

Figure 5.4: Media supplementation with 100 μM ascorbate (ASC) alone does not affect the phenotype of the β-HT, α-HT and A53T-HT strain.

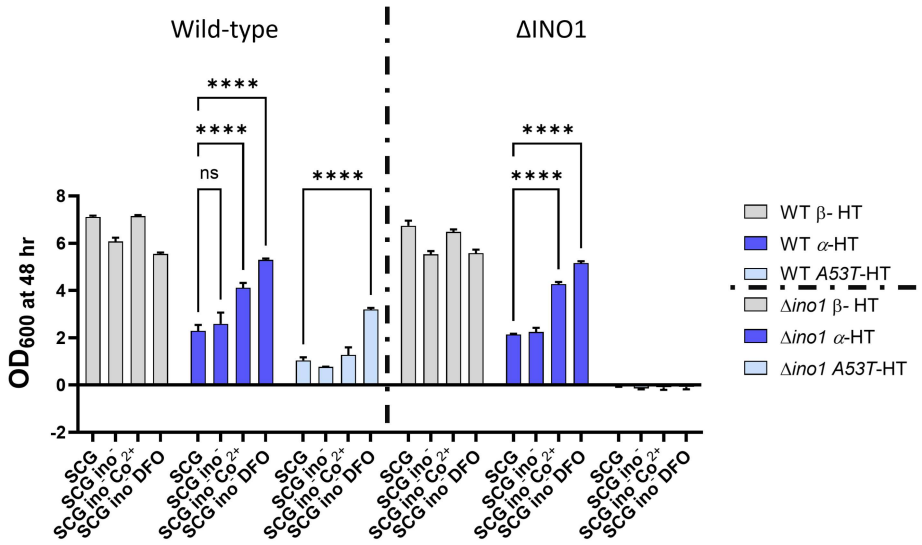

Figure 5.5: Wild-type and Δino1 HiTox strains cultivated in the presence (SCG medium) and absence of inositol substrate (SCG ino_1^-. The Δino1 knock-out in the α-HT strain does not affect the toxicity phenotype induced by the α-syn accumulation even in the absence of this supplement. Interestingly the Δino1A53T-HT strain shows a severe toxicity compared to the correspondent WT strain in all the tested conditions.

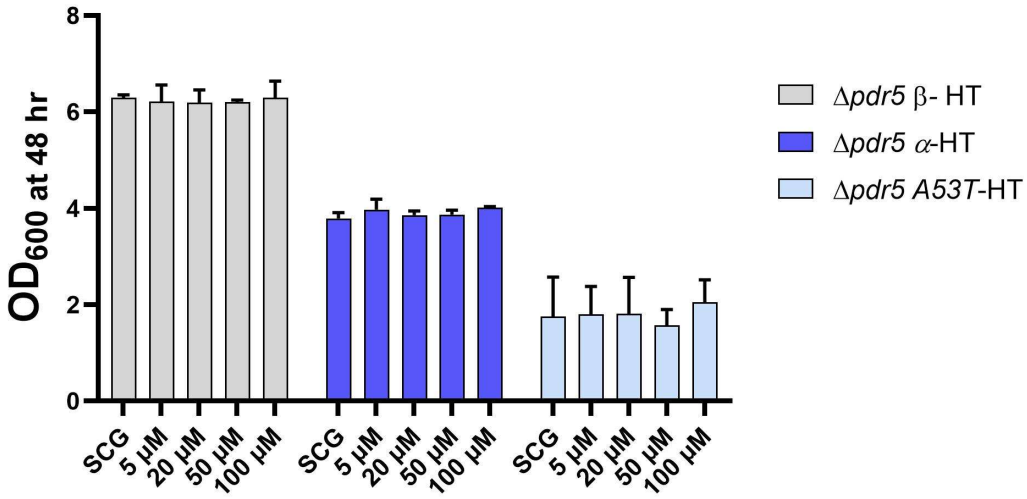

Figure 5.6: The stains β-HT, α-HT and A53T-HT were tested in presence of different concentration of thiamine. The OD_{600} were measured at 48 hours of treatment with 0 μM (SCG), 5 μM, 20 μM, 50 μM and 100 μM of thiamine. Unfortunately, no one of the tested concentrations was able to induce a beneficial effect on the growth of the α-HT and A53T-HT strains.

Table 5.1: List of Strains used in this study

Strain	Genotype	Source
W303a	MATa ura3-52 trp1Δ2 leu2-3,112his3-11 ade2-1 can1-100	Parental strain Dharcom, # YSC1059
W303 HiTox Control (HTC)	MATa can1-100 his3-11,15 leu2-3,112 trp1-1 ura3-1 ade2-1 pdr5Δ::KanMx4 pAG304Gal-ccdB-EGFP pAG306Gal-ccdB-EGFP	Derived Strain
W303 HiTox SNCB (β-HT)	MATa can1-100 his3-11,15 leu2-3,112 trp1-1 ura3-1 ade2-1 pdr5Δ::KanMx4 pAG304Gal-$SNCB^{WT}$-EGFP pAG306Gal-$SNCB^{WT}$-EGFP	Derived Strain
W303 HiTox SNCA (α-HT)	MATa can1-100 his3-11,15 leu2-3,112 trp1-1 ura3-1 ade2-1 pdr5Δ::KanMx4 pAG304Gal-$SNCA^{WT}$-EGFP pAG306Gal-$SNCA^{WT}$-EGFP	Derived Strain
W303 HiTox A53T (A53T-HT)	MATa can1-100 his3-11,15 leu2-3,112 trp1-1 ura3-1 ade2-1 pdr5Δ::KanMx4 pAG304Gal-$SNCA^{A53T}$-EGFP pAG306Gal-$SNCA^{A53T}$-EGFP	Derived Strain
INO1 knock-out strains		
W303 HiTox SNCB Δino1	MATa can1-100 his3-11,15 leu2-3,112 trp1-1 ura3-1 ade2-1 pdr5Δ::KanMx4 ino1Δ::hphMX6 pAG304Gal-$SNCB^{WT}$-EGFP pAG306Gal-$SNCB^{WT}$-EGFP	Derived Strain
W303 HiTox SNCA Δino1	MATa can1-100 his3-11,15 leu2-3,112 trp1-1 ura3-1 ade2-1 pdr5Δ::KanMx4 ino1Δ::hphMX6 pAG304Gal-$SNCA^{WT}$-EGFP pAG306Gal-$SNCA^{WT}$-EGFP	Derived Strain

Continued on next page

Table 5.1 – continued from previous page

Strain	Genotype	Source
W303 HiTox A53T Δino1	MATa can1-100 his3-11,15 leu2-3,112 trp1-1 ura3-1 ade2-1 pdr5Δ::KanMx4 ino1Δ::hphMX6 pAG304Gal-SNCA^{A53T}-EGFP pAG306Gal-SNCA^{A53T}-EGFP	Derived Strain
Thiamine strains (β-HT)		
W303 HiTox SNCB 303GAL	MATa can1-100 his3-11,15 leu2-3,112 trp1-1 ura3-1 ade2-1 pdr5Δ::KanMx4 pAG303Gal-ccdB-HA pAG304Gal-SNCB^{WT}-EGFP pAG306Gal-SNCB^{WT}-EGFP	Derived Strain
W303 HiTox SNCB 303GAL-THI4	MATa can1-100 his3-11,15 leu2-3,112 trp1-1 ura3-1 ade2-1 pdr5Δ::KanMx4 pAG303Gal-THI4-HA pAG304Gal-SNCB^{WT}-EGFP pAG306Gal-SNCB^{WT}-EGFP	Derived Strain
W303 HiTox SNCB 303GAL-THI5	MATa can1-100 his3-11,15 leu2-3,112 trp1-1 ura3-1 ade2-1 pdr5Δ::KanMx4 pAG303Gal-THI5-HA pAG304Gal-SNCB^{WT}-EGFP pAG306Gal-SNCB^{WT}-EGFP	Derived Strain
W303 HiTox SNCB 303GAL-THI11	MATa can1-100 his3-11,15 leu2-3,112 trp1-1 ura3-1 ade2-1 pdr5Δ::KanMx4 pAG303Gal-THI11-HA pAG304Gal-SNCB^{WT}-EGFP pAG306Gal-SNCB^{WT}-EGFP	Derived Strain
W303 HiTox SNCB 303GAL-THI12	MATa can1-100 his3-11,15 leu2-3,112 trp1-1 ura3-1 ade2-1 pdr5Δ::KanMx4 pAG303Gal-THI12-HA pAG304Gal-SNCB^{WT}-EGFP pAG306Gal-SNCB^{WT}-EGFP	Derived Strain

Continued on next page

Table 5.1 – continued from previous page

Strain	Genotype	Source
W303 HiTox SNCB 303GPD	MATa can1-100 his3-11,15 leu2-3,112 trp1-1 ura3-1 ade2-1 pdr5Δ::KanMx4 pAG303Gpd-ccdB-HA pAG304Gal-SNCB^{WT}-EGFP pAG306Gal-SNCB^{WT}-EGFP	Derived Strain
W303 HiTox SNCB 303GPD-THI4	MATa can1-100 his3-11,15 leu2-3,112 trp1-1 ura3-1 ade2-1 pdr5Δ::KanMx4 pAG303Gpd-THI4-HA pAG304Gal-SNCB^{WT}-EGFP pAG306Gal-SNCB^{WT}-EGFP	Derived Strain
W303 HiTox SNCB 303GPD-THI5	MATa can1-100 his3-11,15 leu2-3,112 trp1-1 ura3-1 ade2-1 pdr5Δ::KanMx4 pAG303Gpd-THI5-HA pAG304Gal-SNCB^{WT}-EGFP pAG306Gal-SNCB^{WT}-EGFP	Derived Strain
W303 HiTox SNCB 303GPD-THI11	MATa can1-100 his3-11,15 leu2-3,112 trp1-1 ura3-1 ade2-1 pdr5Δ::KanMx4 pAG303Gpd-THI11-HA pAG304Gal-SNCB^{WT}-EGFP pAG306Gal-SNCB^{WT}-EGFP	Derived Strain
W303 HiTox SNCB 303GPD-THI12	MATa can1-100 his3-11,15 leu2-3,112 trp1-1 ura3-1 ade2-1 pdr5Δ::KanMx4 pAG303Gpd-THI12-HA pAG304Gal-SNCB^{WT}-EGFP pAG306Gal-SNCB^{WT}-EGFP	Derived Strain
W303 HiTox SNCB 423GAL	MATa can1-100 his3-11,15 leu2-3,112 trp1-1 ura3-1 ade2-1 pdr5Δ::KanMx4 pAG423Gal-ccdB-HA pAG304Gal-SNCB^{WT}-EGFP pAG306Gal-SNCB^{WT}-EGFP	Derived Strain

Continued on next page

Table 5.1 – continued from previous page

Strain	Genotype	Source
W303 HiTox SNCB 423GAL-THI4	MATa can1-100 his3-11,15 leu2-3,112 trp1-1 ura3-1 ade2-1 pdr5Δ::KanMx4 pAG423Gal-THI4-HA pAG304Gal-SNCB^{WT}-EGFP pAG306Gal-SNCB^{WT}-EGFP	Derived Strain
W303 HiTox SNCB 423GAL-THI5	MATa can1-100 his3-11,15 leu2-3,112 trp1-1 ura3-1 ade2-1 pdr5Δ::KanMx4 pAG423Gal-THI5-HA pAG304Gal-SNCB^{WT}-EGFP pAG306Gal-SNCB^{WT}-EGFP	Derived Strain
W303 HiTox SNCB 423GAL-THI11	MATa can1-100 his3-11,15 leu2-3,112 trp1-1 ura3-1 ade2-1 pdr5Δ::KanMx4 pAG423Gal-THI11-HA pAG304Gal-SNCB^{WT}-EGFP pAG306Gal-SNCB^{WT}-EGFP	Derived Strain
W303 HiTox SNCB 423GAL-THI12	MATa can1-100 his3-11,15 leu2-3,112 trp1-1 ura3-1 ade2-1 pdr5Δ::KanMx4 pAG423Gal-THI12-HA pAG304Gal-SNCB^{WT}-EGFP pAG306Gal-SNCB^{WT}-EGFP	Derived Strain
W303 HiTox SNCB 423GPD	MATa can1-100 his3-11,15 leu2-3,112 trp1-1 ura3-1 ade2-1 pdr5Δ::KanMx4 pAG303Gpd-ccdB-HA pAG304Gal-SNCB^{WT}-EGFP pAG306Gal-SNCB^{WT}-EGFP	Derived Strain
W303 HiTox SNCB 423GPD-THI4	MATa can1-100 his3-11,15 leu2-3,112 trp1-1 ura3-1 ade2-1 pdr5Δ::KanMx4 pAG303Gpd-THI4-HA pAG304Gal-SNCB^{WT}-EGFP pAG306Gal-SNCB^{WT}-EGFP	Derived Strain

Continued on next page

Table 5.1 – continued from previous page

Strain	Genotype	Source
W303 HiTox SNCB 423GPD-THI5	MATa can1-100 his3-11,15 leu2-3,112 trp1-1 ura3-1 ade2-1 pdr5Δ::KanMx4 pAG303Gpd-THI5-HA pAG304Gal-SNCB^{WT}-EGFP pAG306Gal-SNCB^{WT}-EGFP	Derived Strain
W303 HiTox SNCB 423GPD-THI11	MATa can1-100 his3-11,15 leu2-3,112 trp1-1 ura3-1 ade2-1 pdr5Δ::KanMx4 pAG303Gpd-THI11-HA pAG304Gal-SNCB^{WT}-EGFP pAG306Gal-SNCB^{WT}-EGFP	Derived Strain
W303 HiTox SNCB 423GPD-THI12	MATa can1-100 his3-11,15 leu2-3,112 trp1-1 ura3-1 ade2-1 pdr5Δ::KanMx4 pAG303Gpd-THI12-HA pAG304Gal-SNCB^{WT}-EGFP pAG306Gal-SNCB^{WT}-EGFP	Derived Strain
Thiamine strains (α-HT)		
W303 HiTox SNCA 303GAL	MATa can1-100 his3-11,15 leu2-3,112 trp1-1 ura3-1 ade2-1 pdr5Δ::KanMx4 pAG303Gal-ccdB-HA pAG304Gal-SNCA^{WT}-EGFP pAG306Gal-SNCA^{WT}-EGFP	Derived Strain
W303 HiTox SNCA 303GAL-THI4	MATa can1-100 his3-11,15 leu2-3,112 trp1-1 ura3-1 ade2-1 pdr5Δ::KanMx4 pAG303Gal-THI4-HA pAG304Gal-SNCA^{WT}-EGFP pAG306Gal-SNCA^{WT}-EGFP	Derived Strain
W303 HiTox SNCA 303GAL-THI5	MATa can1-100 his3-11,15 leu2-3,112 trp1-1 ura3-1 ade2-1 pdr5Δ::KanMx4 pAG303Gal-THI5-HA pAG304Gal-SNCA^{WT}-EGFP pAG306Gal-SNCA^{WT}-EGFP	Derived Strain

Continued on next page

Table 5.1 – continued from previous page

Strain	Genotype	Source
W303 HiTox SNCA 303GAL-THI11	MATa can1-100 his3-11,15 leu2-3,112 trp1-1 ura3-1 ade2-1 pdr5Δ::KanMx4 pAG303Gal-THI11-HA pAG304Gal-SNCA^{WT}-EGFP pAG306Gal-SNCA^{WT}-EGFP	Derived Strain
W303 HiTox SNCA 303GAL-THI12	MATa can1-100 his3-11,15 leu2-3,112 trp1-1 ura3-1 ade2-1 pdr5Δ::KanMx4 pAG303Gal-THI12-HA pAG304Gal-SNCA^{WT}-EGFP pAG306Gal-SNCA^{WT}-EGFP	Derived Strain
W303 HiTox SNCA 303GPD	MATa can1-100 his3-11,15 leu2-3,112 trp1-1 ura3-1 ade2-1 pdr5Δ::KanMx4 pAG303Gpd-ccdB-HA pAG304Gal-SNCA^{WT}-EGFP pAG306Gal-SNCA^{WT}-EGFP	Derived Strain
W303 HiTox SNCA 303GPD-THI4	MATa can1-100 his3-11,15 leu2-3,112 trp1-1 ura3-1 ade2-1 pdr5Δ::KanMx4 pAG303Gpd-THI4-HA pAG304Gal-SNCA^{WT}-EGFP pAG306Gal-SNCA^{WT}-EGFP	Derived Strain
W303 HiTox SNCA 303GPD-THI5	MATa can1-100 his3-11,15 leu2-3,112 trp1-1 ura3-1 ade2-1 pdr5Δ::KanMx4 pAG303Gpd-THI5-HA pAG304Gal-SNCA^{WT}-EGFP pAG306Gal-SNCA^{WT}-EGFP	Derived Strain
W303 HiTox SNCA 303GPD-THI11	MATa can1-100 his3-11,15 leu2-3,112 trp1-1 ura3-1 ade2-1 pdr5Δ::KanMx4 pAG303Gpd-THI11-HA pAG304Gal-SNCA^{WT}-EGFP pAG306Gal-SNCA^{WT}-EGFP	Derived Strain

Continued on next page

Table 5.1 – continued from previous page

Strain	Genotype	Source
W303 HiTox SNCA 303GPD-THI12	MATa can1-100 his3-11,15 leu2-3,112 trp1-1 ura3-1 ade2-1 pdr5Δ::KanMx4 pAG303Gpd-THI12-HA pAG304Gal-SNCA^{WT}-EGFP pAG306Gal-SNCA^{WT}-EGFP	Derived Strain
W303 HiTox SNCA 423GAL	MATa can1-100 his3-11,15 leu2-3,112 trp1-1 ura3-1 ade2-1 pdr5Δ::KanMx4 pAG423Gal-ccdB-HA pAG304Gal-SNCA^{WT}-EGFP pAG306Gal-SNCA^{WT}-EGFP	Derived Strain
W303 HiTox SNCA 423GAL-THI4	MATa can1-100 his3-11,15 leu2-3,112 trp1-1 ura3-1 ade2-1 pdr5Δ::KanMx4 pAG423Gal-THI4-HA pAG304Gal-SNCA^{WT}-EGFP pAG306Gal-SNCA^{WT}-EGFP	Derived Strain
W303 HiTox SNCA 423GAL-THI5	MATa can1-100 his3-11,15 leu2-3,112 trp1-1 ura3-1 ade2-1 pdr5Δ::KanMx4 pAG423Gal-THI5-HA pAG304Gal-SNCA^{WT}-EGFP pAG306Gal-SNCA^{WT}-EGFP	Derived Strain
W303 HiTox SNCA 423GAL-THI11	MATa can1-100 his3-11,15 leu2-3,112 trp1-1 ura3-1 ade2-1 pdr5Δ::KanMx4 pAG423Gal-THI11-HA pAG304Gal-SNCA^{WT}-EGFP pAG306Gal-SNCA^{WT}-EGFP	Derived Strain
W303 HiTox SNCA 423GAL-THI12	MATa can1-100 his3-11,15 leu2-3,112 trp1-1 ura3-1 ade2-1 pdr5Δ::KanMx4 pAG423Gal-THI12-HA pAG304Gal-SNCA^{WT}-EGFP pAG306Gal-SNCA^{WT}-EGFP	Derived Strain

Continued on next page

Table 5.1 – continued from previous page

Strain	Genotype	Source
W303 HiTox SNCA 423GPD	MATa can1-100 his3-11,15 leu2-3,112 trp1-1 ura3-1 ade2-1 pdr5Δ::KanMx4 pAG303Gpd-ccdB-HA pAG304Gal-SNCA^{WT}-EGFP pAG306Gal-SNCA^{WT}-EGFP	Derived Strain
W303 HiTox SNCA 423GPD-THI4	MATa can1-100 his3-11,15 leu2-3,112 trp1-1 ura3-1 ade2-1 pdr5Δ::KanMx4 pAG303Gpd-THI4-HA pAG304Gal-SNCA^{WT}-EGFP pAG306Gal-SNCA^{WT}-EGFP	Derived Strain
W303 HiTox SNCA 423GPD-THI5	MATa can1-100 his3-11,15 leu2-3,112 trp1-1 ura3-1 ade2-1 pdr5Δ::KanMx4 pAG303Gpd-THI5-HA pAG304Gal-SNCA^{WT}-EGFP pAG306Gal-SNCA^{WT}-EGFP	Derived Strain
W303 HiTox SNCA 423GPD-THI11	MATa can1-100 his3-11,15 leu2-3,112 trp1-1 ura3-1 ade2-1 pdr5Δ::KanMx4 pAG303Gpd-THI11-HA pAG304Gal-SNCA^{WT}-EGFP pAG306Gal-SNCA^{WT}-EGFP	Derived Strain
W303 HiTox SNCA 423GPD-THI12	MATa can1-100 his3-11,15 leu2-3,112 trp1-1 ura3-1 ade2-1 pdr5Δ::KanMx4 pAG303Gpd-THI12-HA pAG304Gal-SNCA^{WT}-EGFP pAG306Gal-SNCA^{WT}-EGFP	Derived Strain
Thiamine strains (A53T-HT)		
W303 HiTox A53T 303GAL	MATa can1-100 his3-11,15 leu2-3,112 trp1-1 ura3-1 ade2-1 pdr5Δ::KanMx4 pAG303Gal-ccdB-HA pAG304Gal-SNCA^{A53T}-EGFP pAG306Gal-SNCA^{A53T}-EGFP	Derived Strain

Continued on next page

Table 5.1 – continued from previous page

Strain	Genotype	Source
W303 HiTox A53T 303GAL-THI4	MATa can1-100 his3-11,15 leu2-3,112 trp1-1 ura3-1 ade2-1 pdr5Δ::KanMx4 pAG303Gal-THI4-HA pAG304Gal-SNCA^{A53T}-EGFP pAG306Gal-SNCA^{A53T}-EGFP	Derived Strain
W303 HiTox A53T 303GAL-THI5	MATa can1-100 his3-11,15 leu2-3,112 trp1-1 ura3-1 ade2-1 pdr5Δ::KanMx4 pAG303Gal-THI5-HA pAG304Gal-SNCA^{A53T}-EGFP pAG306Gal-SNCA^{A53T}-EGFP	Derived Strain
W303 HiTox A53T 303GAL-THI11	MATa can1-100 his3-11,15 leu2-3,112 trp1-1 ura3-1 ade2-1 pdr5Δ::KanMx4 pAG303Gal-THI11-HA pAG304Gal-SNCA^{A53T}-EGFP pAG306Gal-SNCA^{A53T}-EGFP	Derived Strain
W303 HiTox A53T 303GAL-THI12	MATa can1-100 his3-11,15 leu2-3,112 trp1-1 ura3-1 ade2-1 pdr5Δ::KanMx4 pAG303Gal-THI12-HA pAG304Gal-SNCA^{A53T}-EGFP pAG306Gal-SNCA^{A53T}-EGFP	Derived Strain
W303 HiTox A53T 303GPD	MATa can1-100 his3-11,15 leu2-3,112 trp1-1 ura3-1 ade2-1 pdr5Δ::KanMx4 pAG303Gpd-ccdB-HA pAG304Gal-SNCA^{A53T}-EGFP pAG306Gal-SNCA^{A53T}-EGFP	Derived Strain
W303 HiTox A53T 303GPD-THI4	MATa can1-100 his3-11,15 leu2-3,112 trp1-1 ura3-1 ade2-1 pdr5Δ::KanMx4 pAG303Gpd-THI4-HA pAG304Gal-SNCA^{A53T}-EGFP pAG306Gal-SNCA^{A53T}-EGFP	Derived Strain

Continued on next page

Table 5.1 – continued from previous page

Strain	Genotype	Source
W303 HiTox A53T 303GPD-THI5	MATa can1-100 his3-11,15 leu2-3,112 trp1-1 ura3-1 ade2-1 pdr5Δ::KanMx4 pAG303Gpd-THI5-HA pAG304Gal-SNCA^{A53T}-EGFP pAG306Gal-SNCA^{A53T}-EGFP	Derived Strain
W303 HiTox A53T 303GPD-THI11	MATa can1-100 his3-11,15 leu2-3,112 trp1-1 ura3-1 ade2-1 pdr5Δ::KanMx4 pAG303Gpd-THI11-HA pAG304Gal-SNCA^{A53T}-EGFP pAG306Gal-SNCA^{A53T}-EGFP	Derived Strain
W303 HiTox A53T 303GPD-THI12	MATa can1-100 his3-11,15 leu2-3,112 trp1-1 ura3-1 ade2-1 pdr5Δ::KanMx4 pAG303Gpd-THI12-HA pAG304Gal-SNCA^{A53T}-EGFP pAG306Gal-SNCA^{A53T}-EGFP	Derived Strain
W303 HiTox A53T 423GAL	MATa can1-100 his3-11,15 leu2-3,112 trp1-1 ura3-1 ade2-1 pdr5Δ::KanMx4 pAG423Gal-ccdB-HA pAG304Gal-SNCA^{A53T}-EGFP pAG306Gal-SNCA^{A53T}-EGFP	Derived Strain
W303 HiTox A53T 423GAL-THI4	MATa can1-100 his3-11,15 leu2-3,112 trp1-1 ura3-1 ade2-1 pdr5Δ::KanMx4 pAG423Gal-THI4-HA pAG304Gal-SNCA^{A53T}-EGFP pAG306Gal-SNCA^{A53T}-EGFP	Derived Strain
W303 HiTox A53T 423GAL-THI5	MATa can1-100 his3-11,15 leu2-3,112 trp1-1 ura3-1 ade2-1 pdr5Δ::KanMx4 pAG423Gal-THI5-HA pAG304Gal-SNCA^{A53T}-EGFP pAG306Gal-SNCA^{A53T}-EGFP	Derived Strain

Continued on next page

Table 5.1 – continued from previous page

Strain	Genotype	Source
W303 HiTox A53T 423GAL-THI11	MATa can1-100 his3-11,15 leu2-3,112 trp1-1 ura3-1 ade2-1 pdr5Δ::KanMx4 pAG423Gal-THI11-HA pAG304Gal-SNCA^{A53T}-EGFP pAG306Gal-SNCA^{A53T}-EGFP	Derived Strain
W303 HiTox A53T 423GAL-THI12	MATa can1-100 his3-11,15 leu2-3,112 trp1-1 ura3-1 ade2-1 pdr5Δ::KanMx4 pAG423Gal-THI12-HA pAG304Gal-SNCA^{A53T}-EGFP pAG306Gal-SNCA^{A53T}-EGFP	Derived Strain
W303 HiTox A53T 423GPD	MATa can1-100 his3-11,15 leu2-3,112 trp1-1 ura3-1 ade2-1 pdr5Δ::KanMx4 pAG303Gpd-ccdB-HA pAG304Gal-SNCA^{A53T}-EGFP pAG306Gal-SNCA^{A53T}-EGFP	Derived Strain
W303 HiTox A53T 423GPD-THI4	MATa can1-100 his3-11,15 leu2-3,112 trp1-1 ura3-1 ade2-1 pdr5Δ::KanMx4 pAG303Gpd-THI4-HA pAG304Gal-SNCA^{A53T}-EGFP pAG306Gal-SNCA^{A53T}-EGFP	Derived Strain
W303 HiTox A53T 423GPD-THI5	MATa can1-100 his3-11,15 leu2-3,112 trp1-1 ura3-1 ade2-1 pdr5Δ::KanMx4 pAG303Gpd-THI5-HA pAG304Gal-SNCA^{A53T}-EGFP pAG306Gal-SNCA^{A53T}-EGFP	Derived Strain
W303 HiTox A53T 423GPD-THI12	MATa can1-100 his3-11,15 leu2-3,112 trp1-1 ura3-1 ade2-1 pdr5Δ::KanMx4 pAG303Gpd-THI12-HA pAG304Gal-SNCA^{A53T}-EGFP pAG306Gal-SNCA^{A53T}-EGFP	Derived Strain

Table 5.2: List of Primers used in this study

ORF	Orientation	Sequence
SNCB	**P1** Forward	GGGGACAAGTTTGTACAAAAAAGCAGGCTTCGATGGACGTGTTCATGAAGGG
	P2 Reverse	GGGGACCACTTTGTACAAGAAAGCTGGGTCCGCCTCTGGCTCATACTCCT
SNCA	**P3** Forward	ACAAGTTTGTACAAAAAAGCAGGCTATGGATGTATTCATGAAA
	P4 Reverse	ACCACTTTGTACAAGAAAGCTGGGTCGGCTTCAGGTTCGTAGTC
A53T	**P5** Forward	TCTCAGCCACTGTTGTCACACCATGCACCAC
	P6 Reverse	GTGGTGCATGGTGTGACAACAGTGGCTGAGA
M13	**P7** Forward	GTAAAACGACGGCCAG
	P8 Reverse	CAGGAAACAGCTATGAC
URA3	**P9** Forward	TGCGAGGCATATTTATGGTG
TRP1	**P10** Forward	TAAGCACACAAAGGCAGC
HIS3 ex	**P11** Forward	GGAGTCACTGCCAGGTATCG
SNCA	**P12** Reverse	TGTCTTCTGGGCTACTGC
YOR153W-PDR5	**P13** Forward	TTGGACTCGTGATTCCGTGG
	P14 Reverse	TTGAAATGTAGAAAGCTCGCTGA
INO1-Hyg-frw	**P15** Forward	TTACAACAATCTCTCTTCGAATCTTAGTTCGTTTTGAGAAGGCAATCCAACAGTATAGCGACCAG
	P16 Reverse	TTACAACAATCTCTCTTCGAATCTTAGTTCGTTTTGAGAAGGCAATCCAACAGTATAGCGACCAG
Hyg-int	**P17** Forward	CTGGAGCGAGGCGATG
INO1-ext	**P18** Forward	CCACATACACGCTGGTG
THI5\THI11\THI12\THI13	**P19** Forward	GGGGACAAGTTTGTACAAAAAAGCAGGCTATGTCTACAGACAAGATC

Continued on next page

Table 5.2 – continued from previous page

ORF	Orientation	Sequence
	P20 Reverse	GGGGACCACTTTGTACAAGAAAGCTGGGTC AGCTGGAAGAGCCAATC
THI4	**P21** Forward	GGGGACAAGTTTGTACAAAAAAGCAGGCTA TGTCTGCTACCTCTACTG
	P22 Reverse	GGGGACCACTTTGTACAAGAAAGCTGGGTC AGCAGCAAAGTGTTTC
qPCR Primers		
THI5\THI11\THI12\THI13	Forward	TGTTGCCTCTTTGTTGGACG
	Reverse	TGGCTTCATACCGTAGTGCT
THI4	Forward	TAAATTTGCTCCCATCCGCG
	Reverse	CGCACCGACAATAATCACGT
THI20\THI21	Forward	TACTCATCGTCATGGTGCCA
	Reverse	ATATTCTAGAGCGGCGGTCC
THI80	Forward	TGTGGGTTGTTGCCTATTGG
	Reverse	CACGCTAGTTGGCCAGTTTT
OLE1	Forward	ACCGCTTTCGTCATTCCAAC
	Reverse	TCACGAGGGGTTCTTCTGTC
TDH3 housekeeping	Forward	TCCACTCACGGTAGATACGCT
	Reverse	GTCAACGTTGGAAGAACCCCA

Table 5.3: List of Plasmids used in this study

Vector	Source	Destination\promoter
pAG304GAL-ccdB-EGFP	Addgene plasmid # 14183	TRP1 locus, GAL promoter.
pAG306GAL-ccdB-EGFP	Addgene plasmid # 14187	URA3 locus, gal promoter.
pAG303GAL-ccdB-HA	Addgene plasmid # 14229	HIS3 locus, GAL promoter.
		Continued on next page

Table 5.3 – continued from previous page

Vector	Source	Destination\promoter
pAG303GPD-ccdB-HA	Addgene plasmid # 14230	HIS3 locus, GPD promoter.
pAG423GAL-ccdB-HA	Addgene plasmid # 14245	HIS3 locus, GAL promoter.
pAG423GPD-ccdB-HA	Addgene plasmid # 14246	HIS3 locus, GPD promoter.
pDONR221	ThermoFisher: 12536017	DonorVector
α-syn-pDONR221	Created in this study	α-syn-DonorVector
β-syn-pDONR221	Created in this study	β-syn-Donor Vector
THI4-pDONR221	Created in this study	THI4-Donor Vector. w\o stop codon
THI5-pDONR221	Created in this study	THI5-Donor Vector. w\o stop codon
THI11-pDONR221	Created in this study	THI11-Donor Vector. w\o stop codon
THI12-pDONR221	Created in this study	THI12-Donor Vector. w\o stop codon
THI13-pDONR221	Created in this study	THI13-Donor Vector. w\o stop codon
pAG304GAL-αsyn-EGFP	Created in this study	Destination vector for αsyn-EGFP integration
pAG306GAL-αsyn-EGFP	Created in this study	Destination vector for αsyn-EGFP integration
pAG304GAL-βsyn-EGFP	Created in this study	Destination vector for βsyn-EGFP integration
pAG305GAL-βsyn-EGFP	Created in this study	Destination vector for βsyn-EGFP integration
pAG304GAL-A53T-EGFP	Created in this study	Destination vector for A53T-EGFP integration
pAG305GAL-A53T-EGFP	Created in this study	Destination vector for A53T-EGFP integration
pAG303GAL-THI4-HA	Created in this study	Destination vector for THI4-HA integration

Continued on next page

Table 5.3 – continued from previous page

Vector	Source	Destination\promoter
pAG303GAL-THI5-HA	Created in this study	Destination vector for THI5-HA integration
pAG303GAL-THI11-HA	Created in this study	Destination vector for THI11-HA integration
pAG303GAL-THI12-HA	Created in this study	Destination vector for THI11-HA integration
pAG303GPD-THI4-HA	Created in this study	Destination vector for THI4-HA integration
pAG303GPD-THI5-HA	Created in this study	Destination vector for THI5-HA integration
pAG303GPD-THI11-HA	Created in this study	Destination vector for THI11-HA integration
pAG303GPD-THI12-HA	Created in this study	Destination vector for THI4-HA integration
pAG423GAL-THI4-HA	Created in this study	Destination vector for THI4-HA inducible episomal expression
pAG423GAL-THI5-HA	Created in this study	Destination vector for THI5-HA inducible episomal expression
pAG423GAL-THI11-HA	Created in this study	Destination vector for THI11-HA inducible episomal expression
pAG423GAL-THI12-HA	Created in this study	Destination vector for THI11-HA inducible episomal expression
pAG423GPD-THI4-HA	Created in this study	Destination vector for THI4-HA constitutive episomal expression
pAG423GPD-THI5-HA	Created in this study	Destination vector for THI5-HA constitutive episomal expression
pAG423GPD-THI11-HA	Created in this study	Destination vector for THI11-HA constitutive episomal expression
pAG423GPD-THI12-HA	Created in this study	Destination vector for THI4-HA constitutive episomal expression

Table 5.4: DEGs **UPregulated** at 6 hours in α-HT vs β-HT.

α-HT vs β-HT "Genes upregulated" at 6hours				
Gene	**Enzyme**	**Log2FoldChange**	**padj**	**Function**
YDR007W	TRP1	1.533	1.21E-95	Phosphoribosylanthranilate isomerase that catalyzes the third step in tryptophan biosynthesis. Auxotrophic marker in W303 strain.
YDR107C	TMN2	1.046	6.81E-23	Vacuolar transmembrane proteins essential for the cell adhesion and filamentous growth[609].
YGR213C	RTA1	1.023	4.07E-11	Seven membrane-spanning receptor involved in the resistance against 7-aminocholesterol. Its expression is induced under low-heme and low-oxygen conditions.[610]
YJL153C	INO1	1.785	2.80E-10	Inositol-3-phosphate synthase involved in synthesis of inositol phosphates and inositol-containing phospholipids.
YGL157W	ARI1	1.111	6.26E-9	NADPH-dependent aldehyde reductase member of the short-chain dehydrogenase/reductase superfamily[611].
YFR026C	ULI1	2.133	2.21E-06	Protein of unknown function induced by the unfolded protein response.
YLR194C	NCW2	1.028	2.58E-05	GPI-anchored protein involved in cell wall remodeling and integrity[612].
YIR041W	PAU5	1.069	6.98E-05	Member of the seripauperin family mostly expressed during fermentation, temperature and anaerobic stress.
YJL034W	KAR2	1.027	0.0005	Member of the HSP70 family involved in proteins folding and translocation through the ER.

Continued on next page

Table 5.4 – continued from previous page

Gene	Enzyme	Log2FoldChange	padj	Function
YDR014W-A	HED1	1.068	0.002	Inhibitor protein involved in negative regulation of DNA recombinase mediator complex assembly and mitotic recombination and synaptonemal complex assembly.
YOR383C	FIT3	1.389	0.006	Cell wall mannoproteins, involved in the retention of siderophore-iron in the cell wall[613].

Table 5.5: DEGs **DOWNregulated** at 6 hours in α-HT vs β-HT.

α-HT vs β-HT "Genes downregulated" at 6 hours				
Gene	**Enzyme**	**Log2FoldChange**	**padj**	**Function**
YBR067C	TIP1	-1.100	8.55E-51	Cell wall mannoprotein expressed during heat- and cold-shock with possible lipase activity.
YPR149W	NCE102	-1.165	1.21E-38	Component of the detergent-insoluble glycolipid-enriched complex involved in the pheromone response and in secretion of proteins that lack classical secretory signal sequences.
YDR384C	ATO3	-1.124	1.69E-36	Putative ammonium transporter.
YIL162W	SUC2	-1.179	7.42E-19	Sucrose hydrolyzing enzyme constitutive expressed in the nonglycosylated form, it becomes glycosylated under glucose repression.
YHR139C	SPS100	-1.161	5.98E-16	Protein required for spore wall maturation.

Continued on next page

Table 5.5 – continued from previous page

Gene	Enzyme	Log2FoldChange	padj	Function
YLR303W	MET17	-1.030	4.31E-14	O-acetyl homoserine-O-acetyl serine sulfhydrylase, involved in methionine and cysteine biosynthesis.
YLR162W-A	RRT15	-1.002	4.15E-06	Putative protein of unknown function; identified in a screen for mutants with decreased levels of rDNA transcription.
YLR180W	SAM1	-1.150	2.58E-05	S-adenosylmethionine synthetase, it catalyzes the transfer of the adenosyl group from ATP to the sulfur atom of methionine.
YMR015C	ERG5	-1.128	0.0007	C-22 sterol desaturase, it catalyzes the formation of the C-22(23) double bond in the sterol side chain in ergosterol biosynthesis.
YER011W	TIR1	-1.477	0.02	Cell wall mannoprotein expressed under cold shock and anaerobiosis.
YER091C	MET6	-1.007	0.02	Cobalamin-independent methionine synthase, involved in methionine biosynthesis and regeneration; requires a minimum of two glutamates on the methyltetrahydrofolate substrate.

Table 5.6: DEGs **UPregulated** at 6 hours in α-HT treated with 0.3 mM Co^{2+} vs α-HT.

Cobalt treatment vs α-HT "Genes UPregulated" at 6 hours				
Gene	**Enzyme**	**Log2FoldChange**	**padj**	**Function**
YPL272C	PBI1	2.329	7.94E-46	Enzyme whose function is still unknown, that seems to be involved in the transport machinery responsible for the translocation of phosphatidylserine from the ER, where it is synthesized, to the endosome, where it is converted to phosphatidylethanolamine.
RUF5-1		1.019	5.50E-31	RNA of unknown function.
YOR237W	HES1	1.768	3.78E-15	HES1 is one of the seven oxysterol-binding proteins, conserved in humans[492].These proteins were initially identified for their ability to bind the oxidized form of ergosterol and suppress the expression of mRNAs for sterol-regulated genes [614]. More recently, these proteins have been reclassified as lipid transporters, operating across various membrane contact sites between different subcellular organelles [615].
YDR453C	TSA2	1.046	1.22E-13	Members of the peroxiredoxins antioxidant. A family of proteins well conserved among all organisms ranging from bacteria to humans involved in the detoxification of reactive nitrogen species.
YFL020C	PAU5	1.326	3.32E-12	Member of the seripauperin multigene family, this gene is induced under conditions such as alcoholic fermentation, low temperatures, and anaerobic environments. Its expression is negatively regulated by heme.

Continued on next page

Table 5.6 – continued from previous page

Gene	Enzyme	Log2FoldChange	padj	Function
YOL101C	IZH4	1.148	4.95E-11	Member of the "Implicated in Zinc Homeostasis family" which also includes IZH1, IZH2 and IZH3. IZH4 is expressed in high zinc and fatty acids concentrations. It can work as ergosterol receptor[498] .
YPR145C-A	PDR21	1.547	6.84E-10	Transcription factor that regulates the pleiotropic drug response.
YGR131W	FHN1	1.194	3.61E-06	Protein of unknown function, potentially involved in the regulation of vacuolar morphology, dynamics, and physiology with its homolog NCE102[616].
YER011W	TIR1	1.606	0.005	Cell wall mannoprotein expressed under hypoxia, high pressure and low temperature to ensure cell wall stability in critic conditions[617].

Table 5.7: DEGs **DOWNregulated** at 6 hours in α-HT treated with 0.3 mM Co^{2+} vs α-HT.

Cobalt treatment vs α-HT "Genes DOWNregulated" at 6 hours				
Gene	**Enzyme**	**Log2FoldChange**	**padj**	**Function**
YGL125W	MET13	-1.069	3.22E-09	Major isozyme of methylenetetrahydrofolate reductase; catalyzes the reduction of 5,10-methylenetetrahydrofolate to 5-methyltetrahydrofolate in the methionine biosynthesis pathway.

Continued on next page

Table 5.7 – continued from previous page

Gene	Enzyme	Log2FoldChange	padj	Function
YJL153C	INO1	-1.865	0.0001	Inositol-3-phosphate synthase catalyzes the cyclization of glucose 6-phosphate to inositol 3-phosphate. Its transcription is positively regulated by the transcription factors INO2 and INO4 and repressed by OPI1.
YER091C	MET6	1.768	3.78E-15	Cobalamine independent 5-methyl-tetrahydrofolate homocysteine methyltransferase[502, 503, 504]. It catalyzes the reduction of 5,10-methylene tetrahydrofolate (CH_2-THF) to 5-methyl-tetrahydrofolate (CH_3-THF), the methyl donor for the conversion of homocysteine in methionine[500].

Table 5.8: DEGs **UPregulated** at 12 hours in α-HT treated with 0.3 mM Co^{2+} vs α-HT.

Cobalt treatment vs α-HT "Genes UPregulated" at 12 hours				
Gene	**Enzyme**	**Log2FoldChange**	**padj**	**Function**
YOL101C	IZH4	1.333	0.010	Member of the "Implicated in Zinc Homeostasis family" which also includes IZH1, IZH2 and IZH3. IZH4 is expressed in high zinc and fatty acids concentrations. It can work as ergosterol receptor[498] .
YGR131W	FHN1	1.550	0.023	Protein of unknown function, potentially involved in the regulation of vacuolar morphology, dynamics, and physiology with its homolog NCE102[616].

Table 5.9: DEGs **DOWNregulated** at 12 hours in α-HT treated with 0.3 mM Co^{2+} vs α-HT.

Cobalt treatment vs α-HT "Genes DOWNregulated" at 12 hours				
Gene	**Enzyme**	**Log2FoldChange**	**padj**	**Function**
YMR199W	CLN1	-1.033	0.010	G1 cyclin that regulates the G1 to S phase transition in the cell cycle.
YER070W	RNR1	-1.081	0.023	Tetrameric protein complex that catalyzes the conversion of nucleotides to deoxynucleotides, the rate-limiting step in de novo deoxyribonucleotide biosynthesis, playing an essential role in DNA replication and repair[618] .
YDL227C	HO	-1.645	0.030	Endonuclease responsible for initiating mating-type switching, a gene conversion process where MATa cells change to MATα or vice versa[619] .

Table 5.10: DEGs upregulated in the β-HT vs HTC strain at 12 hours associated with oxidoreductase activity.

Gene	Protein	log2FoldChange	padj
YIR037W	HYR1	1.019522503	2.14E-18
YHR216W	IMD2	2.746018051	2.32E-15
YCL035C	GRX1	1.104880964	2.04E-11
YAR073W	IMD1	2.628771246	5.57E-11
YLR070C	XYL2	1.723726786	7.27E-11
YDR032C	PST2	1.416719008	1.51E-10
YKR076W	ECM4	1.603032135	1.73E-09
YGR256W	GND2	2.031992132	4.74E-09
YMR170C	ALD2	1.159838789	2.33E-08
YLR109W	AHP1	1.213929091	6.54E-08
YDR453C	TSA2	2.377366596	2.37E-07
YAL060W	BDH1	1.141275959	2.37E-07
YMR169C	ALD3	1.212039335	4.54E-07
YCL018W	LEU2	1.261654528	9.61E-07
YKR080W	MTD1	1.096588018	1.55E-06
YBL098W	BNA4	1.226377846	3.13E-06
YJR096W		1.659567321	5.77E-06
YJR009C	TDH2	1.195235789	7.01E-06
YNR073C	MAN2	2.381984068	7.86E-06
YNL241C	ZWF1	1.006544949	1.35E-05
YIR036C	IRC24	1.02850953	1.76E-05
YKL026C	GPX1	1.95986957	2.19E-05
YHR104W	GRE3	1.056270567	4.79E-05
YJL045W		2.516911779	7.59E-05
YEL070W	DSF1	1.972252377	0.000203512

Continued on the next page

(Continued from the previous page)

Gene	Protein	log2FoldChange	padj
YPR037C	ERV2	1.862550013	0.00029886
YOL086C	ADH1	1.192372786	0.000811868
YJL052W	TDH1	2.410380869	0.000855933
YNL274C	GOR1	1.097410782	0.000867495
YPR127W		1.105246582	0.011822162
YAL062W	GDH3	2.256695446	0.014982345
YKL085W	MDH1	1.137146677	0.015708103
YKR009C	FOX2	1.14954847	0.026161656
YKL150W	MCR1	1.012163575	0.027239942
YJR078W	BNA2	1.411122404	0.030507304
YAL061W	BDH2	1.05866938	0.030800735